Measurements of $\delta^{15}N$ of nitrogen gas and composition of trace gases in air from firn and ice cores

Francis Sundresh Mani
March 2010

A thesis submitted for the degree of Doctor of Philosophy at the University of East Anglia, Norwich, UK.

Acknowledgements

---

[a] Sadly passed away in September 2009.

Abstract

An ice core from Berkner Island, Antarctica, a coastal site on the Weddell Sea facing the Southern Atlantic Ocean, provides a new climate record and insights into north-south teleconnections. Isotopic measurements (δD and $\delta^{18}O$) show two distinct peaks during Marine Isotopic Stage 3 corresponding to the Antarctic Isotope Maximum 8 and 12 climate events. A novel extraction method was developed to enable high precision and high resolution measurements of $\delta^{15}N$ of N_2 in air occluded in bubbles in ice from depths spanning these two events. Changes of $\sim$ +0.07‰ in $\delta^{15}N$ were observed. The $\delta^{15}N$ data correlates with δD data ($r^2 = 0.78$) and therefore can be regarded as a climate proxy. Another $\delta^{15}N$ change of +0.18 ‰ was observed around 33 kyr BP, which does not correlate to any events in the δD profile but correlates with the period where large altitudinal changes occurred in the ice sheet at Berkner Island. An important aspect of this study is the opportunity it provides to phase $\delta^{15}N$ with methane, the latter being considered as a proxy for climate change in the northern hemisphere. The data indicate that warming in Antarctica precedes Greenland warming. The time lag estimate between the onset of AIM 12 and the onset of DO 12 is 1600 ± 350 yrs and between AIM 8 and DO 8 is 1100 ± 360 yrs.

A 20th century atmospheric record for perfluorocarbons (CF_4, C_2F_6, C_3F_8, c-C_4F_8), HFC-23, SF_6 and SF_5CF_3 was reconstructed from firn air from the EPICA Dronning Maud Land (EDML) site. The study provides the longest atmospheric history of the perfluorocarbons. The natural variability of CF_4 was also investigated in old air extracted from Berkner Island ice cores, showing that atmospheric CF_4 during the glacial period was higher than in 19th century.

List of Figures

▪▪

**Chapter 3: Isotopic Composition of N_2 gas trapped In Berkner Island ice
cores during the MIS 3 period**

The δ^{40}Ar/4 data plotted together with the δ^{15}N data on the same depth scale.

· ·

Chapter 4: Trace Gas Measurements across the AIM 8 & AIM 12 Event in the Berkner Island Ice core.

GICC05 age-scale. The enclosed methane variations in the box highlight the region of disagreement in Berkner gas age chronology as it does not correspond to the GICC05 age-scale. The disagreement is shown (top) on an expanded scale with correct peak matching indicated by arrows.

∎∎

Chapter 5: Oldest Firn Record of Trace Gases (PFCs, HFC-23, SF$_6$ and SF$_5$CF$_3$) from EPICA Dronning Maud Land, Antarctica.

An illustration of modelled CO_2 firn profile obtained with the effective diffusivity profile matches the observations in the firn.

■■

Chapter 6: CF$_4$ measurements in Berkner Island ice core

List of Tables

The detection limits of the individual compounds based on 100 ml of standard air analysed on 21/02/08.

Table of Contents

_____

Chapter 1: Scientific Background

_____

Chapter 2: Methodology

Chapter 4: Trace gas measurements across the AIM 8 & AIM 12 events in the Berkner Island ice core.

Chapter 5: Oldest firn record of trace gases (PFCs, HFC-23, SF_6 and SF_5CF_3) from EPICA Dronning Maud Land, Antarctica.

Chapter 6: CF$_4$ measurements in Berkner Island ice core

_____

Chapter 7: Conclusions and Recommendations

Chapter 1: Scientific Background

1.1 Introduction

1.2 The ice core record
1.2.1 Ice cores from the Holocene
1.2.2 Ice Core Record of long term climate changes
1.2.2.1 Climate records from the last deglaciation
1.2.2.2 The climate record from the last glacial period
1.2.2.3 Climate record from beyond 100 kyrs

1.3 δ^{18}O as a classical palaeo-thermometer
1.3.1 Limitations of the water isotope palaeo-thermometer

1.4 Firn
1.4.1 Firn structure and processes
1.4.1.1 Convective zone
1.4.2.2 Diffusive zone
1.4.2.3 Non diffusive zone

1.5 Analysis of trace gases in firn air

1.6 Ice age - gas age problem

1.7 Delta ^{15}N as a palaeo-thermometer
1.7.1 δ^{15}N measurements in Greenland ice cores
1.7.2 δ^{15}N measurements in Antarctic ice cores

1.8 Scientific rationale and objectives of the study
1.8.1 Scientific rationale
1.8.2 Objectives of the study

1.1 Introduction

Why study past climates? Palaeoclimatic studies act as a tool for calibrating climatic models. If climate models can reproduce the past then they can be used more confidently to project the future. Studies of past climates can improve our understanding of how the Earth's climate behaved under different conditions and these could be taken into account in the climate models. Palaeoclimatic studies also provide a climate 'base line' against which future climate changes can be compared. The 'base line' climate change could be used to assess future climate changes and isolate the natural climate variability from the human –induced climate change.

Air bubbles trapped in ice cores are valuable archives of past atmosphere and climate change, providing continuous long term profiles spanning hundreds of thousands of years. Ice cores have been used extensively to reconstruct past atmospheric composition of trace gases and aerosols trapped in the ice. Ice cores contain signatures of volcanic eruptions and other polluting agents such as lead (Wolff, 2005). Ice core records have, furthermore, enlightened the scientific community regarding palaeoclimatology through reconstruction of temperature changes from studies of isotopes of the ice and the entrapped air.

The climate system on Earth is a complex interaction between Sun and the Earth - the oceans, the atmosphere, the land masses and the snow and ice masses. The ice core record from Dome C (Figure 1.1.1) shows the temperature change for the last 800, 000 yrs and suggests that climate change is actually cyclic in nature, ranging from slow and gradual to fast and abrupt changes. The transition from the glacial (colder periods) to interglacial periods (warm periods like the present one) is linked to orbital parameters (that is positioning of the Earth relative to Sun) as explained by Milankovitch cycles. Figure 1.1.1 highlighted the positive correlation between CO_2 and temperature change, which is compelling in suggesting that increase in CO_2 in the current atmosphere due to man-made emissions could increase the rate of climate change. The ocean circulation plays an important role in transporting heat between hemispheres and any disruption to this process, such as a large influx of freshwater from ice cap melting, could also impact the climate system.
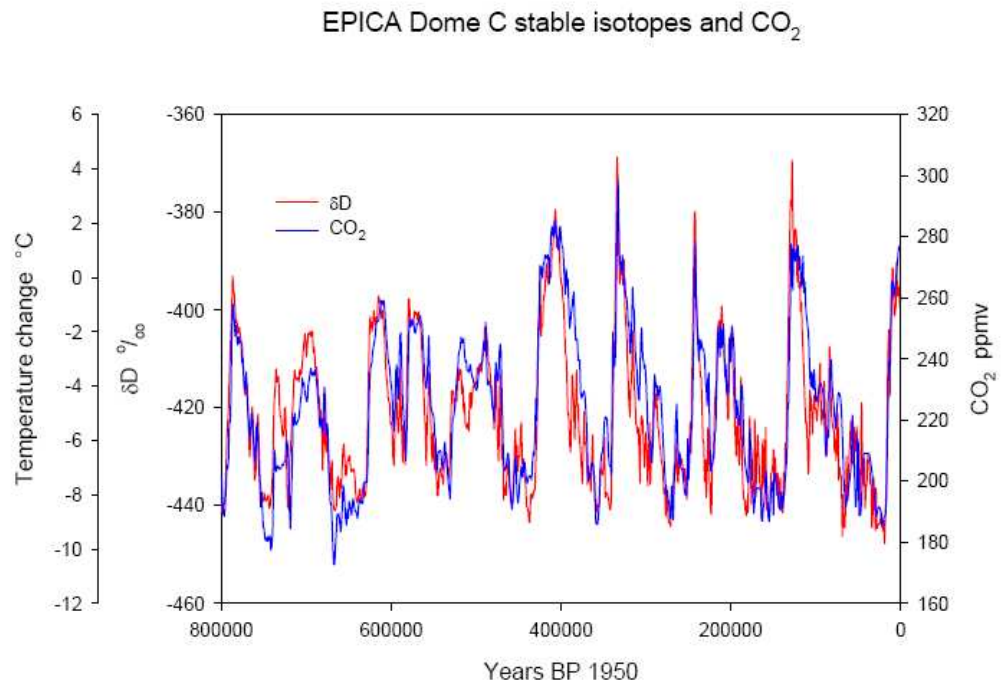
Figure 1.1.1: EPICA Dome C ice core record of the past 800 kyr BP, showing the temperature change (with respect to the last 1000 years) reconstructed from δD (Jouzel *et al*., 2007a) and CO_2 concentrations (Fischer *et al*., 1999; Petit *et al*., 1999; Monnin *et al*., 2001; Siegenthaler *et al*., 2005; Lüthi *et al*., 2008)

We understand just a few parts about the climate system; but beyond this we are less knowledgeable. The understanding of the mechanism of climate change is very limited. More research into understanding the patterns of processes that occur to produce the changes we have observed such as the cycle of glacial advances and retreats is required. Such understanding will assist in answering the fundamental question: "What climate changes will occur as a result of our activities?"

In this thesis, a new climate record is presented from Berkner Island, Antarctica, encompassing the last glacial period from 28,000 -50,000 years before present (28 – 50 kyr BP). The climate record was reconstructed from the isotopes of nitrogen gas ($\delta^{15}N$) trapped in ice cores that reflect the temperature and accumulation changes at the site. This is a novel study which involves the application of a $\delta^{15}N$ technique to characterise the millennial scale climate variability during the Marine Isotopic Stage 3 (MIS 3)

period in Antarctica. Some of the research questions that form the scientific basis of this work are:

- o Was the climate different at the coastal site of Berkner Island during the last glacial period as compared to more in-land sites in Antarctica?
- o Are the temperature reconstructions from the isotopes of gases different from those reconstructed from the water isotopes?
- o Is the modern day $\delta^{18}O_{ice}$ – temperature relationship valid during the glacial period?
- o Was the millennial scale climate variability during the glacial period synchronous with the abrupt climate changes in Greenland?
- o If the abrupt climate changes were asynchronous, which hemisphere leads the abrupt climate changes?
- o Can the phase lag difference be determined without the uncertainty due to 'ice age –gas age' difference?

In this chapter, I will first present the ice core record of palaeoclimatology, and then discuss the classical water isotope palaeo-thermometer and its limitations. A comprehensive discussion on the firn layer and the processes in the firn that modifies the isotopic composition of gases will be given. Finally, I will discuss how the $\delta^{15}N$ palaeothermometer works and its applications in Greenland and in Antarctica ice cores. After the scientific background, the project rationale and specific objectives of the project are given.

1.2 The ice core record

There are many different proxies that can be used to reconstruct the past climate such as tree rings, ocean sediments and corals, lake and bog sediments, speleothems and boreholes. In polar regions, ice cores are one of the most extensively used proxies for palaeoclimate reconstructions. Ice cores are generally well dated and continuous ice core records extend back to 120 kyr BP (kyr BP = 1000 years before present) in Greenland (North Greenland Ice Core Project Members, 2004) and ~ 800 kyr in Antarctica (EPICA Community Members, 2004). Apart from temperature reconstructions from the isotopes of water molecules in ice, that is, the ratio of $^{18}O/^{16}O$

($\delta^{18}O_{ice}$) or $^2H/H$ (δD_{ice}), the ice cores provide the record of the past atmosphere and many other environmental variables and forcing factors for climate such as greenhouse gases in the same core.

1.2.1 Ice cores from the Holocene

The Holocene is a geological epoch that began 10,000 yrs ago and is characterised by relatively stable climate. The mostly widely investigated rapid climate event during the Holocene is the 8.2 kyr cooling event. This climatic event has been investigated extensively in Greenland ice cores and is characterised as a climatic event of rapid cooling of 6 ± 2 °C (Alley *et al*., 1997; Thomas *et al*., 2007). Recently Kobashi *et al*. (2007) used $\delta^{15}N$ of N_2 to estimate a cooling of 3.3 ± 1.1 °C for the 8.2 kyr event. This climatic event is attributed to a temporary reduction in the Northern Atlantic thermohaline circulation due to large flux of freshwater from delayed melting of the North America ice sheets through Hudson Strait to the North Atlantic (Alley *et al*., 1997).

Ice core studies have been carried out in a more recent period sometimes called the "Anthropocene", a period which started during the 18th Century when humans began contributing significantly to global climate change. Ice core records of greenhouse gases during the recent centuries highlighted the preindustrial concentrations and its trend to the present day. The greenhouse gas measurements in ice cores from Law Dome, Antarctica highlighted that CO_2 concentrations increased from preindustrial value of 280 ppmv to 375 ppmv in 1996; similarly CH_4 increased from a pre-industrial value of 700 ppbv to 1800 ppbv, and N_2O increased from 276 ppbv to a value of 315 ppbv (Etheridge *et al*., 1996; Etheridge *et al*., 1998; Macfarling Meure *et al*., 2006). The stable carbon isotope measurements in atmospheric methane ($\delta^{13}CH_4$) from an Antarctic ice core suggested that during the period 0 – 1000 A.D. the major source of atmospheric methane was biomass burning, which could be influenced by both human activities and natural climate change (Ferretti *et al*., 2005).

1.2.2 Ice core record of long term climate changes

The deep drilling programs in Greenland and Antarctica retrieved ice cores that enabled climate reconstructions for thousands of years before present. The two deep ice cores from central Greenland, GRIP and GISP provide climate records back to 105 kyr BP (North Greenland Ice Core Project Members, 2004) and the third deep ice core retrieved from the North Greenland Ice Core Project (NGRIP) site dated back to 123 kyr BP. The deep ice cores from Antarctica provide even longer climate records.

The ice core from the Vostok station in Antarctica provided data for the last four glacial – interglacial cycles, dating back to 420 kyr (Petit *et al*., 1999). The Dome Fuji ice core dated back to 340 kyr (Watanabe *et al*., 2003). More recently the European Project for Ice Coring in Antarctica (EPICA) has provided two deep cores, EPICA Dome C (EDC) and EPICA Dronning Maud Land (EDML). The EDML ice core was drilled to provide a high resolution climatic record for at least two climatic cycles whereas the EDC ice core was drilled to provide the longest record from the Antarctic. The EDC ice core is dated back to 800 kyr BP (Jouzel *et al*., 2007a; Barbante *et al*., 2010).

1.2.2.1 Climate records from the last deglaciation

The climate reconstructions from these deep ice cores confirm that the current Holocene period is ~15 – 20 ℃ warmer than the last glacial maximum in Greenland (NGRIP, 2004). Similar observations were made in the Antarctic ice core, where the present interglacial (Holocene) is about 8 ℃ warmer than the last glacial maximum (Wolff, 2005; Blunier *et al*., 2004). There are numerous ice core studies that investigated the nature and timing of the last glacial termination (Dansgaard *et al*., 1989; Blunier *et al*., 1997; Sowers and Bender, 1995; Stuiver *et al*., 1995; Taylor *et al*., 1997; Cuffey *et al*., 1995; Severinghaus, 2009).

The temperature reconstructions from the central Greenland ice cores show the last glacial termination began at 14.7 kyr BP. During the deglaciation there was a sudden change in temperature of +15 ℃ and then the temperature decreased to the glacial values before increasing to early Holocene values. It is clear that the last deglaciation took place in two steps. The initially warming period called the Bølling/Allerod

transition began at 14.7 kyr BP and this warming was reversed to almost glacial temperatures during the Younger Dryas (YD) period (Severinghaus & Brook, 1999). The YD period began 12.8 kyr BP and ended abruptly at 11.6 kyr BP when the temperature jumped back into the warm phase- a period commonly known as the Preboreal (Severinghaus *et al*., 1998). The termination of the YD is a classic example of an abrupt climate change. The YD climate event is very often compared to the 8.2 kyr event and it has been suggested that the mechanism for these events is similar. The proposed mechanism of YD was a large influx of meltwater from the final deglaciation of the Laurentide ice sheet (Broecker *et al*., 1988).

The termination of the glacial period in Antarctica began around 18 kyr BP (Jouzel *et al*., 2007). The glacial – interglacial warming occurred in two steps interrupted by a slightly colder period called the Antarctic Cold Reversal (ACR), but the signal is not as strong or abrupt as the YD (Blunier *et al*., 1997). The isotopic composition ($\delta^{18}O_{ice}$) of ice cores from GRIP, Vostok and Byrd were synchronised on the same timescales to study the phase relationship of the deglacial climate events between Greenland and Antarctica. The data confirmed that the ACR preceded YD by at least 1.8 kyr (Blunier *et al*., 1997). Severinghaus (2009) suggested that the warming in the Antarctic during the termination began earlier than it did in Greenland. When Antarctica was warming Greenland was in cold phase and when Greenland was warm then Antarctica was cooling. This phenomenon is called the "bipolar see-saw" which resulted from the transport of heat through the thermohaline circulation (Stocker *et al*., 1998) and is explained in details in Chapter 4.

1.2.2.2 The climate record from the last glacial period

The last glacial period spans from 18 kyr BP to 120 kyr BP. The major finding from the ice core studies of the last glacial period is that the glacial climate was very unstable, unlike the Holocene period. The GRIP ice core shows 24 rapid and abrupt warming events during the last glacial period (Dansgaard *et al*., 1993). Such climate oscillations have a consistent pattern of gradual cooling followed by more abrupt cooling and then finally an abrupt warming. These rapid climate oscillations are called Dansgaard/Oeschger (DO) events and were commonly spaced 1,500 yrs apart, although

spacing of 3,000 or 4,500 yrs was also observed (Mayewski *et al*., 1997). The magnitude of temperature changes for these events ranges from 8 – 16 ºC based on the temperature reconstructions from the isotopes of nitrogen gas ($\delta^{15}N$) in the NGRIP ice cores (Huber *et al*., 2006a). Such warmings were very abrupt occurring on the centennial timescale (Huber *et al*., 2006a). The methane profile for the last glacial period is synchronous with the glacial climate instabilities (Chappellaz *et al*., 1993).

Such rapid climate re-organisation in the glacial period is also evident in the Antarctic ice cores (Blunier & Brook, 2001; Blunier *et al*., 1998). Initially it was not clear whether the shorter DO events have counterparts in the Antarctic record but seven major Antarctic warming events (A1 – A7) were identified during the last glacial (Blunier and Brook, 2001). In Antarctica, these millennial scale climate changes during the last glacial period are subdued and more symmetrical in nature as compared to their counterparts in Greenland. However, more recently the high resolution $\delta^{18}O_{ice}$ record from the EDML ice core revealed a one–to-one coupling between all Greenland DO events and Antarctic warm events or Antarctica Isotope Maximum (AIM) events (EPICA, 2006), (see Figure 1.2.1 and Figure 1.2.2). The magnitudes of temperature changes across the AIM events, which are analogous to the DO events, are on the order of 1 – 3 ºC (EPICA, 2006). It was noted that when Antarctic was warming then Greenland was cooling and the amplitude of the AIM events is highly correlated ($r^2 =$ 0.85) with the duration of the concurrent stadial (cooling event) in the north. These observations were explained in terms of bipolar see saw mechanism theory. There are studies which focussed on estimating the time lag between the Antarctic warming events and the corresponding Greenland DO events (Blunier & Brook, 2001; Blunier *et al*., 1998). The phase relationship of climate events in the glacial period between Antarctica and Greenland is discussed in details in Chapter 4.
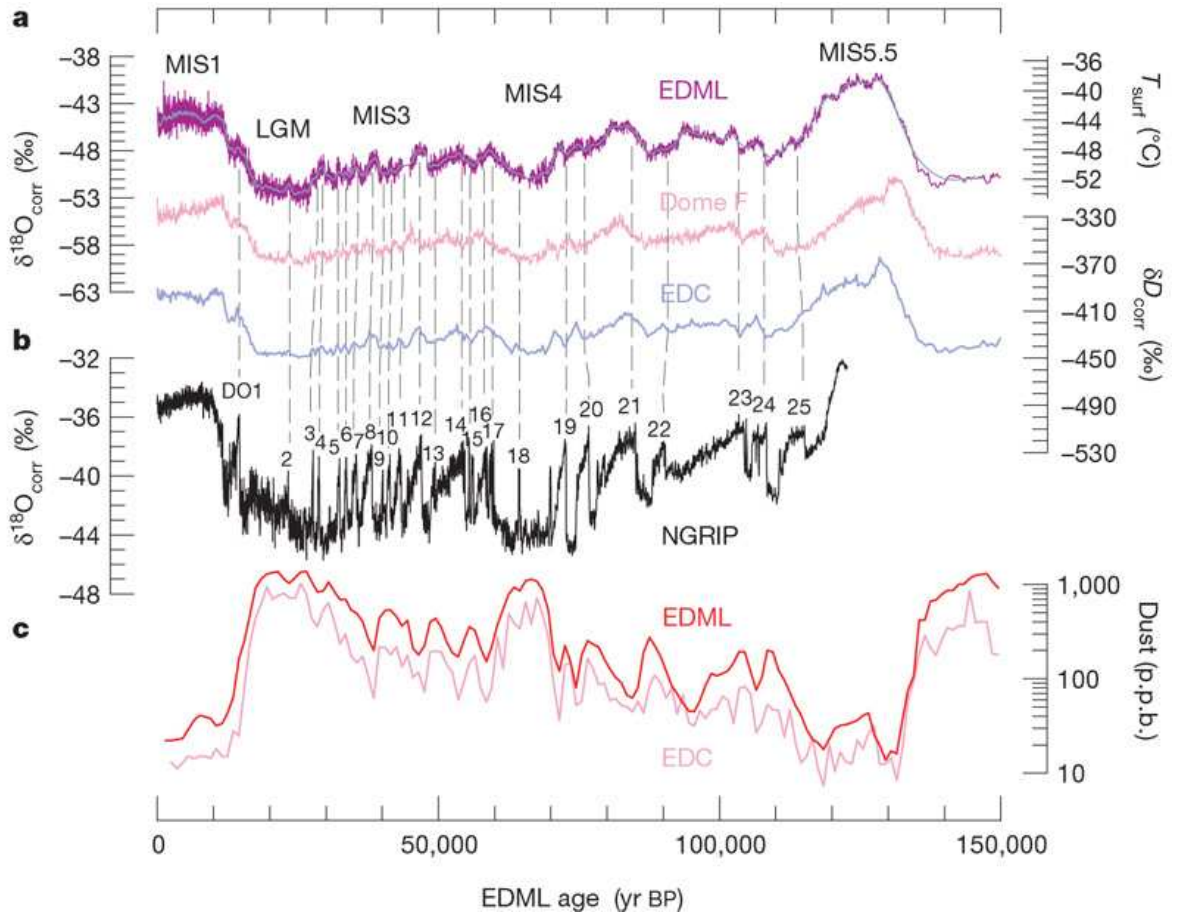
Figure 1.2.1: Antarctic stable isotope records show one to one coupling between the millennial scale climate variations in Antarctica with DO events in NGRIP (Greenland) during the last glacial period. (a) Shows the isotopic record from EDML and EDC were synchronised to EDC3 chronology based on dust profile (c) and from Dome Fuji on its individual age scale. (b) Illustrates the isotopic record from NGRIP ice core showing the rapid DO events (Source: EPICA, 2006).

9
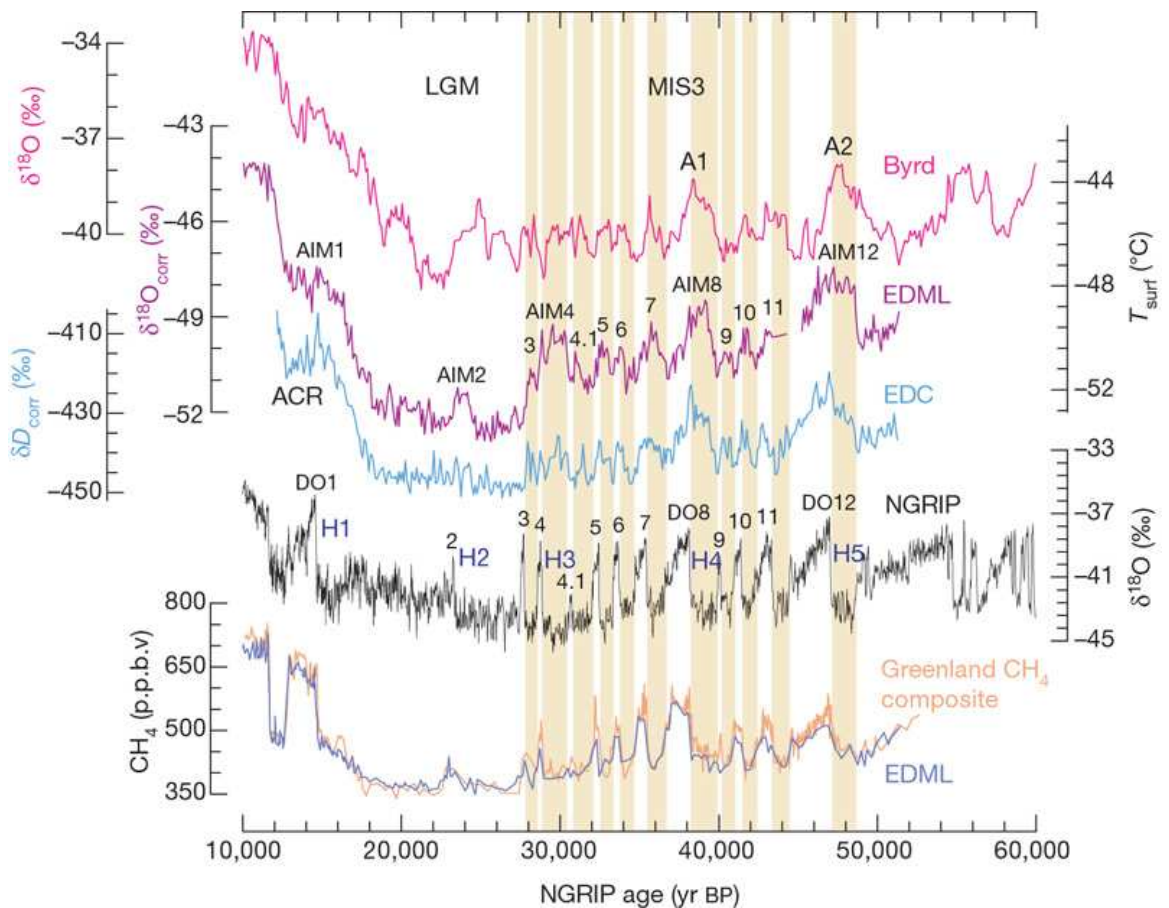
Figure 1.2.2: Methane synchronization of the EDML and NGRIP ice core record reveals a one to one coupling between each Antarctic warming and Greenland stadials. The shaded bars represent the stadials in Greenland, which corresponds to the warming in Antarctica. (Source: EPICA, 2006) H refers to Heinrich events or the Atlantic ice-rafting events which coincides with the onset of warming in Antarctica suggesting that the millenial scale variation results from reduced meridional overturning circulation.

1.2.2.3 Climate record from beyond 100 kyrs

The Vostok and Dome Fuji ice core revealed that the climate variability across East Antarctica over the past three glacial cycles was homogeneous (Watanabe *et al*., 2003). Such long term climate records provide insights into the glacial termination and its mechanism. Comparison of Vostok and Dome Fuji on a common timescale showed that the temperature change across Termination II (T II) was larger than that observed for TI (the last termination). In fact the previous interglacials were warmer than the present interglacial, the interglacial during the Marine Isotopic Stage (MIS) 9.3 was probably 6

ºC warmer than during the Holocene (Watanabe *et al*., 2003). Sime *et al*. (2009) also presented a model study that provided evidence for warmer interglacials in East Antarctic ice cores. The MIS refers to the alternating warm and cold phase of the palaeoclimate derived from the oxygen isotope data. The even numbered MIS events are cold phase and odd numbered MIS events are warm phase. The only exception is MIS 3 which was believed to be a warming phase initially. The Vostok climate record demonstrated that the glacial/interglacial cycles have a periodicity of 100 kyr, which is related to changes in Earth's orbit around the sun according to Milankovitch cycles (Petit *et al*., 1999).

The high resolution profile for the EPICA Dome C ice core extended the climate record to MIS 20.2 (~ 800 kyr B.P.) and provided evidence of climate instabilities in the previous glacial periods and varying intensity of interglacial periods (Jouzel *et al*., 2007). It was noted that the AIM events featured during the past three glacial periods with similar magnitude and pacing as observed in the last glacial period. The record also showed that the AIM events only occurred once the Antarctic temperature has decreased by 4 ˚C (Jouzel *et al*., 2007). The EDC ice core presented a record of eight glacial – interglacial cycles and it highlighted that before 430 kyr the climate was characterised by warmer glacial stages and colder interglacials as compared to the last four glacial/interglacial cycles (EPICA, 2004). The varying intensities of the glacial/interglacial cycles were modulated by variations in the Earth's orbit such as obliquity and precession. However, it is unclear whether the termination events began in the northern or southern hemisphere. Kawamura *et al*. (2007) suggested that the last four deglaciations were triggered by Northern Hemisphere summer insolation. Wolff *et al*. (2009) and Severinghaus *et al*. (2009) suggested that glacial terminations and millennial scale warmings are led from the southern hemisphere.

1.3 δ^{18}O as a classical palaeo-thermometer

The most conventional tool available to reconstruct past temperature changes is from ^{18}O/^{16}O of ice (δ^{18}O$_{ice}$) and ^{2}H/^{1}H (δD$_{ice}$) or more generally the isotopes of water, as highlighted in the previous section. The stable isotopic composition of the precipitation

has been a long standing parameter in reconstructing past local temperatures. It was first used in the 1960s by Dansgaard (1964) and Craig (1961). The Rayleigh Distillation is the process that actually governs the fractionation of isotopes from the evaporating ocean basins until the time of precipitation at the higher polar latitudes. The lighter water molecule (H_2O^{16}) evaporates much faster than H_2O^{18} but H_2O^{18} is preferentially removed during precipitation. The initial isotopic signature of the water vapour is determined by evaporation conditions (seawater isotopic composition, sea surface temperature, relative humidity of the air mass above and surface wind speed) but as the air mass moves towards the poles, it cools and loses water, becoming more depleted in heavy isotopes (i.e. moves to more –ve δ value).

Due to progressive air mass distillation, a linear relationship is observed between modern day precipitation isotopic composition and modern day surface temperature with a slope of 0.67‰ / ˚C for $\delta^{18}O_{ice}$ – T relationship and 6.04‰ / ℃ for δD_{ice} – T relationship (Masson-Delmotte *et al*., 2006).

1.3.1 Limitations of the water isotope palaeo-thermometer

Water isotopes in ice cores ($\delta^{18}O_{ice}$ or δD_{ice}) are useful temperature proxies because it was believed that changes in isotopic composition of precipitation in polar regions are mainly related to variations of temperatures at the site of precipitation. However the slope for water isotopes – T relationship, stated above, is also influenced by variations of the seasonal precipitation distribution, changes in evaporation conditions and atmospheric transport or circulation (Jouzel *et al*., 1997; Masson-Delmotte, *et al*., 2006). Therefore the present day slope should be used with caution to quantitatively interpret past climate shifts. More sophisticated methods resulting from combined measurements of δD and $\delta^{18}O$ of the same samples enable deuterium excess (d = δD - $8\delta^{18}O$) calculations. Jouzel *et al*. (2007b) gives an in-depth review of application and interpretation of deuterium excess in relation to palaeoclimate reconstruction in Antarctica and Greenland. The deuterium excess parameter is used to correct past temperature reconstructions for changes in source or evaporation conditions (Cuffey and Vimeux, 2001; Stenni *et al*., 2004, 2010).

Huber et al. (2006a) suggested that the relation between temperature and $\delta^{18}O_{ice}$ is not linear and should be revised. Their findings support a more complex relationship that is influenced by varying seasonal precipitation distribution and changes in the precipitation source region. During ice core drilling, a thermometer was lowered into the borehole to record temperatures, which can be inverted with heat diffusion model to reconstruct temperature changes (Salamatin et al., 1998).The inversion of the borehole temperature profile for Greenland shows that the glacial to Holocene isotope-temperature slope is 0.33 ‰ / °C, half that of the modern day spatial temperature slope of 0.67‰ / °C (Cuffey et al., 1992 & Dahl-Jensen et al., 1998). An estimate of 0.37 ‰ / °C was explained by a shift in the $\delta^{18}O$ – T relationship for the hydrological cycle linked to cooler tropical source temperatures (Boyle, 1997). Moreover, Salamatin et al. (1998) used borehole thermometry in Vostok ice core to show that the magnitude of temperature change during the last glacial – interglacial transition was underestimated by up to a factor of two. An alternative to borehole palaeo-thermometry in calibrating the water isotope – temperature sensitivity is using the General Circulation Model (GCM), which has been used mostly in Antarctic sites (Jouzel et al., 2003 and Jouzel et al., 2007). Jouzel et al. (2003) disputed the claims of Salamatin et al. (1998) and suggested that the present – day spatial slope can be used to reconstruct temperature changes from the past glacial – interglacial isotopic changes in Antarctica at sites like Vostok and EDC. The temperature changes for the glacial – interglacial transition obtained with isotopic model studies are within -10% to +30% of the corresponding temperature changes estimated from the water isotopes.

Clearly there are limitations for the application of the conventional method to infer temperature changes during the climatic events in the glacial period and for the glacial – interglacial transitions. This qualitative temperature proxy is uncertain because factors other than local mean annual temperature may affect this ratio, such as the seasonality of precipitation at the ice core site and the temperature and proximity of the water vapour source. These issues have raised questions whether the abrupt increases in $\delta^{18}O_{ice}$ in Greenland and Antarctica represent isotopic artefacts rather than local temperature changes as commonly inferred and have created uncertainty about the magnitude of temperature change. Also the validity of the present day water isotope – temperature relationship in the past especially during the glacial period has been questioned (Dahl-Jensen et al., 1998; Cuffey et al., 1992; Salamatin et al., 1998).

Recent research shows that the temperature reconstructions during the glacial times based on the present day isotope – temperature relationship are underestimated (Landais *et al*., 2006b; Huber *et al*., 2006a). Borehole thermometry showed that the general assumption of adapting a spatial relationship between $\delta^{18}O_{ice}$ and surface temperature is not appropriate to calibrate temperature changes of the past. On the basis of this, there is a need for methods to monitor temporal relationships between $\delta^{18}O_{ice}$ and surface temperatures. However borehole temperatures allow us to detect past temperature variations and could be used as a calibrating tool for $\delta^{18}O_{ice}$ and surface temperature relationship but the resolution decreases rapidly with age. Another drawback of the borehole palaeo-thermometry is that it does not allow direct calibration of the isotopic changes at rapid climatic reorganizations such as the Dansgaard Oesheger events and the Younger Dryas event. In addition to uncertainties pertaining to the slope of the glacial $\delta^{18}O_{ice}$ – temperature relationship, the temperature profile reconstructed from the water isotopes cannot be compared directly to greenhouse gas profiles such as CO_2 and CH_4 on the same time domain due to ice age – gas age offset, Δage (explained below).

Due to the associated problems and uncertainties in temperature reconstructions from the water isotopes, an independent palaeo-thermometer was needed to calibrate the slope of $\delta^{18}O_{ice}$ – temperature relationship during the glacial period. This was achieved by the most recent technique of palaeo-thermometry, which is based on the thermal fractionation of isotopes of gases in the firn layer, particularly the isotopic ratios of nitrogen ($\delta^{15}N$) and argon ($\delta^{40}Ar$) gas (Severinghaus *et al*., 1998). Since the temperature signal is in the gas phase and can be directly compared with other greenhouse gas profiles without the need for quantifying the Δage.

Moreover, the $\delta^{15}N$ palaeo-thermometry is affected only by the temperature and accumulation rates at the site and the interplay between these variables and the firn processes. The $\delta^{15}N$ technique is used for reconstructing the magnitude of palaeo-temperature changes for abrupt and rapid climate change events, therefore optimally complementing the borehole temperature technique in calibrating the slope of $\delta^{18}O_{ice}$ – temperature relationship during the glacial period. To understand the concept of $\delta^{15}N$ palaeo-thermometry, it is critical to understand the firn processes and its effect on the

fractionation of the isotopes. To reconstruct palaeo-temperatures, a firn densification model (Goujon *et al*., 2003, Schwander *et al*., 1997) is used to reconstruct past firn conditions to simulate the $\delta^{15}N$ signal. The following section gives an overview of the firn layer and typical isotopic fractionation of gases in the firn and then follows a comprehensive review of application of $\delta^{15}N$ palaeo-thermometry in the Antarctic and Greenland ice cores.

1.4 Firn

In order to extract palaeoclimatology information from isotopic composition of gases trapped in ice cores it is critical to understand the mechanism of bubble entrapment process. Prior to bubble enclosure and air bubbles being preserved in the ice, the air diffuses through the ***firn***, which is the unconsolidated snow that forms the upper first layer of the ice sheet. The firn-ice transition occurs at the bottom of the firn layer called the pore close off depth (COD) where the porosity practically falls to zero. Above the pore close off depth the air in the firn layer still interacts with the atmosphere through the open pores and therefore its composition is modified by variations in the atmosphere, diffusion, convection/advection, gravitation and thermal gradient in the firn layer.

1.4.1 Firn structure and processes

The firn layer is categorized into three layers (Sowers *et al*., 1992) and is primarily based on the porosity of the firn structure and the diffusion of gases. The three layers are the convective zone, diffusive zone and the non-diffusive zone (See Figure 1.4.1).

1.4.1.1 Convective zone

The convective zone is typically confined to the first few meters of the firn and is very porous and well mixed with the overlying atmosphere and thus has a similar composition. The two important processes controlling the movement of air in this zone are wind pumping and thermal convection (Kaspers, 2005).

Thermal convection is the movement of air in the snow or firn due to the temperature gradients. Convection due to temperature gradients is restricted to a few metres of the firn but is more prominent in highly porous layers with large temperature gradients.

Wind pumping causes the movement of air in the snow and firn due to movement of air at the surface (Colbeck, 1989). Wind pumping determines the thickness of the convective zone in response to atmospheric pressure variations. The effect of wind pumping on the thickness of the convective zone is influenced by wind speed, surface topography, porosity and grain size. Usually high wind speed would result in deeper convective zone but such turbulent airflow in the firn is dampened by layers of snow with low porosity and small grain size. Shallower convective zones are characteristic of a high density firn layer owing to its high tortuosity (Sowers *et al*., 1992). Kawamura *et al*. (2006) suggested that there might be a relationship between low accumulation rate and deep convection zones.

Usually the convective zone is restricted to a maximum of 12 m (Landais *et al*., 2006a) but Severinghaus *et al*. (2003) described a 20 m deep convective zone in the megadunes near Vostok with accumulation rate close to zero. Modern firn air isotope measurements from Dome C, Berkner Island and Northgrip suggest a very shallow convective zone less than 2.5 – 5 m deep (Landais *et al*., 2006a). The shallower convective zones at Dome C was surprising when compared to other sites with similar surface characteristics like Vostok and Dome F where convective zones of approximately 10m were observed (Bender *et al*., 1994a).

1.4.2.2 Diffusive zone

In this zone the porosity decreases and the transport of gases is unaffected by surface turbulence and pressure variations. The movement of air is primarily due to molecular diffusion and movement of gases due to gravity. The diffusive layer constitutes most of the firn layer (Schwander *et al*., 1989). The chemical and the isotopic composition deviate from the overlying atmosphere due to ***gravitational settling*** that causes heavier molecules and isotopes to be progressively enriched with depth (Craig *et al*., 1988; Sowers *et al*., 1989). The gravitational fractionation of N_2 isotopes was first

confirmed by Craig *et al.* (1988), who demonstrated that the gravitational separation of isotopes is according to the barometric equation:

$$P_z/P_o = \exp^{(mgz/RT)}$$…………………….(1)

Where P_z is the partial pressure of the gas at depth z, P_o is the partial pressure of the gas at the top of the diffusive air column; m is the mass of 1 mole of gas (kg/mol); g is the gravitational acceleration (9.81 ms^{-2}); R is the universal gas constant (8.314 $J\ mol^{-1}K^{-1}$); T is temperature (degrees Kelvin).

From equation (1) it can be surmised that the $^{15}N^{14}N/^{14}N_2$ ratio of N_2 increases with depth. The standard delta notation to record the $^{15}N^{14}N/^{14}N_2$ ratio of N_2 is:

$$\delta^{15}N = [(^{15}N^{14}N/^{14}N_2)_{sample} / (^{15}N^{14}N/^{14}N_2)_{standard} -1] \times 10^3$$…………………(2)

Combining equations (1) and (2) results in the following equation relating the $\delta^{15}N$ of N_2 in the firn to the depth below the surface of the diffusive air column and the ambient temperature:

$$\delta^{15}N = [\exp^{(0.001gz/RT)} – 1] \times 10^3$$……………………..(3)

The z parameter in equation (3) can be used to reconstruct past diffusive column height (DCH), which could assist in constraining some climate variables such as the accumulation rate. The diffusive column height ranges from 40 m to 100 m in height. The $\delta^{15}N$ of the ice core increases with an increase in the height of the diffusive air column and decreases in proportion to the thickness of the convective zone (Sowers *et al.*, 1992). The $\delta^{15}N$, $\delta^{40}Ar$ and $\delta Kr/Ar$ were measured in Siple Dome ice core to reconstruct the DCH. A 18 m reduction in DCH was revealed during the 18 and 22 kyr climatic event suggesting about 20 – 50 % decrease in accumulation rate according to Herron and Langway (1980) firn densification model (Severinghaus *et al.*, 2003). Another classical example of the application of DCH to understand past climate change was a net ablation event at 15.3 kyr BP in Siple Dome ice core. During this time all of the firn was removed through an interval of sustained net ablation and resulting in the unique result of $\delta^{40}Ar$ being zero. However reconstructing past DCH in both climatic

events illustrates the possibility that the ice record from Siple Dome has a short hiatus in deposition during those time intervals.

Thermal diffusion is another process that may fractionate isotopes or gases in the diffusive layer. **_Thermal fractionation_** results from the existence of a temperature gradient in the firn due to atmospheric seasonal temperature variations or abrupt rapid warming in climates. The atmospheric temperature variations only penetrate down to about 5 – 10 m depth and the thermal diffusion is of significance only to a depth of 20 - 30 m (Landais *et al*., 2006a; Huber *et al*., 2006b). The thermal fractionation effect was predicted with the solution of the Boltzmann equation and the development of the kinetic theory of gases which postulate that:

$$\delta = [R/R_o - 1]10^3 = ([T_o/T]^\beta - 1)10^3 \ldots\ldots\ldots\ldots\ldots\ldots..(4)$$

Where δ is the fractional deviation of the isotope ratio R from the ratio R_o, T and T_o are temperature in K, β is the thermal diffusion factor. According to equation (4) the heavier gases become enriched in colder regions.
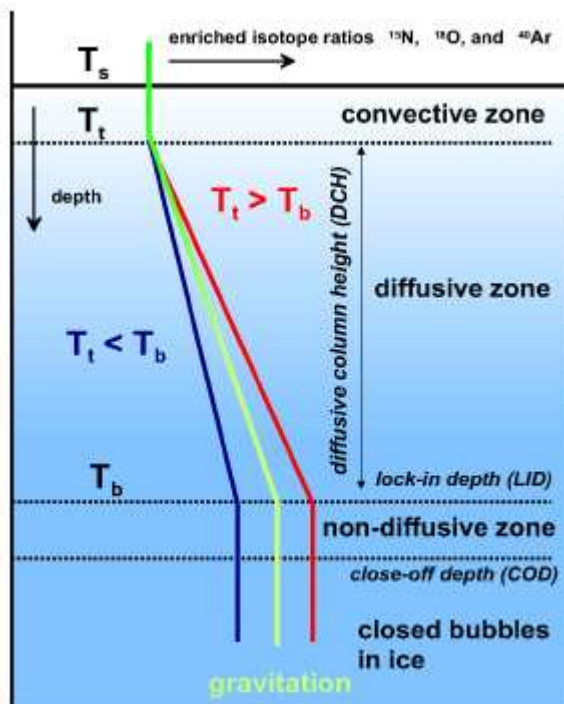
Figure 1.4.1: An illustration of three zones of the firn layer showing the effect of gravitational and thermal fractionations on isotopic composition.

18

1.4.2.3 Non diffusive zone

This lies between the bottom of the diffusive air column and the bubble close off region or the firn-ice transition zone. Many firn studies have shown that this zone is generally less than 10 m at most sites (Schwander *et al*., 1997, Landais *et al*., 2006a). However the depth of this zone varies from site to site depending on the site temperature and accumulation rates. Larger non-diffusive columns are typical of high accumulation sites. The diffusivity in this zone is so low that the gas transport ceases and the trapped gas and isotopic composition are said to be below the "Locked In Depth" (LID), which is few meters above the bubble Close Off Depth (COD) (see Figure 1.4.1). LID has open porosity and firn air could still be pumped and collected but at the close-off depth the open porosity is zero and firn air cannot be sampled or pumped any longer. Since the air in the non diffusive zone cannot equilibrate with the overlying diffusive column the isotopic composition or the mixing ratio of a gas reaches a constant value and remains unchanged throughout this zone. The constant $\delta^{15}N$ values observed in the firn air acts as a stratigraphic marker for this zone.

COD is at the bottom of the non diffusive zone where complete pore close off occurs isolating the air from the overlying atmosphere. The air parcel in the non diffusive column is being occluded into bubbles during the firn - ice transition and is then preserved for thousands of years in the ice. The COD is characterised by the critical density interval between 0.800g cm^{-3} and 0.830g cm^{-3} (Schwander *et al*., 1997). Usually sites with higher accumulation rate and colder temperature will have deeper CODs whereas shallower CODs are attributed to sites with higher temperatures and lower accumulation rates (Sowers *et al*., 1992). However during the last glacial maximum the accumulation rates and temperatures were lower and the COD was 15-30 m deeper than the interglacial period (Sowers *et al*., 1992). This is explained in terms of predominant role of temperature effect on snow grain size, increasing the porosity of the firn that leads to deeper COD during the glacial periods (Sowers *et al*., 1992).

It is now apparent that prior to bubble enclosure in ice, the air isotopic composition is altered due to two prominent processes that are gravitational and thermal fractionation in the diffusive column. The movement of gases in the diffusive zone could also be driven by the presence of concentration gradients in the firn. The concentration gradient

effect is not relevant in interpreting the isotopic data, such as $\delta^{15}N$, but is of great significance in reconstructing the trace gas history and is parameterised in the firn diffusion model (Rommelaere *et al*., 1997) used in the interpretation of trace gas mixing ratios from firn air measurements.

It was believed that in the non diffusive column the movement of the gases cease, hence the air composition is no longer modified past the LID zone and reaches the COD where it is occluded into air bubbles. However recent research has highlighted another fractionation process occurring in the non diffusive zone that could alter the firn and bubble air composition. It is called ***bubble close off fractionation***.

Gases in bubbles become fractionated during the bubble close-off process. Severinghaus and Battle (2006) measured noble gas ratios, O_2 and isotopes of N_2 in firn air from Siple Dome and South Pole and observed large enrichments in O_2/N_2, Ne/N_2 and Ar/N_2 ratios up to 10 ‰, 90 ‰ and 3 ‰ respectively in the COD. This indicates that Ne, O_2 and Ar are preferentially excluded when the bubbles are closing. The bubble close off fractionation results from the existence of pressure gradient between the newly formed ice bubble and the open pore air, which causes the diffusion of gases with smaller molecular diameters into the open pores. The larger atoms like Kr and Xe do not show bubble close off fractionation. The finding reveals a threshold atomic diameter of 3.6 Å above which the chance of gas escape from the bubble is negligible.

Similar studies were carried out on Devon Island and NGRIP firn air by Huber *et al*. (2006b), who also suggested a molecular size dependent gas fractionation near the COD. A critical threshold diameter of 3.6 Å was also cited but offers a different explanation to that of Severinghaus and Battle (2006). Huber *et al*. (2006b) believe that the plausible mechanism for such size dependent fractionation during bubble close-off is the diffusion of molecules through the channels in the ice lattice. The ice crystal has a hexagonal passage formed by six H_2O molecules the dimension of which is similar to critical size of 3.6 Å (Huber *et al*., 2006b).

 Despite different approaches being used in the explanations, both studies (Severinghaus and Battle (2006) and Huber *et al*. (2006b) highlighted selective gas permeation across the very thin ice film and the effect is size dependent. Fortunately such fractionation

does not affect the reconstructed profiles for larger molecules like Xe, Kr, N_2, CO_2, CH_4 and N_2O, hence the integrity of polar ice cores as an archive of the ancient atmospheric composition of these gases is still maintained. However it does affect elemental ratios such as O_2/N_2 and Ar/N_2 profiles from the ice cores. It is still questionable how to apply correction for such effects and whether such process is related to site specific parameters because Devon Island showed 4 times more enrichment at the bottom of the firn, which might probably be due to the presence of melt layers (Huber *et al*., 2006b).

1.5 Analysis of trace gases in firn air

Firn air provides an archive of older air which is ideal for reconstructing atmospheric composition over the past century. Because of the porous structure of the firn, large volumes of air can be sampled for a wide range of trace gas analyses. Firn air analysis has increased the scientific knowledge of these trace gases by providing longer term trends of many important trace gases in the atmosphere.

The key aspect of reconstructing the longest atmospheric record is to sample the oldest firn air and Kaspers *et al*. (2004) demonstrated model calculations that can be used to find a site in Antarctica for the oldest air. Currently the longest 80 year record is derived from the South Pole firn air (Kaspers *et al*., 2004) and could be paralleled by the EDML firn air record obtained in this study (Chapter 5). There are several studies documenting atmospheric records of trace gases from firn air. Butler *et al*. (1999) obtained records for CFCs and chlorocarbons at the South Pole (Antarctica), Siple Dome and Tunu (Greenland). Sturges *et al*. (2001) presented reconstructed atmospheric trends for several organobromine gases ($CHBr_3$, CH_2Br_2, $CHBrCl_2$, $CHBrCl$ and CH_2BrCl) in firn air sampled at Dronning Maud Land (DML), and Dome C. Kaspers *et al*. (2004) obtained non-methane hydrocarbons and methyl chloride records for DML site. Concentrations of CO_2, CFCs and chloroform have been reported by Trudinger *et al*. (1997, 2002 & 2004). Sturges *et al*. (2000) presented atmospheric record of SF_6 and SF_5CF_3 from Dome C firn air. Worton *et al*. (2007) presented the long term trends of CF_4 and C_2F_6 in Berkner Island and NGRIP firn air. In this study the longest

reconstructed atmospheric trends of PFCs (CF_4, C_2F_6, C_3F_8, $c-C_4F_8$), HFC-23, SF_6 and SF_5CF_3 from the EDML firn air are discussed in Chapter 5. A comprehensive literature review of the individual species is also presented in Chapter 5.

1.6 Ice age - gas age problem

The permeability and diffusivity of the firn layer not only play the critical role of altering the isotopic composition of the gas as compared to the overlying atmosphere but also affect the ice age-gas age difference (Δage). The bubbles of air are isolated from the atmosphere at some depth below the surface and are therefore younger than the surrounding ice hence resulting in Δage. A firm understanding of Δage is a necessity in order to compare the trapped trace gas composition and isotopic gas composition profiles with profiles from ice such as $\delta^{18}O$ and δD (markers for past temperatures) in similar time domains. An accurate determination of Δage is critical in determining the ice chronology and in studying the north – south teleconnections (Blunier *et al*., 1998).

The diffusive and the convective mixing of air in the firn layer tend to smooth the atmospheric record stored in the firn. Hence, at a certain depth in the firn layer the age of air is not expressed as a single number, but contains a distribution of ages. Schwander (1993) show calculated age distributions for CO_2 at different depths and to obtain the corresponding age distribution for other gases, simply divide the age scale by the diffusion coefficients of the particular trace gas. The age difference between a trapped bubble and the surrounding ice is equal to the age of the firn air and ice at the bottom of the diffusive layer (Sowers *et al*., 1992). It is clear that the depth and the extent of the bubble close-off region and the mixing of the air in the firn system influence the age difference and distribution (Schwander *et al*., 1988, Schwander, 1993).

In palaeoclimate reconstructions the Δ_{age} is calculated by the diffusion model (Schwander, 1993). However the model does not take into account additional mixing due to convection or ventilation by turbulent wind or pressure variations. It also assumes that the firn is horizontally homogeneous and has no melt layers and that

diffusivity decreases monotonically with depth (Schwander *et al.*, 1989; Schwander, 1993).

An independent check on the model Δ_{age} calculation is derived from DCH reconstructed from the nitrogen and argon isotopic measurements (Brook *et al.*, 2005). To calculate Δ_{age} from DCH, it was assumed that convection is negligible so that gravitational fractionation is expressed throughout the firn column. Also some assumptions were incorporated into the Herron and Langway (1980) model. The calculation uses the DCH to find the accumulation rate consistent with the specified firn thickness (DCH), close off density and temperature. Δ_{age} is then determined from these parameters. The Δ_{age} calculated from the DCH data from Siple Dome (Severinghaus *et al.*, 2003) agrees reasonably well with the Herron and Langway (1980) calculation (Brook *et al.*, 2005).

1.7 $\delta^{15}N$ as a Palaeothermometer

Measurements of isotopic composition of nitrogen in firn air and ice cores came into existence approximately two decades ago. It was primarily used to demonstrate the gravitational enrichment component in ice cores (Craig *et al.*, 1988), which was later adopted as an important component in the determination of Δage (Schwander *et al.* 1993; Sowers *et al.*, 1992). The $\delta^{15}N$ in the firn at Vostok Station was also used in the $\delta O_2/N_2$ measurements, which was used to constrain the recent rate of the atmospheric oxygen decrease (Bender *et al.*, 1994a). More recently it was highlighted that thermal signals can be extracted from $\delta^{15}N$ of nitrogen gas in ice cores making it a palaeo-thermometer, an alternative to the classical method of temperature change estimation based on $\delta^{18}O$ of ice (Severinghaus *et al.*, 1998).

Initially, Severinghaus *et al.* (1998) highlighted the validity of $\delta^{15}N$ as a paleothermometer, deriving the protocol from his earlier studies on thermal diffusion of gases in sand dunes (Severinghaus *et al.*, 1996). During an abrupt climate warming there is a temperature gradient in the firn layer causing the heavier species such as $^{15}N^{14}N$ and ^{40}Ar to be preferentially driven downwards towards the colder regions of the firn. Since gases diffuse 10 times faster than heat the thermally fractionated gas will

penetrate to the close off depth (COD) and become locked in depth long before the temperature of the firn column equilibrates. The temperature change during past abrupt climate change is approximated from a term called $\delta^{15}N_{excess}$, which is defined as follows:

$$\delta^{15}N_{excess} = \delta^{15}N - \delta^{40}Ar/4$$

As discussed above gravitational and thermal fractionation are the main processes that fractionate gases in the firn layer. The $\delta^{40}Ar/4$ is the gravitational component in the above term. The gravitational fractionation is dependent on mass difference between the gas pairs. The unit mass difference between ^{36}Ar and ^{40}Ar is 4 and therefore the gravitational fractionation for argon is four times more than $^{15}N^{14}N$, which has the mass difference of 1. Unequivocally the gravitational fractionation component for nitrogen is one quarter of $\delta^{40}Ar$. Hence $\delta^{15}N_{excess}$ is a gravitational corrected term and only contains the thermal fractionation signal. The above equation can be written as follows:

$$\delta^{15}N_{excess} = \Delta T(\Omega^{15} - \Omega^{40}/4)$$

where Ω is thermal diffusion sensitivity which has been determined in the laboratory (Grachev and Severinghaus, 2003a,b). The $\delta^{40}Ar$ is less sensitive to thermal fractionation, in fact it is four times less than $\delta^{15}N$, due to lower thermal diffusivity (Dreyfus, 2010). The $\delta^{15}N_{excess}$ quantity can be used directly to estimate temperature changes during abrupt climate events by using appropriate thermal diffusion sensitivity and taking into account the correction for heat transfer in the firn (Grachev and Severinghaus, 2005). This approach is the least complex as it does not involve a model, which is uncertain to some extent and uses assumptions to estimate changes due to gravitational settling in response to firn thickness or convective zone changes.

There are numerous studies that employed $\delta^{15}N$ and $\delta^{15}N_{excess}$ quantity to estimate temperature changes for the climatic events in Greenland and Antarctic events (See Table 1.1)

Table 1.1: Review of studies utilizing δ^{15}N in characterising abrupt climate changes in Greenland and Antarctic ice cores.

Location	Climate Event	Reference
Greenland Ice Cores		
GISP2[a]	Termination of the Younger Dryas	Severinghaus *et al*., 1998 Kobashi *et al*., 2008a
	Termination of the Pre-boreal Oscillation	Kobashi *et al*., 2008b
	8.2 Kyr event	Kobashi *et al*., 2007
GRIP[b]	The Bølling transition	Severinghaus & Brook, 1999
	8.2 Kyr event DO[c] 19 DO 12	Leuenberger *et al*., 1999 Lang *et al*., 1999 Landais *et al*., 2004a
NorthGRIP	DO 19 DO 18, 19, 20 DO 23 & 24 DO 9 – 17	Landais *et al*., 2004b Landais *et al*., 2004c, 2005 Landais *et al*., 2006b Huber *et al*., 2006a
West Greenland Ice margin	The last glacial termination from a horizontal ice core	Petrenko *et al*., 2006
Antarctic Ice cores		
DSS[d] **EDML**[e]	LGM[f] transition	Landais *et al*., 2006b
Vostok	The MIS[g] 5d/5c transition	Caillon *et al*., 2001
Siple Dome	2 rapid climatic events during the termination of the LGM	Severinghaus *et al*., 2003
	Abrupt climate change around 22,000	Taylor *et al*., 2004

[a] Greenland Ice Sheet Project 2
[b] Greenland Ice Core Project
[c] Dansgaard Oescheger event
[d] Dome South Summit ice core from Law Dome
[e] EPICA Dronning Maud Land
[f] Last Glacial Maximum
[g] Marine Isotopic Stage

1.7.1 δ^{15}N measurements in Greenland ice cores

The first study of extracting thermal signals from fractionation of nitrogen and argon was carried out in Greenland ice cores, GISP2 (Severinghaus *et al*., 1998). The results suggested a step-like temperature change of +5 - +10 °C in less than a decade at the end of the Younger Dryas interval approximately 11.6 kyr BP. The δ^{15}N rose from +0.4‰ during a cold stable climate to +0.56‰. These measurements had an analytical precision, determined from replicate ice cut from the same depth, of ±0.02‰ for δ^{15}N and ±0.03‰ for δ^{40}Ar. Also in this study Δ_{age} was accurately determined by counting the annual layers between the gas isotopic anomaly that marks the end of the Younger Dryas and the corresponding isotopic changes recorded in the ice. This Δ_{age} was related to absolute temperature by using the empirical densification model, suggesting that the temperature at the termination of the Younger Dryas event in Greenland was 15 ± 3 °C colder than present. However this temperature estimate is limited by large analytical uncertainties and the actual thermal diffusion factors for N_2 and Ar at -40°C were not known.

Severinghaus and Brook (1999) performed a similar study for the Bølling Transition at ~14.6 Kyr in GISP2 ice cores. The δ^{15}N values rose across the transition from baseline glacial values of +0.48‰ to peak values of +0.63‰ corresponding to an estimate of 9 ± 3°C for the magnitude of the abrupt warming. However, in this study the thermal diffusion sensitivity (Ω) of pure gases was experimentally determined in a known temperature gradient and was proposed that they be utilized in direct estimation of temperature change from the strength of the isotopic anomaly. The preliminary values of Ω used in this study are +0.0145 ‰K^{-1} for δ^{15}N and +0.036 ‰K^{-1} for δ^{40}Ar at a mean temperature of -43°C. The δ^{18}O$_{ice}$ increased by 3.4‰ across the transition and with a temperature change of 9 ± 3°C (from δ^{15}N and δ^{40}Ar signal), implies oxygen isotope temperature sensitivity (α) of 0.38‰, which is very close to the borehole temperature calibrated value of 0.33‰. Hence δ^{15}N in this study provided an independent verification of the borehole calibration.

Much of the earlier work of Severinghaus was reported using the thermal diffusion constants based on pure gases rather than air mixture and had very poor precision. However Grachev and Severinghaus (2003 a, b) measured the thermal diffusion of

$^{29}N_2/^{28}N_2$ and $^{40}Ar/^{36}Ar$ in air and in the temperature range (-60 to -10°C) relevant to reconstruction of palaeo-temperatures. The precision of the thermal diffusion measurement was improved five to ten fold, compared with early pure gas studies. Using the newly acquired laboratory determinations of thermal diffusion sensitivity (Ω), the data for the Younger Dryas/Pre-Boreal (YD/PB) transition in the pioneering work (Severinghaus *et al*., 1998) was revisited and the original estimate of 15 ± 3°C warming was revised to 10 ± 4°C (Grachev & Severinghaus, 2005). The magnitude of 9 ± 3°C during the Bølling transition (Severinghaus & Brook, 1999) was revised to 11 ± 3°C (Severinghaus *et al*., 2003).

Leuenberger *et al*. (1999) obtained a temperature of – 7.4 K for the 8.2 kyr BP event and Lang *et al*. (1999) obtained a warming of 16 K for the Dansgaard Oescheger (DO) event 19(~80 kyr BP) in GRIP ice cores. The results in these studies were limited to only nitrogen isotope measurements or the temperature change estimates for these two events were derived without argon isotope data needed for gravitational correction. The data were corrected for gravitational fractionation by the firn densification model with incorporated heat transfer and molecular diffusion (Schwander *et al*., 1997). The modelled $\delta^{15}N$ obtained for different temperature scenarios were compared to measured $\delta^{15}N$ and the measured values were slightly lower than the modelled values using the 0.33 ‰/K T-$\delta^{18}O_{ice}$ dependence. After regression analysis the α value of 0.30 ‰/K was obtained with the best estimate of temperature change of 7.4 K for a $\Delta\delta^{18}O_{ice}$ drop of 2.23‰ during the 8.2 kyr event (Leuenberger *et al*., 1999). Lang *et al*. (1999) used high resolution measurements of nitrogen isotopes on the GRIP ice core to show an increase in $\delta^{15}N$ by 0.17 ± 0.02‰ in 160 years. This signal in $\delta^{15}N$ equates to a temperature change of 10.4 ± 1.6 K, assuming no change in the diffusive column height but was corrected for modelled gravitational fractionation. The value of α obtained by Lang *et al*. (1999) was 0.42 ‰/K, providing further evidence of the invalidity of the modern $\delta^{18}O_{ice}$- surface temperature correlation during the glacial period.

The uncertainties in the studies by Leuenberger *et al*. (1999) and Lang *et al*. (1999) were high due to limited resolution of the data, noise in the $\delta^{18}O_{ice}$ record, and variations in α value. The major drawback of the model results could be due to the assumptions such as the convective zone remaining constant and the uncertainties associated with the approximation of accumulation rate. Hence this approach may not be the ideal way to

assess palaeo-temperature and isotopes of noble gases like Ar are needed especially for periods of strong changes in accumulation rate, temperature and where significant variations in close-off depth are expected. Also in these studies a thermal diffusion factor of 0.00347 ± 0.00003 for nitrogen was calculated, which was significantly lower than the value adopted in the work of the Severinghaus *et al.* (1996, 1998).

In order to overcome the assumption of constant gravitational corrections it is vital to measure $\delta^{40}Ar$ and estimate the thermally fractionated $\delta^{15}N$ or $\delta^{15}N_{excess}$. Landais *et al.* (2006b) performed 130 duplicate measurements of $\delta^{15}N$ ($\pm0.006‰$) and 47 measurements of $\delta^{40}Ar$ ($\pm0.025‰$) between 2,870 and 3,085m depth in the NGRIP ice core. The $\delta^{15}N$ profile depicts rapid variations over Dansgaard Oescheger (DO) event 23 and 24 and the corresponding signal is recorded 7 - 8m shallower in $\delta^{18}O_{ice}$. The $\delta^{15}N_{excess}$ was calculated to be 0.06‰ and 0.04‰ for the DO 24 and DO 23 respectively. The $\delta^{15}N_{excess}$ profile was fitted with a modelled $\delta^{15}N_{excess}$ obtained as output of the firnification and heat diffusion model by Goujon *et al.* (2003). The best fit was obtained with temperature increases of 10 ± 2.5 °C and 16 ± 2.5 °C, for DO 23 and DO 24 respectively (Landais *et al.*, 2006b).

Landais *et al.* (2004a) investigated the profile for $\delta^{15}N$, $\delta^{40}Ar$ and methane over the depth range from 2270 to 2370 m in the GRIP ice core encompassing the DO 12 event. The $\delta^{15}N_{excess}$ profile obtained was used to quantify past surface temperature variation through the firn densification model developed by Goujon *et al.* (2003). The temperature change across the DO event 12 was estimated to be 12 ± 2.5 ºC as compared to 6.8 ºC changes deduced from the water isotopes (Landais *et al.*, 2004a). It was proven again that the conventional use of water isotopes in ice cores largely underestimates the actual amplitude of rapid temperature change in Central Greenland. Landais *et al.* (2004a) also concluded that the temperature rise was synchronous with an increase in CH_4 at Greenland. Landais *et al.* (2004b, 2005) also used $\delta^{15}N_{excess}$ to reconstruct temperature changes of 11 ºC for DO 18 and 20, and 16 ºC for DO 19 in the NorthGRIP ice core. The corresponding value of α were 0.3, 0.4 and 0.5 ‰/K for DO 18, DO 19 and DO 20 respectively, which were significantly lower than the present day value of 0.67 ‰/K. Kobashi *et al.* (2008a) reconstructed a temperature change of 4.0 ± 1.5 ºC at 11.27 Kyr BP in the GISP2 ice core from the simultaneous measurements of

δ^{15}N and δ^{40}Ar in the same sample. The temperature change was reconstructed with the firn temperature gradient obtained with the firn densification model.

More recently, Huber *et al*. (2006a) and Kobashi *et al*. (2007) utilized only the δ^{15}N data to reconstruct the temperature changes for the abrupt climate events. Kobashi *et al*. (2007) did measure δ^{40}Ar but the data were too noisy and as a result the observed δ^{15}N data were corrected for gravitational fractionation using the model. Kobashi *et al*. (2007) used high resolution and high precision δ^{15}N measurements (precision = 0.004 ‰) to conclude a cooling of 3.3 ± 1.1 ℃ for the 8.2 kyr event, which occurred in less than 20 years in GISP ice core. The temperature change observed for 8.2 kyr event by Kobashi *et al*. (2007) is much lower than the previous estimate of cooling of 7.4 ℃ by Leuenberger *et al*. (1999) at the GRIP site. It was suggested that the precision of 0.03 ‰ in Leuenberger *et al*. (1999) would certainly make the identification of the 8.2 Kyr event difficult, as the δ^{15}N signal for this particular event was ~ 0.035‰ (Kobashi *et al*., 2007). The oxygen isotope temperature sensitivity α = 0.55 ± 0.05 ‰/K was obtained for an average cooling of 3.3 ± 0.5 ℃.

The high resolution δ^{15}N measurements were carried out across the DO 9 – 17 in the NorthGrip ice core during the MIS 3 period for which temperature changes of 8 to 15 ℃ were estimated (Huber *et al*., 2006). In this study, a combined firn densification/temperature/gas diffusion model (Goujon *et al*., 2003; Schwander *et al*., 1997) was used to simulate the evolution of δ^{15}N using an assumed temperature and accumulation rate history both derived from the δ^{18}O$_{ice}$ empirical relationship. The temperature history and accumulation history were tuned in order to minimize the differences between the model and the measured δ^{15}N. Several model simulations were conducted. In the first approach the convective zone was assumed to be non–existent, the accumulation rate history used in the NorthGrip age scales ss09sea was used and the α values were varied. This basic approach matched the timing and the amplitudes of the abrupt changes (see Figure 1.7.1). To reconcile the vertical offset between the modelled and the measured δ^{15}N, convective zones were assumed, larger shifts in the absolute temperature (approach 2) and decreasing the accumulation rate (approach 3) were considered. The best fit was obtained when the accumulation rate was decreased by 20% compared to the assumptions made in the ice flow dating model for the NorthGrip

ss09 sea age scale. In order to maintain the chronology of the ice core, the ice thinning function had to be changed accordingly.
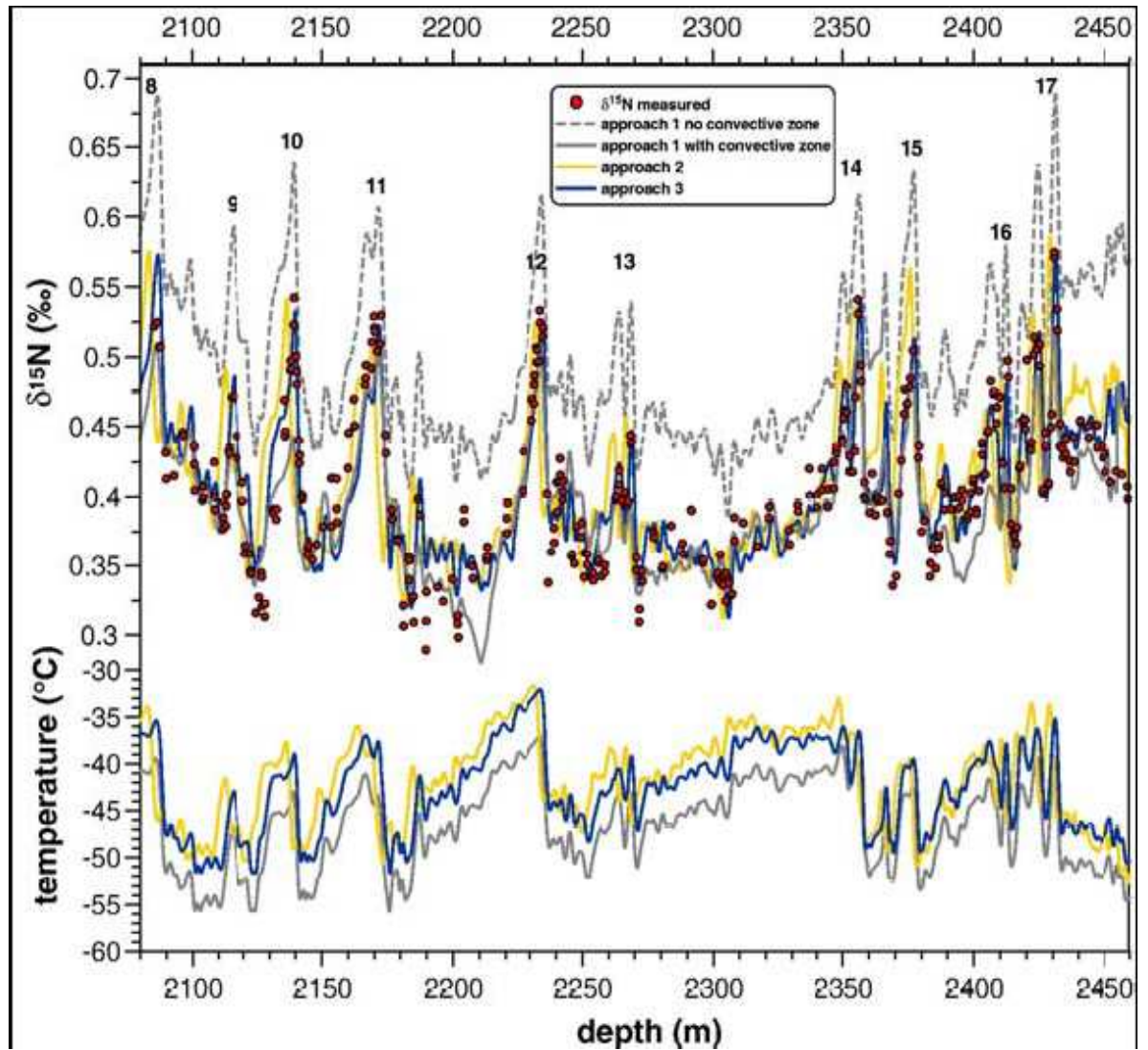
Figure 1.7.1: Top panel shows $\delta^{15}N$ measurements (red dots) in NorthGrip ice core from DO 9 – 17 events and firn model calculations versus ice depth. Bottom panel shows the surface temperature evolution used as model input. The different approaches are described in the text. (Adapted from Huber *et al.*, 2006a)

Huber *et al.* (2006a) also highlighted some other interesting facts regarding the temperature and CH_4 relationship. A detailed comparison of temperature reconstructions from $\delta^{15}N$ and CH_4 concentrations suggested that the start of CH_4 rise lags temperature rise at the onset of the DO events by 25 – 75 yrs. This study also concluded that the

modern day $\delta^{18}O_{ice}$ - T relationship (α) was not valid during the glacial period, the data suggest a slope of 0.41 ± 0.05 ‰/K during the stadial – interstadial transitions.

1.7.2 $\delta^{15}N$ measurements in Antarctic Ice cores

This new method of $\delta^{15}N$ as a palaeo-thermometer had been extensively applied to Greenland ice cores initially because the gas isotopic anomaly records abrupt climate changes only. In Antarctica the magnitude of such abrupt climate changes is muted and not as rapid as those observed in Greenland. However Caillon *et al*. (2001) were the first to suggest that this technique can be applied to Antarctic sites although the isotopic signals would be small. A theoretical estimation of $\delta^{15}N$ signal of 0.02‰ was calculated for the period between 110 and 104 kyr BP using thermal diffusion model. The $\delta^{15}N$ and $\delta^{40}Ar$ measurements were performed in the depth range from 1546 – 1587 m in the Vostok Ice core encompassing the marine isotope stage (MIS) 5d/5c transition (ca 108 kyr B.P.). In this study CODs were estimated from the combined $\delta^{15}N$ and $\delta^{40}Ar$ data to be between 64m and 70m. The temperature at the surface is the main driving factor for varying CODs if the accumulation was constant. The CODs were calculated using the firn densification model (Barnola *et al*., 1991; Arnaud *et al*., 2000) for different values of temperature change by varying the deuterium/temperature coefficient used to infer the Vostok temperature change and keeping the accumulation unchanged around the 5d/5c transition. For the CODs to equal to 64 and 70m temperature difference in the range -6.6 to -8.6 ºC was estimated with respect to the present day temperature at Vostok. This was slightly lower than the estimate of -6.5°C reported by Petit *et al*. (1999). This result suggest that the use of present day spatial slope to interpret the Vostok Deuterium data underestimates $\Delta T_{5d/modern}$ by 20% ± 15%, which contrast the findings of the borehole calibration that suggest that temperature changes based on spatial changes are underestimated by up to 50% (Salamatin *et al*., 1998). However, the major drawbacks of this study were that the precision of the measurements was on the similar order of the $\delta^{15}N$ signal obtained and the accumulation rate was assumed to be constant in the model.

Recently, the precision of $\delta^{15}N$ measurements has improved to 0.003 - 0.006‰ (Severinghaus *et al*., 2001; Landais *et al*., 2006b), which is an order of magnitude lower than the signals in the Antarctic ice cores. This improved precision benefits from the

standard corrections to take into account the formation of CO^+ (mass 28) from CO_2 and the sensitivity of $\delta^{15}N$ measurements to the varying ratios of O_2/N_2. Taking advantage of such precision more studies were carried in the Antarctic sites such as DSS and EDML (Landais et al., 2006a), Dome C (Dreyfus, 2010), Siple Dome (Taylor et al., 2004, Brook et al., 2005).

The $\delta^{15}N$ profile from the DSS ice core shows an increase from 0.19 ‰ during the Last Glacial Maximum (LGM) to 0.27‰ during the Early Holocene (EH) (Landais et al., 2006a). However the validity of these results was initially questioned due to larger analytical uncertainty. With the improved high precision method, the $\delta^{15}N_{excess}$ profile during the last deglaciation was reconstructed from the EDML ice core. Like the DSS, the $\delta^{15}N$ profile illustrated similar magnitude of isotopic signal, $\delta^{15}N$ increased from 0.41‰ during the LGM to 0.46‰ during the EH (Landais et al., 2006a). The measured $\delta^{15}N$ was compared to modelled $\delta^{15}N$ profile from the steady state firnification model by Arnaud et al. (2000) and for both sites, the simulations show opposite LGM to EH trends to the measured $\delta^{15}N$ increases. The same firnification model was used for the existing deglaciation $\delta^{15}N$ profiles from Vostok (Sowers et al., 1992), Dome F, Dome C and the results share the same pattern of model-data mismatch (Landais et al., 2006a).

The model-data mismatch could be due to a number of reasons such as the thickness of the convective and the non-diffusive zones, which were assumed to be constant but may actually vary with time. Certainly it shows that the parameterisations in the firn model are not accurate. Such disagreement is not only invoked by invalid temperature input but also by highly uncertain past accumulation rates. The past accumulation rates are inferred from water isotopes which tend to underestimate the accumulation rate by as much as 30% in NGRIP (Landais et al., 2006b). It seems that estimating past accumulation rates is really challenging and would be the most likely reason for model-data mismatch especially for the East Antarctic sites. To overcome this problem of estimating highly uncertain accumulation rates from water isotopes, an alternative method of assessing accumulation rates needs to be explored or the model should be modified so that they become less dependent on the uncertain accumulation rates.

Taylor et al. (2004) reported a temperature change of ~6 °C from the $\delta^{15}N_{excess}$ in less than 50 years at Siple Dome around 22 ka BP. However, such abrupt climate change did

not occur at 500 km away in the Byrd ice core, demonstrating significant spatial heterogeneity in the Antarctic climate, or perhaps that the isotopic data was biased due to stratigraphy distortions or a hiatus in accumulation. Another possibility for such observation could be due to changes in the altitude-induced lapse-rate related change in surface temperature. A 6 °C change in temperature in several decades would imply ~600 m decrease in surface elevation. Such a decrease in altitude in several decades would require an extensive decrease in snowfall or perhaps due to glaciological drawdown of the ice in response to increased drainage from sudden onset of ice stream. However it is unlikely that a decrease in snowfall alone can account for 600 m decrease in several decades. The model predicted from the calculated DCH that the accumulation rate did not decrease around the time in question. The chemistry of the ice cores (Na^+ and Ca^{2+}) rules out the possibility of any large-scale atmospheric circulation patterns and sea ice extent changes or absence of winter snow, which could cause a step increase in δD_{ice}. Hence, in the absence of any evidence of stratigraphic disturbances, the isotopic anomaly was interpreted as a local warming of about 4 – 6 °C in less than 50 years. This local warming at Siple Dome suggested that occurrence of abrupt climate change events may not be consistent in Antarctica and perhaps the coastal sites experience different climate regime than the more continental sites in Antarctica. Is the warming more significant at the coastal sites? This needs to be confirmed with more climatic records from coastal sites.

To summarise the above studies, the principal issues relevant to the study conducted here are:

- The $\delta^{15}N$ palaeo-thermometry has been used to characterise the DO events (DO 9 – 24) in Greenland ice cores. The temperature reconstruction from $\delta^{15}N$ serves as a tool for calibrating the $\delta^{18}O$ – T coefficient. Studies carried out in Greenland suggest that the temperature reconstructions based on modern day $\delta^{18}O$ – T coefficient were underestimated. The methane record from NorthGrip ice core is almost synchronous with temperature changes reconstructed from $\delta^{15}N$.

- In Antarctica, the use of $\delta^{15}N$ technique is very scarce because the thermal anomaly is very small and high precision measurement is required to detect such anomalies.

- The $\delta^{15}N$ data is combined with $\delta^{40}Ar$ to calculate $\delta^{15}N_{excess}$, which is then modelled with firn densification model with different temperature scenarios. However, there are some studies where $\delta^{40}Ar$ measurements were not carried out and the firn densification model was used to separate the thermal and gravitational signal from the total $\delta^{15}N$ measured.

- The major drawbacks of the application of the $\delta^{15}N$ technique in some studies were low data resolution, precision of the measurements, and the assumptions used in the model like the convective zone remaining constant. If the convective zones were greater than the assumed depth then the temperature reconstructions from $\delta^{15}N$ would be underestimated.

- The firn densification model does not work for the east Antarctic sites and it was suggested that the past accumulation rates derived from the water isotopes were underestimated.

- The $\delta^{15}N$ palaeo-thermometry suggested a local warming at Siple Dome, a coastal site in west Antarctic. This finding suggests that the climate regime at the coastal site is different as compared to more continental site. However, this finding needs to be replicated with other ice core records from coastal sites.

1.8 Scientific rationale and objectives of the study

1.8.1 Scientific rationale

There are limited applications of $\delta^{15}N$ palaeo-thermometry in Antarctic ice core. The technique has not been applied to study the AIM events during the MIS 3 period because high precision technique is needed to measure the small signal of $\delta^{15}N$ in Antarctic ice core. It has been used extensively to characterise the DO events during the last glacial period in Greenland. The temperature reconstructions from the $\delta^{15}N$ technique in Greenland ice cores were used to calibrate the modern $\delta^{18}O$ – temperature sensitivity, which was used to reconstruct temperature changes across abrupt climate changes from water isotopes in the glacial period. Another significance of $\delta^{15}N$ measurements in ice cores is to independently validate the model derived Δage estimate,

which is used in obtaining the chronology through synchronisation of gas records (Blunier *et al*., 2007).

The EPICA (2006) showed that there is a strong one – one coupling between all the DO events and the Antarctic warming during the last glacial period, although the magnitude of temperature changes in Antarctica are not as large as the Greenland DO events. The $\delta^{15}N$ technique is not applied to characterise these warming events in Antarctica except the MIS 5c/d transition (Caillon *et al*., 2001). The precision is the limiting factor in its application to assess abrupt climate changes in Antarctic ice cores due to the smaller magnitude of southern hemisphere temperature changes (Caillon *et al*., 2001; Blunier *et al*., 2007). The $\delta^{15}N$ data obtained in the Antarctic ice cores, to evaluate the temperature change during the LGM and MIS 5d/5c transition, had to be corrected for chemical interference from other constituents of air such as O_2 and CO_2 (Landais *et al*., 2006a; Caillon *et al*., 2001). The combined corrections are 0.03 ‰ (Sowers *et al*., 1989) and represents as much as 30 % or more of the likely recorded isotopic shifts during the LGM in the Antarctic ice core (Landais *et al*., 2006). Hence to investigate these smaller warming events in Antarctica during the last glacial period it is vital to develop a method that removes all the interfering species before measurement.

Some studies indicate that the climate events are not synchronous in Antarctica but may represent the possibility of a complex local pattern of millennial-scale temperature variability in high latitudes of southern hemisphere. The climate record from the Taylor Dome ice core from a coastal east Antarctic site suggests that the timing of the deglacial event was more synchronous with Greenland than with Byrd ice cores (Steig *et al*., 1998). A local warming at a coastal Siple Dome site of 6 ºC around 22 kyr was not observed in other ice core records (Taylor *et al*., 2004). There was a suggestion that the coastal sites experience different climate regime compared to more in-land sites and this needs to be confirmed with climate records from more coastal sites in Antarctica such as Berkner Island. The climate records from such coastal sites could also provide further insights into phasing relationship of climate change between northern and southern hemisphere.

1.8.2 Objectives of the Study

- To develop a high precision $\delta^{15}N$ method by removing all the interfering species and eliminating all the correction procedures associated with $\delta^{15}N$ measurements previously.

- To utilise the improved high precision $\delta^{15}N$ method to obtain high resolution data for two climatic warming during the last glacial period, namely AIM 8 (A1) that occurred approximately ~38 kyrs and AIM 12 (A2) that occurred approximately ~ 46 kyrs.

- To combine the $\delta^{15}N$ and $\delta^{40}Ar$ data to estimate $\delta^{15}N excess$ to reconstruct the temperature changes across the two warming events with a firn densification model.

- To obtain the climate record in gas phase from the coastal site in Antarctica and validate the Δage derived from the model and verify the ice chronology.

- To obtain high resolution methane measurements that could be coupled with $\delta^{15}N$ signal to investigate the lead and lag of the onset of climate change between northern and southern hemisphere.

- To measure halocarbons in the EDML firn air and to reconstruct atmospheric histories from the firn diffusion model, providing the updated and probably the longest atmospheric record of man-made gases reconstructed from Antarctic firn air.

- To measure CF_4 in Berkner Island ice core to investigate the variability in natural background level of CF_4 beyond pre-industrial times and in the glacial period.

Chapter 2: Methodology

2.1 Introduction

2.2 Methodology for $\delta^{15}N$ measurements in ice cores

2.2.1 Existing methodologies for $\delta^{15}N$ method
    2.2.1.1 Corrections for isobaric interferences
2.2.2 Experimental instrumentation
    2.2.2.1 Basic mass spectrometry concepts
    2.2.2.2 Isotopic ratio mass spectrometry
    2.2.2.3 SIRA description
2.2.3 Extraction procedure
2.2.4 Measurement on IRMS
    2.2.4.1 Data acquisition
    2.2.4.2 Reference gas
    2.2.4.3 Pressure imbalance corrections
2.2.5 Normalization to atmospheric N_2 isotopic composition
2.2.6 Quality control and method validation
    2.2.6.1 Zero enrichment
    2.2.6.2 Precision
    2.2.6.3 Testing for fractionation effects during the extraction procedure
    2.2.6.4 Long term stability
    2.2.6.5 Inter-laboratory comparison of Berkner Island firn air
    2.2.6.6 Analysis of Holocene ice cores
2.2.7 Influence of oxygen on $\delta^{15}N$ measurements

2.3 Methodology for $\delta^{40}Ar$ measurements in ice cores

2.3.1 Extraction
2.3.2 Analysis

2.4 Trace gas measurements

2.4.1 Experimental instrumentation
    2.4.1.1 Gas chromatography
    2.4.1.2 Mass spectrometry
2.4.2 GC-MS Analysis
    2.4.2.1 Autospec tuning and mass calibration
    2.4.2.2 Sample pre-concentration
    2.4.2.3 Manual inlet system
    2.4.2.4 Sample analysis
    2.4.2.5 Peak identification
2.4.3 Analytical precision
2.4.4 Blanks
2.4.5 Calibration
2.4.6 Detection limits

2.5 CF$_4$ analysis in ice cores

2.5.1 Extraction
2.5.2 Sample analysis
2.5.3 Simulated ice core extraction with the EDML firn air standard
2.5.4 System blanks

2.6 Methane analysis in Berkner Island ice cores

2.1 Introduction

In Chapter 1 it was highlighted that high precision $\delta^{15}N$ measurements are needed for successful application of $\delta^{15}N$ techniques in reconstructing small temperature changes during the last glacial period in Antarctica. In-house development of high precision $\delta^{15}N$ ice core measurements at the Stable Isotope Laboratory at the University of East Anglia (UEA) was an essential prerequisite for this study. The $\delta^{15}N$ method developed does not require any corrections for isobaric or chemical interferences.

Details of $\delta^{15}N$ methodology developed during this study for ice core measurements are presented in Section 2.2. The $\delta^{40}Ar$ measurement technique is summarised in Section 2.3 and the methodology for halocarbon measurements in EPICA Dronning Maud Land (EDML) firn air are presented in Section 2.4. In this study, I also developed a technique for gas extraction from ice cores for CF_4 analysis and this is discussed in Section 2.5. The methodology for methane measurements in ice cores is presented in Section 2.6.

2.2 Methodology for δ^{15}N measurements in ice cores

2.2.1 Existing methodologies for $\delta^{15}N$ measurements in ice cores

Stable nitrogen isotope analysis of trapped nitrogen gas in ice cores has been used for almost three decades now. Over this time, the understanding of how the $\delta^{15}N$ measurements can be interpreted has improved, as has the precision of the measurements. It was initially measured as an indicator of isotope enrichment due to gravitational settling in the firn (Craig et al., 1988, Sowers et al., 1989) and its relation to close-off-depth was used to estimate Δage (Schwander et al., 1989, Sowers et al., 1992). Prior to $\delta^{15}N$ of trapped N_2 gas measurements, elemental N_2 ratios were combined with oxygen data in the form of $\delta O_2/N_2$, which were used to constrain the biogeochemical rates of the global carbon cycle (Bender et al., 1994a, b). The $\delta O_2/N_2$ ratios were also used in Vostok ice cores to support orbital tuning chronology based on $\delta^{18}O_{atm}$ (Bender et al., 2002). The $\delta^{15}N$ method made a breakthrough in palaeoclimatology ice core science in the late 1990s (Severinghaus et al., 1998, Leuenberger et al., 1999), illustrating that the thermally fractionated isotopes can be used to interpret the magnitude of temperature changes during abrupt climate changes.

Since then $\delta^{15}N$ measurements have become increasingly important and are recognised as a good/reliable proxy for temperature change during abrupt climate change.

Better understanding of how ice core $\delta^{15}N$ measurements could be interpreted led to a pursuit for more robust and higher precision methods of extraction and analysis. Initially, Craig *et al*. (1988) used wet extraction to extract trapped gases, which were subsequently cycled over hot carbon to convert O_2 to CO_2, which was then removed cryogenically. Carbon monoxide (CO) was removed using I_2O_5 before injecting the remaining N_2-Ar fraction into the mass spectrometer. The working standard was a N_2/Ar gas mixture and experimental precision was 0.05‰. Sowers *et al*. (1989) used a melt and refreeze extraction technique in which the released gases were collected cryogenically in a stainless steel tube dipped in a dewar filled with liquid helium. The melt-refreeze cycle was repeated to ensure complete transfer of any occluded gases that were not released during the first cycle. The precision of the technique was in the range of 0.02 – 0.03 ‰, however this method required corrections (as discussed below) for chemical interferences due to the presence of CO_2 and O_2 in the analyte. Severinghaus *et al*. (1998 & 1999) used the method of Sowers *et al*. (1989) but obtained higher precision by using horizontal pieces of ice and applying an additional correction for pressure imbalances.

Most experimental work in which $\delta^{15}N$ measurements were made on extracted ice core nitrogen until 2006 referenced the methodology of either Sowers *et al*. (1989) or Severinghaus *et al*. (2001 & 2003). Petrenko *et al*. (2006) used the melt-refreeze method described by Sowers *et al*. (1989) with slight modifications. The ice was melted using a warm water bath rather than at room temperature and during the cryo-transfer step a liquid nitrogen trap was used in between the extraction vessel and the dipping tube in liquid helium to remove water vapour and carbon dioxide. This was the first mention of extracting water vapour and carbon dioxide using liquid helium in the $\delta^{15}N$ measurements since Mariotti *et al*. (1980), who measured $\delta^{15}N$ of N_2 in ambient air samples.

More recently Kobashi *et al*. (2007 & 2008), outlined a method similar to the method developed here at UEA. In addition to removing CO_2, hydrocarbons, water vapour and trace gases using a liquid helium trap, O_2 was also removed by passing the analyte

40

through hot copper granules at 550°C (Kobashi et al., 2007). The reason for removing CO_2 was already well understood (and is explained in detail in Section 2.2.1.1). The reason for removing H_2O vapour is that it generates N_2H^+ in the source which isobarically interferes with $^{15}N^{14}N^+$ (Kobashi et al., 2007). Kobashi et al. (2007) report a pooled standard deviation of 0.004 ‰ for their $\delta^{15}N$ measurements. Kobashi et al. (2007) state that oxygen was removed because $^{18}O^{18}O$ interferes with ^{36}Ar and therefore affect $\delta^{40}Ar$ measurements but they do not explain how it affects the $\delta^{15}N$ measurement or why its removal improves the $\delta^{15}N$ precision. Neither do they explain in detail the composition of their gas standard and whether any corrections were applied. In this chapter, a detailed description of the method used at UEA, which was being developed at the same time as Kobashi et al. (2007) were developing their method, is presented. In addition, some possible explanations for how the presence of O_2 interferes with $\delta^{15}N$ measurements are proposed.

2.2.1.1 Corrections for isobaric interferences

The presence of CO_2 in a sample results in isobaric interferences at masses 28 ($N^{14}N^{14}$) and 29 ($N^{15}N^{14}$). This interference results from ionization of CO_2 to $^{12}C^{16}O^+$ and $^{13}C^{16}O^+$ in the ion source and therefore requires correction of the measured $\delta^{15}N$ of the sample. If the sample and reference have the same CO_2 concentration, then this interference would cancel out but any slight differences between sample and reference could cause a differential isobaric interference. A correction procedure is described in Sowers et al., (1989), which entails measuring the $\delta^{12}CO_2$ content of the sample and then applying the following equation to correct the $\delta^{15}N$ measurement:

$$\delta^{15}N_{corrected} = \delta^{15}N_{measured} - [0.03 \text{ x } (\delta^{12}C^{16}O_2/^{14}N_2)/1000]$$

The magnitude of this correction was $\leq 0.03‰$ for all the samples analysed by Sowers et al. (1989).

Another important correction needs to be made for the sensitivity of $\delta^{15}N$ to $\delta O_2/N_2$ ratios. To date, this effect has not been well understood and has been mainly attributed to ion-molecule reactions in the mass spectrometer source (Headley et al., 2007). We

designed an experiment to investigate the cause of this effect (See Section 2.2.7). This correction is sometimes referred to as the "chemical slope" correction (Severinghaus *et al.*, 2003; Headley *et al.*, 2007). The $\delta^{15}N_{corrected}$ ($\delta^{15}N$ corrected for CO_2 isobaric interference) can be further corrected for the $\delta O_2/N_2$ sensitivity using the following equation:

$$\delta^{15}N_{true} = k'(\delta O_2/N_2)_{measured} + \delta^{15}N_{corrected}$$

where k' is the chemical slope determined by adding aliquots of pure O_2 to a sample of dry air and subsequently measuring the $\delta^{15}N$ and $\delta O_2/N_2$. Sowers *et al.* (1989) showed that the chemical slope ranged from 0.004 ‰ / ‰ to 0.000 ‰/ ‰ and the overall $\delta^{15}N$ correction was in the order of 0.01‰.

2.2.2 Experimental instrumentation

An Isotope Ratio Mass Spectrometer (IRMS) was used for isotopic ratio measurements and a Gas Chromatography Mass Spectrometer (GC-MS) was used for measuring trace gas concentrations. Although these are different types of mass spectrometer, the principle of operation is similar and a brief explanation follows in Section 2.2.2.1.

2.2.2.1 Basic mass spectrometry concepts

Mass spectrometry is an analytical technique used to measure the mass to charge ratio (m/z) of a gas. The basic principle of the technique is to accelerate an ion of mass M and charge Z with potential V into a uniform magnetic field B. Upon entering the magnetic field the ions move in a circular orbit of radius R, which is defined by the equation;

$$M/Z = B^2R^2/2V$$

Ions of differing masses are separated based on the radius of their path through the magnetic field (See Figure 2.2.1).

In order to be analysed, a gas sample must undergo five processes in the mass spectrometer. These five processes are outlineded below in order of their execution:

-

(i)   Ionization

Ion generation is fundamental to mass spectrometry and takes place in the ion source. There are different types of ion sources but Electron Ionization (EI) and Chemical Ionization (CI) are the common methods utilized for ion generation. In this study only the EI method was used, in which a sample is bombarded by high energy electrons that are produced by thermal ejection from a filament. The ions tend to acquire a large amount of excess energy (~10 eV) from the ionizing electrons which leads to additional fragmentation. The CI technique transfers less energy to the sample and leads to less fragmentation and therefore is known as a softer ionization technique.

(ii)   Ions formed into beam

This process takes place in the source. The positive ions produced from the sample gas during ionization are formed into a well defined beam by increasing the positive potential of the ionisation chamber.

(iii)   Acceleration of ions

The ions are accelerated from the source slit to a second defining slit (called alpha slit) at ground potential.

(iv)   Deflection in magnetic field

This process takes place in the flight tube, which forms an arc between the poles of a fixed or electro-magnet. As the ion beam travels down the flight tube, it is separated into beams with different radii corresponding to different masses (See Figure 2.2.1)

(v)   Detection

The final detection takes place in the collector. Ions of the chosen mass pass through a resolving slit and are detected by a Faraday cup. The ion current of the cup is proportional to the number of incident ions and hence to the partial pressure of the corresponding isotopic molecular species in the sample gas.

-

DETECTION

Faraday
collectors

Mass 46
Mass 45
Mass 44

Positive ion beam

Magnet

Amplifiers

current

Ratio
output

ION SOURCE

Beam focussing
Ion accelerator
Electron trap
Ion repeller
Gas inflow (from behind)
Ionizing filament
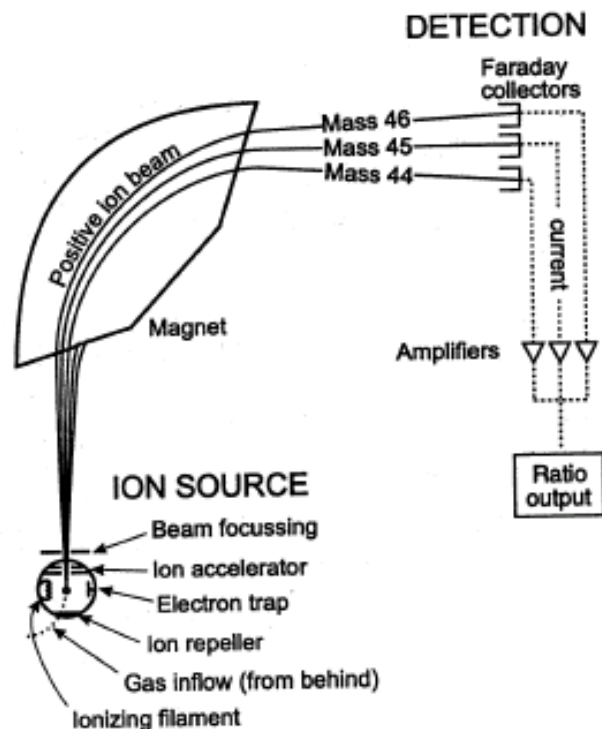
Figure 2.2.1: A simple schematic of a mass spectrometer used to determine the isotopes of $CO2$ (m/z = 44, 45, 46)**.** The different masses had different radii in the magnetic field and are separated accordingly.

2.2.2.2 Isotopic ratio mass spectrometry

Isotope ratio mass spectrometry (IRMS) is a specialization of mass spectrometry, which allows precise and accurate determination of the isotopic composition of a sample by comparing measured isotopic ratios of the sample to that of a standard. The principle of operation is similar to conventional mass spectrometry except for few minor differences. In this study, a dual inlet approach was used. The dual inlet system enables repeated measurements of sample and reference gas to be made by supplying continuous gas streams of reference and sample gas which are alternated rapidly and measured sequentially. In conventional mass spectrometry, a wide mass range is scanned to obtain a spectrum of mass peaks which reveals the chemical composition of the sample. In IRMS, the gas species being analysed is known and therefore the fields are held constant so that the variations in the isotopes can be detected with high precision. A characteristic of IRMS is that its collector consists of an array of Faraday cups or "multi-collectors" which allow simultaneous detection of multiple isotopes.

Faraday cups are widely used in IRMS to measure the relative isotope abundance of a gas species with high accuracy and precision (Gross, 2004). A Faraday cup consists of a conductive metal vessel that acts as an electrode where ions deposit their charge and become neutralized. The charge deposited in the Faraday cup passes through a resistor and is converted to a signal that is reported as a voltage.

There are two types of IRMS commonly in practise today; the dual inlet and the continuous flow IRMS. The dual inlet as the name suggests has a sample and a reference inlet side and is measured alternately as described above. The sample is prepared or purified separately before it is introduced into the sample side of the IRMS and measured repeatedly. In the continuous flow system the sample is prepared immediately on an on-line preparation system before injection into the IRMS and the sample is measured just once. Hence the continuous flow system results in higher sample throughput and is more convenient to use but it yields lower precision. A dual inlet system (SIRA Series II) was used in this study.

2.2.2.3 SIRA description

A SIRA Series II (VG Isogas Ltd) instrument was employed to measure nitrogen isotopes in air, firn air and ice core samples. The instrument uses a dual inlet system and 3 Faraday collector cups that allows simultaneous measurement of major and minor isotopes as well as an accurate comparison between a sample of unknown isotopic composition and reference gas. The high vacuum in the system, which is critical, is obtained by the use of rotary and diffusion pumping. Control and data acquisition for the SIRA instrument was provided by an IBM PS/2 Model 50.

The inlet system comprises two identical halves, each containing a variable volume gas reservoir. One half is used to store a reference gas of known isotopic composition whilst the other is used to introduce the sample gas to be analysed. The two reservoirs are connected to the ion source by equal lengths of stainless steel capillary tubing crimped such that equal pressures in the two reservoirs give rise to identical ion beams in the ion source. The bellows may be expanded or compressed by the action of software controlled stepper motors to equalise sample and reference major ion beams, either manually or automatically.

A micro changeover valve is fitted between the capillaries and the ion source such that either the sample or the reference gas is admitted. Whilst one gas is flowing into the ion source, the other is flowing at exactly the same rate into a waste line, connected to a high vacuum pump. In this way all the relative isotopic fractionation and mass discrimination effects associated with gas handling and ion beam formation are held equal for both gases. Since these effects are cross-cancelling, they need not be considered in the calculation of isotopic enrichments for the samples being measured.

2.2.3 Extraction procedure

A "wet" extraction method was employed to remove trapped gases from ~20g of inner ice core sample. The surfaces of the ice samples were trimmed in an ice core laboratory at -25°C and placed in a pre-chilled glass extraction vessel, containing a magnetic stirrer. The extraction vessel was sealed with a Viton o-ring using a glass flange and a metal clamp. The effectiveness of the o-ring seal was tested by evacuating the extraction vessel to less than 20 Pa and isolating the vessel from the pump for 24 hours; no significant increase in pressure was noted. The vessel was then attached to a glass vacuum manifold, chilled to -30°C in a liquid nitrogen/ethanol mixture, and evacuated for 20 minutes. During evacuation the pressure in the vessel reduced to ~20 Pa which is the vapour pressure of water over ice at ~ -30°C. This continual flux of sublimed vapour assists in the evacuation of room air, and also cleans the surface of the ice sample of any gaseous contamination (Severinghaus *et al*., 2003).

After evacuation, the vacuum tap on the lid of the extraction vessel was closed and isolated from the vacuum manifold. The vessel was placed in warm water to melt at least half of the ice sample, and was then placed on the magnetic stirrer plate to agitate the melt vigorously in order to accelerate the melting process. Whilst melting was taking place, the extraction vessel was attached to the extraction line (See Fig. 2.2.2) via Cajon Ultratorr fittings, and the extraction line evacuated to 8×10^{-4} Pa with a diffusion pump backed by a rotary pump. Once the melting was complete, the air was expanded through a glass trap at -80°C (dry ice and ethanol slurry) to remove water. The gas was

then expanded into a column containing copper granules (Aldrich, 10 - 40 mesh) and heated to 600°C for 10 minutes to remove oxygen.

During the oxygen removal process a dip tube was prepared to receive the sample. The tube was a ¼″ x 1.5 m stainless steel tube with a Nupro metal bellows valve attached, evacuated to a pressure of 1 x 10^{-4} Pa before being immersed into a dewar filled with liquid helium. After removal of oxygen the gas stream was then passed into a second glass trap held at -196°C (liquid nitrogen) for a further 5 minutes to remove CO_2, after which the vacuum valve downstream of the second glass trap was slightly opened so that the pressure upstream decreased by ~10 Pa/min. This ensured a slow consistent flow across the furnace for complete removal of any residual oxygen in the sample.
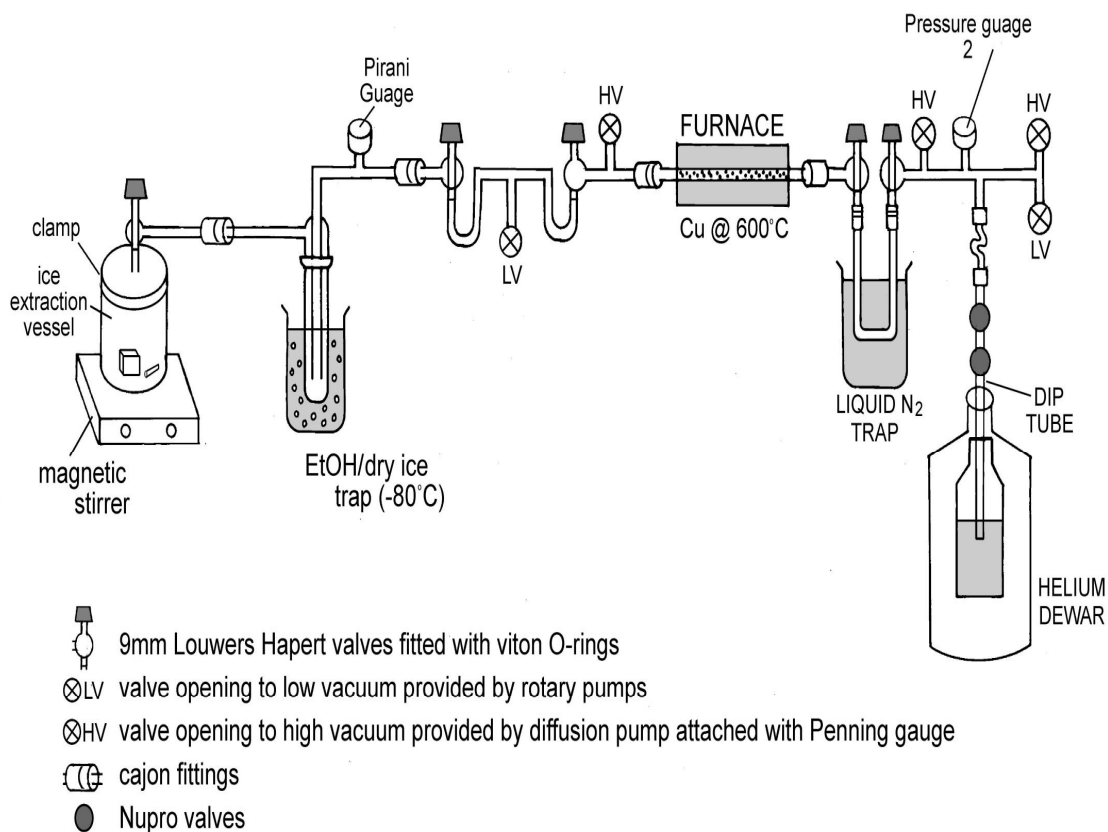
Figure 2.2.2: A schematic of the extraction line used for $\delta^{15}N$ measurements.

The gas was transferred into the dip tube immersed in the liquid helium for 35 minutes, or until the pressure downstream decreased to < 1 Pa on a $0 – 1 \times 10^5$ Pa capacitance manometer. After collection, the valves to the high vacuum pump and associated pressure gauge were opened, at which point the residual pressure in the extraction line was observed to be ~1×10^{-2} Pa.

While the gas was being cryopumped into the dip tubes, the sample flow through the furnace was controlled by metering the valve immediately downstream of the liquid nitrogen trap to increase the residence time of the sample in the furnace and to ensure complete removal of oxygen. If the valve was fully opened the pressure upstream decreased very rapidly, and the oxygen was not removed completely in the furnace, resulting in an interference with the $\delta^{15}N$ measurements (see below). Another potential source of error, resulting from sample fractionation, could occur if the sample is not completely collected in the dip tube. To investigate this, the sample freezing time was increased to 50 minutes, and to 75 minutes, for which the residual pressure decreased to 8×10^{-3}, and 5×10^{-3} Pa respectively, but this did not affect the measured $\delta^{15}N$ values. This confirms that essentially the entire sample is recovered in the dip tubes after the chosen transfer time of 35 minutes.

The method of removing oxygen using a copper reduction furnace has been previously applied to $^{15}N/^{14}N$ measurements in ambient air by Mariotti (1983), but silica gel was used in that study to trap N_2 gas at 77K. We initially attempted to replicate this procedure, but it resulted in a lower precision of 0.020‰, which is in good agreement with the precision of 0.025‰ obtained in Mariotti's work. The sample was trapped in a glass tubing with vacuum valves containing silica gel dipped in liquid nitrogen and then after equilibration at room temperature, the trapped gases were desorbed into the headspace of the glass tubing which was expanded in the sample bellow in the IRMS for measurements. Further tests with silica gel tubes revealed that the samples were fractionated during the desorption stage, with the ratios becoming heavier by as much as 0.05‰ (See Table 2.2.1), suggesting that the lighter fraction was being preferentially retained on silica gel. The silica gel tubes were heated to accelerate desorption of the lighter fractions, but incomplete recovery of the lighter fractions was still experienced.

This unusual behaviour of nitrogen isotopes trapped on silica gel remains unexplained. If the method of Mariotti (1983) had proved successful then it would be have been a relatively simple and cost effective procedure.

Table 2.2.1: Three sample vials, each containing Si gel, were filled with reference gas and the $\delta^{15}N$ composition determined without the nitrogen being adsorbed onto the Si gel.The remaining gas was then frozen onto the Si gel and then subsequently desorbed by heating with a hot air gun. The nitrogen isotope composition was then re-measured.

Sample	STD 1		STD 2		STD 3	
Procedure	Not adsorbed	Adsorbed and then desorbed	Not adsorbed	Adsorbed and then desorbed	Not adsorbed	Adsorbed and then desorbed
Trial 1	0.004	0.038	-0.003	0.049	-0.007	0.015
Trial 2	-0.002	0.027	0.004	0.042	0.006	0.039
Trial 3	-	0.031	0.006	0.056	0.009	0.030

2.2.4 Measurements on IRMS

2.2.4.1 Data acquisition

The dip tubes were equilibrated at room temperature for at least 2 hours before the gas sample was measured for the $m/z = 29/28$ ratio on a SIRA Series II (VG Isogas Ltd) dual inlet mass spectrometer. The gas was expanded into the sample bellows and allowed to equilibrate for 10 minutes before being isolated in the inlet of the mass spectrometer. The pressure in both the reference and sample bellows were equalized by adjusting the corresponding bellow volumes. The mass spectrometer was operated in the 'normal' reference/sample switching mode, performing 12 cycles per run with an integration time of 15 s per cycle, and an inter-cycle delay of 20 s. If the internal precision of the measurement was $\geq 0.006‰$ then the analysis was repeated automatically. This is an automated function of the instrument control software. Each sample was analysed in duplicate or triplicate. The ion intensities of $m/z = 32(O_2)$, $40(Ar)$ and $44(CO_2)$ were also monitored by peak jumping, which served as a diagnostic

tool for rejecting any sample that showed higher mass 32 or 44 signals due to incomplete removal of O_2 or CO_2, or leakage during the extraction process. Monitoring mass 40 was also useful in identifying any potential leaks in the inlet system, and inspecting the possibility of reference drift in the reference gas (see below).

2.2.4.2 Reference gas

The reference gas was prepared by mixing commercial oxygen free nitrogen with pure argon in a 20 L round-bottomed flask fitted with 9 mm Louwers-Harpert, Viton o-ring sealed valves. The volume of the reference flask was calibrated and a 78:1 mixture of N_2 and Ar prepared, closely resembling the composition of the extracted and deoxygenated air samples. The 20 L flask was placed on its side in a box filled with insulating material, and the exit port fitted with a glass tube fixed to the valve extending to the middle of the flask to minimise any thermal fractionation. During analyses the mass 40 beam signal in both the reference and the sample were similar, indicating that the reference gas was correctly prepared.

2.2.4.3 Pressure imbalance correction

In high precision dual inlet analysis it is important to ensure that the sample and reference gas pressure, capillary characteristics, and depletion rates are identical to minimise the effect of small pressure imbalances on the measured isotopic composition. During this study we carefully adjusted the capillary crimps to ensure identical flow characteristics through both the reference and sample sides of the inlet system. We also characterised the effect of small pressure imbalances by measuring the variation in the 29/28 ratio as a function of the major beam signal intensity. This is carried out by varying the gas pressure in the reference bellows over a factor of two. This is commonly referred to as a linearity test. For the analyses that we report here, the change in the 29/28 ratio is less than 1 ppm per nA imbalance in the major beam current. This is equivalent to a change in $\delta^{15}N$ of 0.13‰ per nA of difference in beam current between sample and reference. We analysed samples at a major beam signal strength of approximately 6 nA, and balanced the sample and reference signals to significantly better than 1%. Thus any correction needed due to an initial pressure imbalance was significantly less than 0.007‰ and could be ignored.

Finally, after balancing the sample and reference gas beams, the variable volume bellows were isolated from the carefully matched inlet volumes (0.2 mL) in the sample and reference valve blocks. This ensured that the measurements were made with identical gas depletion rates with matched signals throughout the measurement period.

2.2.5 Normalization to atmospheric N_2 isotopic composition

In common with studies of this type, outside ambient air was used as a standard gas for $\delta^{15}N$ measurements because it is assumed that outside air has a constant $\delta^{15}N$ of zero. The air sample was collected in glass fingers fitted with vacuum 9 mm Louwers-Harpert vacuum valves from outside the UEA laboratory. Before collection of the outside air, the glass fingers were prepared by evacuating to 10^{-4} Pa whilst heating with a hot air gun to desorb any gases on the glass surfaces. Evacuation was allowed to continue whilst the glass fingers cooled to room temperature. The glass fingers were then equilibrated with outside air for two hours. This sampling technique avoids any sample fractionation due to temperature gradients, insufficient flow, or pressure fluctuations.

The air samples were processed in exactly the same manner as the ice core samples, mimicking the exact process for ice core extraction to ensure that any minor fractionation effects, or contamination in the extraction procedure, would cancel out. To illustrate the importance of this, when an outside ambient air sample was processed without passing through the drying trap at the front of the line, this resulted in enriched $\delta^{15}N$ values (~0.800 ‰) and when passed through the water trap it gave a lower value (~0.720‰). We believe that fractionation takes place in the water trap which is held at about -80 ˚C. All other steps of the extraction procedure were tested and shown not to give rise to any fractionation (See Section 2.2.6.3). The residual pressure of 1x 10^{-2} Pa suggests that 99.998% of the gas was collected and prolonging the freezing time did not change the measured isotopic composition as discussed above. The fractionation effect observed with/without the water trap for the outside air samples is therefore perplexing and we cannot explain it at this stage. To overcome this effect, the samples and the outside air were extracted in exactly the same way and each step was carried out consistently. The data shown in Table 2.2.2 proves that this precautionary measure

eliminates any bias in data calculation. The firn samples, 0 m and 12 m, measured in September of 2006 were processed through the extraction line without the extraction vessel and water trap at -80 °C and the air values that were used in the normalization calculation were also processed exactly the same way. The same firn samples and the outside air were analysed again in March/April 2007 and were processed in exactly the same way as the ice core samples, that is, through the water trap and the extraction vessel. The data show that the normalized $\delta^{15}N$ value was within the error limit as long as the extraction procedure for the sample and the outside air was exactly the same.

Over the entire period of ice core analysis, 53 outside air samples were measured with respect to the working standard (Fig 2.2.3). The measurements had a mean value of 0.717‰ and a standard deviation of 0.025‰. This latter value is much higher than the precision of the method (0.006 ‰, see Section 2.2.6.2) and can probably be attributed to variations due to gas handling or drift in the mass spectrometer or standard gas over time (Severinghaus *et al.*, 2003). In our mass spectrometer we record a small fractionation of the reference gas towards enriched $\delta^{15}N$ compositions as the gas is used up and the bellows become compressed towards small volumes over a period of several days to weeks. Because we calibrate the reference gas composition regularly to an air standard as described above this drift in reference gas composition is not significant. Figure 2.2.3 illustrates that towards the end of the analysis period (June 2008), the working standard had become heavier and consequently the $\delta^{15}N_{uea\ air}$ with respect to the working standard became lighter.
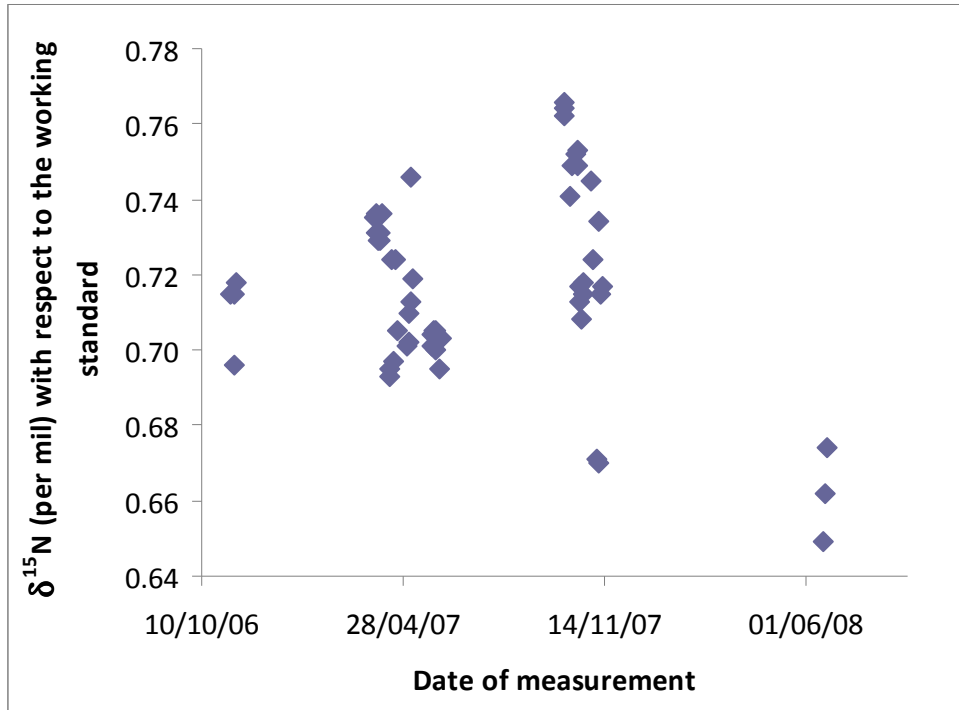
Figure 2.2.3: A plot of all $\delta^{15}N_{uea\ air}$ measurements with respect to the working standard used in the normalization procedure.

The principle used in normalizing the ice core samples to atmosphere was to try to find the best estimate of outside air, during the period in which the ice core samples were measured and was normalized as follows (Severinghaus *et al.*, 2003):

$$\delta^{15}N_{normalised} = (\{[\delta^{15}N_{measured}]/1000 + 1\} \, / \, \{[\delta^{15}N_{uea\ air}]/1000 + 1\} - 1)* 10^3‰$$

Since the air samples were analysed everyday or every other day it was not difficult to estimate the best air value to be used in the calculation. During the period where the reference gas was stable in the bellows then an average value was used in the calculation, but if the reference gas in the bellows became depleted then the air values obtained either immediately before or after the sample analysis was used in the calculation. In fact analysing air samples frequently served as an important tool in detecting reference drift in the bellows. As soon as the air values started getting lighter, the reference gas was evacuated from the reference bellow and loaded with fresh standard from the reference tank.

53

2.2.6 Quality control and method validation

2.2.6.1 Zero enrichment experiment

A zero enrichment experiment was conducted by expanding the reference gas into both bellows and expected zero value of δ^{15} N should be measured. This test reflects any fractionation of sample or reference *en route* to the source, for example during diffusion through the capillaries, and also assesses the effects of any leaks in the inlet system. The zero enrichment test was carried out three times during the course of analysis (See Table 2.2.2) and the mean zero enrichment value obtained was 0.001‰. The zero enrichment tests therefore confirm the satisfactory functioning of the mass spectrometer and the sample and reference side inlets to the mass spectrometer.

Table 2.2.2: Zero Enrichment experiment results

Date	16/03/07	02/10/07	29/05/08
Mean zero enrichment value obtained	0.001 ± 0.001‰ (n = 7)	0.001 ± 0.005‰ (n = 9)	-0.001 ± 0.006 (n = 8)

2.2.6.2 Precision

Precision was determined by analysis of replicate ambient air samples, and also from replicate analysis of ice samples collected from similar depths during the Holocene period. The climate during the recent Holocene period has been relatively stable and as a result the δ^{15}N of the extracted nitrogen in these samples should be almost invariant, and so should allow a measure of the reproducibility of the technique. The ambient air samples, collected simultaneously and subjected to the entire extraction and analytical procedure, resulted in a precision of 0.003‰ (1σ, n = 7). These air samples were analysed on seven different days, and consequently the precision obtained includes effects that may be associated with any instrumental or reference gas drift over the period of one week.

54

-

Reproducibility tests on Holocene ice core samples were carried out on a 55 cm length of ice core from Berkner Island, Antarctica (79°S, 45°W). Ten samples from a depth range of 451.55 – 452.10 m (~3950 ± 50 years BP) with a depth resolution of 2.5 - 7.5 cm were subjected to the entire extraction procedure and measured (one measurement was rejected due to procedural error). The precision of these measurements was 0.006‰ (1σ, n = 9). The precision obtained with ice replicate samples was higher as compared to that obtained with outside air. The larger variability observed with ice samples could not be due to the extraction procedure as both the air and the ice samples were subjected to exactly the same treatment. The larger variability observed in the ice core measurements is most likely due to real sample heterogeneities in the ice as the samples used in the test were not really identical. Even so, the precision of the ice-core measurements is an order of magnitude better than the precision of 0.02 – 0.05‰ reported in numerous other studies (Huber *et al*., 2006; Leuenberger *et al*., 1999, Lang *et al*., 1999, Sowers *et al*., 1989) and is comparable to work by Landais *et al*.(2004, 2005 & 2006) and Severinghaus *et al*. (2003), who reported a pooled standard deviation of 0.006‰.

Pooled standard deviation is calculated from duplicate or triplicate analysis of samples and the deviation of replicates from each other can be used as a measure of reproducibility. The pooled standard deviation is defined by Severinghaus *et al*. (2003) as the square root of the summed squared standard deviations of replicates, δi, from their respective means, divided by the degrees of freedom (the number of samples '*n'* minus the number of reported means '*m'*). Kobashi *et al*. (2007 & 2008) suggest that an efficient oxygen removal step results in high precision with a pooled standard deviation of 0.004‰ (n = 238). In this study, samples from 18 sampling depths were analysed in duplicate and gave a pooled standard deviation of 0.007‰. Our value of 0.007‰ is comparable to the precision of 0.004‰ quoted by Kobashi *et al*. (2007) considering the fact that duplicate samples were not taken from exact same depths but were 2.5 cm apart and the subset of samples used in the calculation was very small as compared to Kobashi *et al*. (2007).

2.2.6.3 Testing for fractionation effects during the extraction procedure

To investigate if the extraction process fractionated the samples, the reference gas was subjected to the entire extraction process (except that the water trap was at room temperature), and then measured against the same reference gas. The reference gas was expanded into 6 glass vials. Five samples were processed through the extraction line and one sample was analysed without any treatment and acted as a reference point. A value of 0.005 ± 0.004‰ was obtained for the sample without any treatment, and values in the range of 0.003 - 0.007‰ were obtained for the samples that underwent the complete extraction process. The absence of any significant difference between the values suggests that there is no fractionation or any leakage during the extraction process. In addition, the values are on either side of the 0.005‰ reference point indicating a lack of systematic bias in the extraction procedure.

2.2.6.4 Long term stability

To investigate the long term stability of measured $\delta^{15}N$ values, firn air samples with known (see Section 2.2.6.5) nitrogen isotopic composition were analysed on different days and the results are displayed in Table 2.2.3. The results for 0 and 12 m depth samples analysed on different occasions show that the variability due to effects associated with reference drift, instrumental drift, and sample processing is very small and is on the order of the overall procedural error.

Table 2.2.3: $\delta^{15}N$ of firn air samples (0m & 12m) measured on different days

Firn Sample	Date of Analysis	$d^{15}N$ (‰)	Average	1σ
0 m	15/09/2006	0.003		
	21/03/2007	0.004		
	*02/04/2007	0.006	0.004	0.002
12 m	28/09/2006	0.105		
	21/03/2007	0.095		
	*31/03/2007	0.089	0.096	0.008

* The extraction of the firn air samples was simulated as ice core extraction

2.2.6.5 Inter-laboratory comparison of Berkner Island Firn Air

The Berkner Island firn air samples from 9 depths that had been initially measured by University of Bern were re-analysed on our mass spectrometer using the oxygen removal method. The data obtained are show in Figure 2.2.4. There is excellent agreement between the Bern and UEA data, thus increasing our confidence in our measurement technique. The error estimate on Bern data was ±0.020 ‰, based on a recent publication by the Bern group on $\delta^{15}N$ firn data (Huber *et al*., 2006), stating that the precision is in the range of 0.02‰. The precision obtained at UEA (0.006‰) is an order of magnitude better than that obtained with the Bern $\delta^{15}N$ method (Leuenberger *et al*., 1999; Huber et al., 2006b), which reported precision in the range of 0.03 – 0.05‰.

The full profile of $\delta^{15}N$ in the Berkner Island firn air is published elsewhere (Landais *et al*., 2000b) and therefore it was not my intention to characterise the full firn profile. Only selected samples were analysed for the inter-laboratory comparison exercise. However, it is worth mentioning that the incomplete profile of $\delta^{15}N$ obtained in this study does compare well with the published firn data of Landais *et al*. (2006a). The $\delta^{15}N$ values close to 0‰ were measured in the first few metres of the firn column. These values are typical of the convective zone of the firn as it represents the isotopic composition of modern air. In the diffusive zone, $\delta^{15}N$ values increase with increasing depth until the lock-in-depth zone. The lock-in-depth is characterized by constant $\delta^{15}N$ values until the close-off–depth is reached. At this point, bubbles close-off, capturing the isotopic signal at the bottom of the firn and preserving it in the ice.
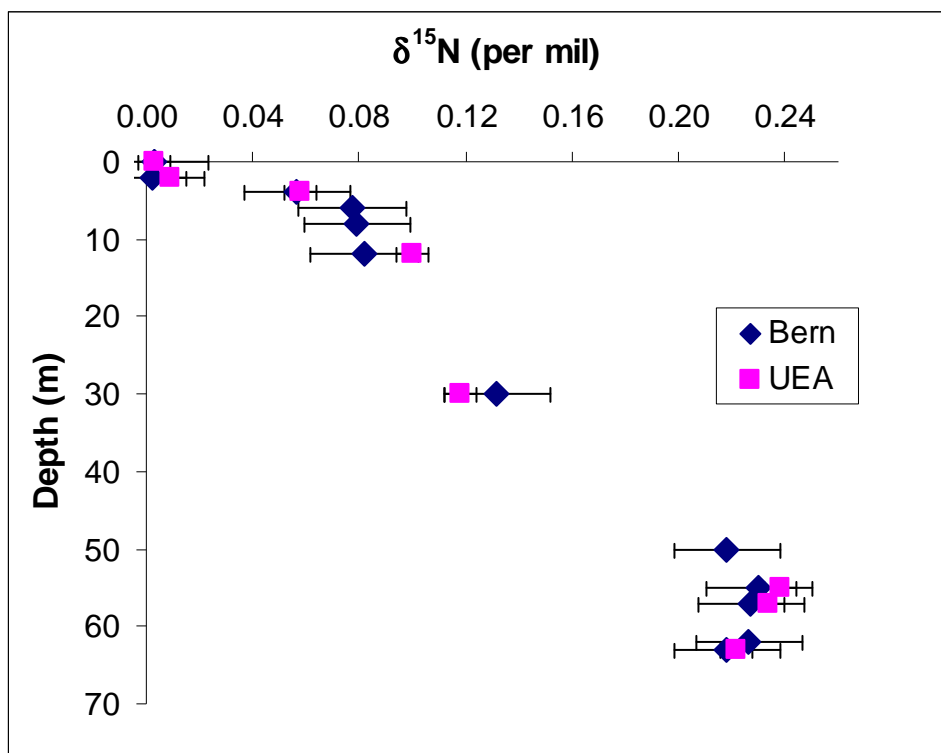
Figure 2.2.4: A comparison between the University of Bern and UEA $\delta^{15}N$ measurements for the Berkner Island firn air.

2.2.6.6 Analysis of Holocene ice core samples

In addition, seventeen samples from a depth of 446.60 – 562.68 m were analysed, and values in the range of 0.209 – 0.228 ‰ were obtained with $1\sigma = 0.006$‰. The $\delta^{15}N$ values obtained were similar, within error, to those observed at the bottom of the firn layer (See Figure 2.2.4) at the same location. Assuming that climate, accumulation rate and diffusive column height during the last 3000 – 5000 years BP is similar to present day then we would expect the $\delta^{15}N$ composition of these samples to be typical of those observed at the bottom of the firn layer. The δD_{ice} profile for Berkner Island suggests that the climate was stable and the accumulation rate derived from $\delta^{18}O_{ice}$ is not significantly different from the present day (J.-M. Barnola, pers. Comm.) supporting the data we observed for the seventeen samples from the Holocene period and enhancing our confidence in the method.

2.2.7 Influence of oxygen on $\delta^{15}N$ measurements

To investigate the influence of oxygen on the measured nitrogen isotope composition we adopted an experimental strategy in which air samples were analysed both with oxygen present and after oxygen was removed (see Table 2.2.4). The results clearly show that when oxygen is present the measured $\delta^{15}N$ composition of samples has an apparent enrichment of between 0.8 and 1.0‰. Sowers *et al*. (1989) reported a similar effect when measuring $\delta^{15}N$ of air samples using air as reference gas in the mass spectrometer. Their observed change of 0 to 0.004‰ in $\delta^{15}N$ per ‰ change in $\delta(O_2/N_2)$ is consistent with the magnitude of change observed in this study. They were unable to draw definitive conclusions regarding the origin of this variation.

Table 2.2.4: $\delta^{15}N$ of N_2 measurements in air samples with and without O_2 removal, $\delta^{15}N$ (‰) values are expressed with respect to the working standard. Values shown are the mean $\pm$ 1 standard deviation of 12 measurements of each sample on the instrument.

Date	$\delta^{15}N$ measured with O_2 removed	$\delta^{15}N$ measured with O_2 present
19/03/07	0.828 ± 0.006	1.703 ± 0.007
	0.822 ± 0.008	1.884 ± 0.016
	0.830 ± 0.004	1.771 ± 0.015
21/03/07		
	0.793 ± 0.001	1.661 ± 0.018
	0.794 ± 0.007	1.611 ± 0.080

Outside air samples were collected in six different vials simultaneously on 19/03/07 (following the procedure outlined in Section 2.2.5).Three were processed through the hot copper furnace at 600°C, and three were processed through the copper furnace at room temperature. All samples were passed through the glass trap at -196K to remove CO_2. Another suite of four air samples were collected on 21/03/07 and two vials were subjected to each treatment. The $\delta^{15}N$ values for the air samples shown in Table 2.2.4 are expressed with respect to the working standard. As already discussed (Section 2.2.5), the $\delta^{15}N$ of the working gas standard exhibits a slight increase as the gas depletes. Hence the apparent 0.03 ‰ change in air $\delta^{15}N$ composition with respect to the working standard between 19/03/07 and 21/03/07.

For the air samples in Table 2.2.4, those that were not subjected to the oxygen removal process had an analyte gas composition of approximately 78% N_2, 21% O_2 and 1% Ar. However, enrichment in the measured $\delta^{15}N$ composition of samples at much lower oxygen concentrations was also observed. Figure 2.2.5 shows the difference ($\Delta\delta^{15}N$) between the expected $\delta^{15}N$ and the measured $\delta^{15}N$ compositions for a range of samples (modern and Holocene air) as a function of the m/z = 32 ($I(O_2)$) ion beam intensity. Enrichment starts to become significant at oxygen concentrations 10^4 times lower than in air. The functional dependency of $\Delta\delta^{15}N$ on $I(O_2)$ is of the form $\Delta\delta^{15}N \propto I(O_2)^{1/2}$.

Log of m/z =32 signal beam

y = 0.44x + 3.65
R^2 = 0.81
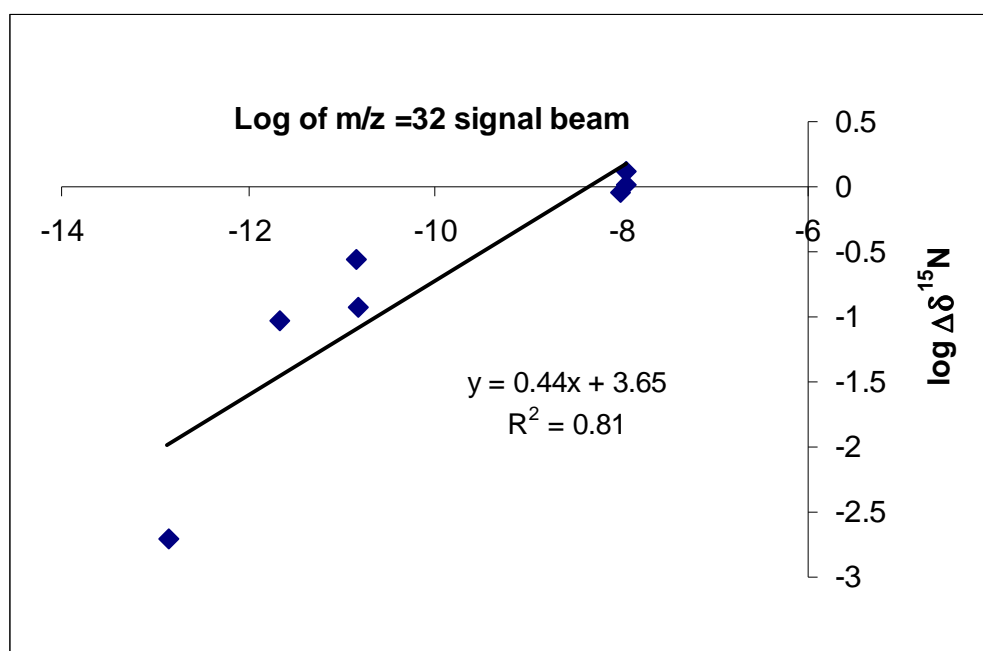
Figure 2.2.5: A log – log plot of the change in $\delta^{15}N$ ($\Delta \delta^{15}N$) with intensity of the measured oxygen signal. The results show that small amounts of oxygen lead to changes in measured $\delta^{15}N$ composition. The gradient of 0.44 is close to that expected for the reaction $C + \frac{1}{2} O_2 \rightarrow CO$ in the source of the mass spectrometer.

The most likely cause of the apparent enrichment in $\delta^{15}N$ is isobaric interference of CO with N_2. CO has isotopic species at m/z = 28 ($^{12}C^{16}O$), 29 ($^{13}C^{16}O$) and 30 ($^{12}C^{18}O$) with isotopic ratios of approximately 1% (29/28) and 0.2% (30/28). Assuming similar ionisation efficiencies for N_2 and CO then a mixing ratio of just 7.6×10^{-4} for CO in N_2 is all that is required to cause a 1‰ enrichment of the 29/28 ratio and hence the measured $\delta^{15}N$ composition. Carbon monoxide and hydrogen are the most common residual gases in clean vacuum systems. In the presence of oxygen, CO is readily

formed by oxidation of impurity carbon in tungsten filaments and their supports (Brion and Stewart, 1968; Singleton, 1966). It has also been suggested that atomic oxygen, desorbed from a hot tungsten filament, can interact with the walls of a vacuum chamber to produce CO (Singleton, 1966).

We have observed that the intensity of the m/z = 44 peak also increases with oxygen content of the analyte gas. This is shown in Figure 2.2.6. It is tempting to suggest that the rise in the mass 44 signal is the result of the following gas phase reaction at the ion source and ion gauge filaments (Singleton, 1966):

$$2CO + O_2 \leftrightarrow 2CO_2$$
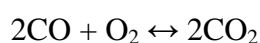
However, Leuenberger et $al.$ (2000) show that, rather than CO_2, the major component of the m/z = 44 beam is $^{14}N_2{}^{16}O$ resulting from the reaction:

$$2N_2 + O_2 \leftrightarrow 2N_2O$$
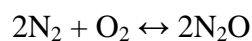
They observed an increase in signal only when both nitrogen and oxygen are present. When analysing pure oxygen they see no change in the m/z = 44 signal.

It is unlikely that isotopic fractionation during production of N_2O according to this reaction can account for the apparent enrichment of ^{15}N in N_2. Maximum m/z = 44 intensities for air samples containing oxygen are just 5×10^{-13} A and are some 10^4 times smaller than the N_2 beam intensity at m/z = 28. An unrealistically large isotopic fractionation of 10,000‰ between N_2 and N_2O would be required to produce 1‰ enrichment in the 29/28 ratio.
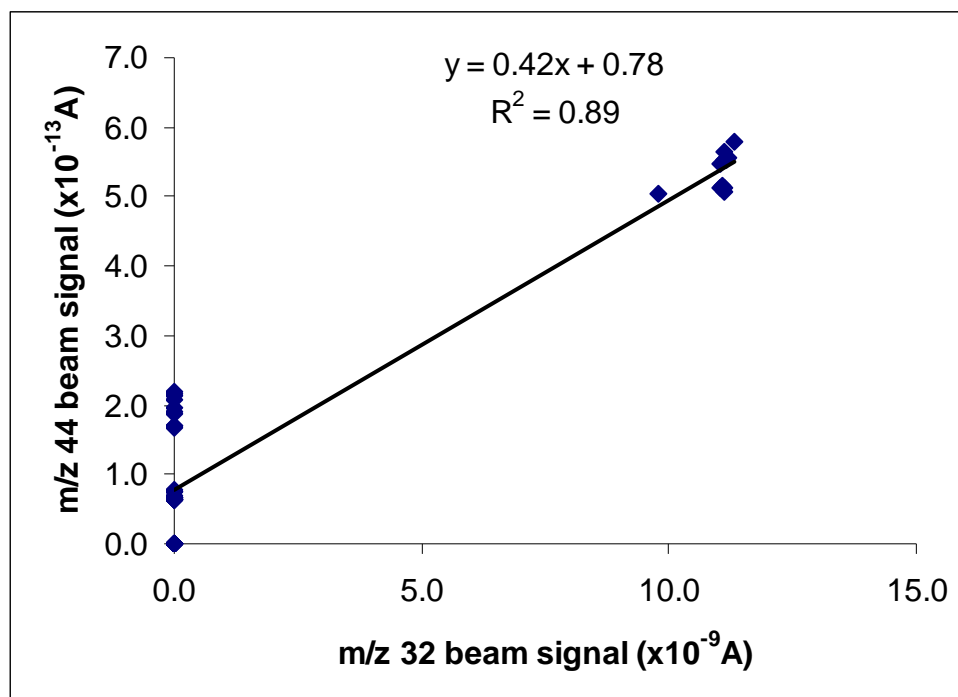
Figure 2.2.6: An illustration of mass 32 and mass 44 correlations suggesting that the presence of oxygen could potentially lead to in situ CO_2 or N_2O production.

Our preferred explanation is that when oxygen is present, measured $\delta^{15}N$ compositions of nitrogen are enriched due to CO production in both the ion source and on the walls of the mass spectrometer.

To test this, we extracted five ambient air samples as previously described, including the oxygen removal step, and then added approximately 20% $^{18}O^{18}O$ gas (98% purity, CK Gases Ltd) to two air samples. Any CO production in the source from the added $^{18}O^{18}O$ gas should contribute to m/z = 30 and m/z = 31, and not 28 and 29 as with oxygen of natural isotopic abundance, and should therefore not affect $\delta^{15}N$ measurements. The $\delta^{15}N$ composition measured with respect to the reference gas for air stripped of oxygen gave an average value of 0.845. The two samples enriched with $^{18}O^{18}O$ gas gave values of 0.878‰ and 0.923‰. We did not observe any large enrichment in $\delta^{15}N$, compared to the 0.8 - 1‰ enrichment observed in the case of samples containing $^{16}O^{16}O$. The small enrichment in measured $\delta^{15}N$ obtained for samples containing $^{18}O^{18}O$ (~ 0.03 to 0.08‰) may result from the fact that the CK Gases $^{18}O^{18}O$ gas contained 1% ^{16}O. In addition, we measured the 30/28 ratio for N_2 –

$^{18}O^{18}O$ gas mixtures and obtained a value of 5.43 x 10^{-4}. The expected 30/28 ratio, based on the known amount of N_2 in the sample and the amount of $^{18}O^{18}O$ gas added, was 1.37 x 10^{-5}.We attribute the much higher30/28 ratio observed (~40x) to the formation of $^{12}C^{18}O$.

This contribution of oxygen to the isobaric interference at m/z = 28 and 29 is not accounted for when making the usual CO^+ correction in which the magnitude of the correction is based on the CO_2 content of the sample. This approach assumes that the sample and reference gases have similar oxygen contents and therefore that the oxygen effect will be cancelled out. However, our results show that small differences in the oxygen content of samples and reference gases have a measurable effect on the 29/28 ratio and lead to errors/uncertainties in the measured nitrogen isotope composition. It is well known that different amounts of oxygen in the sample and standard gas cause an artefact in measured $\delta^{15}N$ composition, often described as the "chemical slope". To date, laboratories have applied empirical "chemical slope" corrections to adjust measured $\delta^{15}N$ values (Sowers *et al*., (1989), Headley and Severinghaus (2007)). Although such corrections have previously been applied, the origin of the effect has never been fully understood. Our study elucidates the chemistry of the effect in the mass spectrometer source.

Another feature, shown in Table 2.2.4, is the degree of reproducibility obtained between samples measured with and without oxygen stripping. Reproducibility between replicate samples is in the range 0.001 to 0.003‰ with oxygen removed, compared to 0.07 to 0.13‰ for samples with oxygen. Clearly, the presence of oxygen affects both the accuracy and precision of measurements.

2.3 Methodology for δ⁴⁰Ar measurements in ice cores

The δ^{40}Ar measurements were carried out at the Laboratoire des Sciences du Climat et de l'Environnement (LSCE) in Gif-sur-Yvette, France under the supervision of Amaelle Landais. In total 33 samples were extracted and measured. The extraction and measurement procedure is exactly the same as the high precision method developed by Severinghaus *et al*., (2003) for measurement of argon 40/36 and krypton/argon ratios in trapped air in polar ice. The procedure involves wet extraction and followed by use of a getter, a metal strip of Zr/Al alloy heated to 900 ºC, which removes all reactive gases leaving behind the noble gases. To speed up the extraction process, three samples were prepared and melted for extraction simultaneously.

2.3.1 Extraction

Approximately 35 g of ice sample was placed in a pre-chilled glass vessel containing a magnetic stirrer. The glass vessel was joined to a Conflat vacuum fitting which allows a gas-tight glass to metal transition to be made. The glass vessel containing the sample was lowered into a dewar of liquid nitrogen and ethanol (held at -20 to -25˚C) to prevent the ice from melting whilst being bolted onto the vacuum manifold. A copper gasket was used to make the Conflat seal and each copper gasket was used for up to 6 extractions before being replaced. Once the extraction vessel was secured tightly to the manifold, it was fully immersed in the dewar and evacuated to remove room air for 5 minutes. The glass vessel was then isolated from the pump and leak tested. If any increase in the pressure on the pressure gauge was observed, then nuts and bolts on the Conflat fittings were further tightened. In very exceptional cases, tightening the bolts did not improve the vacuum, in which case the copper gaskets were replaced. If no evidence of any leaks was found, then the glass vessels were evacuated for a further 35 minutes. To speed up the extraction process, three sample vessels were evacuated simultaneously. The temperatures of the different ethanol dewars were kept as similar as possible to minimise differences in vapour pressures between the different vessels.

After 35 minutes, the extraction vessels were isolated from the pumps by closing the two valves on each port (See Figure 2.3.1). The ethanol dewars were removed and replaced by warm water baths. During melting of the ice, the water traps were attached to the line and evacuated and immersed in ethanol/liquid nitrogen slurry held at

64

approximately -100°C. After complete evacuation and leak testing across the water trap, the sample was cryo-trapped in a stainless steel tube dipped in dewar containing liquid helium, after passing through the water trap. During the cryo-transfer, the melt was agitated vigorously with the magnetic stirrer in order to ensure complete extraction of all the gases. The cryo-transfer process took 8 minutes and during the course of the transfer, the dipping tube was lowered twice into the liquid helium dewar to improve freeze-down of the gas by exposing a fresh metal surface. During these 8 minutes three getter sheets were loaded into a quartz glass wrapped with heating wire.
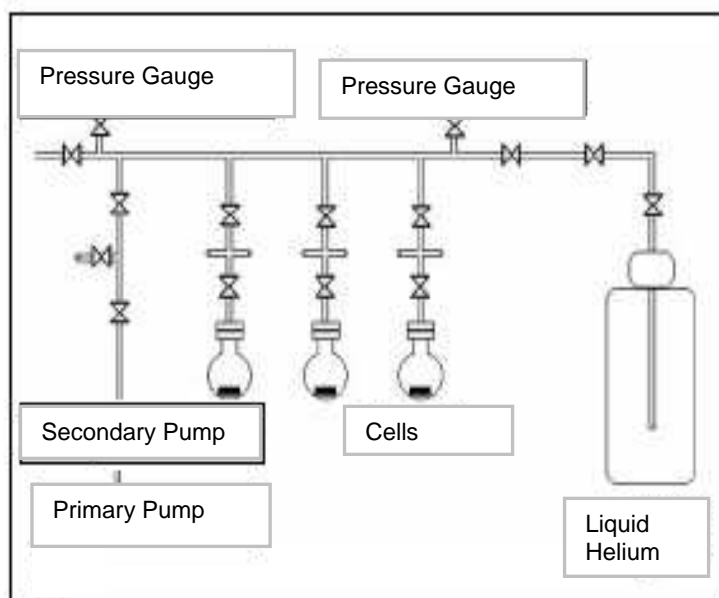
Figure 2.3.1: Schematic of the extraction line for gas extraction for δ^{40}Ar Analysis.

On completion of cryo-transfer, the stainless steel tube containing the sample was isolated from the line and attached to the getter pump. The next step in the extraction procedure was to remove N_2, O_2 and other reactive gases by exposing the sample gas to a Zr/Al (SAES) getter at high temperatures. Before the gettering process, the getter set-up was prepared by evacuating the room air from the system and heating the getter pump to 900°C to desorb any gaseous contaminants under vacuum. During the heating stage, an increase in pressure was observed. Once the pressure began to decrease, no further heat was applied. The entire getter preparation step took 10 minutes. After 10

minutes, the getter was isolated from the turbo pump and the nupro-valve on the dipping tube opened to allow sample to pass into the getter. The sample was gettered for 8 minutes at 900°C followed by an additional 2 minutes at 300°C to remove H_2 gas. Heating was then stopped and the sample was expanded into the entire extraction line. After noting the pressure in the line, the sample was frozen into a second pre-evacuated stainless steel tube dipped in dewar containing liquid helium for 3 minutes. An aliquot of Ultrahigh purity N_2 of pressure equal to 9.63 times the sample gas pressure in the extraction line was added to the sample and was frozen with the sample by pushing the dipping tube further into liquid helium dewar. The addition of nitrogen was to increase the sample volume. This is necessary in order to maintain an adequate pressure in the mass spectrometer capillaries. The reason for adding exactly 9.63 times the sample gas pressure was because the standard had similar Ar : N_2 composition, hence minimizing the "chemical slope" correction needed for varying Ar/N_2 ratios.

Once the N_2 was added, the tube was removed from the liquid helium and warmed to room temperature. The sample was then allowed to equilibrate in the tube for 40 minutes before analysis by mass spectrometry (see Section 2.3.2).

2.3.2 Analysis

Argon isotope ratios ($^{40}Ar/^{36}Ar$) were analysed on a Finnigan MAT 252 mass spectrometer. The sample and standard were expanded into their respective bellows and allowed to equilibrate. After equilibration period, an aliquot of sample and standard was isolated in their respective bellows and the bellow pressures were adjusted so that the pressures were matched as closely as possible. The side that had less quantity of the gas was started off with little high pressure so that during the run the pressure on both sides would equalise hence minimizing the pressure imbalance corrections. Each sample was measured twice on the instrument. Each sample 'measurement' consisted of a set of 32 measurements by the instrument (16 sample measurements and 16 reference measurements). $\delta Ar/N_2$ ratios were also analysed for each sample by peak jumping. At the end of the run, the ISODAT software was used to statistically analyse the data. The $\delta^{40}Ar$ value obtained was corrected for any pressure imbalances and varying $\delta Ar/N_2$ ratios.

-

2.4 Trace gas measurements

Trace gases (CF_4, C_2F_6, C_3F_8, $c-C_4F_8$, CHF_3, SF_6 and SF_5CF_3) were measured in firn air samples from EPICA Dronning Maud Land (EDML). Methane and CF_4 concentration during the last glacial period in ice cores from Berkner Island in Antarctica were also measured. The methodology for the analysis of atmospheric halocarbons is well established at UEA. A brief description is included below and further details can be found in Oram (1999) and Worton (2005).

2.4.1 Experimental instrumentation

Measurements were performed on a Waters[®] Micromass[®] AutoSpec Premier[TM] Mass Spectrometer, which is a double-focusing magnetic sector instrument providing high sensitivity, high resolution and low background noise. The tri-sector double focusing geometry design has an electric sector (electrostatic analyzer) on each side of the magnet. The first electric sector has de-magnifying optics that give high resolution and sensitivity whereas the second electric sector improves abundance sensitivity by filtering unwanted metastable ions and reducing background noise. The instrument uses electron ionization (EI) and samples were introduced after separation by gas chromatography (see below).

2.4.1.1 Gas chromatography

A general introduction to Gas Chromatography and the principles of Gas Chromatography-Mass Spectrometry (GC-MS) is beyond the scope of this thesis. A thorough explanation of the technique and its applications can be found in Heard (2006); Skoog *et al*., (1996).

In gas chromatography, a mobile phase, known as the carrier gas, transports components of a gas mixture to be separated through or over a stationary phase (column), separating them according to differences in the rates of migration. In this study a Hewlett Packard GC oven was used in a temperature programmed mode. Table 2.4.1 below shows the characteristics and the operating conditions used for the GC.

Table 2.4.1: Operating Conditions for Gas Chromatography

Column: Al$_2$O$_3$/KCL PLOT Capillary Column

Length = 50 m; Internal Diameter = 0.53 mm; Film thickness = 15 μm

Carrier Gas: He

Pressure: 5.02 KPa

Temperature Programme for the Oven:

Initial temperature: -30˚C

Initial time: 5.00 min

Temperature Ramps

Ramp #	Rate (˚C/min)	Temp (˚C)	Hold time (min)
1	8	50	0
2	20	120	0
3	10	180	60

2.4.1.2 Mass spectrometry

A short length of deactivated fused silica tubing was used to connect the outlet of the GC to the ion source of the MS. In the ion source, the gases eluting from the GC undergo electron ionisation and produce molecular ions and ion fragments of lower mass. For example, consider the ionisation of CF$_4$. The initial step is that the CF$_4$ molecule gains a high energy electron and produces the CF$_4^{+\bullet}$ molecular ion:

$$CF_4 + e^- \rightarrow CF_4^{+\bullet} + 2e^-$$
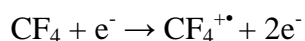
Due to sufficient excess energy the charged CF$_4^{+\bullet}$ ions may undergo further fragmentation into lower mass ions by losing one or more fluorine atoms. For example, the loss of one F atom will produce a CF$_3^+$ ion:

$$CF_4^{+\bullet} \rightarrow CF_3^+ + F^\bullet$$
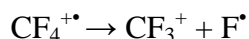
This would give a peak with mass 69 in the mass spectrum in addition to the molecular ion peak at mass 88. Similarly, peaks at masses 50 and 31 may also be present, due to CF$_2^+$ and CF$^+$ ions respectively. These ions are focused and accelerated towards the

magnetic sector by a series of electrostatic slits and then to a photomultiplier tube for detection.

Instrument operation and data acquisition were controlled by a Mass Lynx software package provided by Waters Micromass. The software includes a chromatographic peak detection and integration package for identification and quantification of peak areas. The Autospec mass spectrometer can be operated in two modes. In scan mode, the magnet is programmed to record over a specific, pre-selected mass range and this is useful for identifying unknown compounds. However, in scan mode, detector time is wasted in recording masses of little interest or in scanning parts of a spectrum where no ions are found. The detector response time is also consumed whilst the magnet jumps from one mass to the next. Quicker response times and better detection limits can be obtained using the Selective Ion recording (SIR) mode, in which the mass analyser is set to pass only ions of a particular m/z. Table 2.4.2 shows the SIR programme used in the analysis.

2.4.2 GC-MS analysis

2.4.2.1 Autospec tuning and mass calibration

Before analysis, the mass spectrometer needs to be tuned and mass calibrated every day. This was done by introducing hexadecane reference into the source and tuning the electron energy and emission current to maximise ionisation efficiency. The ion repeller and the focusing lenses were also adjusted to optimise peak shape and intensity. Once the maximum peak intensity was attained, the mass calibration procedure was carried out. In the mass calibration process, the accelerating voltage is scanned over the selected mass range and the major peaks matched with a reference file containing the known peaks of the hexadecane reference. This ensures that the peak positions and the masses are correctly identified. Each function in the SIR programme is calibrated separately. After mass calibration, it was necessary to ensure that there was sufficient hexadecane reference to act as a lock mass. A lock mass provides corrective measures for small changes in the peak position that can be caused by slight fluctuations in the magnetic field during SIR experiments. The fragment ions of hexadecane reference are different from those of the halocarbons normally analysed and therefore do not interfere with the analysis. As a result a mass corresponding to a hexadecane ion is included in

69

each SIR function as a lock mass (Table 2.4.2). The computer software makes sure that the top of the lock mass peak is monitored for maximum sensitivity. If the lock mass peak position changes from its position then the mass calibration is automatically corrected accordingly for all the masses monitored in that function.

2.4.2.2 Sample pre-concentration

Air samples were pre-concentrated to increase the sensitivity of the method. During the pre-concentration step, the main aim is to separate the compounds of interest from the bulk of the air sample (primarily N_2 and O_2) by cryogenic trapping. In this study, a 1/8" stainless steel tubing packed with Tenax^{TM} and immersed in liquid nitrogen (-196˚C) was used for sample pre-concentration. After pre-concentration, the analytes of interest were thermally desorbed using boiling water and injected onto the analytical column of the GC.

There is a possibility that sample breakthrough from the trap could occur during the pre-concentration step especially if large volumes are introduced. To establish the capacity of the trap, several analyses of different volumes of standard gas were carried out. Figure 2.4.1 shows that after 100ml of the sample, the area of the CF_4 peak is no longer linearly correlated with the volume of sample injected whereas for SF_6, peak area is linearly correlated with the volume of sample injected up to 200 ml of sample volume (See Figure 2.4.2). The reason for this is that CF_4 is the least well retained of the gases of interest on the trap and is consequently the first compound to be lost from the trap. If more sample volume is pre-concentrated into the trap then CF_4 is "pushed out" from the other end and this result in part of the sample being lost.

Table 2.4.2: Experimental SIR programme used in the GC-MS analysis of fluorinated compounds in the EDML firn air

Function #	Start Time mins	End Time mins	Compound	Retention Time mins	Monitored m/z	Monitored Ion
1	0.00	5.00	CF_4	2.75	68.9952	CF_3^+
			$C_{16}H_{34}$	Lock mass	71.0861	
2	5.00	13.00	SF_6	7.10	126.9641	SF_5^+
			C_2F_6	7.20	118.9920	$C_2F_5^+$
			CFC – 13	9.80	86.9627	$CClF_2^+$
			$C_{16}H_{34}$	Lock mass	85.1017	$C_6H_{14}^+$
3	13.00	18.60	C_3F_8	14.20	68.9952	CF_3^+
			SF_5CF_3	15.50	88.9673	SF_3^+
			CFC-115	16.10	68.9952	CF_3^+
			H-1301	16.20	78.9138	$^{79}Br^+$
			HFC-23	17.35	68.9952	CF_3^+
			$C_{16}H_{34}$	Lock mass	71.0861	
4	18.60	21.00	c-C_4F_8	20.70	68.9952	CF_3^+
			$C_{16}H_{34}$	Lock mass	71.0861	

Linearity test for CF$_4$ trapping
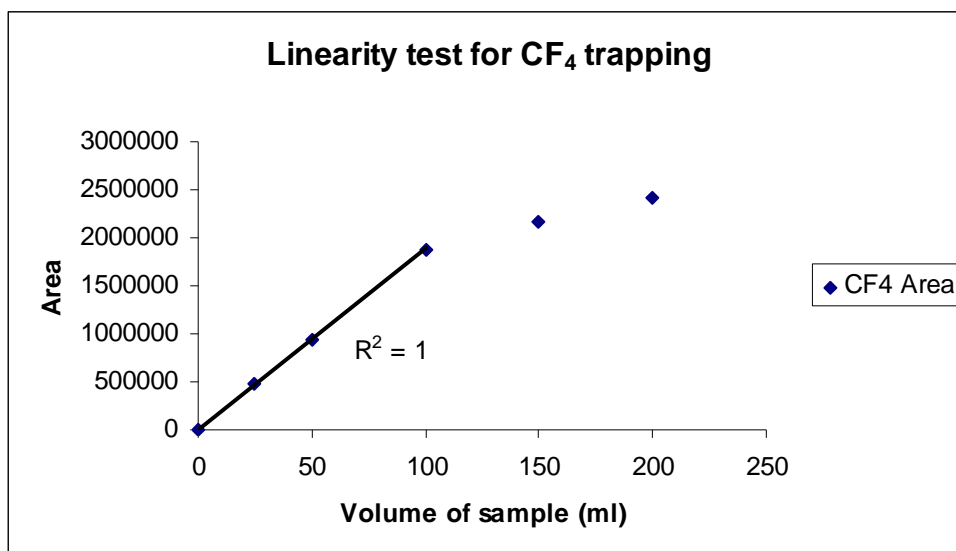
Figure 2.4.1: Sampling linearity test for CF$_4$ trapping. The linear correlation ($r^2 = 1$) between volumes of the sample and the area response is maintained until at least 100 ml of volume sample trapped.

Linearity test for SF$_6$ trapping
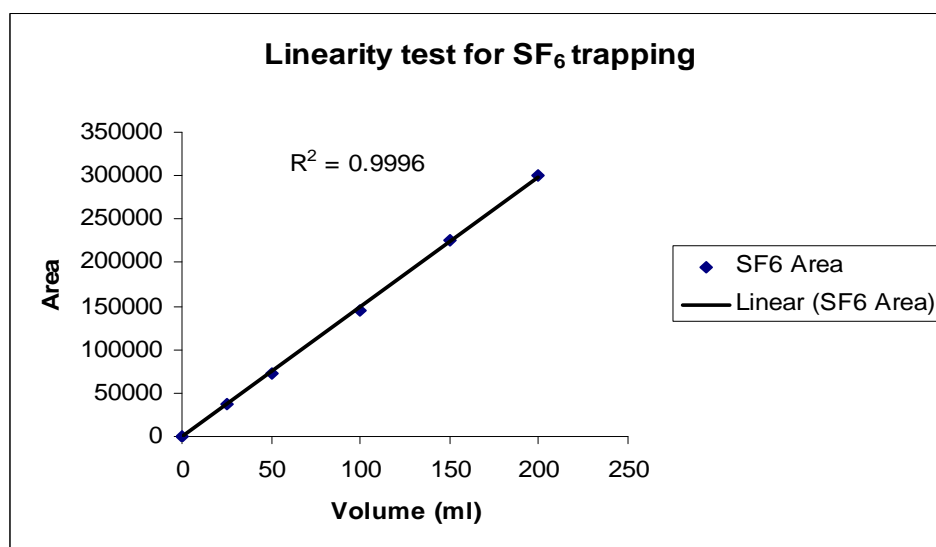
Figure 2.4.2: Sampling linearity test for SF$_6$ trapping

2.4.2.3 Manual inlet system

A schematic of the manual inlet system used for GC-MS analysis during this work is shown in Figure 2.4.3. The inlet system consists of Nupro valves used to isolate the inlet line from the vacuum, glass tubing packed with magnesium perchlorate to remove

Figure 2.4.3: Schematic diagram of the inlet and pre-concentration set-up for GC-MS analysis

V9

Column

Carrier gas in

To detector

6 Port Valve

PG

1L glass void volume

Needle valve

Baratron

Standard

V6

V7

V8

V5

V2

MPC Trap

Tenax pre-concentration trap

V4

V3

To Vacuum

To Vacuum

To Vacuum

Liquid Nitrogen

= Nupro Valve

72

PG = Pressure Gauge

Sample

MPC = Magnesium PerChlorate
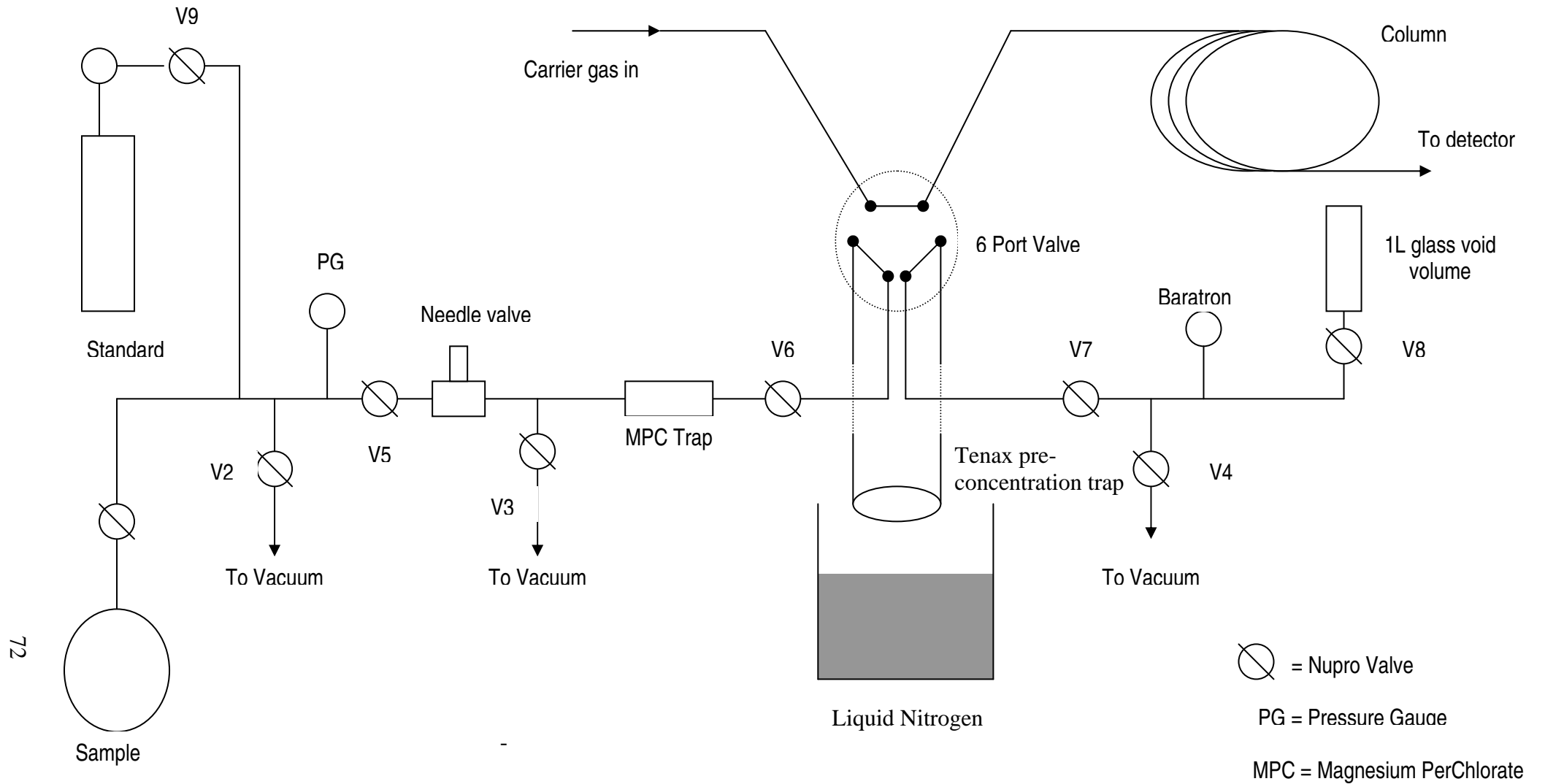
any water vapour from the samples, a piece of 1/8" stainless steel tubing packed with Tenax[TM] for sample pre-concentration and a manually operated Valco 6 port Valve (VICI) for injecting samples into the GC.

The flowrate of sample through the pre-concentration trap (<10 ml min^{-1}) was controlled by a needle valve. A flowrate of less than 10 ml min^{-1} is important in order to achieve efficient trapping and to avoid sample breakthrough. The ballast volume located downstream of the sampling loop had an approximate volume of 1 L. The pressure was measured downstream by a baratron and the temperature of the ballast volume was recorded. The ballast volume prevented any back diffusion of lab air into the inlet system and also made it possible to measure the sample volume.

2.4.2.4 Sample analysis

Once the instrument was tuned and calibrated, the inlet line and pressure gauge on the standard tank was evacuated. The pressure gauge and the inlet line were then filled with standard and then re-evacuated. This step was repeated three times to remove any contaminants that had built up in the pressure gauge. The sample pre-concentration step, as described above, was carried out with the sample flowrate controlled by a Nupro needle valve. Once the desired sample volume was collected then the pre-concentration trap was isolated from the sample flow. The residual air (non-trapped air) in the pre-concentration trap was then evacuated and the sample injected onto the GC column. Soon after the switching the Valco valve into the sample injection position, the liquid nitrogen dewar was swapped with a dewar containing hot boiling water to desorb the analytes from the Tenax[TM] pre-concentration trap. After sample injection, the entire line including the ballast volume was evacuated.

At the beginning of each analysis day, a long term air standard (ALM-39753) held at UEA was analysed several times to allow for the instrument to settle down. Once the instrument response was stable, a real air sample was analysed two or three times in succession with the working standard analysed between samples. Peak areas were used to quantify each compound of interest in a sample. Data were initially calculated as a relative ratio to the average area of the working standard, and then multiplied by the concentration of that compound in the working standard (See Section 2.4.5 below).

During the day the instrument response factor may change (instrumental drift) and therefore the same standard may record slight variations in area response values. Therefore data for every sample needed to be corrected for this instrumental drift. The drift correction was applied by fitting a straight line to all the peak areas of the working standard and sample peak areas were normalised to this line. The precision of replicate measurements of the same sample was further improved by correcting the peak areas for differences in sample volumes. A correction for the sample volume analysed was made for every sample analysed.

2.4.2.5 Peak identification

The analysis of trace gases in firn air, archive air and in background air is a well established at UEA. Peak identification was made based on retention time and the ion being monitored in each SIR function (See Table 2.4.2). Below are the typical chromatograms of a CF_4 peak (Figure 2.4.4), C_2F_6 and SF_6 (Figure 2.4.5), C_3F_8, SF_5CF_3 and CHF_3 (Figure 2.4.6) and c-C_4F_8 (Figure 2.4.7).

74
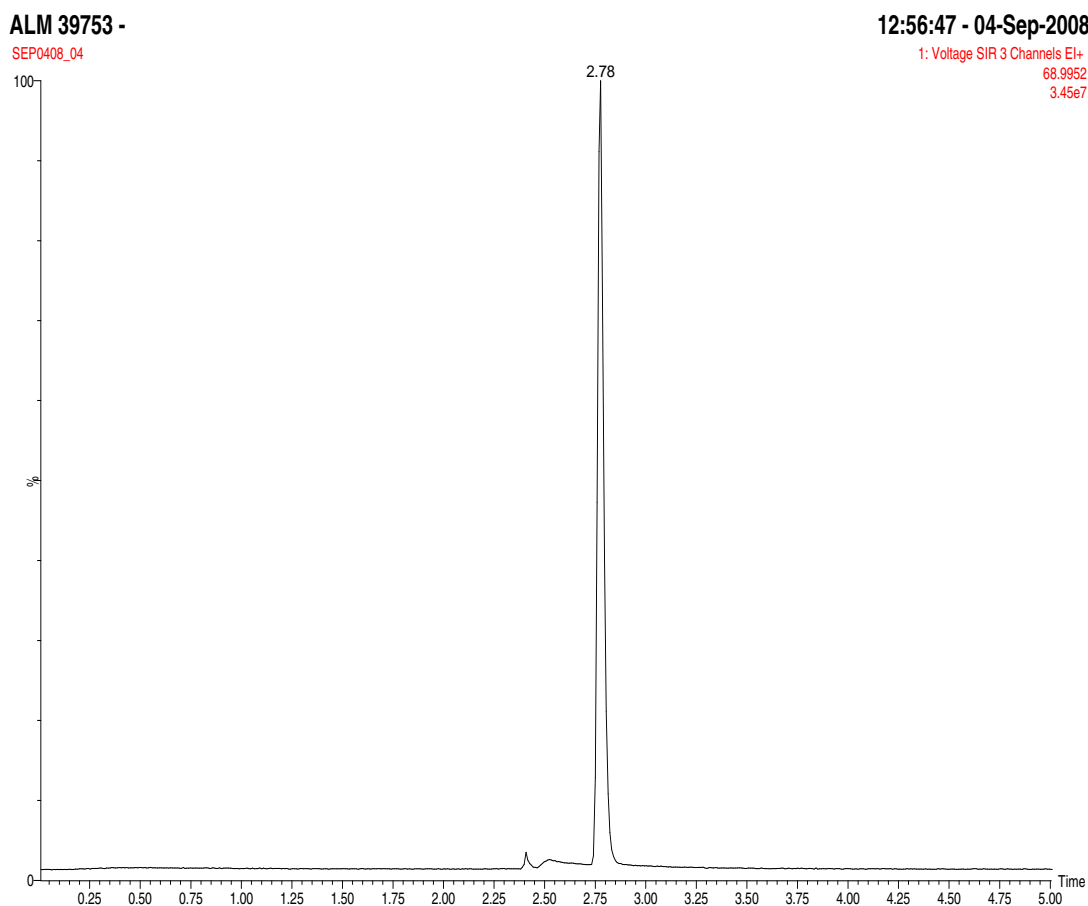
Figure 2.4.4: A typical chromatogram of CF$_4$ peak monitored on m/z = 68.9952 in 100 ml of ALM 39753 standard air.
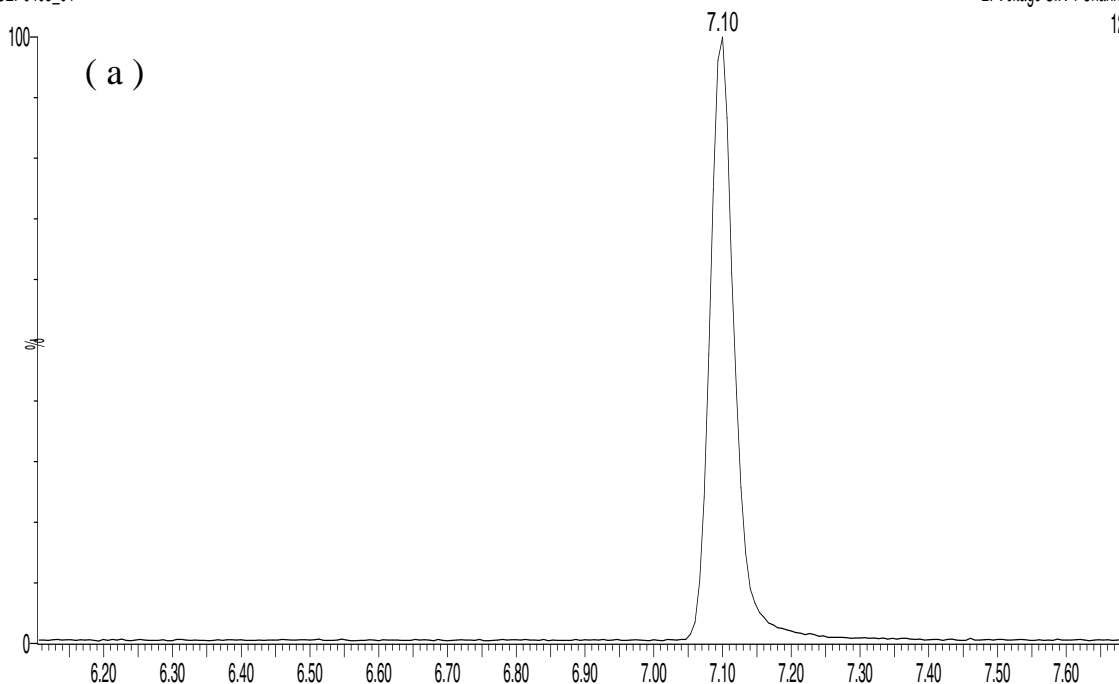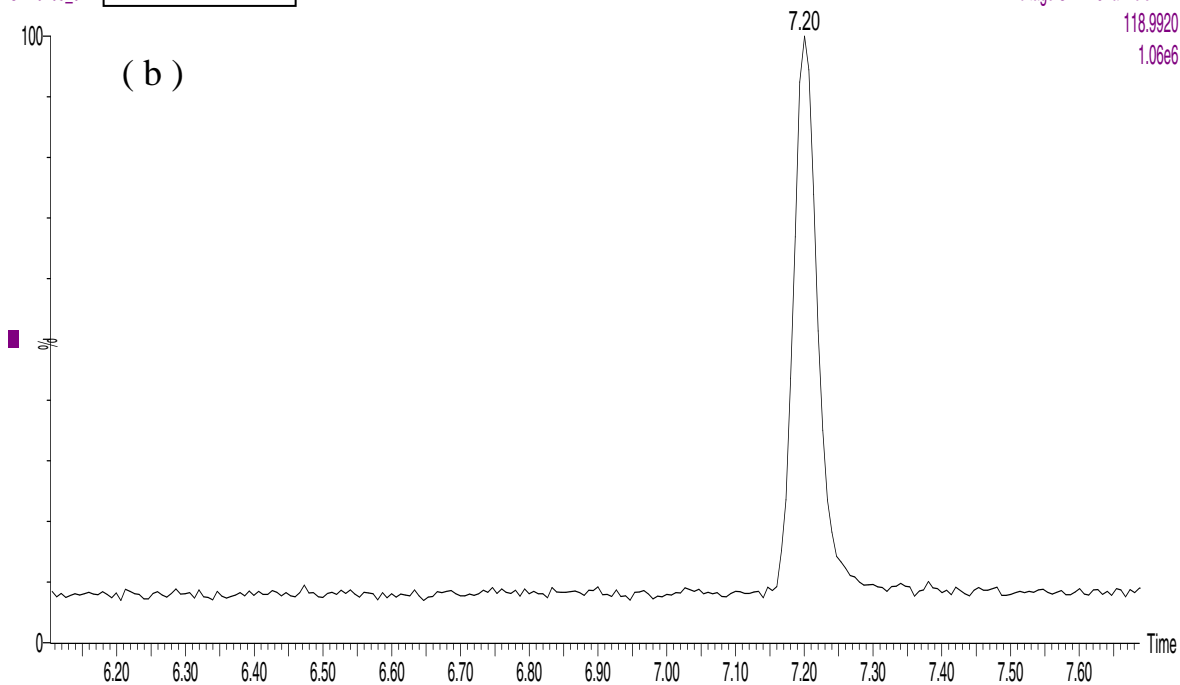
Figure 2.4.5: (a) Typical chromatogram of SF$_6$ monitored on m/z = 126.9641 **and (b)** typical chromatogram of C$_2$F$_6$ monitored on m/z = 118.9920 measured in 100 ml of ALM 39753 standard air.
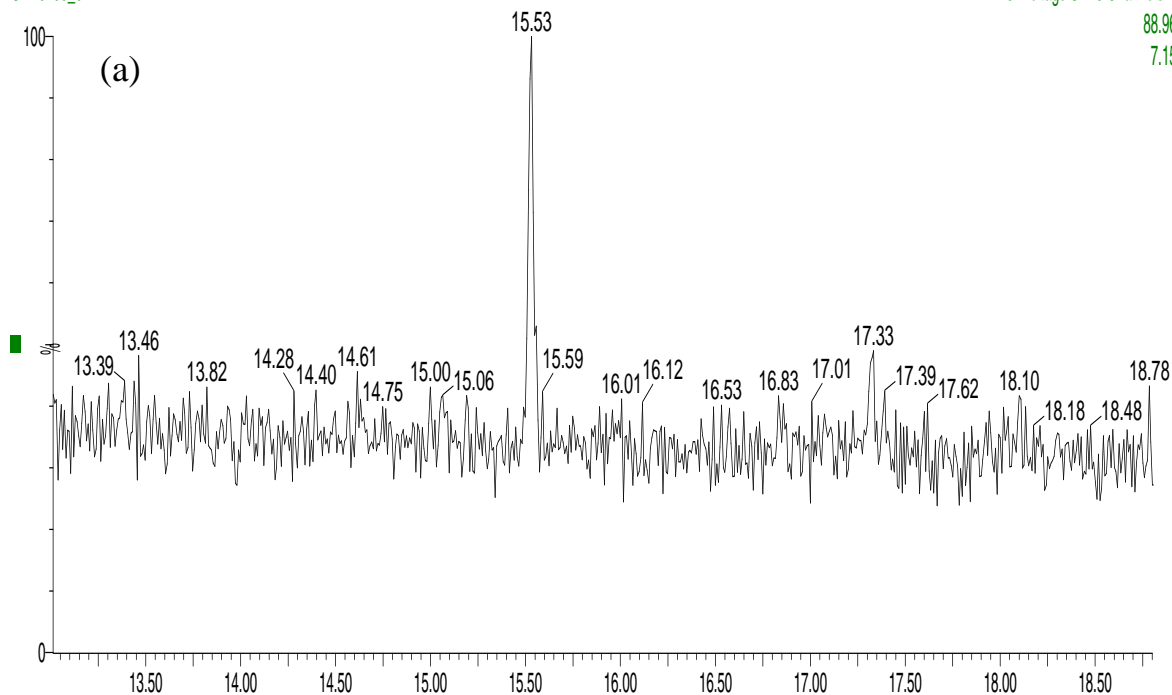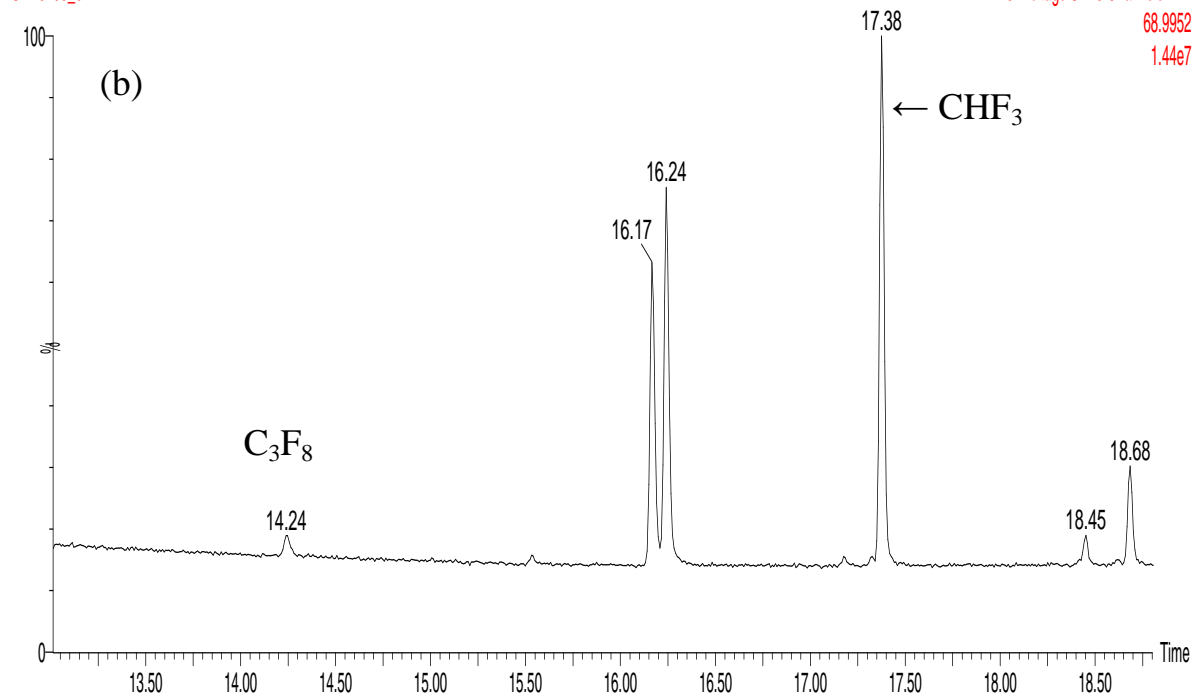
Figure 2.4.6: (a) A typical chromatogram of SF$_5$CF$_3$ monitored on m/z = 88.9673 **and** **(b)** typical chromatogram of C$_3$F$_8$ and CHF$_3$ monitored on m/z = 68.9952.

ALM39753 -
FEB1208_01

09:43:55 - 12-Feb-2008
4: Voltage SIR 3 Channels EI+
99.9936
4.09e5
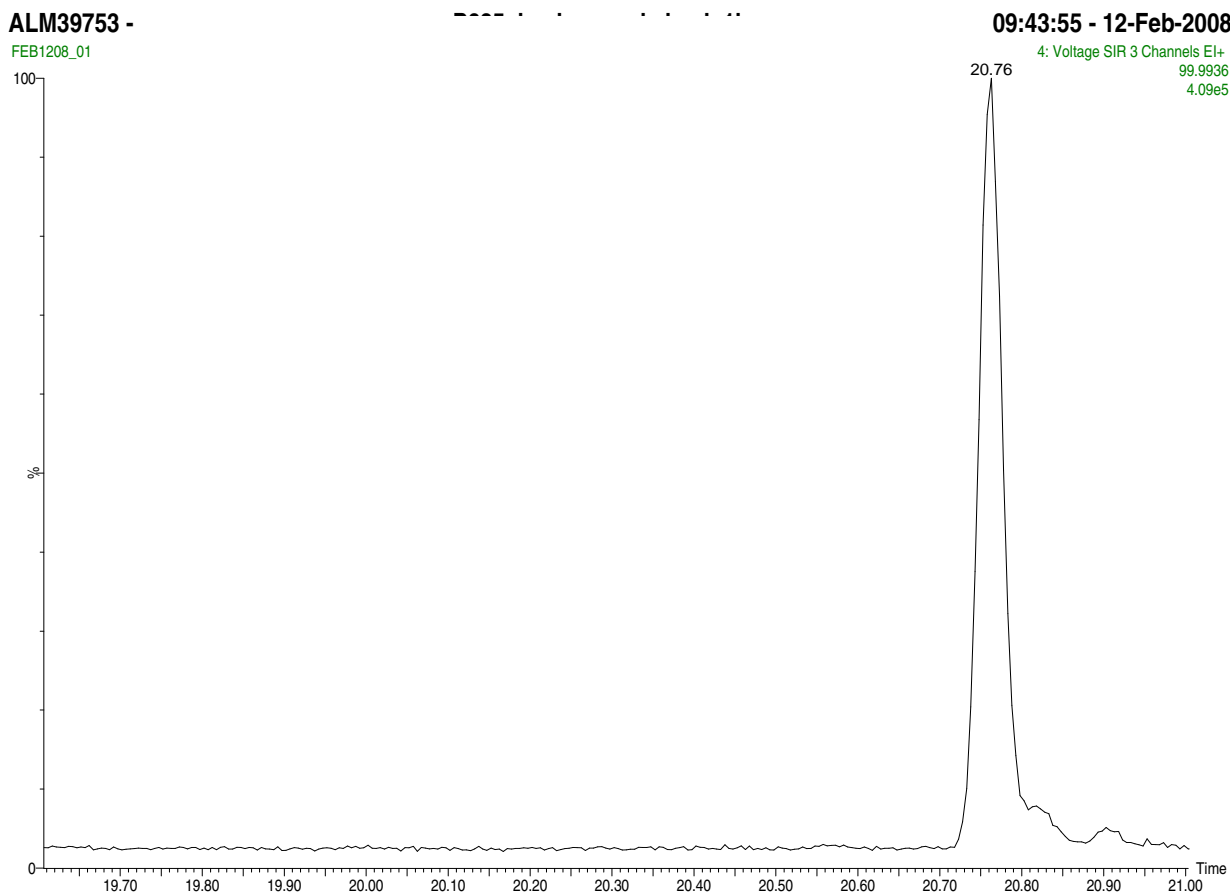
Figure 2.4.7: A typical chromatogram of c-C_4F_8 monitored on m/z = 99.9935 in 100 ml of ALM 39753 standard air.

2.4.3 Analytical precision

The analytical precision was calculated as one standard deviation (1σ) of replicate analyses of each air sample. The mean analytical precision based on the average standard deviation of volume and drift corrected replicate analyses for each compound of interest are shown in Table 2.4.3.

77

Table 2.4.3: Analytical precision of individual species studied in this project.

Compound	Precision (%)
CF_4	0.9
C_2F_6	2.1
C_3F_8	1.8
$c\text{-}C_4F_8$	0.9
HFC-23	1.2
SF_6	0.8
SF_5CF_3	2.2

2.4.4 Blanks

System blanks were run to check for any possibility of sample contamination due to leaks in the system or from the carrier gas. Blank runs were performed by pre-concentrating 100 ml of aliquots of the helium carrier gas. The peaks of the analytes of interest were completely absent in the blank chromatograms. Vacuum blanks were performed to asses the cleanliness of the inlet system, without the need for pre-concentrating helium. The sample loop was immersed in liquid nitrogen for the same length of time used to pre-concentrate 100 ml of air sample, before injection onto the column in the usual way. The absence of any of the analyte peaks of interest in the vacuum blanks eliminate the possibility of any leaks in the inlet system and any sources of contamination from the various manifold components such as the valves, tubing etc.

2.4.5 Calibration

All measurements were referenced to one working standard (ALM-39753) contained in a pressurised Aculife-treated aluminium cylinder. This standard was purchased from the National Oceanic and Atmospheric Administration (NOAA) and consists of a real air sample collected at Niwot Ridge, Colorado (40ºN) in 1994. In addition, the NOAA standard was pre-calibrated at NOAA-CMDL (Climate Monitoring and Diagnostic laboratory) for a number of compounds enabling us to report our values on the NOAA calibration scale. For example, SF_6 values reported in this study are on NOAA-CMDL

calibration scale. Most of the compounds studied here were calibrated in ALM-39753 in previous studies and the calibration procedures are described therewithin. These include: HFC-23 (Oram, 1999), CF_4 and C_2F_6 (Worton *et al*., 2007), c-C_4F_8 (Lee, 1994) and SF_5CF_3 (Sturges *et al*., 2000). The mixing ratios of various halocarbons in ALM-39753 used for calibration are shown in Table 2.4.4.

Table 2.4.4: Concentration of species of interest in ALM 39753 working standard

Compound	Mixing ratio (ppt)
CF_4	72.00
C_2F_6	2.23
C_3F_8	0.30[1]
c-C_4F_8	1.13
HFC-23	22.50
SF_6	3.23
SF_5CF_3	0.094

[1]**The concentration of C_3F_8 in ALM 39753 was not calibrated but was on a UEA preliminary scale.**

2.4.6 Detection limit

The limit of detection is the lowest concentration that can be determined by an analytical method. By convention, detection limit is often defined as the analyte concentration that has a signal three times the standard deviation of the blank/background signal (i.e. a signal-to-noise ratio of 3:1). The Autospec automatically calculates the signal-to-noise ratio and the detection limits were calculated from this value. Table 2.4.5 shows the typical value of the detection limit for each individual species. The detection limit varies, depending on the compound being analysed, the choice of monitored ion, background noise, the ionising conditions and the volume of air sample analysed.

Table 2.4.5: The detection limits of the individual compounds based on 100 ml of standard air analysed on 21/02/08.

Compound	Method Detection Limit (ppt)
CF_4	0.07
C_2F_6	0.03
C_3F_8	0.04
$c-C_4F_8$	0.007
HFC-23	0.01
SF_6	0.004
SF_5CF_3	0.006

2.5 CF_4 Analysis in ice cores

An extraction technique for CF_4 measurements from gas trapped in ice cores was developed in this study. There is only one previously published work (Harnisch *et al*., 1996) in which CF_4 data from ice core samples have been presented and few details of the extraction method used in that study are given. In this study, a dry extraction technique was used whereas Harnisch *et al*., 1996) used wet extraction technique. Since CF_4 is sparingly soluble in water, wet extraction technique was avoided.

2.5.1 Extraction

The outer surfaces of the ice core samples were trimmed to remove any contaminants introduced during drilling and storage in cold rooms. The samples were weighed and approximately 180 g of sample cut into smaller pieces so that it could be packed into the pre-chilled perforated cylinder or "cheese grater" (see Figure 2.5.1) in the cold room. This perforated metal cylinder packed with samples was carefully lowered into another stainless steel metal pot and tightly sealed. To make a good vacuum seal, pure indium wire was used in between the two metal flanges. Indium wire was used because of its ductile properties and because the sealing properties of the indium are not affected by

cold temperatures compared to Viton^{TM}, which loses its elasticity at sub zero temperatures. After sealing the sample in the extraction vessel, the vessel was connected to the extraction line and evacuated.

Figure 2.5.1: Shows the extraction vessel used in milling the ice core to release the trapped air bubbles.

The ice sample was pumped for 10 minutes under vacuum. The extraction vessel was then isolated from the vacuum pump and leak tested. If there was a leak then the indium wire seal was removed and replaced with new indium wire and the vessel was resealed. Once it was established that the extraction vessel was leak proof, the Nupro valve on the extraction vessel was closed and the vessel containing the sample removed from the extraction line.

The extraction vessel was placed onto a milling device in -25 ° C cold room and shaken slowly at a rotating speed of 5 Hz for 5 minutes and then the speed was increased slowly to 8 Hz. After 35 minutes, about 98% of the sample was grated into fine "snow", the air trapped in the bubbly ice having been released into the headspace of the extraction vessel. The extraction vessel was then removed from the milling device and attached to the extraction line (See Figure 2.5.2).

The extraction line was maintained at very high vacuum using a turbo-molecular pump (Pfeiffer Vacuum). The extraction line consists of a rotary pump, a pressure gauge, a water trap immersed in liquid N_2/ethanol slurry (-80 ºC), a turbo-molecular pump and a stainless steel tubing filled with activated charcoal for trapping the gas samples. While

the ice was being pulverized, the stainless steel tubing packed with activated charcoal was prepared for sample collection. The tubing was evacuated and then after few minutes of pumping on the high vacuum pump, the tubing was heated with a hot air gun to desorb any remaining gases from the activated charcoal. The readings on the high vacuum pump would initially increase and then begin to decrease. When the readings began to decrease consistently, the heating was stopped and the stainless steel tubing allowed to cool to room temperature.

Once the extraction line and the stainless steel tubing for sample collection were prepared, the sample was initially introduced only into the extraction line and the water trap. The sample was then gradually introduced to the rest of the extraction line. This procedure ensures sufficient residence time of the sample in the water trap for efficient removal of water vapour. Finally the sample was introduced into the stainless steel tubing packed with activated charcoal. The stainless steel tubing was immersed into a dewar containing liquid nitrogen for cryo-trapping. The sample was collected within 15 minutes and when the sample was isolated from the line, the residual pressure was less than 1×10^{-3} mbars.
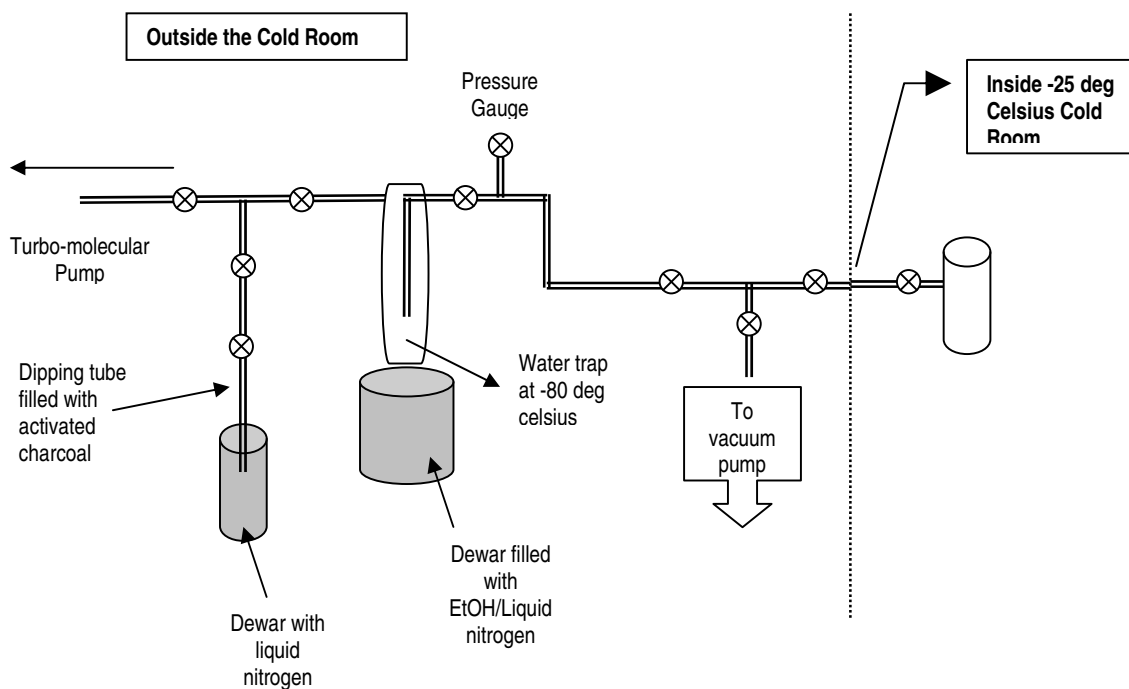
Figure 2.5.2: Schematic diagram for CF_4 gas extraction line.

2.5.2 Sample analysis

Once the sample was frozen onto the activated charcoal at liquid nitrogen temperature, the stainless steel tube was isolated and detached from the extraction line. The tubing was attached to the manifold of the inlet system of the GC-MS described earlier. A hot air gun was used to heat the tubing to desorb the trapped gases from the activated charcoal. The stainless steel tubing containing the sample was heated for 5 – 8 minutes and then placed in a dewar of boiling water just before introduction of the sample into the inlet and pre-concentration on the Tenax^{TM} (as described in Section 2.4.2.3). The pre-concentration step takes about 8 – 10 minutes. During this step, it is critical that the temperature of the stainless steel tubing does not reach room temperature and therefore the stainless steel tube was kept near the boiling point of water. When the activated charcoal approached room temperature, it was observed that some of the gases were adsorbed back onto the activated charcoal resulting in incomplete extraction and subsequent loss of some component of the sample. Typically, 15 ml of each air sample was pre-concentrated and injected onto the GC column and the same SIR method was used for analysis as described previously (see Table 2.4.2). The whole suite of fluorinated compounds were analysed for each ice core sample as a test to ensure that the sample was not contaminated during extraction. This is possible since most of fluorinated compounds are man-made and do not exist in ancient air from ice cores. Any samples that showed high levels of any of the modern man-made fluorinated gases had clearly become contaminated and were discarded. During the course of the measurement period only two samples were rejected on the basis of high levels of SF_6 and CFC-12. The results were treated and analysed in the same way as the other trace gases as discussed in Section 2.4.2.4 . A typical chromatogram of CF_4 from an ice extract is shown below (Figure 2.5.3).

B550 - Berkner Ice Core Sample Bag #550
OCT1608_07

16:19:14 - 16-Oct-2008
1: Voltage SIR 3 Channels EI+
68.9952
7.32e6
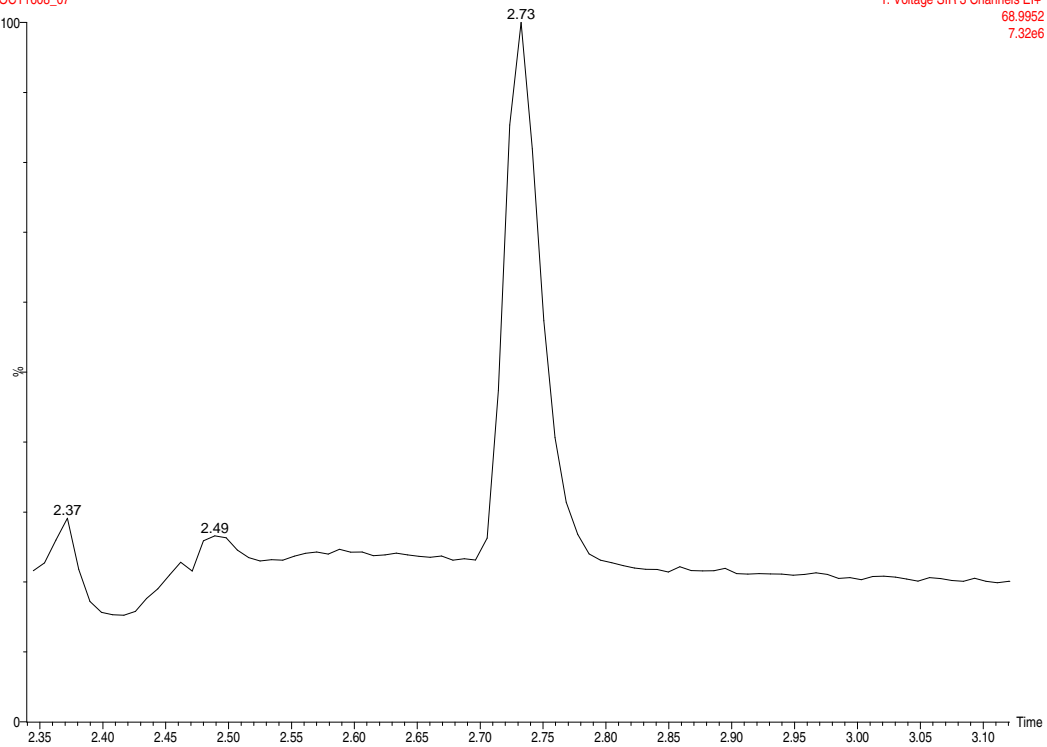
Figure 2.5.3: A typical chromatogram of CF_4 peak in ~ 15 ml of air extracted from Berkner Island ice core.

2.5.3 Simulated ice core extraction with the EDML firn air standard

Before extracting real ice samples, the ice core extraction technique was simulated with the EDML firn air of known CF_4 concentration. This test was designed to test the suitability of the developed extraction and trapping method for CF_4 measurements. The ice was crushed and then evacuated so that the ice extraction vessel only contained ground ice. About 50 ml of the EDML firn air (from between depths of 92.75 m and 20.12 m) was expanded into the extraction line from the sample storage canisters. The firn air samples were trapped and measured as described above. Table 2.5.1 shows that the data obtained from the simulated ice core extraction is in good agreement with the CF_4 concentration in the firn air measured directly from the sample storage canisters. The reproducibility of the EDML firn air

84

standard used to simulate ice core extraction proves that the sample was not contaminated during extraction due to leaks or from the components of the manifold and also demonstrates the efficiency of the activated charcoal as an absorbent for CF_4 analysis.

Table 2.5.1: Ice core extraction method simulated with the EDML firn air.

EDML Firn Air sample	[CF_4] measured in firn air (ppt)	[CF_4] for ice core extraction simulations (ppt)
20.12 m	78.5 ± 2.1	79.5 ± 1.2[a]
92.75 m	37.4 ± 0.3	37.4 ± 1.5

a: the error is based on the standard deviation of two aliquots of each sample that were separately simulated for ice core extractions.

2.5.4 System Blanks

To eliminate any artefacts in measurements due to the extraction, Oxygen Free Nitrogen (OFN) gas was expanded into the extraction line and the extraction vessel containing snow (crushed ice), and was milled for 30 minutes, trapped and measured in exactly the same way as the ice core extraction. The concentration of CF_4 measured in two OFN transfers had an average value of 0.14 ppt and is within the error limit of the measurements. The minute amount of CF_4 in the OFN could be due to residual CF_4 present in the extraction vessel from the previous ice sample or could be due to some very small leaks in the extraction system. As usual He blanks were also performed to investigate any contaminants from the inlet manifold or leaks in the inlet system, which could affect the CF_4 results. Figures 2.5.4 and 2.5.5 shows the chromatogram for the OFN blank run and He blank run respectively. The CF_4 peak was absent in the He blank run whereas a very small peak was observed in the OFN transfer blank.

N2 BLANK -
OCT3108_08
P685, background check 1k res
19:08:29 - 31-Oct-2008
1: Voltage SIR 3 Channels EI+
68.9952
2.48e6
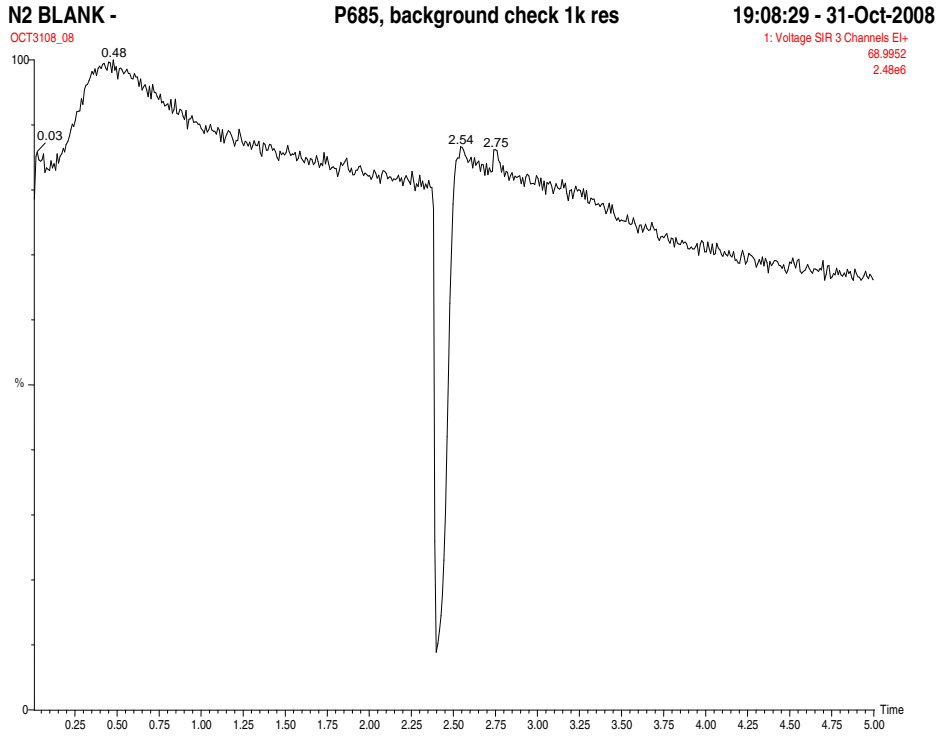
Figure 2.5.4: Chromatogram of CF_4 peak in 25 ml of OFN transfer from the extraction method.

He BLANK -
OCT2908_10
P685, background check 1k res
21:05:21 - 29-Oct-2008
1: Voltage SIR 3 Channels EI+
68.9952
1.17e8
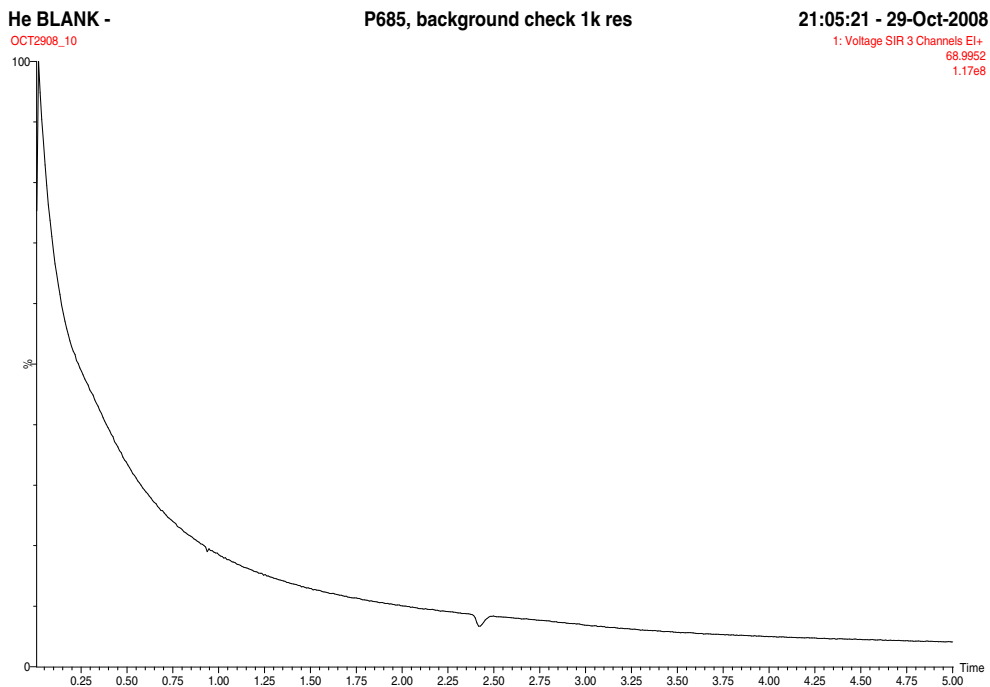
Figure 2.5.5: Absence of CF_4 peak in the He blank run. A 50 ml sample was trapped for Blank run and as a result has a greater sensitivity than the run shown in Figure 2.5.1.

2.6 Methane Analysis in Berkner Island Ice Core

Methane measurements were performed at Laboratoire de Glaciologie et Géophysique de l'Environment in Grenoble, France. These measurements were possible due to collaboration with Jerome Chapellaz. Approximately 65 samples were measured across the depth of 693 – 750 m. A melt-refreeze technique was used to extract the trapped gases from the ice core samples and measurements made on a GC (Varian 3300) with a Flame Ionization Detector (FID). The GC was equipped with a Porapak N column using high purity helium (99.9995%) as the carrier gas. An overview of the methane measurement methodology is given here. A full description of the extraction line and the methodology can be found in Chapellaz *et al*. (1990) and Raynaud *et al*. (1988).

Approximately 40 g of inner ice-core sample was placed in a pre-chilled glass cell and sealed with Viton O-rings. A conductive paste was applied to the bottom of all the 11 cells, which were then quickly loaded onto individual ports on the metal support tray with tripods. A liquid nitrogen/ethanol bath was raised manually so that the tripods were in the bath and cooled the glass cells. The 11 glass cells were then attached to the extraction line and the contemporary air evacuated whilst the temperature was maintained below -20 ℃. Each glass cell was checked for leaks and if any were found then that particular cell was detached from the extraction line and placed in the cold room to be used in the next extraction. Once all the cells were leak tight, then the rest of the automated extraction and measurement procedure was initiated. This procedure involved 5 steps:

Step 1: Pumping
The metal stands supporting the glass cells are immersed in liquid nitrogen/ethanol bath at -60 ℃. The sample was pumped for 30 minutes without any melting of the ice samples.

Step 2: Melting of ice samples

After 30 minutes the bath was automatically lowered and the resistors were turned on to heat the metal tripods and the glass cells to 80 ℃. The ice samples started to melt and after 15 minutes each cell was closely examined to ensure complete melting of the ice. Once all the ice in the cell had melted, heating was stopped manually for that particular cell. This was done to prevent the melt water boiling and increasing the water vapour content of the sample.

Step 3: Refreezing of the melt water

Once the ice in all the cells was melted, the liquid nitrogen and ethanol bath was again lifted and the metal tripods immersed in the bath refreezing the melt water. The entire procedure took about 2 hours before the first sample was ready to inject onto the GC.

Step 4: Running calibration standard

About 1 hour into Step 3, 17 runs of the calibration standard were performed. The [CH_4] of the standard was 499 ppb and peak areas of the standard runs were integrated. Comparison of the methane peaks from the ice core samples with the peaks from the calibration standard enabled quantification of methane in the air extracted from the ice core samples.

Step 5: Sample Analysis

An aliquot of sample air was expanded into the extraction line. The pressure of the sample air in the extraction line was measured by a baratron before the sample was injected onto the GC column. The pressure gives an indication of the volume of the sample injected and enables corrections to be made accordingly during the data processing. Each cell was measured in turn and when all were measured once, the measurements were repeated for each cell. Hence each sample was measured twice, with a delay of several minutes between the two runs. This method of analysing the cells means that it should be possible to detect any micro-leaks that may have occurred during the measurements. If the standard deviation on the sample measurement was poor then the data were rejected.

Chapter 3: Isotopic composition of N₂ gas trapped In Berkner Island ice cores during the MIS 3 period

3.1 Introduction

3.2 Berkner Island site description & ice core chronology

3.3 Water isotopes: δD and δ¹⁸O

3.4 δ¹⁵N Data: Timing and structure of the events

3.5 Temperature reconstructions for AIM 8 and AIM 12 events

3.6 Summary

3.1 Introduction

Isotopic compositions of ice and gases trapped in ice cores provide valuable information about past climates. The water isotopes (δD and $\delta^{18}O$) of ice provide the classical palaeo-thermometer but it has been proven by numerous studies that this palaeo-thermometer, which is dependent on the modern spatial $\delta^{18}O$ – temperature relationship, is not valid during the glacial period at Greenland sites. The classical palaeo-thermometer generally underestimates the magnitude of temperature change between glacial and interglacial periods in Greenland and in the Antarctic, although the underestimate is not as marked in the latter. Measuring $\delta^{15}N$ in the trapped air provides an independent means of calibrating the classical palaeo-thermometer. However, whilst the $\delta^{15}N$ palaeo-thermometry technique is suitable for large abrupt climate changes like DO events, it is generally not considered applicable for measuring smaller, slower temperature changes and has not been applied to interpret the Antarctic warming events during MIS 3 period. Nevertheless Berkner Island, which is a coastal site on the Weddell Sea and is facing the Southern Atlantic Ocean, offers the opportunity to test the $\delta^{15}N$ palaeo-thermometer on a site that differs from more in-land sites and which could experience different climate regimes.

In this project a high precision $\delta^{15}N$ method was developed at UEA with the specific aim of identifying small signals in the Antarctic, and was applied to two Antarctic warming events, the Antarctic Isotope Maximum (AIM) 12 and the AIM 8 events. It is believed to be challenging to obtain a signal in $\delta^{15}N$ for the DO counterparts in Antarctic and even more difficult to obtain a thermal isotopic anomaly in $\delta^{15}N$ (Caillon *et* al., 2001; Blunier *et* al., 2007). The information regarding the site description, derivation of the ice core chronology and a brief description of the δD profile from the Berkner Island ice core are discussed initially in this chapter. However, the principal focus is the interpretation of the $\delta^{15}N$ data obtained from 27 kyr BP to 50 kyr BP. The $\delta^{15}N$ data were used in the calculation of Δage (ice age – gas age difference) and Δdepth (change in depth for the same signal in ice phase and in gas phase), which provided additional constraints on the Berkner Island ice core chronology. The approaches that utilise the $\delta^{15}N$ dataset in the temperature reconstructions across the two warming events are discussed in detail, highlighting the limitations of the current measurements and the modelling techniques.

3.2 Berkner Island site description & Ice Core chronology

3.2.1 Site description

Berkner Island is located in the Weddell Sea, embedded between the Ronne and Filchner Ice Shelves and is the largest island of Antarctica (Fig. 3.2.1). It holds an ice sheet which is independent of the Antarctica at present and has two domes approximately 140 km apart: the north dome called Reinwarthhöhe at 720 m above sea level (a.s.l)., and the south dome called Thyssenhöhe at 890 m a.s.l. The domes are separated by a trough, known as the McCarthy Inlet. The deep Berkner ice core was drilled close to the summit of the Southern Dome over three austral summer seasons by a joint British/French project. The three principal motivations for deep drilling at Berkner Island were:

1. To provide a new climate record of the deglaciation period from a coastal site facing the Southern Atlantic Ocean that could provide further insights into the spatial pattern of the phasing of the Northern and Southern hemisphere climate.

2. The Weddell sea is a major contributor for the deep Antarctic Bottom Water (AABW) in the thermo-haline circulation. Therefore Berkner Island could provide knowledge about the evolving climate of the source region for cold AABW since the Last Glacial maximum (LGM), the extent of the ice sheet and the timing of its withdrawal from the continental-shelf break, which are relevant in the modelling of the palaeo-ocean circulation system.

3. To understand glaciological issues regarding the ice sheet thickness, ice flow and volume in the Weddell Sea at the LGM, the timing of the retreat of the ice and the point at which Berkner Island became an independent ice cap.

The deep Berkner Island ice core drilling site was in the vicinity of the South Dome. The airborne radio-echo sounding measurements through the ice cap indicated a relatively flat and horizontal bed. The over-snow radar measurements confirmed an undisturbed stratigraphic column through the ice thickness, ruling out any distortion in the layers due to ice flow or any discontinuity in the age-depth profile (Mulvaney *et* al., 2007). The success of the drilling project and the technical details are provided in Mulvaney *et* al. (2007). The

site specific parameters for the drilling site are given in Table 3.1. Ice cores were drilled to the bedrock and the deepest core contained basal sediments.
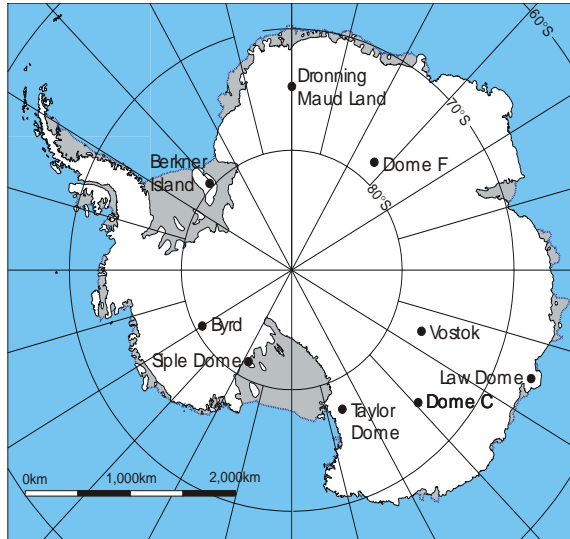
Figure 3.2.1: Map of Antarctica showing Berkner Island in relation to other deep ice core drilling sites in Antarctica.

Table 3.1*:* Site specific parameters for Berkner Island

Location	79˚34'S 45˚42'W
Altitude	890 m
Accumulation	130 kg m^{-2} a^{-1}
10 m temperature	- 26.5˚C
Basal temperature	-11.6 ˚C
Ice thickness	948 ± 2 m

Ice sheet modelling suggests that the ice sheet on Berkner Island increased and then decreased in altitude from the last glacial to the present day altitude (Huybrechts 2002). Total air volume content measured in cm^{3}g^{-1} is a proxy for estimating elevation changes. Figure 3.2.2 shows the depth profile of the total air volume content of Berkner Island. Despite very poor data resolution the long term trend shows that the mean air volume content was ~ 0.115 cm^{3}g^{-1} in the LGM and then it increased to 0.120 cm^{3}g^{-1} in the late Holocene. This change in total air volume content equates to approximately 50 – 60 mbars of pressure and calculations using the altimeter equation suggest that Berkner Island was 500 m higher in LGM than its present altitude. This estimation is subject to uncertainties due to other factors that influence the total air content such as variations in atmospheric pressures, temperature at the ice formation site, wind speed and the ice porosity when the air bubbles close-off.
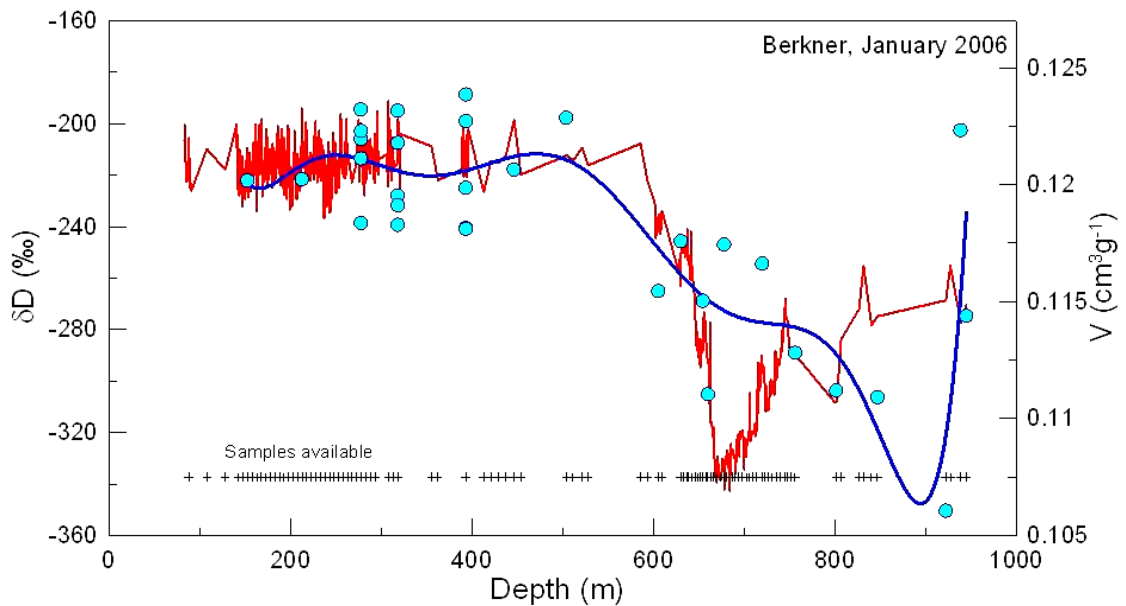
Figure 3.2.2: A depth profile of δD (red line) and total air volume content measurements (blue dots) in Berkner Island. The dark blue line shows the long term trend in total air volume content (V. Lipenkov, pers. comm.).

3.2.2 Dating of the ice core

The chronology of the Berkner ice core was determined by Jean-Marc Barnola at LGGE. The gas age of the ice core was assigned by gas matching or more commonly known as "wiggle- matching". The CH_4 results obtained for Berkner Island were compared to CH_4 gas age profiles for EPICA Dome C (EDC) and Vostok and CO_2 results were compared to CO_2 gas age profiles for Vostok and Byrd. The Vostok and Byrd data were fitted to EDC3 (EDC 3rd generation age scale) timescales and therefore the gas age obtained for Berkner is also on EDC3 timescale (Parrenin et al., 2007). Although CH_4 is considered as the best marker, CO_2 was very useful around 70 kyr BP and in the deepest part of the ice core to decipher if the gases and ice records were coherent. The CO_2 wiggle matching was considered useful particularly around 70 kyr BP because there were not significant variations in the CH_4 records. This procedure provides the annual layer thickness between the time markers and thus the gas chronology. Figure 3.2.3 shows CH_4 and CO_2 results fitted to gas profiles of EDC, Vostok and Byrd to obtain gas age.

93
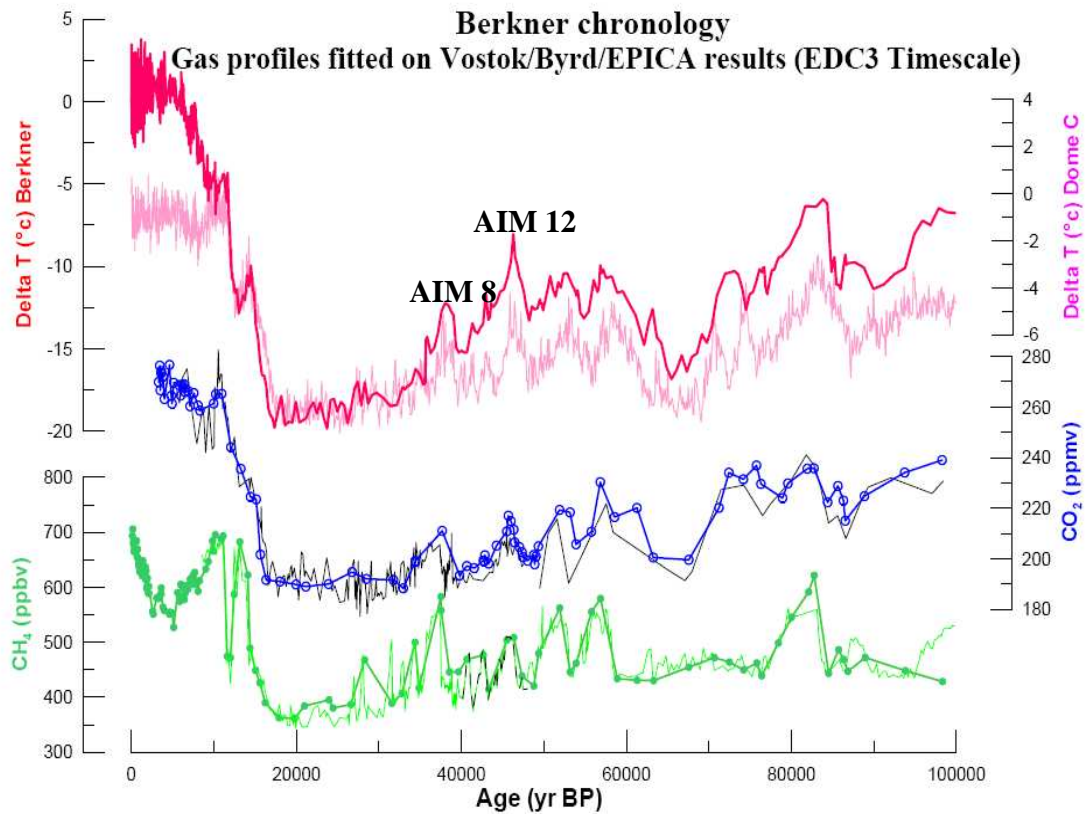
Figure 3.2.3: The CH_4 (dark green) and CO_2 (blue) gas profile from Berkner Island fitted to gas profiles from EDC (light green), Vostok (black line, CH_4 from 50 – 40 kyr BP, CO_2 from 50 kyr BP - Holocene) and Byrd (black line, CO_2 from 100 – 50 kyr BP). The figure also shows the change in temperature (deduced from Berkner δD profile using the classical relationship of 6.04 per mil/°C) as compared to change in temperature in EDC. There is a strong 1-1 coupling between the AIM 8 and AIM 12 events in EDC and Berkner Island. (J-M Barnola, pers. Comm.).

Once gas ages were obtained the ice age was determined through the firn densification model of Goujon *et* al., (2003). In order to run the model, delta temperature and accumulation rates had to be defined. The δD profile was interpolated to get 1 m resolution, which was then converted into delta temperature by the classical 6.04 per mil/°C relation (Parrenin et al., 2007) (shown in figure 3.2.3). The accumulation rates were deduced through the relation used for DC, that is, accumulation rate = $accu_0 * exp(.0150 * 6.04 * delta\ T)$ where $accu_0$ = present day accumulation rate (Parrenin et al., 2007). The delta

temperature profile was smoothed (20 m running averages) and converted into surface temperature (T). Following this the model was run in a static mode with temperature and accumulation rates as inputs in the firn densification model to generate delta age (Δage), which was then used to assign ice age (ice age = gas age + Δage).

The EDC3 chronology for the EPICA DC ice core is robust as it was derived from a combination of age markers and ice flow modelling. The dating error in the EDC3 age scale, which would be reflected in Berkner chronology, was assessed based on the age markers (Parrenin *et* al., 2007). The error is about 3 – 8 years (estimated by volcanic horizons) back to AD1100 and thereafter increases to 100 years at 2000 yr BP and stays stable until 6000 yr BP (age constrained by ^{10}Be marker). The uncertainty of the age scale then increases to 400 yr at 14 kyr BP, which is approximately the error arising from the CH$_4$ age markers. The dating error increased to 1 kyr at 18 kyr BP (LGM), 1.5 kyr at 40 kyr BP (comparison to Laschamp event) and finally to 3 kyr at 100 kyr BP (Parrenin *et* al., 2007).

The Berkner chronology could be in debate if the spatial relationship obtained between accumulation rates and delta temperature for EDC is not valid at Berkner Island. The Berkner ice core chronology was synchronised to a common EDC3 timescale by matching gas profiles, and therefore the total uncertainty in Berkner chronology would be a summation of any uncertainties associated with the EDC3 timescales, errors in the synchronisation process and in the firn densification model.

The Berkner chronology could be constrained by the dated horizons or age markers such as volcanic eruptions/signatures (Severi *et* al., 2007; Udisti *et* al., 2004) and ^{10}Be measurements. ^{10}Be is a cosmogenic radionuclides with its production rates controlled by solar activity and by the strength of the Earth's magnetic field. It has been used to date the last 6 kyr BP in EDC but is particularly useful in identifying the Laschamp event, which gives rise to a structured peak in ^{10}Be records around 41.2 kyr BP. The identification of Mount Berlin ash layer dated at 92.5 ± 2 kyr BP and proxies of local summer insolation

such as air content (Raynaud *et* al., 2007) and $^{18}O_{atm}$ (Dreyfus *et* al., 2007) could potentially be used in future to constrain the chronology.

3.3 Water Isotopes: δD and δ18O

3.3.1 $\delta^{18}O$ and δD profile for Berkner Island

High precision water isotopes were measured at the Natural Environment Research Council (NERC) Isotope Geosciences Laboratory (NIGL) using a VG SIRA stable isotope mass spectrometer. The analytical precision is typically ± 0.05‰ for $\delta^{18}O$ and ± 1.0‰ for δD. The water isotopic ratios are expressed with respect to the international standard, VSMOW (Vienna Standard Mean Ocean Water). Figure 3.3.1 shows the δD and $\delta^{18}O$ profiles for Berkner Island. Both profiles exhibit virtually identical trends, conforming to what was expected and therefore assures the data quality.
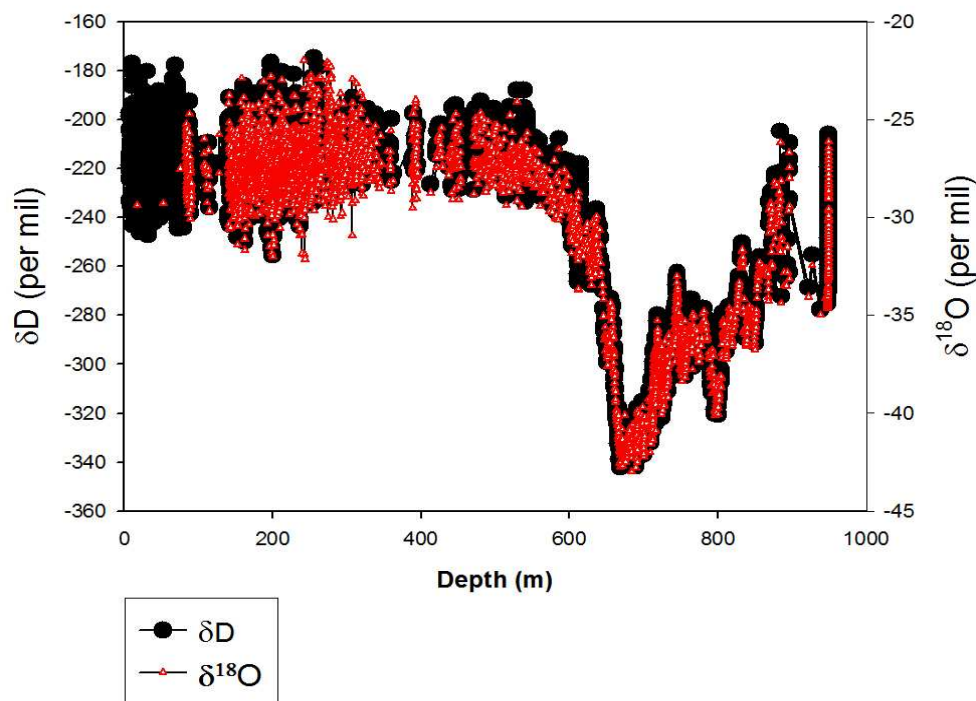
Figure 3.3.1: A depth profile of δD (black) and $\delta^{18}O$ (red) for Berkner Island. The black and red coloration in the figure is due to merging of numerous data points in that region.

As discussed earlier δD and $\delta^{18}O$ are classical palaeo-thermometers but also have some relevance in palaeo-accumulation rate estimation and constraining the elevation history of an ice sheet. The combined measurements could provide the deuterium excess profile (d = δD - $8\delta^{18}O$), which is a signature for changes in moisture sources or oceanic source conditions such as SSTs and sea surface humidity at the initial evaporation site (Jouzel *et al.*, 1997, 2007; Petit *et al.*, 1991; Uemura *et al.*, 2004). Masson-Delmotte *et al.* (2005) used a simple isotopic modelling approach to quantify the observed fluctuations in the water isotopes in terms of changes in the source and site temperatures. There is considerable scientific knowledge that can be drawn from the detailed study of the water isotopes, however such a study is beyond the scope of this work. The discussion on water isotopes, which follows is restricted to highlighting the fact that the climatic record obtained from the Berkner Island ice core is coherent with other Antarctic deep ice cores and it was used as a criterion for identifying sampling depths that encompass the isotope maximum anomaly. Later in the discussion δD has been correlated with the $\delta^{15}N$ profile obtained in this study to constrain the Δdepth or Δage estimations and to explain the behaviour of the $\delta^{15}N$ signal.

3.3.2 Comparison with other Antarctic sites

The δD profile of Berkner Island was compared to either the $\delta^{18}O$ or the δD profile from EDML (EPICA community members, 2004), EDC (EPICA community members, 2004), Dome Fuji (Kawamura *et al.*, 2007) and Vostok (Petit *et al.*, 1999) (see Figure 3.3.2). The water isotopes data from the different sites were plotted with their respective age scale and were not synchronised to a common timescale. Consequently there were some very minor disagreements in the absolute timings of the climatic events that could be easily compensated by making allowance for the uncertainties in the age scales.

It is evident from Figure 3.3.2 that the climate records from Berkner Island are coherent with other deep ice core records from Antarctica. The figure shows the major climatic events such as the Antarctic Cold Reversal (ACR), the last glacial – interglacial transition and the Antarctic warming events during the last glacial period. The structure and timing of
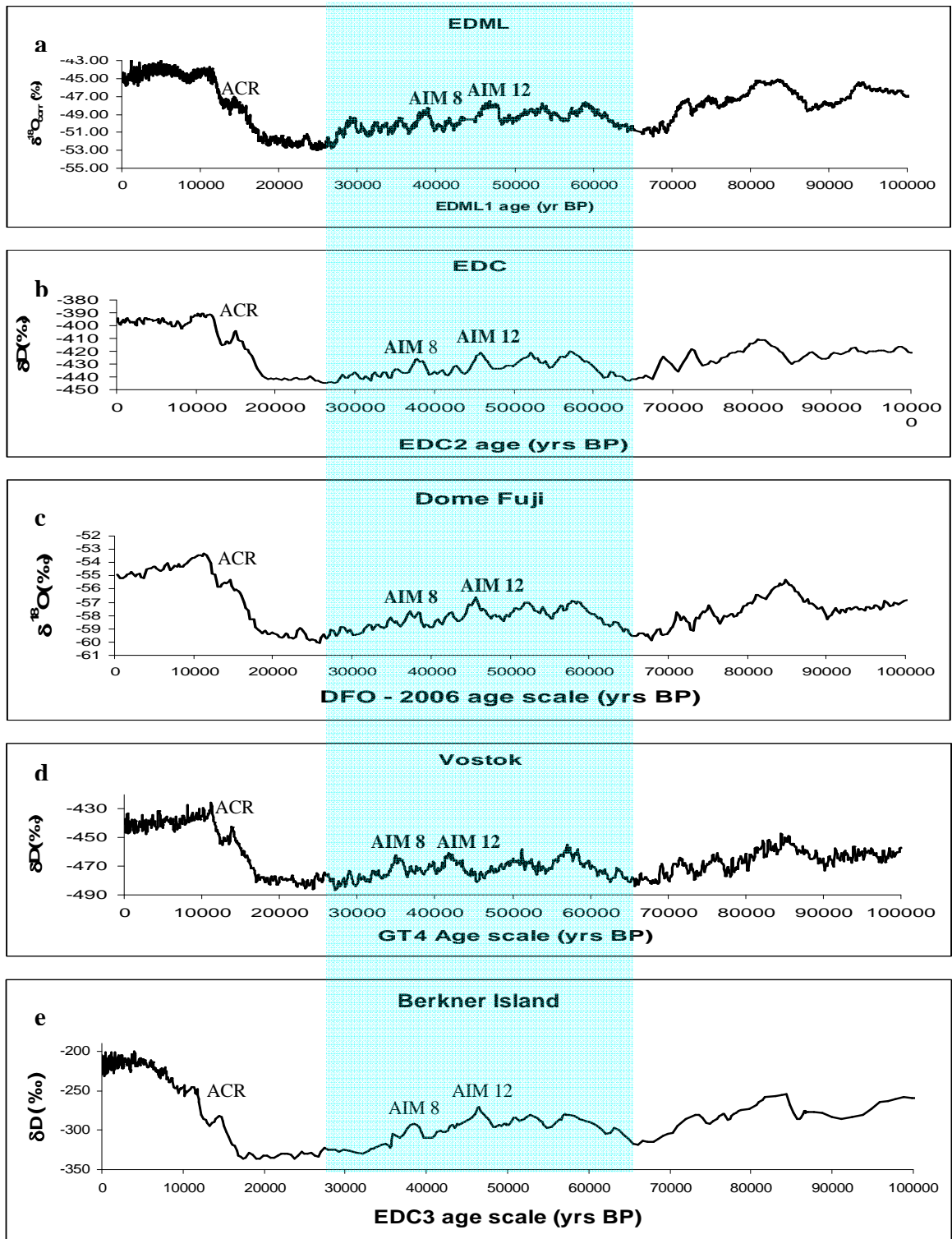
Figure 3.3.2: Comparison of water isotopes on an age scale from different sites in Antarctica. The shaded region shows the MIS 3 period. Climate events such as AIM 8, AIM 12 and ACR are also marked.

these events are remarkably similar to other ice core records and therefore proves the integrity and the broad chronology of the Berkner ice core.

Despite similar characteristics in the timing and structure of the climatic events, the absolute values of δD were different. The δD values range from -342.6 ‰ to ~ -200.0 ‰ in the Berkner ice core and are higher than the other Antarctic continental drilling sites such as the EPICA DC with values ranging from -450 ‰ – -360‰ and Vostok with values ranging from -480 ‰ – -420‰. The δD values for Berkner Island are more comparable with the δD profiles from near coastal sites like Byrd or Law Dome (Masson *et* al., 2000). The difference in δD values from various sites can be explained by colder temperature conditions in continental sites, varying altitudes and varying accumulation rates.

Another distinctive feature between δD profiles of Berkner Island and other sites shown in Figure 3.3.2 is the evolution trend of δD after the climatic optimum at ~ 11 kyr BP, that is, after the last glacial – interglacial transition. The δD tends to stabilise after the transition in EDML and EDC cores whereas in Vostok and Dome Fuji ice cores it stabilises and then exhibits a slow gradual decrease during the Holocene. However, in Berkner it shows a completely different trend. The δD values at Berkner continue to increase from -259.9 ‰ to -207.2 ‰ after the transition and start to stabilise around mid Holocene with higher values of -215.5 ‰. This change in δD is not due to any global climatic change but is, rather, attributed to ice sheet altitude changes. The ice sheet was thinning gradually leading to lower altitudes and higher temperatures and as a result increasing δD values. The altitude changes in Berkner Island ice sheet will be discussed in detail in Section 3.4.6.2.

The change in δD across the glacial – interglacial transition is larger at Berkner as compared to the more continental sites. A change of ~100 ‰ is observed at Berkner whereas ~50‰ change in δD is observed at Vostok, EDC, Dome Fuji and ~64‰ change at EDML. A large shift in isotopic values does not necessarily imply that larger temperature changes were observed at Berkner during the LGM transition. Interpretation of the water isotopes in terms of temperature changes needs to be treated cautiously especially with the coastal sites where elevation changes contribute significantly or even predominantly to

isotopic signals (Jouzel *et* al., 1989). The dynamics of ice sheet/ice shelves/sea ice growth and decay all contribute to the isotopic variations. The coastal sites have larger amplitude of isotopic variations than the more inland sites and this argument has been supported by a model simulation, which removes all sea ice around Antarctica and shows a limited impact on the eastern plateau but a very large impact at coastal locations especially near Taylor Dome (Masson *et* al., 2000). The effects of complex combination of factors such as temperature and elevation can be resolved with the aid of ice sheet models forced with different temperature variation scenarios.

3.3.3 Sample selection

The sampling strategy was based primarily on the deuterium profile and the initial firn densification model results to identify the approximate location of the δ^{15}N isotopic thermal anomaly in the ice core. The deuterium profile showed two distinct peaks in the depth range corresponding to the Marine Isotopic Stage 3 (MIS 3) period, which is a warm period during the last glacial, centered at around 50 kyrs BP. The two peaks correspond to AIM 8 and AIM 12 warming events in Antarctica. The transition of the warming phase of AIM 8 event, which is the Antarctic counterpart to DO 8 event in Greenland, was identified from ~724.5 - ~719 m with a positive signal of ~ 30 ‰ in deuterium (see Figure 3.3.3). The warming phase of AIM 12 (analogous to DO 12 event in Greenland) event was identified in the depth range of ~752 - ~745 m with a positive change of ~ 40 ‰ in deuterium. The firn densification model predicted that gas signals would appear 1.5 – 2 m deeper than the signal in ice due to ice age – gas age difference. To encompass the warming and cooling phase of both these events and to account for the Δdepth calculations and its related uncertainties, it was decided to sample as much as possible across these two events to avoid the risk of missing an isotopic anomaly in δ^{15}N. For AIM 8 event samples were selected at a 55 cm resolution from ~709 – ~733 m and for AIM 12 the samples were selected at 55 cm resolution from ~742 – ~758 m (see Figure 3.3.3). The ice core was cut to 55 cm sections in the field and was packed for transport. The 55 cm section is commonly referred to as 'bags'. Samples were taken from each bag and the resolution of each bag is ~ 200 yrs. Upon measurements of all these samples it was realized that the δ^{15}N signal was very

peculiar after the AIM 8 event. In order to understand this behaviour additional sampling was carried out between ~693 – ~708 m.
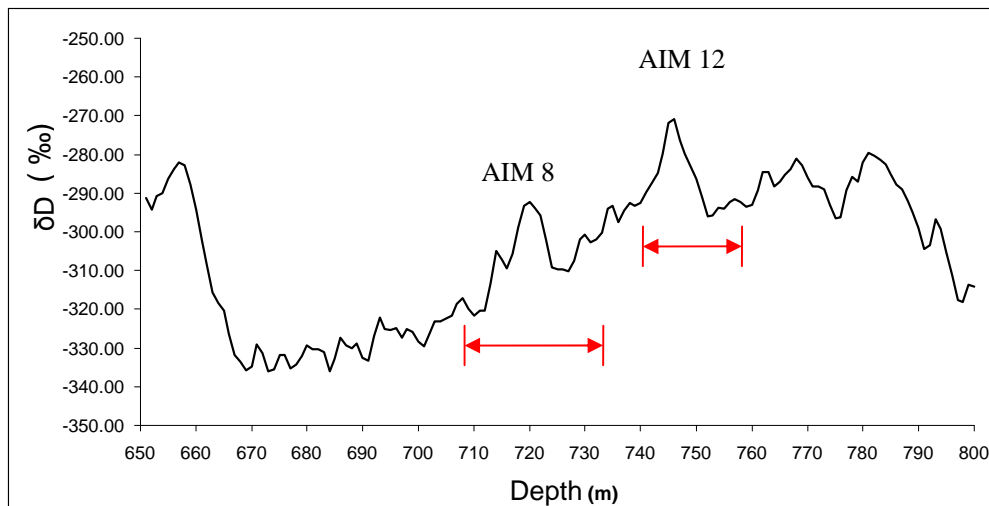
Figure 3.3.3: Using the water isotopic signals for AIM 8 and AIM 12 to choose the depths where ice core to be sampled for $\delta^{15}N$ measurements.

3.4 $\delta^{15}N$ Data: Timing and structure of the events

A high resolution record of $\delta^{15}N$ was obtained for the period 26.4 – 49.1 kyr BP on a gas age scale. Figure 3.4.1 shows $\delta^{15}N$ data obtained in this study on a gas age scale. The figure shows three distinct peaks in the $\delta^{15}N$ profile during the measurement period. The peak from 49 – 44 kyr BP corresponds to the AIM 12 event, the peak from 39.5 – 36.4 kyr BP corresponds to the AIM 8 event whereas the largest peak from 35.6 – 27 kyr BP does not correspond to any Antarctic warming events documented to date. Samples from 44 – 39.5 kyr BP were not measured.

3.4.1 AIM 12 event

The $\delta^{15}N$ values started increasing gradually from an average lowest value of 0.18 ‰ around 48.7 kyr BP to a maximum of 0.25 ‰ near 46.3 kyr BP. The amplitude of the signal

is +0.07 ‰ over a period of 2400 years. The initial rate of increase was very slow but the rate increased from 47 kyr BP, accounting for 50% of the signal in only ~800 years. After reaching the maximum the signal decayed to ~ 0.19 ‰ almost at a similar rate at which it started increasing rapidly.
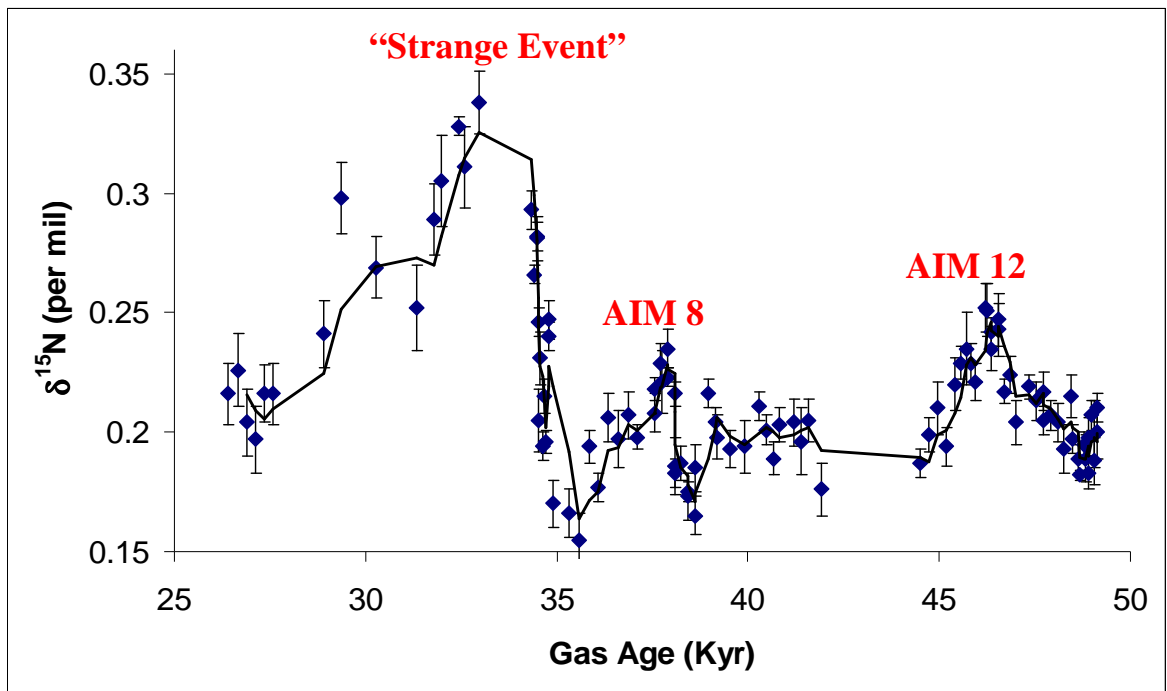
Figure 3.4.1: A high resolution $\delta^{15}N$ profile from Berkner Island ice core during the Marine Isotope Stage 3. The two Antarctic warming events, AIM 8 and AIM 12 signals are observed in addition to an enormous "strange" signal at ~ 35 kyr BP.

During the DO 12 event in NorthGRIP ice core, the $\delta^{15}N$ values changed by +0.17‰ in less than 400 years. The magnitude of change is larger (more than twice as much) and the rate of change is 6 times faster than the AIM 12 event. Despite the slow rate in change of temperature as depicted by δD and $\delta^{15}N$ (proxies for temperature changes), a signal of +0.07 ‰ change in $\delta^{15}N$ was obtained, which is similar to a change of +0.08‰ in $\delta^{15}N$ observed during the last deglaciation in Law Dome DSS ice core and a change of +0.05‰ observed for similar period in EDML ice core (Landais *et* al., 2006). The measurement

technique developed in this study allows better quantification of the $\delta^{15}N$ signal, which is comparable to the signals observed during the Antarctic deglaciation in previous studies.

3.4.2 AIM 8 event

The $\delta^{15}N$ values remained almost constant at 0.20 ± 0.01 ‰ from 41.7 – 39.9 kyr BP after which it showed a steady increase from 0.19 ‰ to 0.22 ‰ in approximately 500 years (from ~ 39.5 kyr BP – 39.0 kyr BP) then it suddenly decreased to 0.16 ‰. The values increased slowly to 0.19 ‰ and then increased very abruptly to 0.216 ‰ in less than 50 years (based on 3 samples measured across a 10 cm core from a bag). The $\delta^{15}N$ values continued to increase before reaching a maximum of 0.2 ‰ around 37.9 kyr BP and then decreasing to ~0.2 ‰. The structure or shape of $\delta^{15}N$ profile for the warming event AIM 8 is complex when compared to the AIM 12 event. It does not show the smooth increase and decrease coinciding with the warm and cold phase of the warming event. The structure of the AIM 8 peak makes it difficult to identify the starting point of the transition of this warming event. Later in sections 3.4.5 and 3.5.1, the $\delta^{15}N$ data are combined with δD and $\delta^{40}Ar$ data to understand the $\delta^{15}N$ signal for this particular event. The data clearly shows an increase of +0.07 ‰ from 38.6 – 37.9 kyr BP.

3.4.3 The "Strange Event"

At the end of the AIM 8 event peak the $\delta^{15}N$ values decreased to 0.16 ‰ and then increased rapidly to 0.29 ‰ in approximately 800 years. Such a large enrichment in $\delta^{15}N$ was not observed during any of the warming events and this enrichment is not associated with a warming in the δD signal. To further investigate this anomalous behaviour of $\delta^{15}N$ more samples from the depth range of 693 – 708 m were analysed. After analyses of the additional samples it was realized that the values peaked at 0.34 ‰ around 33 kyr BP, however it could be possible that the peak value could have been missed as samples in the depth range of 706.2 – 708.8 m were not measured. Nevertheless the measurements do confirm that the values increased rapidly and then decrease to 0.2 ‰ very slowly over a period of 5000 years. The shape of this strange peak is similar to a warming event

consisting of a warming and a cooling phase. An apparent enrichment of 0.2 ‰ would reflect a large increase in Diffusive Column Height (DCH) or temperature or both or due to some other isotopic fractionation mechanism in the firn column which has not been documented to date (discussed further in section 3.4.6). If the enrichment was due to an abrupt warming event then this has to be a local warming because such event was not observed at any other sites in Antarctica during that period and certainly not larger than AIM 8 and AIM12 events. If the strange event is indeed linked to an abrupt climate change then it may suggest that the climate regime of the coastal sites may be different from the more inland sites of Antarctica. A localised warming event has been observed in the past for a coastal site like Siple Dome, where a 6 °C warming has been observed at 22 kyr BP. Detailed analyses of δD and $\delta^{40}Ar$ and paleo-accumulation rate estimation may help to interpret this strange event.

3.4.4 Estimating Δdepth and Δage

At the close-off depth gases are younger than the surrounding ice due to diffusion of gases in the porous firn layer. This leads to ice age – gas age difference (Δage) on the age scale and in terms of depth scale it is referred to Δdepth. An important outcome of high resolution and high precision $\delta^{15}N$ data obtained in this study would be to verify the modelled Δage or Δdepth, which was used to obtain the chronology of the Berkner Island ice core. The Δage or Δdepth can be calculated from the difference in position of a signal in ice (δD or $\delta^{18}O$) and in the gas phase ($\delta^{15}N$, CH_4, CO_2). Figure 3.4.2 shows the plot of $\delta^{15}N$ and δD on a depth scale. The difference in the position of the maxima in $\delta^{15}N$ and δD peaks for each warming event equates to Δdepth. The calculated Δdepth was then compared to the model predicted Δdepth (from herewithin referred to as Δdepth$_{modelled}$), which was estimated from the ice age – gas age difference predicted by the firn densification model.

The measured Δdepth for the AIM 8 event (~ at 720 m) is 2.1 m and for the AIM 12 event (~ at 745 m) is 2.2 m. The uncertainties in these calculated values arise from the sampling resolution and therefore are not more than ± 0.5 m. For the AIM 12 event it is possible that the peak value may have been omitted as a sample (at 746.9 m) adjacent to the sample

currently containing the peak values was not measured due to extraction errors. Regardless of the degree of error associated with the calculations, the calculated Δdepth is in agreement with the Δdepth$_{modelled}$ of 2.15 m. The calculated Δages are 724 and 569 years for the AIM 8 and the AIM 12 events respectively.
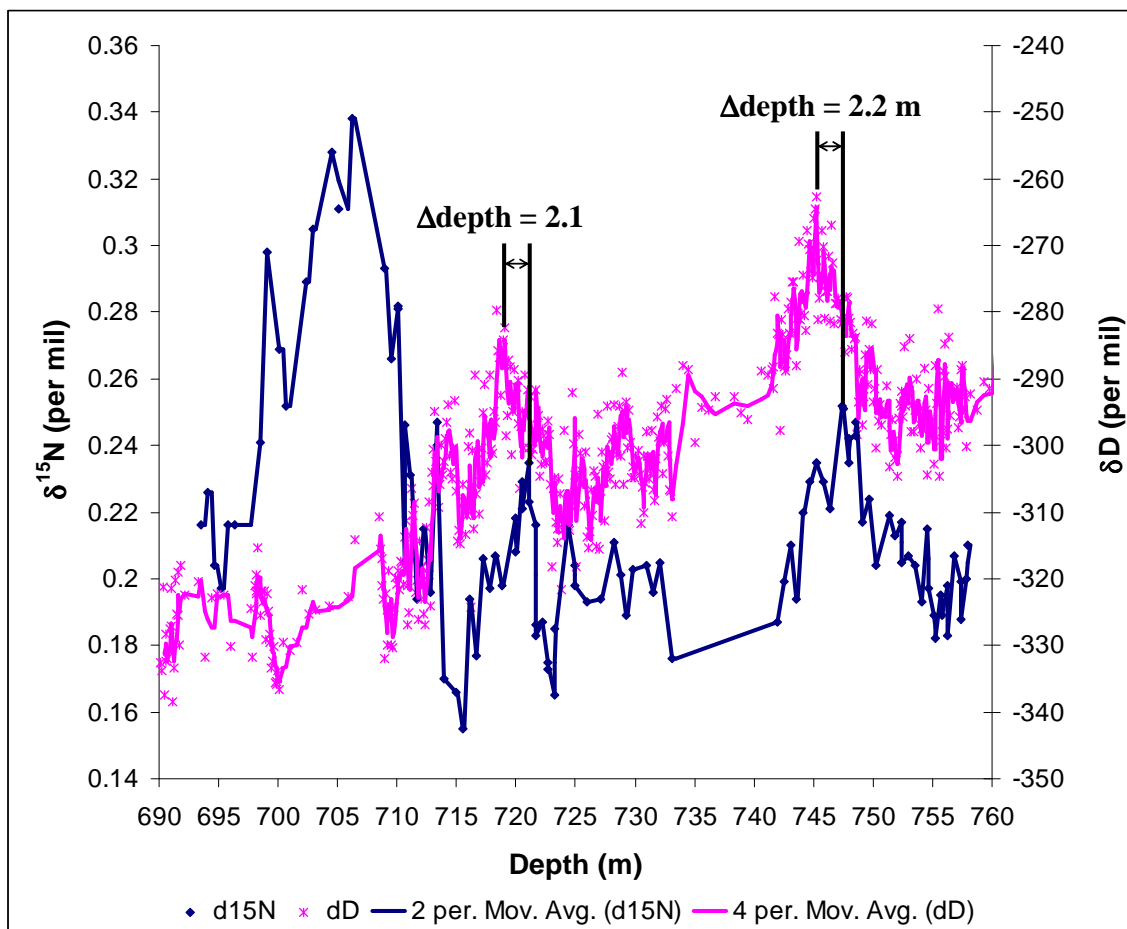
Figure 3.4.2: A plot of δ^{15}N and δD on the same depth scale to estimate the Δdepth between the maxima in ice signal and in the gas signal.
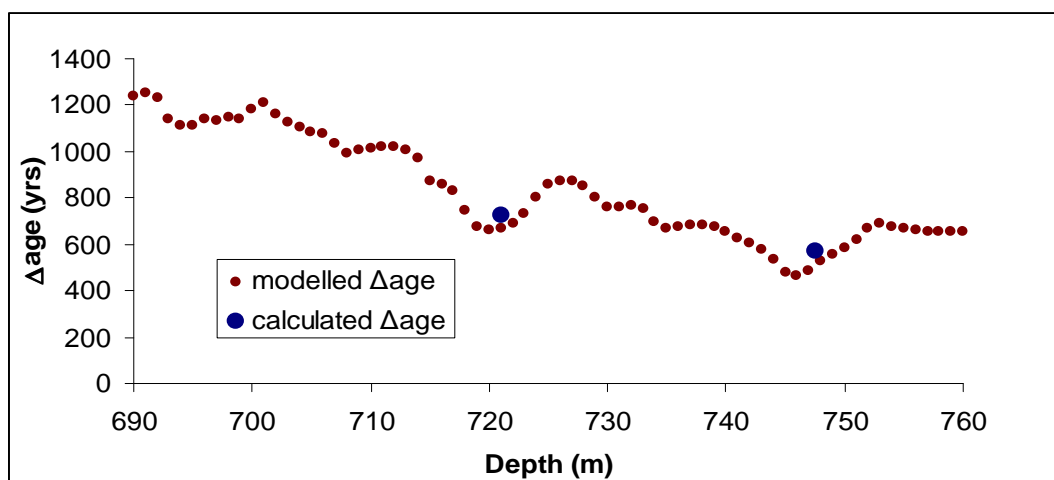
Figure 3.4.3: A comparison between the calculated Δage and the modelled Δage obtained with the firn densification model (Goujon *et* al., 2003) that was used to derive the ice age for the Berkner Island ice core.

These calculated values are also closer to the model estimates of Δage of 670 years for the AIM 8 event and 507 years for the AIM 12 event (see Figure 3.4.3 above). The calculated Δdepth and Δage are in close agreement with the predicted Δage and Δdepth obtained with the firn densification model (Goujon *et* al., 2003). The validity of the assumption that the maximum in deuterium should be contemporaneous with the maximum in $\delta^{15}N$ signal really depends on the mechanism which is not very well understood at this stage. More recently Severinghaus et al. (2010) suggested that during the glacial period there is a possibility of larger convective zones in the order of 30 m due to lower accumulation rates and macro-cracks. However during the warming events in the glacial period the accumulation would increase and then the dense layer of snow could possibly reduce the ventilation of the firn and increase the gravitational signal. To explain an increase of 0.07 ‰ in $\delta^{15}N$ only 6 m of reduction in convective zone is needed and should take place simultaneously with increasing temperature. This mechanism is just a mere speculation at this stage.

Hence $\delta^{15}N$ measurements were able to verify the chronology of the Berkner Island ice core across the AIM 8 and AIM 12 events and to some extent proves the validity of the reconstructions for paleo-temperature and paleo-accumulation rates based on the water

isotopes that were used as the input variables in the firn densification model to derive the ice age. However the chronology across the strange event could not be verified by the δ^{15}N measurements due to the lack of any corresponding signals in the δD profile. In Chapter 4 high resolution methane measurements were obtained and it revealed that there were some discrepancies in the Berkner gas age scale during the occurrence of the "strange" event.

3.4.5 δD versus δ^{15}N

It is evident from the δ^{15}N measurements that the Δdepth is approximately 2 m across the AIM 8 and AIM 12 events. To gain a better understanding of the behaviour of the δ^{15}N signals across these two events, the δ^{15}N data were depth corrected by applying an average Δdepth of 2 m (subtracting 2 m from the measured depth). The Δdepth corrected δ^{15}N data were plotted together with the δD data so that both profiles are on the same depth scale (see Figure 3.4.4 below). There is a remarkable resemblance between δD and δ^{15}N data for the AIM 12 event ($r^2 = 0.78$). Dreyfus *et al*. (2010) also observed high correlation between δ^{15}N and δD during the termination events in EDC ice core and suggested that δ^{15}N signal could be used as a climate proxy in gas phase.

The identification of the starting point for the warming transition of the AIM 8 event became obvious by matching variations in δD and δ^{15}N after correcting for the Δdepth effect. It is evident that the climate started warming at approximately 39 kyr BP (~724 m), which was confirmed by the overlapping of increasing signals in both the δD and δ^{15}N profiles (see Figure 3.4.4). The δD values continued to increase although the rate of change was slow as compared to the initial phase of this event whilst the δ^{15}N values decreased rapidly by approximately 0.06 ‰. The decrease in the δ^{15}N signal during the warming period tends to suggest that an abrupt increase in temperature caused the thinning of the firn and therefore resulted in depleted δ^{15}N values. The δ^{15}N values then started to increase and were most likely to be caused by thickening of the firn and the temperature gradient. The δ^{15}N values increased very rapidly and coincided with the maxima in δD. The firn thinning during the transition of the warming phase of the AIM 8 event is discussed further in Section 3.5.1, where argon isotope measurements are used to determine DCH.
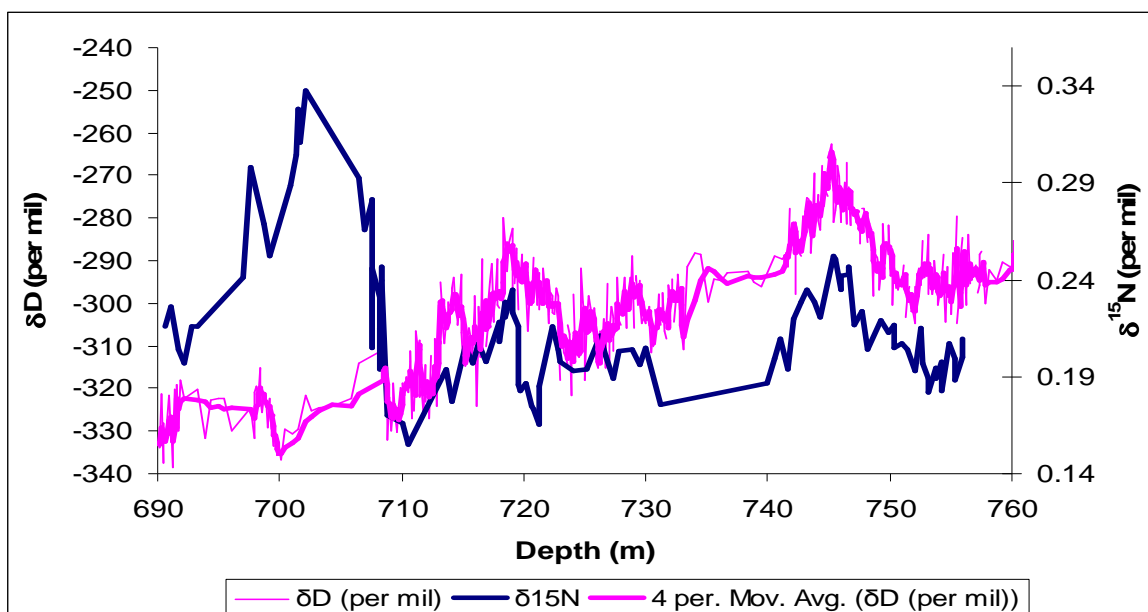
Figure 3.4.4: Correlation between δD and $\delta^{15}N$ after taking into account an average Δdepth correction of 2 m across the warming events and estimating Δdepth from the model from 690 m – 715 m.

Figure 3.4.3 shows that the modelled Δage increases from approximately 700 years across the AIM 8 event to 1200 years at 700 m, the depth where the strange signal in $\delta^{15}N$ was observed. Due to such large variations in Δage between the two events it was not appropriate to apply a constant Δdepth correction of 2 m. In fact from 717 m – 690 m, the depth corrections were estimated from the modelled ice age – gas age difference and were typically in the range of 1.5 – 6 m. It is intriguing to see that the Δdepth corrected $\delta^{15}N$ signal of this strange event does not coincide with any peak in δD profile. Hence this confirms that the large peak in the $\delta^{15}N$ profile, which is referred to as the strange event, is definitely not caused by any abrupt warming event. In actual fact the $\delta^{15}N$ values continue to increase from 0.14 – 0.34 ‰ while the δD profile shows a decreasing trend during this strange event. There could be many factors attributing to such $\delta^{15}N$ anomaly and these are discussed in Section 3.4.7.

3.4.6 Correlation between deuterium excess (*dxs*) and δ^{15}N

The δ^{15}N data were compared to the deuterium excess (*dxs*) profile for the MIS 3 period (Figure 3.4.5) and it revealed that there was a decrease in *dxs* values before the onset of the warming events. A decrease in *dxs* indicates a shift in the moisture source region to a colder source waters with reduced evaporation (Thomas *et* al., 2009). Usually the *dxs* profile is in anti-phase with the δ^{18}O and δD profile and is commonly observed in all Greenland interstadials (Jouzel *et* al., 2007; Masson-Delmotte *et* al., 2005); however such characteristic was not observed at the Berkner Island site. A more detailed analysis of the *dxs* profile would elucidate the mechanisms of warming in Antarctica during the last glacial period as the signals of the moisture source migration were observed near the warming events.
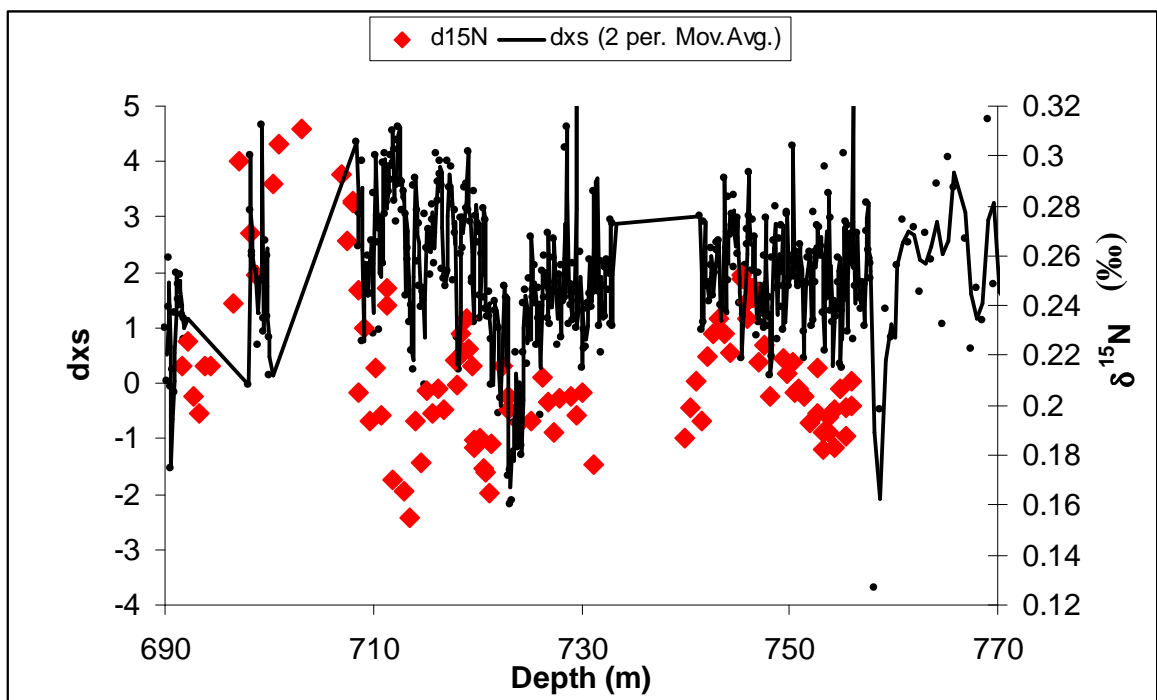
Figure 3.4.5: A phasing between δ^{15}N (corrected for Δdepth) and *dxs* profile shows that the moisture source migrates to a colder source before the warming events.

For the AIM 8 event, the *dxs* values reached a minima, which coincided with the onset of the warming phase of δ^{15}N and δD signal. As for the AIM 12 event the minima in *dxs* was observed before the rise in δ^{15}N. Suppose there is a consistent pattern, such that the minima in *dxs* coincide with the onset of warming, then it raises the question whether the beginning of the δ^{15}N signal for the AIM 12 warming event has been missed. Maybe extending the sampling depth to deeper depths would resolve this issue in the future.

Thomas *et* al. (2009) highlighted similar observation about the warming starting to accelerate only after the complete transition of the *dxs* to a minimum across the DO 8 event in the NGRIP ice core. It was noted that the moisture source location shifted north to cold but ice-free Greenland-Norwegian Sea that accelerated the warming (Thomas *et* al., 2009). This enhanced warming is consistent with a transfer of oceanic heat to the atmosphere after the insulating sea-ice has been removed. Probably this analogy could be applied to the AIM 8 event at Berkner Island to explain the mechanism of climate change.

3.4.7 Causes of δ^{15}N enrichment at 700 m ("Strange Event")

The enrichment of δ^{15}N in the firn layer is usually attributed to two factors:
(i) increased gravitational fractionation due to increase in diffusive column height
(ii) a transient temperature gradient due to an abrupt warming event.

It is evident from Figure 3.4.4 that the strange event does not coincide with any warming event. There are two small warming events (at 700 m and 709 m) within the depth range of the strange signal, characterised by positive changes of 20 ‰ in δD that coincides with the "jumps" within the strange event. In the absence of any large abrupt warming event coinciding with the strange peak, all the explanations for the occurrence of the strange event are more focussed on the increase in DCH and factors influencing the DCH.

An enrichment of 0.2 ‰ could be accounted for by an increase of 39 m in DCH, under the assumption that all the apparent enrichment in δ^{15}N was caused by gravitational fractionation. The increase in DCH could be due to the thickening of the firn layer, which

could be influenced by an increase in the accumulation rate. In order to increase the DCH by 39 m from accumulation alone takes an extreme minimum of 39/α years where α is the accumulation rate in metres/yr. The increase in DCH could also be explained by a decrease in convective zone depth or deepening of the close-off depth. The depth of the convective zone is influenced by wind pumping or wind speed and is generally less than 10 m. Wind pumping in the firn could be significantly dampened by layers of snow with low porosity and small grain sizes (Sowers et al., 1992). If the wind speed decreased or if an impermeable melt layer at the top was formed then the depth of the convective zone would decrease. It would be difficult to obtain an increase in DCH by 39 m due to the loss of 39 m in convective zone although a large convective zone of 20 m has been observed in megadunes at the Vostok site (Severinghaus, et al., 2003). A decrease in convective zone may contribute partially in the increase of the DCH, which could be confirmed in the future from detailed measurements of Ca^{2+} ions or from the conductivity measurements of two cores drilled parallel to each (Barnes et al., 2006) Generally higher $\delta^{15}N$ values are associated with deeper close-off depths (CODs), which are characteristic of colder sites with higher accumulation rates (Sowers et al., 1992). It is evident from the δD profile that the site was cooling during the period of the strange event and if it is proven that the accumulation rates increased during the strange event then this would suggest deeper CODs which inevitably means larger DCH resulting in an enrichment of $\delta^{15}N$ signal.

3.4.7.1 Palaeo-Accumulation rate estimation

An increase in the accumulation rate during the period of the strange event could account for the increase in DCH resulting in the observed enrichment in $\delta^{15}N$. Figure 3.4.6 shows the accumulation rate deduced from the water isotopes as there is a direct relationship between water isotopes and accumulation rates. It clearly shows that the accumulation rate increased from 4.5 to 9.5 $g.cm^{-2}.yr^{-1}$ during the warming phase of the AIM 12 event and from 3.5 – 7.5 $g.cm^{-2}.yr^{-1}$ during the warming phase of the AIM 8 event. This suggests that most of the $\delta^{15}N$ signals observed across these warming events may be due to gravitational fractionation rather than thermal fractionation if the temperature change was slow and gradual. The accumulation rate estimation from water isotopes did not record any increase

in accumulation rate during the strange event. Since the accumulation rates were deduced from the δD profile, it shows similar trends to δD and also recorded a decrease during the strange event.

It is well understood that the accumulation rates derived from water isotopes is not valid at certain times. The detailed accumulation rates across sections of interest needs to be verified by other independent method such as Na^+ (to estimate annual cycles) or from high resolution CH_4, which could then potentially be used to validate the deuterium – accumulation relationship.
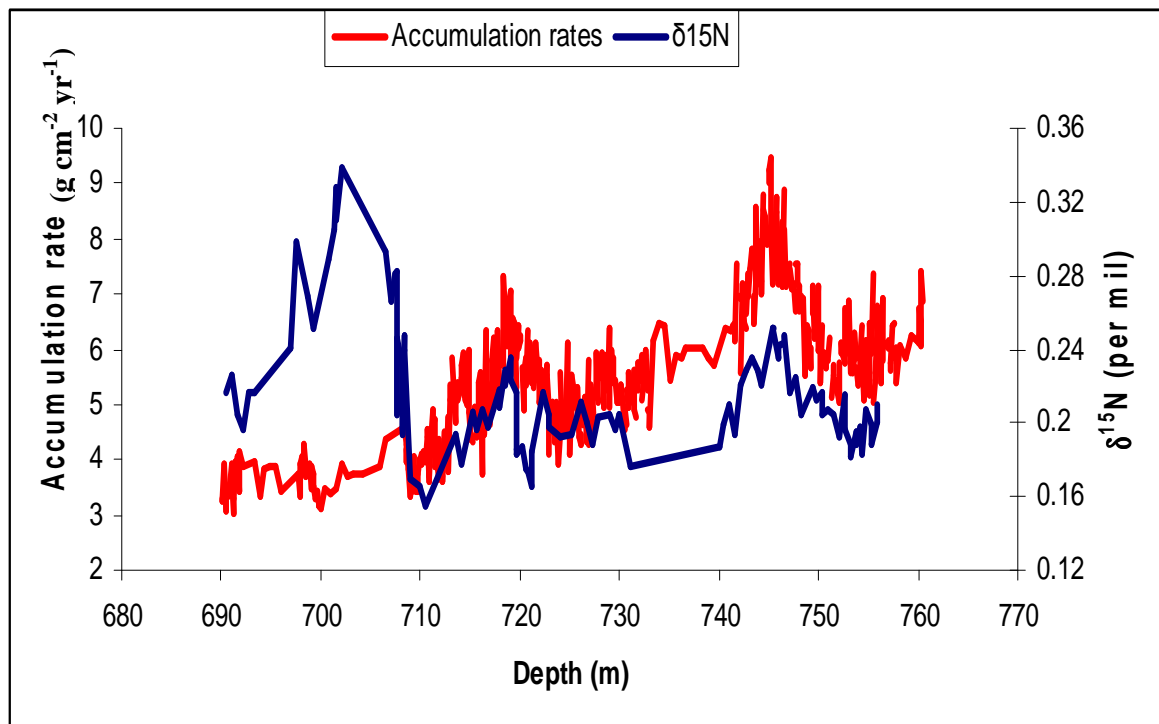
Figure 3.4.6: An illustration of accumulation rate derived from δD phased with Δdepth corrected δ15N.

3.3.7.2 Change in altitude

During the last glacial period Berkner Island ice sheet experienced large altitudinal changes. The lapse rate calculations showed that the altitude started to increase in mid 40 kyr BP and had increased by 200 – 400 m by mid 20 kyr BP. Figure 3.4.7 clearly shows that the changes in altitude took place in two steps. The rate of change accelerated around mid 30 kyr BP and then the altitude change stopped momentarily before starting to increase steeply around 28 kyr BP. The increase in altitudinal rate of change at 34 kyr BP coincided with the timing of the strange event. The rate of change in altitude stated here is questionable and is very much dependent of the data resolution and smoothing of the data. The rapid increase in altitude could be attributed to increased accumulation rate or decreased mass flow or combination of both.
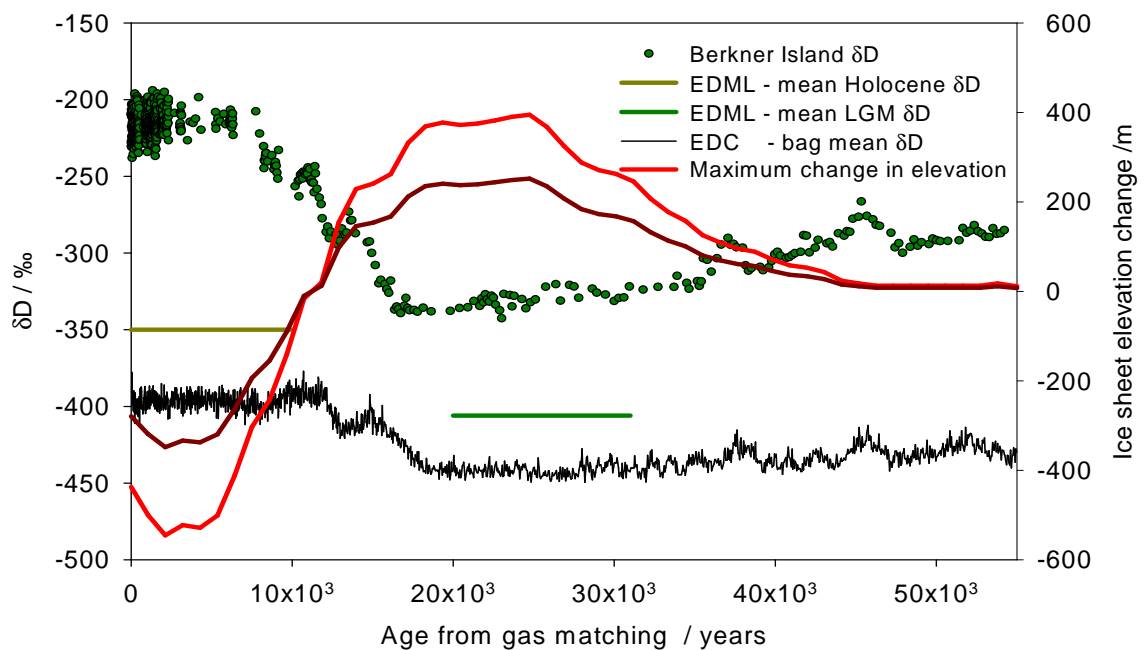
Figure 3.4.7: Estimating Altitude change at Berkner Island from comparing δD profiles of Berkner Island and EDML and applying lapse rate calculation. (Mulvaney, pers. comm.)
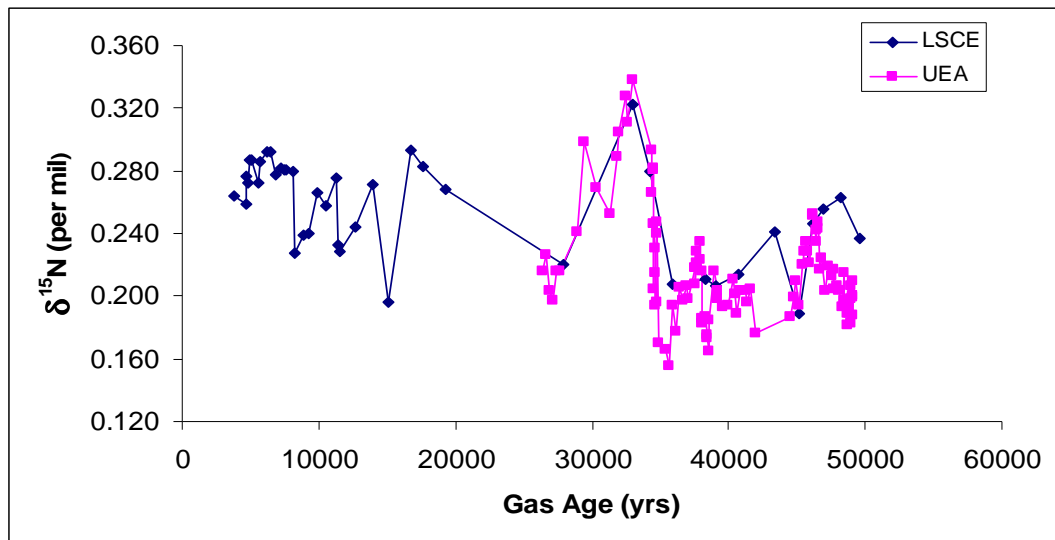
Figure 3.4.8: A comparison between UEA and LSCE δ^{15}N dataset shows good agreement particularly for the strange event. The low resolution LSCE data shows two strange peaks before the deglaciation and both these peaks coincide with the time when the altitude was increasing.

At present the coincidence of the strange event with increasing altitude indicates that the large enrichment in δ^{15}N values could be linked to an increase in DCH due to increased accumulation during the altitudinal change. However, in the absence of rigorously quantified palaeo-accumulation rates this explanation could not be satisfactorily tested. Figure 3.4.8 shows δ^{15}N measured in samples across the ice core at LSCE at a very low resolution. Generally there is a good agreement between UEA and LSCE measured values except two data points around 50 kyr BP. The measurements at LSCE also confirm the occurrence of the strange event and exactly match the timing and the magnitude of this event. The LSCE data also show another peak or enrichment in δ^{15}N which coincides with the increase in the rate of altitudinal change around 28 kyr BP. This observation substantiates the connection between the observed large enrichments in δ^{15}N during the strange event and large increases in altitude.

The agreement between the timing of enrichment in δ^{15}N and increase in altitudinal change suggests changes in the firn column could account for the δ^{15}N signal. This could be

explained by increase in DCH during large altitudinal change but in order to explain the decrease when the ice sheet stopped changing altitude is quite challenging. A decrease of 0.14 ‰, which equates to a decrease of 27 m in DCH over 6,000 yrs tend to suggest that the accumulation rate decreased or the densification rate was faster. The altitudinal change calculations do not show either a decrease or an increase during the decreasing phase of the $\delta^{15}N$ but these calculations are questionable as the δD measurement resolution is poor in these depths to draw any conclusive remarks. A high resolution δD measurements need to be conducted in future and if the detailed data shows a decreasing altitude during the fall of the strange signal then certainly this would confirm that these apparent enrichment and decrease in $\delta^{15}N$ values are linked to altitude changes, which in turn could be directly related to large accumulation rate variations obtained with high resolution chemistry measurements in the near future.

Another speculation for the occurrence of the strange event could be due to some fractionation mechanism not documented to date, such as, the existence of a pressure gradient and the effect of rapid altitude change on the bubble close-off fractionation. Severinghaus & Battle (2006) proposed that gases could be fractionated during bubble close-off process and is caused by pressure gradient, between the newly formed bubbles and the adjacent open pores, that drives a permeation flux of selective gases through the thin ice wall. The flux of a gas from the bubble is directly proportional to $x_n P/\gamma$ (where x_n is the mole fraction of gas n in the bubble, P is the barometric pressure in the open pores and the γ is regarded as the wall thickness). This suggests that when pressure decreases, the wall thickness also decreases to maintain constant flux. It was suggested that the extent of this effect was mostly dependent on the atomic/molecular size with a threshold atomic diameter of ~3.6 Å, above which the probability of a gas escaping from the bubble becomes very small. It is understood that the bubble close-off fractionation is almost negligible for N_2 however during the altitude change the pressure gradient could be possibly higher leading to the escape of lighter isotopes across the thin wall.

3.5 Temperature reconstructions for AIM 8 and AIM 12 events

The $\delta^{15}N$ measurements across the AIM 8 and AIM 12 events show a signal of +0.07 ‰, which is significantly larger than the signal of +0.02 ‰ observed during the MIS 5d/5c transition at Vostok (Caillon *et* al., 2001). The magnitude of changes in $\delta^{15}N$ observed are comparable to the magnitude of change observed during the last deglaciation at the EDML and Law Dome DSS ice cores, where temperature changes in the range of 8 – 10 ℃ were observed (Landais et al., 2006a). Usually the temperature changes for the AIM events in inland Antarctic sites like EDC and EDML are in the range of 2 – 4 ℃ (EPICA, 2006). Does this imply that Berkner Island being a coastal site experienced larger temperature changes during the AIM events than the more inland sites during the Antarctic warming events in the last glacial period?

Larger magnitude of change in $\delta^{15}N$ does not necessarily imply large temperature changes just like the occurrence of the "strange event". Any temperature increase is generally accompanied by an increase in accumulation rate with a concurrent increase in the DCH. The warming also causes the firn to thin as the transformation of snow to ice proceeds faster in warmer temperatures as it is a temperature–activated metamorphic process. Hence the observed $\delta^{15}N$ anomaly is due to a combination of gravitational and thermal fractionation. The $\delta^{40}Ar$ data are used to correct for the gravitational fractionation in the measured $\delta^{15}N$ and the remaining term known as the $\delta^{15}N_{excess}$, which is the thermal fractionation component is then used to reconstruct temperature changes .

3.5.1 $\delta^{40}Ar$ Results

To extract the thermal counterpart of the observed $\delta^{15}N$ isotopic anomaly, $\delta^{40}Ar$ measurements were carried out to enable $\delta^{15}N_{excess}$ calculations. The argon isotopes in the depth range of the climatic events were measured at Laboratoire de Science du Climate *et* de l'Environment (LSCE) in Gif-sur-Yvette, France under the supervision of Dr Amaelle Landais.

The δ^{40}Ar data obtained were noisy therefore the use of these data in any quantitative assessment would be inconclusive. Figure 3.5.1 plots the data as δ^{40}Ar/4 and theoretically should be equivalent to δ^{15}N in the absence of any thermal fractionation. In total 16 samples were measured across the AIM 12 event, out of which 3 samples could be eliminated on the basis of procedural error and another sample as an outlier. Despite the elimination of the suspected data there was still a certain degree of scatter. Taking into consideration the values which were assumed to be real implied that most of the observed δ^{15}N signal across the AIM 12 event was due to gravitational fractionation.
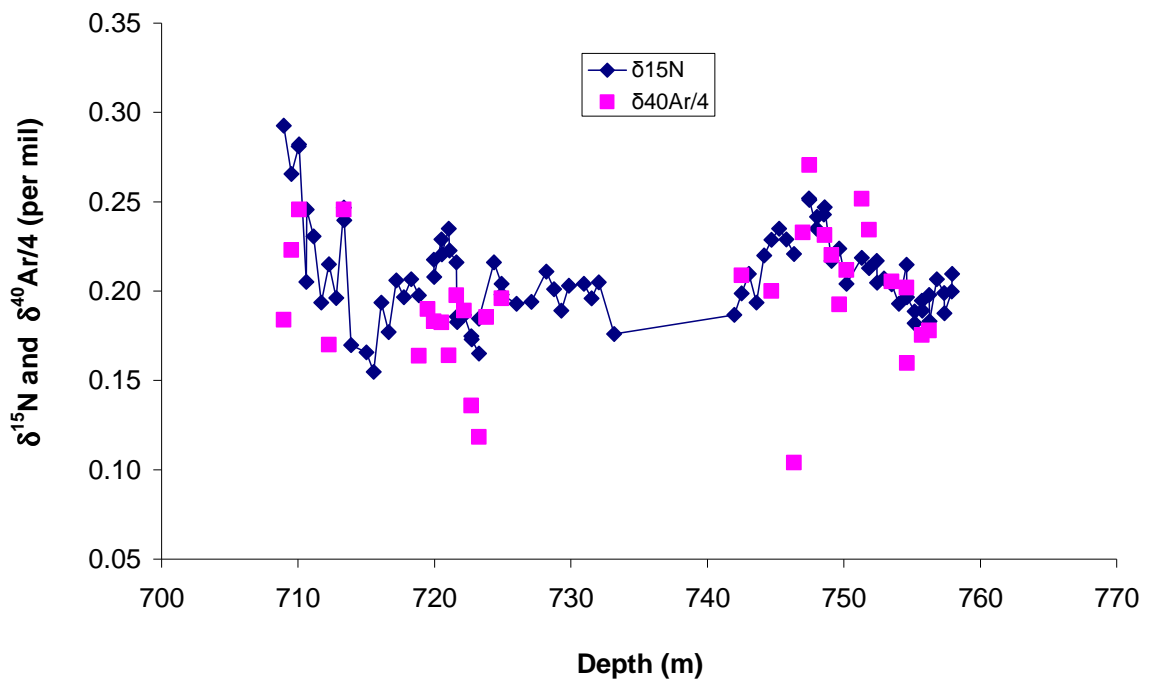
Figure 3.5.1: The δ^{40}Ar/4 data plotted together with the δ^{15}N data on the same depth scale.

The δ^{40}Ar measurements were performed on 11 samples across the AIM 8 event and four samples had δ^{40}Ar/4 values extremely lower than δ^{15}N. The validity of these data is questionable and needs to be re-analysed in future. An important observation for this period is that the δ^{40}Ar/4 also shows a sudden decrease during the transition of the AIM 8 event. The δ^{40}Ar measurements confirm that during the transition of the AIM 8 event the temperature rise caused the thinning of the firn layer. The δ^{40}Ar/4 data matched the δ^{15}N data at the beginning of the transition and when it started to decrease. However, when the

117

temperature reached its maximum, according to the δD_{ice} profile, the $\delta^{40}Ar/4$ values were lower than the recorded minimum in $\delta^{15}N$. This difference could be attributed to a temperature gradient in the firn resulting in $\delta^{15}N_{excess}$ or could simply be due to an artefact in the analytical method. However if the $\delta^{40}Ar$ data during this period were real then it would suggest that the DCH decreased by approximately 14 m. The deuterium profile implies an increase in temperature of approximately 3°C across the AIM 8 event. The estimated decrease in the DCH is in agreement with Caillon *et al.* (2003), which suggested that a rapid increase in temperature of 2 °C could lead to a 10 m reduction in the DCH.

The samples were not analysed in duplicate but the total analytical error for $\delta^{40}Ar$ measurements using the same extraction technique and instrument has been previously reported in the range of 0.016 – 0.020 ‰ (Amaelle Landais, personal communication). In future some of these measurements should be repeated in duplicate to gain better estimates on the accuracy of the method. One of the reasons for such large scatter in the dataset could be due to poor quality of the samples. Some of the samples may have been sampled from a fractured column of the ice or some of the samples were being exposed to temperatures above -25 ºC during transportation from Norwich to Gif-Sur-Yvette. The samples were shipped in thermally insulated box packed with solid CO_2 and the box was sent by air freight for next day delivery. The delivery was delayed by 24 hours and therefore there could be a possibility that some ice samples in the box (probably those at the top) had warmed up slightly although there were enough solid CO_2 remaining in the box and ice melting was ruled out upon visual inspection of the samples.

Ikeda-Fukazawa *et al.* (2005) demonstrated that the storage temperature affects the composition of the trapped gases. Gases could leak out of the ice lattice depending on the molecular size of the molecules (Huber *et al.*, 2006a; Severinghaus and Battle, 2006). Gases in ice leak through micro-cracks causing mass dependent fractionation, often observed in poor quality ice and the gas-clathrate transition zone where ice samples are typically fractured (Bender *et al.*, 1995; Kobashi *et al.*, 2008). Argon is relatively more susceptible to the gas loss processes than nitrogen during core retrieval and storage (Bender *et al.*, 1995). The depth of our study is out of the gas-clathrate transition zone but the

quality of these samples may have been compromised during transportation. There are contrasting opinions about the influence of gas loss process on the isotopic composition of the gases. Kobashi *et* al. (2008) observed argon loss but the isotopic composition appeared to be unaffected whereas some other studies (Severinghaus *et* al., 2003; Severinghaus et al., 2001) indicated that gas loss process affects isotopic composition. In order to eliminate the possibility of gas loss fractionations and to infer the quality of the ice core samples, $\delta O_2/N_2$ (a proxy indicator for the quality of the ice core samples) and $\delta Ar/N_2$ should have been measured. The $\delta Ar/N_2$ ratio is a very good proxy indicator for the amount of argon isotopic fractionation by gas loss (Severinghaus *et* al., 2003). Unfortunately these ratios were not measured as the N_2 and O_2 gases were removed from the sample prior to analysis.

3.5.2 $\delta^{15}N_{excess}$ approach for temperature change reconstructions

Measurements of both nitrogen and argon isotopes allow the extraction of the thermal isotopic anomaly, a parameter called $\delta^{15}N_{excess}$ or $\delta^{15}N_{xs}$, which can be related to change in temperature (ΔT) during an abrupt climate change (Grachev & Severinghaus, 2005; Severinghaus and Brook, 1999; Landais *et* al., 2004a, b). There are numerous ways in which $\delta^{15}N$ and $\delta^{40}Ar$ could be used in the evaluation of ΔT. Severinghaus *et* al., (1998) forced a gas and heat diffusion model with boundary conditions of a 5 °C step function to simulate the observed $\delta^{15}N$ and $\delta^{40}Ar$ datasets. A similar approach of using an initially prescribed magnitude of warming in some form of a step function in the model of heat and gas diffusion combined with firn thickness estimates from a firn densification model (Schwander *et* al., 1997) was employed in the work of Severinghaus *et* al., (2003) and Taylor *et* al., (2004). The magnitude of the initially prescribed warming is adjusted until a best fit to the observed data is obtained. A temperature history from the borehole temperature calibrated $\delta^{18}O_{ice}$ was used to drive the model to fit the $\delta^{15}N$ and $\delta^{40}Ar$ datasets to obtain ΔT during the Bølling Allerod Transition in the GISP2 ice core (Severinghaus and Brook, 1999).

Another possibility of generating surface temperature history from $\delta^{18}O_{ice}$ is through a linear relationship with a constant slope ($\alpha = d\delta^{18}O_{ice}/dT_s$) across the transition of the climatic events. Landais *et* al. (2004) used α values ranging from 0.26 to 0.70 in the firn densification model developed by Goujon *et* al., (2001) to simulate $\delta^{15}N_{excess}$. This particular approach was validated by sensitivity tests of the modelled $\delta^{15}N_{excess}$ to different surface temperature scenarios, derived independently of the $\delta^{18}O_{ice}$ profile. A similar approach was used to model the $\delta^{15}N_{excess}$ profile to interpret temperature changes during the DO 18, 19 and 20 events at the NorthGRIP site (Landais *et* al., 2004b).

This project was designed to measure a high resolution $\delta^{15}N$ and $\delta^{40}Ar$ across the AIM 8 and AIM 12 events to calculate $\delta^{15}N_{excess}$, which could be modelled by firn densification model to interpret ΔT across these climatic events. An important outcome of this study would have been to calibrate the classical $\delta^{18}O_{ice}$ palaeo-thermometer and to establish if Berkner Island had a different or rather warmer climate than the more inland Antarctica sites. Due to the scatter in $\delta^{40}Ar$ measurements these objectives could not be fulfilled at this stage.

On a hypothetical basis it is possible to calculate $\delta^{15}N_{excess}$ by eliminating samples that were subjected to procedural error such as leaks or low sample volumes or outliers and samples that had unexplained low values across the AIM 8 event. Figure 3.5.2 a,b shows the $\delta^{15}N_{excess}$ profile for the AIM 8 and the AIM 12 events and the following data interpretation should be treated with caution as data points were eliminated to reduce the scatter. Grachev and Severinghaus, (2005) stated that the $\delta^{15}N_{excess}$ could be utilised directly to calculate temperature changes by taking advantage of the laboratory determined thermal diffusion coefficients for $^{29}N_2/^{28}N_2$ and $^{40}Ar/^{36}Ar$ for a typical glacial temperature range of -60 to 0 ºC. This is a very simple and direct approach of converting $\delta^{15}N_{excess}$ into ΔT and does not involve any modelling and its associated assumptions and uncertainties. However due to the lack of confidence in $\delta^{40}Ar$ data further interpretation would be unjustified.
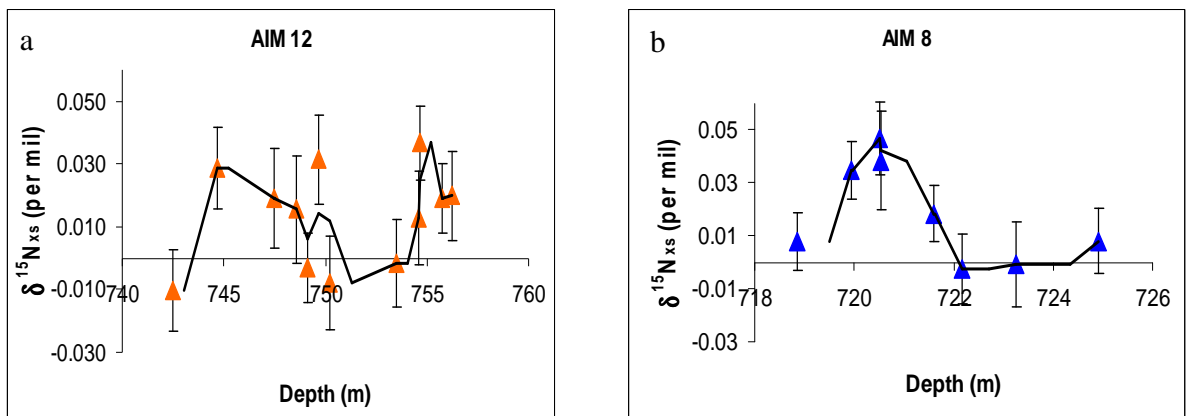
Figure 3.5.2: Presumed $\delta^{15}N_{XS}$ for (a) AIM 12 event and (b) AIM 8 event.

The $\delta^{15}N_{excess}$ profile obtained for AIM 12, after rejecting the suspected data (4 points), shows that there might be a small thermal signal of +0.02 ‰ but the uncertainties on these measurements are quite large to draw any conclusive remarks. Interestingly it shows that there was a cooling before the warming of the AIM 12 event. Although the cooling is much more dramatic here (may be due to poor quality Ar data), this particular observation is very similar to what has been observed for DO 12 at NGRIP (Landais *et* al., 2005, Landais *et* al., 2004). The presumed $\delta^{15}N_{excess}$ evolution for AIM 8 is very impressive as the shape and the position of the peak coincides with the predicted shape and timing. In addition, the $\delta^{15}N_{excess}$ clearly shows an increase of 0.04 ‰, a significantly pronounced signal as compared to AIM 12 event. This may suggest that surface temperature change was larger and more abrupt during AIM 8 than during AIM 12. This also raises the question regarding the validity of the modern spatial $\delta D - T$ relationship (α) during the AIM 8 event. To fully answer this question, more precise $\delta^{40}Ar$ measurements and a rigorous modelling with a firn densification model is needed. There has been documented evidence that coastal sites may have lower isotope-temperature coefficients and could experience larger temperature changes (Masson-Delmotte, 2003). The Law Dome site has a coefficient of approximately 3‰ per ºC, which is almost half the observed value at more in-land sites (Masson-Delmotte, 2003). Certainly the changes in $\delta^{15}N$ across the AIM 8 were more abrupt but this does not imply large changes in temperature but could also be attributed to changes in the hydrological cycles that influence the accumulation rates.

3.5.3 Using the firn densification model to reconstruct temperature changes

3.5.3.1 Temperature reconstruction from the measured $\delta^{15}N$ data only: examples from previous studies

As discussed in the previous section that the $\delta^{15}N_{excess}$ approach to reconstruct temperature changes was not successful due to poor quality $\delta^{40}Ar$ data. However, there are numerous studies that estimated temperature changes across the abrupt climate events without the use of $\delta^{15}N_{excess}$ or $\delta^{40}Ar$ measurements (Leuenberger *et* al., 1999; Lang *et* al., 1999; Huber *et* al., 2006a; Kobashi *et* al., 2007). The $\delta^{15}N$ data were explicitly corrected for gravitational influence (provided if the accumulation rate is accurately known) by the firn densification model and then the residual $\delta^{15}N$ variations were attributed to firn temperature gradient. Below is the summary of data interpretation of the individual studies that only used the measured $\delta^{15}N$ to reconstruct temperature changes.

Leuenberger *et* al. (1999) corrected the observed $\delta^{15}N$ profile in NGRIP ice cores by applying gravitational correction obtained with the firn densification model. The residual $\delta^{15}N$ profile was simulated with a dynamic firn densification model with incorporated heat transfer and molecular diffusion (Schwander *et* al., 1997). The model was run for three temperature scenarios: (1) the quadratic temperature dependence on $\delta^{18}O_{ice}$, calibrated by borehole measurements and using two isotope – temperature sensitivity; (2) $\partial\delta^{18}O_{ice}/\partial T = 0.67‰/K$ and (3) $\partial\delta^{18}O_{ice}/\partial T = 0.33‰/K$. The accumulation rate changes were estimated from the calcium and ammonium records, which showed a reduction in the accumulation rate of 25% for the study period. The $\delta^{15}N$ profile generated with the temperature dependencies of $\partial\delta^{18}O_{ice}/\partial T = 0.33‰/K$ closely matched the measured $\delta^{15}N$. Kobashi *et* al. (2007) used the firn densification model (Goujon *et* al., 2003), surface temperature proxy derived from $\delta^{18}O_{ice}$ with an adjustable scaling α as a surface temperature proxy, and independently estimated accumulation rate from annual layer counting with ice flow corrections to calculate the DCH and thermal gradient in the firn. The thermal and gravitational fractionation of $\delta^{15}N$ was separated and a cooling of 3.3 ± 0.5 ºC was

estimated for 8.2 kyr BP event based on an oxygen isotope temperature sensitivity of $\alpha = 0.55 \pm 0.05$ ‰/°C.

Lang *et* al. (1999) assumed no significant change in the DCH although the measured δ^{15}N was corrected for gravitational fractionation by the model. The two approaches taken here to reconstruct temperature change were slightly different from the one adopted in Leuenberger *et* al. (1999). Lang et al. (1999) derived α from the Δage calculations obtained with the model, which was then used in the firn densification model to simulate the measured δ^{15}N. However, assuming constant DCH or applying constant gravitational correction is not favoured because of the variability in accumulation rates that could have an effect on the firn thickness and subsequently on the δ^{15}N signal. The approach of Huber et al. (2006) (discussed in Section 1.7.1) seems to be an ideal way of reconstructing temperature changes across the warming events from the measured total δ^{15}N signal.

3.5.3.2 Firn densification model results for Berkner Island

The firn densification modelling work was carried out in collaboration with Jean-Marc Banola from LGGE. A firn densification model developed by Goujon *et* al. (2003) was used in this study to simulate the measured δ^{15}N signals. The temperature history and the accumulation rates used in the model were derived from the deuterium isotope profile, using empirical relationships which are valid at EDC. In addition an independent estimation of accumulation rates were also obtained from gas markers (CH_4, CO_2) from EDC and Berkner Island gas profiles. The annual layers were calculated from the gas markers, which were then divided by the thinning rate obtained from the ice flow model to calculate paleo-accumulation rates. There are large discrepancies between the two accumulation rates estimation approach. For the time period of interest to this study (27 – 50 kyr BP) the discrepancies are as large as 70%. It has been proven that the temperature dependency derived accumulation rates can be lower during the glacial times (Cuffey and Clow, 1997; Huber *et* al., 2006a) and that the empirical relation between accumulation and temperature may not be valid during glacial times. On the other hand there is a significant uncertainty in the accumulation rates derived from the gas markers due to poorly constrained thinning rate

from the ice flow model and poor gas data resolution. It is difficult to decide which palaeo-accumulation estimation is the best scenario for the model simulations and as a result both scenarios were used.

Figure 3.5.3 & Figure 3.5.4 shows the model output for $\delta^{15}N$ using both accumulation scenarios and temperature history derived from deuterium data. The model works well for the Holocene period as it closely matches the measurements. Figure 3.5.6 also shows that the model output with the accumulation rate derived from deuterium fits the data for the Holocene period and therefore suggests that the relationship between accumulation, temperature and deuterium valid at inland Antarctica such as Dome C is also valid at Berkner.
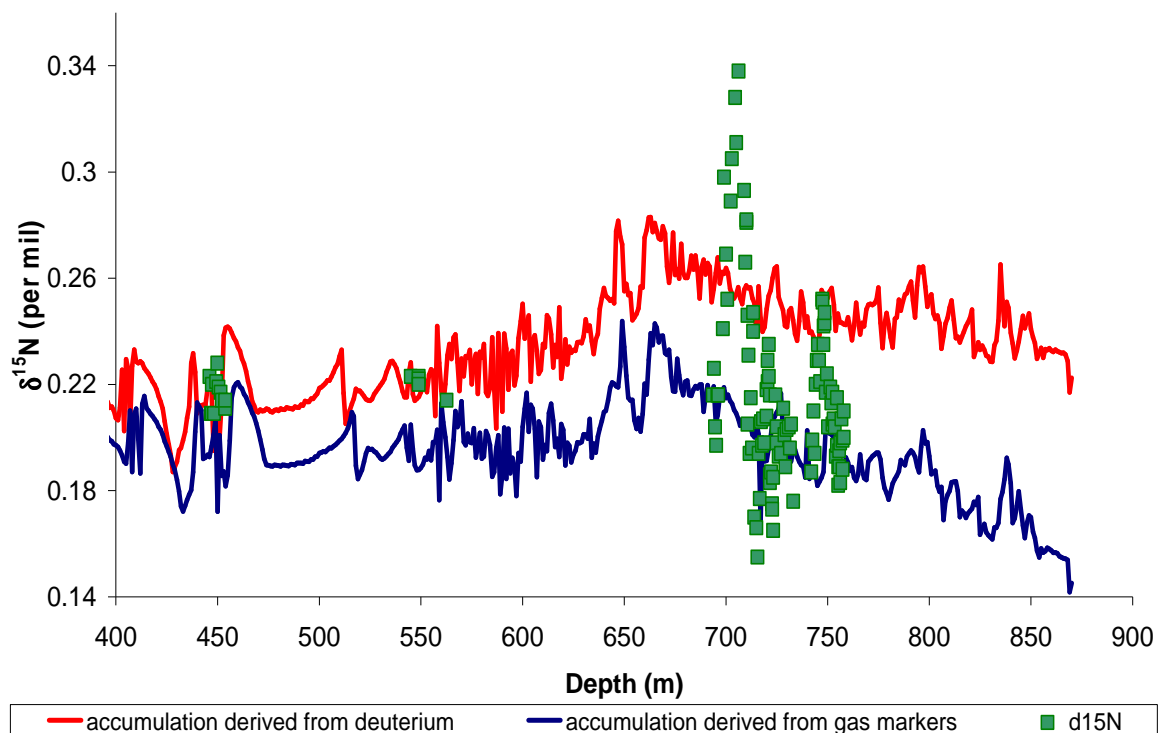
Figure 3.5.3: Modelled $\delta^{15}N$ output from the firn densification model with the accumulation history derived from deuterium profile (red) and gas synchronisation (blue) fitted to the measured $\delta^{15}N$ (green squares).
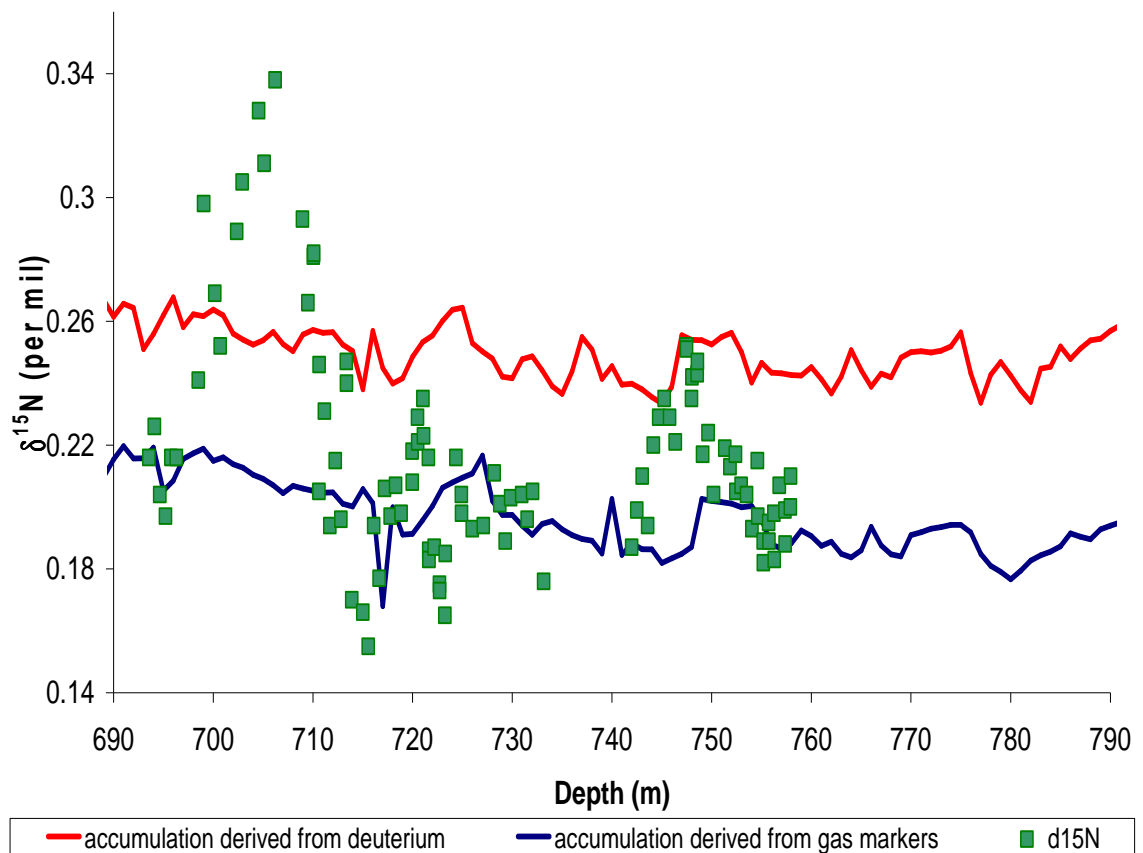
Figure 3.5.4: Modelled δ^{15}N from the firn densification model fitted to measurements for the depth range of 690 – 760 m.

Both model runs disagree with the measurements in the 690 – 760 m depth range. The modelled δ^{15}N from temperature history and accumulation rate derived from the deuterium isotopes were overestimated across the warming events. Although the peak measured values for AIM 12 event were matched by the model, the amplitude and the timing of the signals for both events could not be reconciled with the model.

Landais *et al.* (2006a) noted similar observation of model-data mismatch during the glacial periods in Antarctica. In that study the Arnaud *et al.* (2000) model was forced with the water isotopes derived accumulation rate and the model outputs for δ^{15}N were overestimated by 0.1 ‰ and 0.25 ‰ during the LGM for EDML and Law Dome DSS ice

cores respectively (see Figure 3.5.5 & 3.5.6) (Landais *et* al., 2006a). The disagreement between the modelled $\delta^{15}N$ and measurements in this study is not as large as those observed by Landais *et* al. (2006a) and there is an excellent match during the Holocene period, which in contrast to the EDML model-data match (see Figure 3.5.7). The annual layer counting in EDML ice cores during the early Holocene suggested that the accumulation rate inferred from water isotopes was underestimated by 30%. The revised accumulation rate from annual layer counting resolved the data-model mismatch for the early Holocene period in EDML (Landais *et* al., 2006a). Lower estimates for accumulation rate during the LGM, obtained from Dome C – EDML dust and volcanic peaks synchronisation, reduced the mismatch in EDML ice core to some extent.
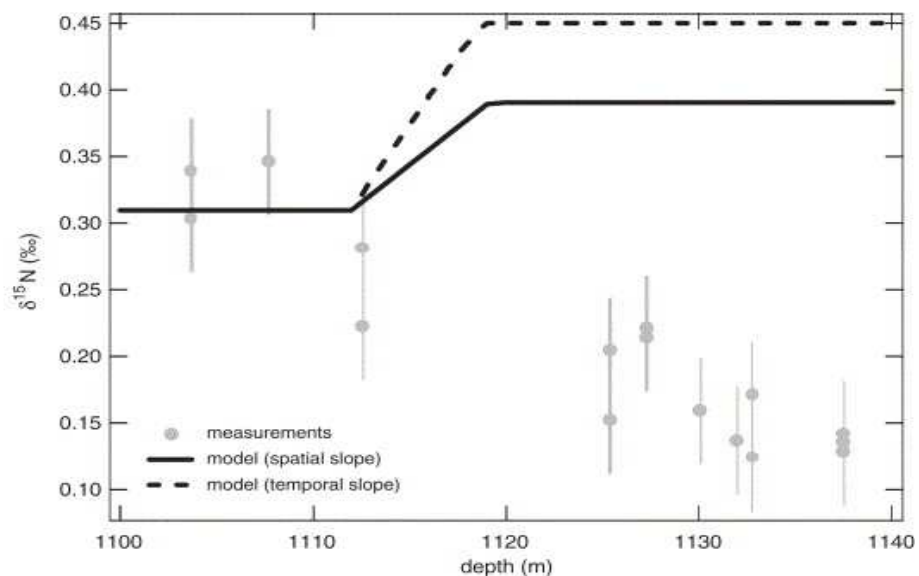
Figure 3.5.5: $\delta^{15}N$ measurements on the Law Dome DSS ice core (grey circles). $\delta^{15}N$ evolution from the <u>Arnaud *et* al. (2000)</u> model forced by modern surface conditions for EH and deduced from the water isotopes for LGM (the black continuous line is inferred when using the spatial slope, 0.67‰ °C^{-1}, and the black dotted line when using the temporal seasonal slope, 0.44‰ °C^{-1}). (Figure adapted from Landais et al., 2006)

126
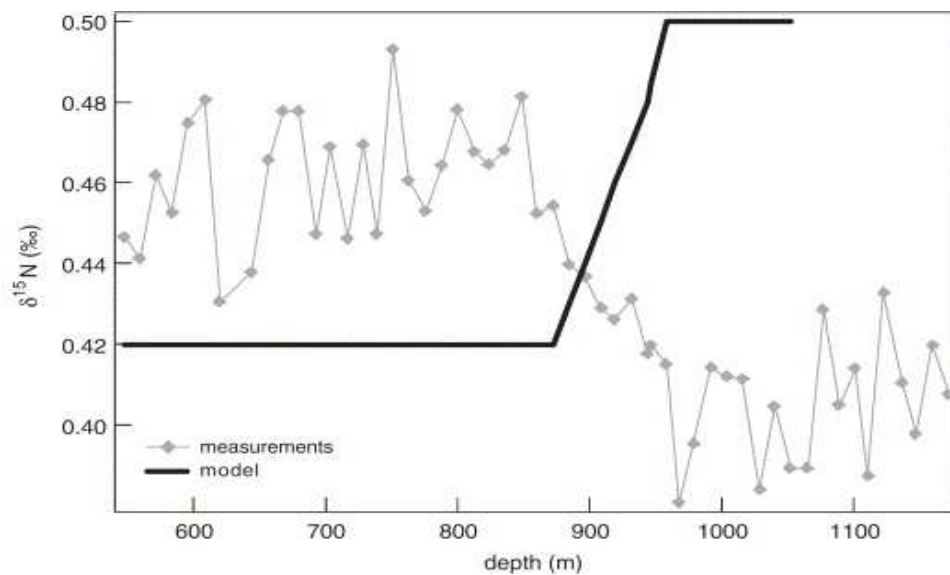
Figure 3.5.6: $\delta^{15}N$ measurements on   the EDML ice core (grey circles). $\delta^{15}N$ evolution from the Arnaud *et* al. (2000) model forced by surface conditions (accumulation rate and temperature) assumed to be modern levels for EH and deduced from the water isotopes for LGM (black dotted line). (Adapted from Landais *et* al., 2006a)

Previous studies have indicated that the accumulation rate derived from water isotopes may not be accurate and should be treated with caution for Antarctic sites, e.g. Taylor Dome (Monnin *et* al., 2004), Siple Dome (Taylor *et* al., 2004; Severinghaus *et* al., 2003), Vostok (Parrenin *et* al., 2004) and Dome C (Udisti *et* al., 2004). The atmospheric conditions especially for the coastal sites could distort the accumulation – water isotopes relationship. The Holocene accumulation rate variability at Law Dome DSS site was not linked to fluctuations in water isotopes because this coastal site is affected by strong cyclonic activity as compared to more inland East Antarctic, where local temperature controls the atmospheric moisture content (van Ommen *et* al., 2004).

The accumulation derived from synchronising gas profiles (CH_4 and CO_2) of Berkner Island and Dome C, indicated by the blue line in Figure 3.5.4 shows lower modelled $\delta^{15}N$ values as compared to those values obtained with the accumulation rate derived from water isotopes. This model run does not simulate either the amplitude of the measurements or the timing of the event but is not in vast disagreement as observed for the other Antarctic sites

such as Law Dome and EDML (Landais *et* al., 2006a). There is some time – depth offsets between the two model runs. This is not unusual as different accumulation scenarios were used and such mis-match in finer detail is not a concern here because both model runs did not match the amplitude well enough. However, the modelled δ^{15}N values obtained with the accumulation rate derived from synchronisation of gas records reproduced the baseline values of the climatic events whereas the modelled δ^{15}N values obtained with the accumulation rate derived from the deuterium isotopes captured the maximum values of the measurements, particularly for the AIM 12 event. On the basis of the two model runs we can speculate that during the transition of the warming events the accumulation rate increased rapidly. If the isotope – temperature coefficient (α) observed at inland Antarctica (6.04 ‰ per °C at EDC) is also valid at Berkner Island then an increase in accumulation rate from ~2 cm a^{-1} – 6 cm a^{-1} for the AIM 8 event and an increase from ~ 2.5 cm a^{-1} – 9 cm a^{-1} for the AIM 12 event would reconcile the mis-match between the model data and the measurements (Barnola, J.-M., pers. comm.). Hence a site such as Berkner Island with these high resolution δ^{15}N measurements may give the best chance of resolving the δ^{15}N data – model mismatch and to provide insights about past accumulation rate changes and its relationship to temperature during an Antarctic warming event for coastal sites.

In order to calculate the absolute temperature changes from the observed δ^{15}N signals and to calibrate the δD – temperature coefficient of 6.04 ‰ per °C, an accurate accumulation rate history needs to be known. More reliable approach of estimating accumulation rate such as high resolution Na$^+$ ion measurements across the climatic event should be considered in future. The annual layers can be inferred from high resolution Na$^+$ ion measurements which then can be multiplied by thinning rate to obtain accumulation rates. Once the accumulation rate history is known and supposing the model can replicate the amplitude and timing of warming events, then the other parameters such as the depth of the convective zone and temperature sensitivity could be tuned to fit the measurements.

Currently the Δdepth and Δage inferred from the difference in the position of the peak signal in δ^{15}N and δD agrees well with the model results. Consequently, the δ^{15}N measurements validate the chronology of Berkner Island ice core through the warming

events and therefore support the assumptions regarding the accumulation rate history and temperature history. If the accumulation rates across the warming events are different and are not linked to water isotopes then it could change the existing age scale of the ice core. In order to conserve the age scale of the ice core, two protocols could be adopted as highlighted by Huber *et al*. (2006a): (1) change the accumulation rate and thinning rate accordingly since the age scale depends only on the product of accumulation and the ice thinning and (2) change the slope of the accumulation to δD dependency but maintain a constant average accumulation rate over a certain period. The slope could be increased during the warming phase to give a higher accumulation rate and decreased to give a lower accumulation rate during the cold phase of the climatic event. Hence changing the accumulation rate does not imply that the current chronology verified by our δ^{15}N data would be destroyed.

3.5.4 Phasing firn temperature gradient with δ^{15}N profile

The model of Goujon *et al*. (2003) also calculates the past firn temperature gradients. The firn temperature gradient is not so sensitive to accumulation rate changes but is sensitive to temperature changes imposed by rapid warming. The accumulation rate changes will influence the positioning of these temperature gradients. Figure 3.5.7 shows the phasing between the temperature gradients and the δ^{15}N measurements. The firn temperature gradient, obtained from the model using the deuterium derived accumulation rate, is in phase with the δ^{15}N measurements for both climatic events. Not only has it matched the two climatic events but also the cold dip before the strange event as well. The increase in firn temperature gradient matches the variation and positioning of the δ^{15}N peak and therefore fully confirms that we have identified a warming signal in a gas phase.
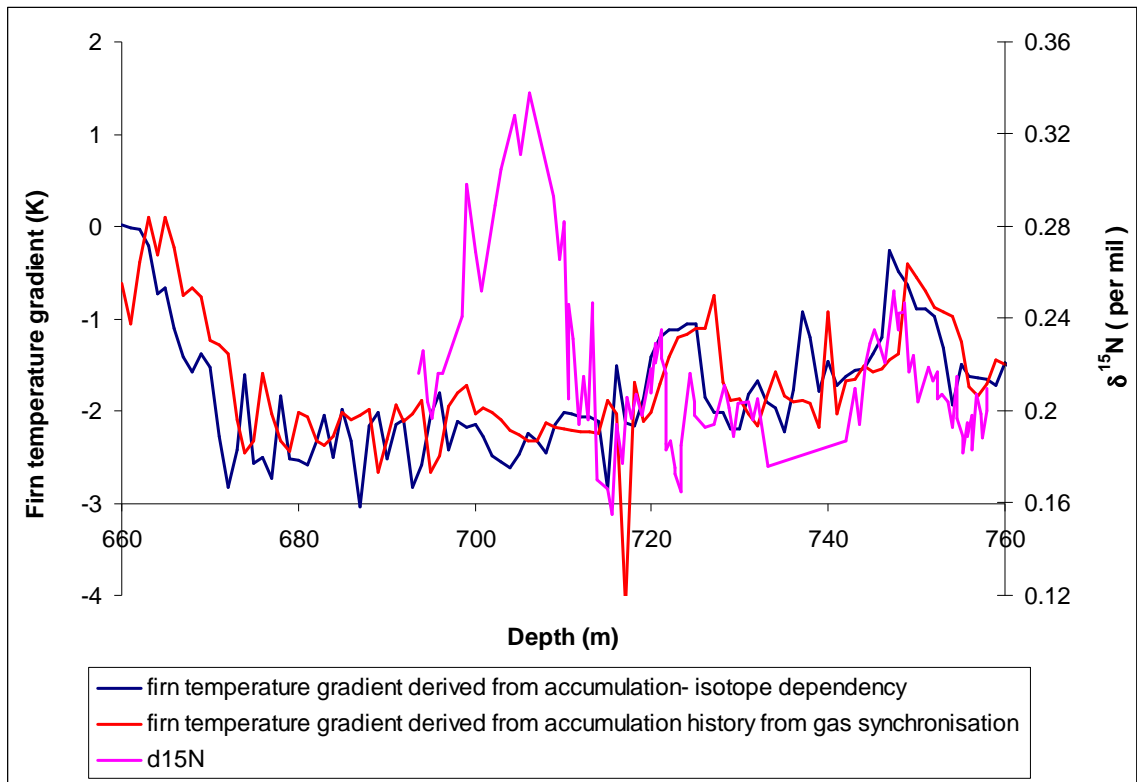
Figure 3.5.7: Phasing of the measured $\delta^{15}N$ (pink) with firn temperature gradients obtained from the model forced with the accumulation history derived from the deuterium profile (blue) and gas synchronisation (red).

The phasing correlation suggests that the relationship between deuterium and accumulation established for the central part of the Antarctic ice sheet is also valid at Berkner Island for the two warming events. This may be contradictory to what was stated earlier regarding the relationship between deuterium and accumulation rate. However it may be true that during the warming events the relationship between deuterium and accumulation rate may not be valid. It could be changing quite drastically over a short period of time which could potentially induce greater gravitational fractionation of nitrogen isotopes. On a longer time scale the accumulation rate derived from deuterium gives an average accumulation for that particular period and therefore does not affect the chronology.

The firn temperature gradient obtained using the accumulation rate derived from gas synchronisation is out of phase with the $\delta^{15}N$ signal. This suggests that the thinning rate obtained from the ice flow model to calculate accumulation rate is not correct.

3.5.5 Use of the firn temperature gradient to estimate surface temperature changes

More recently Kobashi *et al*. (2007, 2008) stated that the firn temperature gradient from the model can be successfully used to reconstruct surface temperature changes in Greenland ice cores based on two assumptions: (1) gravitational influence is very minimal and (2) the change in the temperature gradient in the firn layer mimics the surface temperature evolution if it is a rapid surface temperature change on a decadal – centennial timescales, or if it is faster than heat diffusion in the firn. Kobashi *et al*. (2008) modified the firn densification-heat transfer model (Goujon *et* al., 2003) to calculate surface temperature changes from the firn temperature gradient history and accumulation rate. The accumulation rate history was obtained from visual layer counting coupled with ice flow corrections. The surface temperature (T_s) was generated by adding the calculated temperature (T_b) at the bottom of the firn in the previous model year to the firn temperature gradient calculated from $\delta^{15}N$ and $\delta^{40}Ar$.

The approach adopted by Kobashi *et al*. (2008) of using the firn temperature gradient could not be used to calculate the surface temperature changes in this study because the $\delta^{40}Ar$ data were noisy, and because the temperature change across the two events occurred on a longer timescale of 800 – 2400 yrs. Consequently the firn temperature would have completely equilibrated and therefore we only see a very small temperature gradient in the range of 1 – 1.5 ℃. This may indicate that the $\delta^{15}N$ technique may not be an appropriate method to estimate temperature changes for the Antarctic warming as the temperature changes occur on longer timescales as compared to Greenland sites. Nevertheless the $\delta^{15}N$ signal obtained for the AIM 8 and AIM 12 is definitely a climatic signal. It may not be directly related to temperature changes but is related more indirectly through an increase in accumulation rate due to the increase in temperature and concurrent increase in the DCH.

3.6 Summary

The δD profile reveals that the climate record from the Berkner Island ice core is consistent with climate records from the other sites in Antarctic. The climate instabilities during the last glacial period are evident in the ice core record, showing two Antarctic warming events, the AIM 8 and the AIM 12 event which occurred at approximately 38 kyr BP and 46 kyr BP respectively. The $\delta^{15}N$ measurements of the trapped nitrogen gas in the ice cores across these two warming events revealed a signal of +0.07 ‰. In addition to these signals across the Antarctic warming events an enrichment of 0.2 ‰ in $\delta^{15}N$ was observed after the AIM 8 event.

The observed changes in the $\delta^{15}N$ data across the two warming events were small and the rate of change was slow as compared to the analogous DO events in Greenland ice cores. Nevertheless the newly obtained high precision $\delta^{15}N$ measurements during the MIS 3 period produced isotopic anomaly that were larger than the documented $\Delta\delta^{15}N$ for the last glacial–interglacial signal observed in EDML and Law Dome DSS ice cores. These small signals could be observed partly due to the improved method adopted in this study, which was specifically designed for identifying small signals in Antarctic ice cores. The data for the AIM 12 event reveal a cooling event preceding the major warming event, a pattern consistent with the DO 12 event in Greenland. During the AIM 8 event the temperature rose very abruptly resulting in rapid thinning of the firn as indicated by the depleted $\delta^{15}N$. After the AIM 8 event the $\delta^{15}N$ signal increased anomalously and does not correlate with any known Antarctic warming events during the MIS 3 period.

The Δdepth and Δage values were calculated by plotting $\delta^{15}N$ and δD data on the same depth scale. The calculated Δdepth and Δage agrees well with the modelled Δdepth and Δage, which was used to derive the chronology of the Berkner Island ice core. Hence the $\delta^{15}N$ measurements verified the derived chronology across the AIM 8 to AIM 12 event and also validate the assumptions used in the temperature, accumulation and deuterium isotope relationships. The Δdepth corrected $\delta^{15}N$ data show a high correlation with the δD data for the AIM 12 event ($r^2 = 0.78$) and there is also a high degree of coincidence between the onset and the peak of the warming signal in $\delta^{15}N$ and δD for the AIM 8 event. The very

large peak around 700 m, referred to as the "strange event" does not coincide with any peak in the δD record and therefore could not be to attributed to any climatic warming event. An increase of 0.2 ‰ could be accounted for by an increase of 39 m in the DCH. An increase in the DCH seems to be a logical explanation because the occurrence of this strange event coincides with the time when the ice sheet at Berkner Island was undergoing change in altitude. The hypothesis that the strange event is linked to rapid increase in altitude change could be further validated by independent evidence of increasing accumulation rate during this period. The accumulation rate derived from deuterium does not record any increase in accumulation rate during this period. It is possible that the deuterium – accumulation relationship failed during this time and therefore there is a need for a palaeo-accumulation rates estimation that is independent of water isotopes.

The quantification of the thermal isotopic anomalies from the observed δ^{15}N data is important in evaluating the magnitude of the temperature change during these climatic events and also to calibrate the δD – temperature sensitivity. The δ^{40}Ar measurements were very noisy, and any estimation of the δ^{15}N excess parameter was inconclusive. The firn densification model was incapable of simulating the observed δ^{15}N signal and failed in interpreting the δ^{15}N signal in terms of gravitational and thermal components. Due to these limitations it was not possible to quantify the temperature change during the climatic events. The fact that there is an agreement between the modelled and the calculated Δage, suggest that the modern isotope – temperature sensitivity of 6.04 ‰/°C could be valid for the glacial period. Therefore based on the water isotopes the temperature change for the warming events would be in the range of 4 – 5 °C, which is not significantly different from the inland Antarctic sites. This δD – temperature sensitivity should be calibrated in future by firn densification modelling. It is obvious that the main reason for the current failure of firn densification model is the highly uncertain accumulation rates. The model-data mismatch suggests that Berkner Island experienced large variations in accumulation rate during the warming and strange events. An independent assessment of palaeo-accumulation rates such as high resolution Na^+ measurements to infer seasonal cycles could explain the strange event and also reconcile the model-data mismatch.

An interesting outcome of the modelling work was phasing the firn temperature gradient with the $\delta^{15}N$ signal. The firn temperature gradients during the two warming events, obtained from the model using the accumulation rate derived from the deuterium isotopes, are in phase with the $\delta^{15}N$ signal. The firn temperature gradient is less sensitive to rapid variations in accumulation rate changes but is more dependent on the surface temperature changes during the warming events. An excellent phasing between the positive firn temperature gradient and the $\delta^{15}N$ signal confirms that the isotopic signal obtained is definitely a climatic warming event. This phasing also validates the timing of the observed $\delta^{15}N$ signal and therefore provides further constraints on the chronology of the Berkner Island ice core in addition to the constraints provided by the Δage calculations. The absolute values of the firn temperature gradient are very small and suggest that the change in temperature was slow and gradual therefore most of the observed $\delta^{15}N$ signal was gravitational in nature. Nevertheless, the signal observed is clearly a climatic event. The $\delta^{15}N$ signal may not be directly related to temperature changes but more indirectly through an increase in accumulation rate due to increases in temperature resulting in a larger gravitational fractionation and again argues for better accumulation rates via detailed chemistry.

Temperature can have two main effects on $\delta^{15}N$. Firstly the thermal fractionation effect should cause a transient change wherever a temperature gradient exists in the firn. In this case the firn temperature gradient of $1 - 2$ °C in thousand of years across the two warming events. The thermal fractionation for the two warming events studied here would be in the order of 0.01 ‰. Increasing temperature could influence the gravitational signal of $\delta^{15}N$ signal either way; increase in temperature is generally associated with an increase in accumulation rates that would increase the firn thickness thereby increasing $\delta^{15}N$ values but if the accumulation rate is not changing then increasing temperature could decrease the firn thickness due to faster densification process and lowers the COD thereby decreasing $\delta^{15}N$ values. The decrease in $\delta^{15}N$ values across the warming event AIM 8 is not unusual and Caillon et al. (2001) have observed similar behaviour for $\delta^{15}N$ signals during the warming events in Vostok ice cores. In common with other authors we are therefore unable

quantitatively to explain the δ^{15}N signal although it seems to correlated with temperature or δD proxy.

Currently it is impossible to isolate the thermal signals from the δ^{15}N measurements due to the limitations mentioned above. The δ^{15}N technique could not successfully be applied to Berkner Island, implies that this site does not record rapid temperature changes on the order of decadal-centennial timescales during the warming events. Nevertheless indirectly the δ^{15}N signal obtained is likely to be a complex proxy for climate change at Berkner Island responding to both temperature and accumulation. The high resolution δ^{15}N data could be correlated with methane (regarded as a proxy for climate change in the Northern Hemisphere) from similar depths, which would provide insights into the phasing relationship between the Northern and the Southern Hemisphere climate. The δ^{15}N signal and methane are proxies for changes in the gas phase, and therefore thus overcomes uncertainties in phasing due to Δage, which is crucial in synchronising the climate change records between the two hemispheres.

Chapter 4: Trace Gas Measurements across the AIM 8 and AIM 12 Event in the Berkner Island Ice core.

4.1 Introduction

4.1.1 Timing of millennial-scale climate change in Antarctica and Greenland during the last glacial period

4.1.2 Bipolar seesaw mechanism

4.2 Methane Data

4.2.1 Sample selection

4.2.2 Discussion

4.3 Phase relationship between Antarctic and Greenland climate during the last glacial period

4.4 Phasing of atmospheric CO_2 and $\delta^{15}N$ for the AIM 12 Event.

4.5 Summary

4.1 Introduction

Gases trapped in air bubbles in ice cores provide valuable information about the past atmospheric composition of greenhouse gases such as CH_4 and CO_2. Reconstructing the atmospheric histories of these gases provides a basis for understanding past climate dynamics particularly by determining the phasing between climate change and the greenhouse gases. In May – June 2009 I measured CH_4 across the AIM 8 and AIM 12 events in an ice core from Berkner Island. Measurements were made at the Laboratoire de Glaciologie et Geophysique de l'Environment (LGGE), Grenoble, France under the supervision of Jerome Chappellaz. These data are presented in this chapter. Also discussed are the CO_2 data for the AIM 12 event measured by Hinrich Schaefer at LGGE.

The primary aim of the high resolution methane measurements across the two warming events is to try to establish the phase relationship between Antarctic and Greenland climate change. Due to rapid inter-hemispheric mixing times of ~ 1 year, large scale changes in methane or any other long lived atmospheric gases are globally synchronous at the timescales that we are investigating here. As a result, methane measurements in ice cores provide a valuable tool for synchronising ice core chronologies and comparing the timing of climate events, which are recorded by various proxies in the ice cores, between the hemispheres. It has been shown that increases in methane are almost synchronous with increases in temperature in the Northern Hemisphere (Huber *et al*., 2006a; Landais *et al*., 2004a; Severinghaus *et al*., 1998). Atmospheric methane is generally considered as a useful time marker for climate change in the Northern Hemisphere (Petit *et al*., 1999).

The previous chapter presented data that show a climatic $\delta^{15}N$ signal for the two Antarctic warming events (AIM 8 and AIM 12). Measuring methane in the same ice core samples therefore provide information on the time leads/lags of rapid climate change events in the North and of its Antarctic counterpart. Since the proxy for climate change at Berkner ($\delta^{15}N$) and the proxy for climate change in Greenland (CH_4) are both derived from trapped gases, this circumvents the need to consider uncertain Δage

calculations to study the phase relationship between the two hemispheres. Such a direct approach has previously been applied to study the phase relationship between Antarctic and Greenland climate in the Vostok ice core for the MIS 5d/c transition (approximately 108 kyrs BP) but the data quality and data resolution were poor (Caillon et $al.$, 2003). Coupling the high resolution $\delta^{15}N$ data obtained in this study with the methane data should better constrain the timing of the millennial scale Greenland and Antarctic climate events. In addition, Berkner Island is an ideal site to study the phase relationship between the two hemispheres as it is located on the Weddell Sea in the South Atlantic Ocean facing Greenland. The Weddell Sea plays a critical role in the Thermo-Haline Circulation (THC).

This chapter provides a summary of previous research findings on the issue of the timings of the climate events in both hemispheres. The phase relationship between Antarctic and Greenland climate based on the methane and $\delta^{15}N$ data from this study are discussed in detail. There is also a brief discussion of the time lag between temperature increase and carbon dioxide rise across the AIM 12 event.

4.1.1 Timing of millennial-scale climate change in Antarctica and Greenland during the last glacial period

Paleoclimate proxies such as ice cores and speleothem records suggest periods of climate instability during the last glacial period. The records suggest that the climate oscillated very rapidly between cold and warm phases and that these rapid oscillations occurred over a period of several thousand years. These millennial-scale climate instabilities are common to both hemispheres, although the rate and magnitude of the changes are much greater in Greenland than in Antarctic (EPICA, 2006).

Blunier et $al.$ (1998) synchronised the GRIP (Greenland), Byrd and Vostok (both Antarctica) water isotopic records using methane to compare the timing of the millennial-scale events between 10 and 45 kyrs BP. Their conclusion was that the warming in Antarctica began before the warming in Greenland for DO events 8 and 12 by more than 1 kyr. This particular study was extended to cover the entire last glacial period (90 kyrs BP) in Blunier and Brook (2001) and it was revealed that this phase relationship was a common feature for the seven identified warming events in Antarctic

labelled A1 to A7. The A1 to A7 events precede D-O events 8, 12, 14, 16/17, 19, 20 and 21 by 1.5 to 3 kyrs (Blunier and Brook, 2001).

The study of Blunier *et al.* (1998) and Blunier and Brook (2001) estimated the time lag of 1.5 – 3 kyr after taking into account the Δage estimations. The Δage estimation for Byrd during the last glacial period was on the order of 500 years, which was verified independently by $\delta^{15}N$ of nitrogen gas. Therefore it is highly unlikely that the time lag between the Antarctic and Greenland is an artefact of the Δage calculations. Caillon *et al.* (2003a) used a different approach to study the phase relationship, whereby methane and climatically fractionated isotopes of gases ($\delta^{15}N$ and $\delta^{40}Ar$) were measured in the same Vostok ice core during the MIS 5d/c transition. Such a phasing study circumvents the need to accurately constrain the Δage and the errors associated with the synchronisation of the records from both hemispheres. From this study, Caillon *et al.* (2003) suggested that warming in the Northern Hemisphere occurred 2 kyrs after warming in the Southern Hemisphere.

The above studies suggest that warming in the Southern Hemisphere precedes warming in the Northern Hemisphere. However, there are some contradictory studies which suggest that climate change is in phase in both hemispheres. Bender *et al.* (1999) used $\delta^{18}O$ of atmospheric oxygen in trapped gases in the ice to synchronise the GISP2 (Greenland) and Vostok (Antarctica) time scales. Bender et al. (1999) concluded that the DO events found in GISP2 between 35 and 75 kyr BP are also found at Vostok and were in phase within ± 1.3 kyrs. Furthermore, $\delta^{18}O$ data from the Taylor Dome Ice Core in coastal East Antarctica suggests that the timing of the deglacial warming is synchronous with GISP2 rather than with Byrd ice core records (Steig *et al.*, 1998). This has led to the suggestion that perhaps climatic change in coastal region of Antarctica is synchronous with Greenland rather than with central Antarctica. However, the chronology of the Taylor Dome ice core is believed to be in error and has been questioned by Mulvaney *et al.* (2000). Evidence for synchronous climate events in both hemispheres from the Taylor Dome ice core record may raise questions about the possibility of a complex regional pattern of millennial-scale temperature variability in high latitudes of the Southern Hemisphere (White and Steig, 1998). In addition, Raisbeck *et al.* (2002) used high resolution [10]Be to synchronise GRIP and Dome C

records and suggested that the time lag between the onset of the DO 10 event and the corresponding Antarctic δD maximum is approximately 200 yrs. It should be noted that the Antarctic δD peak for the AIM 10 event is very small and Steig (2006) questioned why it should be regarded as a climatic signal when similar sized peaks between AIM 1 and AIM 2 are not considered to be a climatic signal (Steig, 2006).

It is apparent that the issue of the timing of millennial scale Greenland and Antarctic climatic events is complex and new information is required to gain a better understanding of the elusive climate dynamics responsible for these variations. Recently, it was highlighted by the EPICA community members (2006) that there is a strong one-to-one coupling of glacial climate variability in Greenland and EPICA Dronning Maud Land (EDML), Antarctic (although with a phase lag for Greenland climate change). Similarly to Blunier and Brook (2001), EPICA (2006) not only showed a correlation between the larger Antarctic warming events and the longest DO events but the high resolution record also showed a corresponding Antarctic counterpart for almost all the DO events in the Greenland ice core. The data suggested that the Antarctic warm events began before the DO events but the time lag estimates could not be determined more precisely than the synchronisation error of 600 ± 200 yrs (EPICA, 2006). An interesting finding of EPICA (2006) was that the amplitude of the Antarctic warm event was found to be linearly dependent on the duration of the concurrent stadial in the North suggesting a reduction in the Atlantic Meridional Overturning Circulation (AMOC). This, in turn, supports the bipolar seesaw mechanism, which is described in more detail below.

4.1.2 Bipolar seesaw mechanism

The connection between the hemispheres may take place via the ocean or via the atmosphere. However, it seems that the ocean plays a critical role in regulating the past climate of both polar regions and that Thermo-Haline Circulation (THC) plays an important part in linking the two hemispheres. The most common mechanism proposed to explain asynchronous millennial scale climatic change in both hemispheres is commonly known as the "Seesaw Effect".

The Seesaw Effect theory postulates that through disturbances in the THC in the North Atlantic, the climate signals in both hemispheres exhibit anti-phase behaviour (Stocker,

2000). Climate changes in Greenland are caused by disturbances in the Atlantic thermohaline circulation and are closely linked to ice-rafting events (Heinrich events) and the associated melt water that occurs in the North Atlantic region (Blunier *et al.*, 1998). An influx of freshwater reduces North Atlantic Deep Water (NADW) formation and initiates cooling in the North Atlantic region. This disruption in the THC prevents northward migration of heat and could lead to warming of the southern hemisphere. Cooling in the North Atlantic region reduces melting and induces the re-establishment of NADW formation, rapidly bringing heat to the North Atlantic. Model simulations demonstrate the sensitivity of NADW formation to freshwater inputs and also highlighted that the resumption of the conveyor belt circulation after a shutdown is a rapid process (Stocker, 2000). The ocean models also suggest that initiation of North Atlantic THC cools at least parts of the Southern Hemisphere, hence justifying the see-saw mechanism. However the nature of the Southern cooling is a gradual rather than abrupt change and takes about 1000 years to cool off due to large reservoir of heat represented by the Southern Ocean (Severinghaus, 2009).

4.2   Methane Data

4.2.1   Sample selection

Samples for methane measurements were selected across the two warming events (AIM 8 and AIM 12) to study the phase relationship and additional samples were selected in the depth range of 693 – 716 m. These additional samples were measured to provide better constraint on the Berkner gas age chronology and high resolution methane measurements could also provide some insights into paleo-accumulation rates across the "strange" event at 708 m. The resolution of the methane data across the warming events are in the range of 0.55 – 1.10 m (1 or 2 bags) or 200 – 400 yrs. The resolution of the data across the strange event is typically 0.55 m.

4.2.2   Discussion

Figure 4.2.1 presents the methane data measured for the Berkner Island ice core in the depth range of 680 – 760 m. Altogether 59 samples were measured and only data for four samples were rejected either due to leaks in the sample vessels or poor standard

deviation on replicate measurements. The standard deviation of duplicate samples is generally better than 10 ppbv.
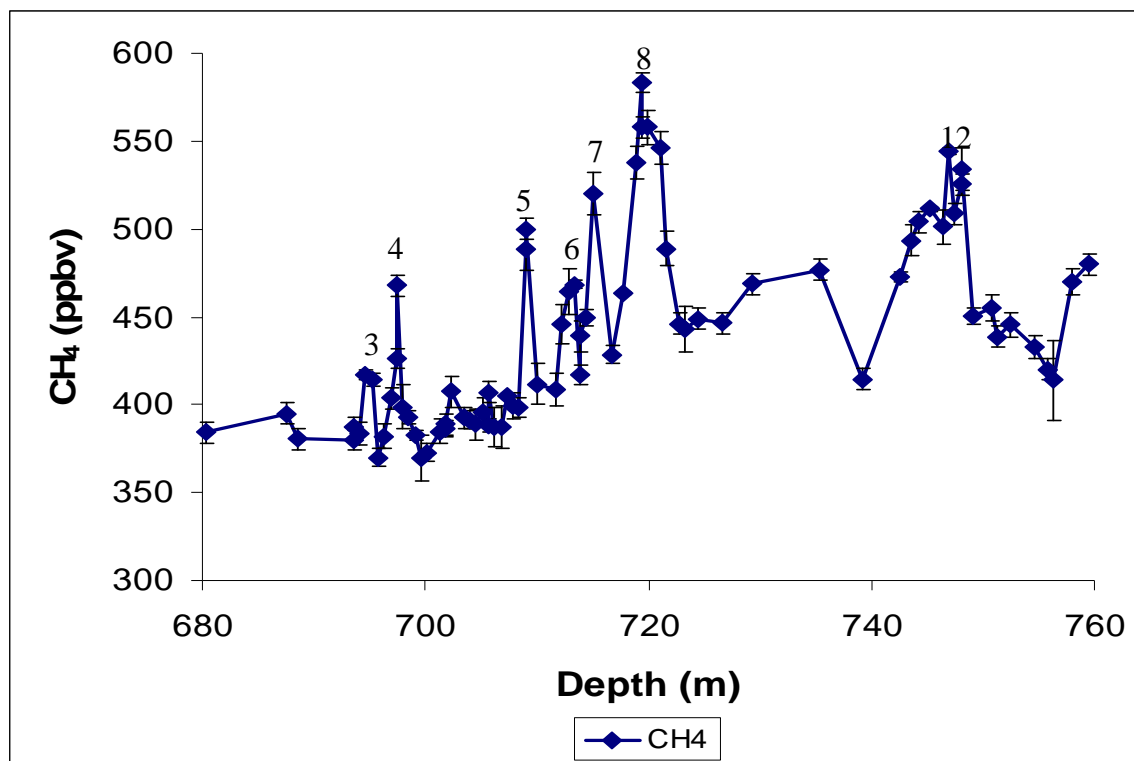
Figure 4.2.1: Shows the methane data measured here plus some earlier data from Grenoble in the depth range of 680 – 760 m for Berkner Island ice core, encompassing the MIS 3 period. The numbers 3 – 8, 12 above the methane peaks denote DO events by comparison to Greenland methane records. Error bars show 1 standard deviation for 3 replicate measurements.

The methane peak at 747 m corresponds to the DO 12 event and the methane peak at 719 m corresponds to the DO 8 event seen in the δD_{ice} and $\delta^{15}N$ of trapped N_2 from this ice core. The magnitude of changes in methane concentrations across these climatic transitions during the last glacial period is about 100 ppbv, which is consistent with the findings of other studies (Huber, *et al.*, 2006a; Landais *et al.*, 2006b). The methane values increased rapidly from 450 ppbv to 550 ppbv during the transition of the DO 12 event and an increase from 450 ppbv to 580 ppbv during the transition of the DO 8 event. The magnitude change across the transition of these events is in close agreement with the Byrd data (Blunier *et al.*, 1998), Dome C data (Spahni *et al.*, 2005) and the

Greenland CH_4 records. This gives confidence in the validity of the methane data obtained in this study. The slight differences between different methane records could be attributed to interpolar differences and signal attenuation at low accumulation sites (Chappellaz *et al*., 1997; Spahni *et al*., 2005). The variations in the concentration and the magnitude of change in methane during different DO events could be attributed to variations in the extent of the glacial wetlands and factors controlling emissions from the wetlands, which are the largest natural source of atmospheric CH_4.

Although the chief objective for methane measurements was to study phase relationships between the two Antarctic warming events observed in the $\delta^{15}N$ profile, additional high resolution CH_4 measurements were carried out in the depth range of 690 – 716 m to obtain better synchronisation of gas records and to estimate paleo-accumulation rates that could possibly explain the anomalous behaviour in $\delta^{15}N$. This work is in progress and will be developed further in collaboration with Jean-Marc Barnola and his colleagues at LGGE. The methane data (See Figure 4.2.1) show signals for DO 3 – 7. These variations or methane peaks closely resemble the Greenland methane composite record (Blunier *et al*., 2007) (See Figure 4.2.2).

Preliminary inspection of the methane data for the DO 3 – 7 events shows that the Berkner gas age chronology for the DO 5 event does not correspond to the GICC05 age scale (see Fig. 4.2.2). There is an apparent disagreement of ~ 2000 years between the Berkner and GICC05 age scales for the timing of the DO 5 event methane peak. The Berkner age scale for DO 5 is older by 2000 years compared to the GICC05 age scale. It is also noteworthy that according to the GICC05 there are ~1800 years between the maxima of DO 7 and DO 6 and ~1300 years between DO 6 and DO 5 event. Figure 4.2.1 shows that the difference in depth between the peak maxima of DO 7 and DO 6 is 2 m whereas the difference in depth between the peak maxima of DO 6 and DO 5 is 4 m. These observations tend to suggest that if the thinning rate was constant throughout DO 5 – DO 7 events then the accumulation rate between DO 6 and DO 5 would have increased by a factor ~ 2.5. Consequently the doubling of the accumulation rate could explain most of the anomalous behaviour in $\delta^{15}N$ at 710 m depth, which also occurred between DO 6 and DO 5 events (See Fig. 4.2.3). However appropriate thinning rates and annual layer thicknesses should be calculated with the aid of an ice flow model in order to confirm an increase in paleo-accumulation rate.
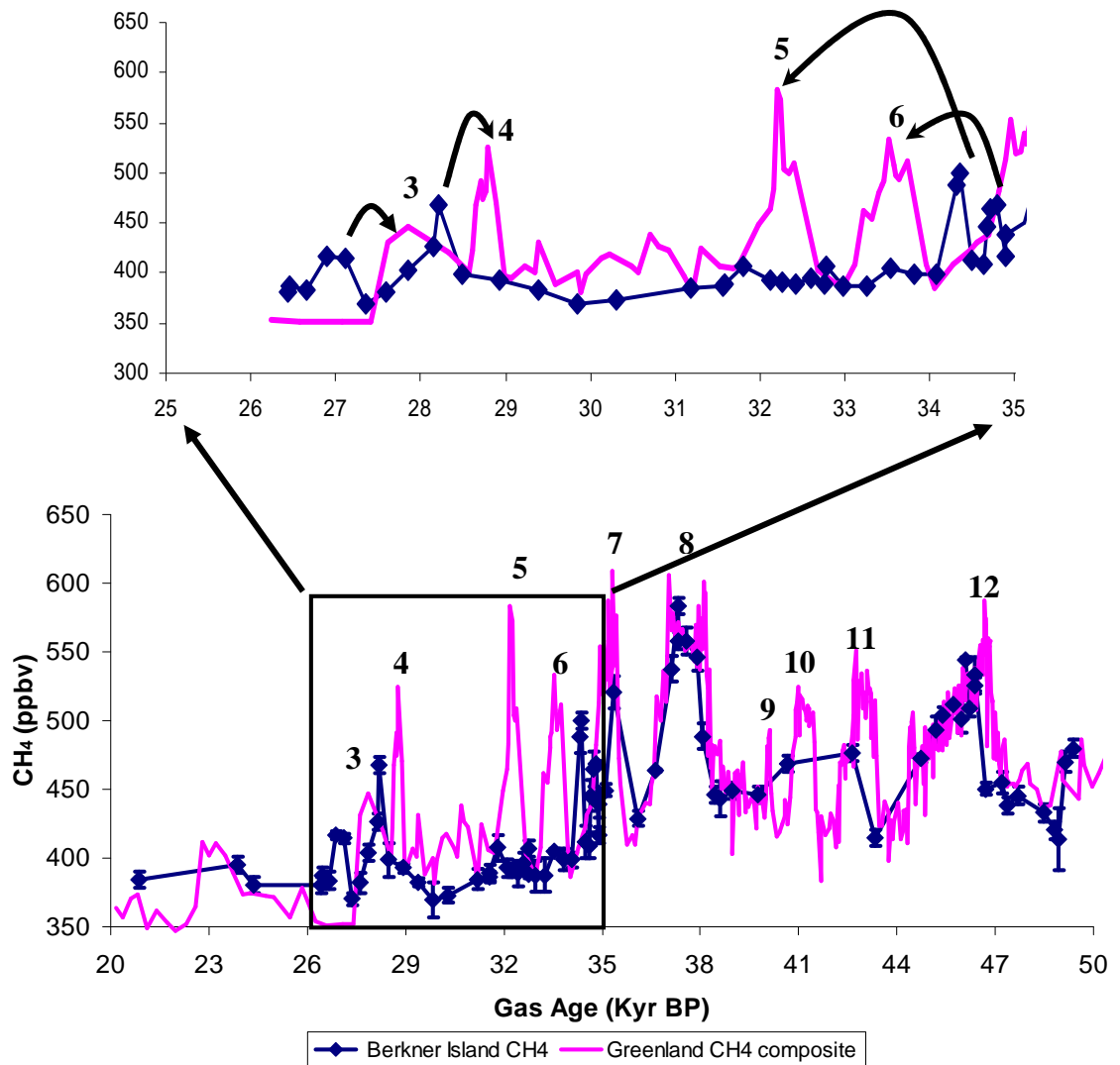
Figure 4.2.2: Methane data (blue diamonds) from Berkner Island are plotted on the Berkner gas age chronology and are compared to the Greenland Methane Composite (pink solid line) on GICC05 age-scale (Blunier *et al.*, 2007). The enclosed methane variations in the box highlight the region of disagreement in Berkner gas age chronology as it does not correspond to the GICC05 age-scale. The disagreement is shown (top) on an expanded scale with correct peak matching indicated by arrows.

The depth of the maximum values of the CH_4 peak for DO 8 and 12 events are correlated with the maxima of the $\delta^{15}N$ peaks for the AIM 8 and AIM 12 events respectively (see Figure 4.2.3). An interesting feature of Figure 4.2.3 is the rate of change in methane across the DO 8 and 12 events, which is very rapid compared to the rate of change in $\delta^{15}N$ at Berkner Island. This observation reinforces the earlier argument that the climate change in Antarctica was much slower than the climate

144

change in Greenland. The methane increased from its stadial values to maximum values in approximately 300 and 600 years for the DO 12 and DO 8 event respectively. The methane increase for the DO 12 event seems to occur in two stages, a slow gradual increase of 30 – 50 ppbv and then a rapid increase of 100 ppbv, consistent with the findings of Landais *et al*. (2004a).
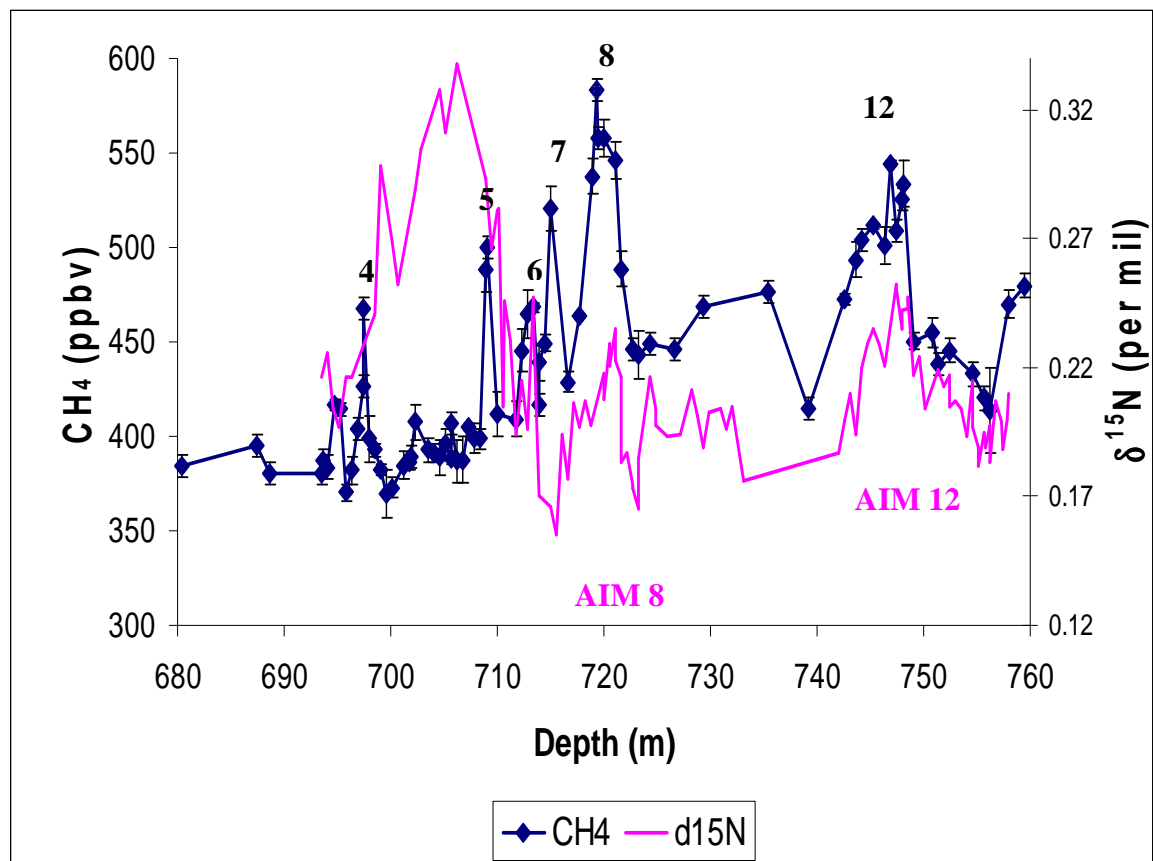
Figure 4.2.3: Comparison of $\delta^{15}N$ and CH_4 data from Berkner Island plotted on the same depth-scale. The numbers 4 – 8 and 12 above the methane peaks represent DO events.

4.3 Phase relationship between Antarctic and Greenland climate during the last glacial period

Methane increased almost synchronously with climate change in the Northern Hemisphere (Huber *et al*., 2006b; Severinghaus *et al*., 1998). Almost 75 % of the natural sources of methane occur in the Northern Hemisphere. Generally, increases in

methane concentration lag DO events by ~ 25 - 75 years (Huber *et al*., 2006b) and by 0 – 30 yrs during the last deglaciation (Severinghaus *et al*., 1998). Huber *et al*. (2006b) showed that for the DO 12 event methane lagged temperature by 50 ± 25 yrs and by 70 ± 25 yrs for the DO 8 event. Synchronous changes in methane concentration and Greenland temperature are thought to be caused by changes in the source emissions from tropical and/or northern mid-latitude wetlands (Dällenbach et al., 2000). Methane increases during DO events could also be due to thawing of permafrost regions (Huber *et al*., 2006).

To study the phasing relationship it is crucial to identify precisely the onset of the warming events in the $\delta^{15}N$ profile. This was achieved by matching the $\delta^{15}N$ variations and the Δdepth corrected δD profile to identify the onset of the warming event both in the gas and in the ice phase (refer to Top panel of Figure 4.3.1). Also the phasing between the firn temperature gradient and $\delta^{15}N$ (refer to Figure 3.5.7) was used as another approach in deciding the onset of the AIM 12 warming event. Once the onset of the warming was identified in the $\delta^{15}N$ profile then the time lag estimate was simply calculated as the difference between the onset of warming in the $\delta^{15}N$ profile and the onset of the rise in methane signal.

It is apparent from Figure 4.3.1 that $\delta^{15}N$ was increasing in response to local climate changes at Berkner Island whilst the methane values were almost stable or near its stadial values. The methane values only increased very rapidly once the $\delta^{15}N$ reached its maximum. This behaviour was expected and according to the seesaw theory the rates of climate changes in the Northern Hemisphere are supposed to be rapid due to the fast re-establishment of the THC. It has been previously reported that the maxima of the Antarctica warming events coincide with the onset of the DO events in Greenland (EPICA, 2006). The maxima of the methane peak is in phase with the $\delta^{15}N$ maxima for the AIM 12 event but there is apparently a time lag between the methane peak and the $\delta^{15}N$ peak for the AIM 8 event. However the Greenland methane composite record (see Figure 4.2.3) shows a double methane peak rather than a single peak for the DO 8 event. If the resolution of the Berkner methane measurements were increased then the peak of the methane transition may be in phase with the maxima of the $\delta^{15}N$. Therefore it is concluded that the peak of the methane signal is in phase with the peak of the $\delta^{15}N$
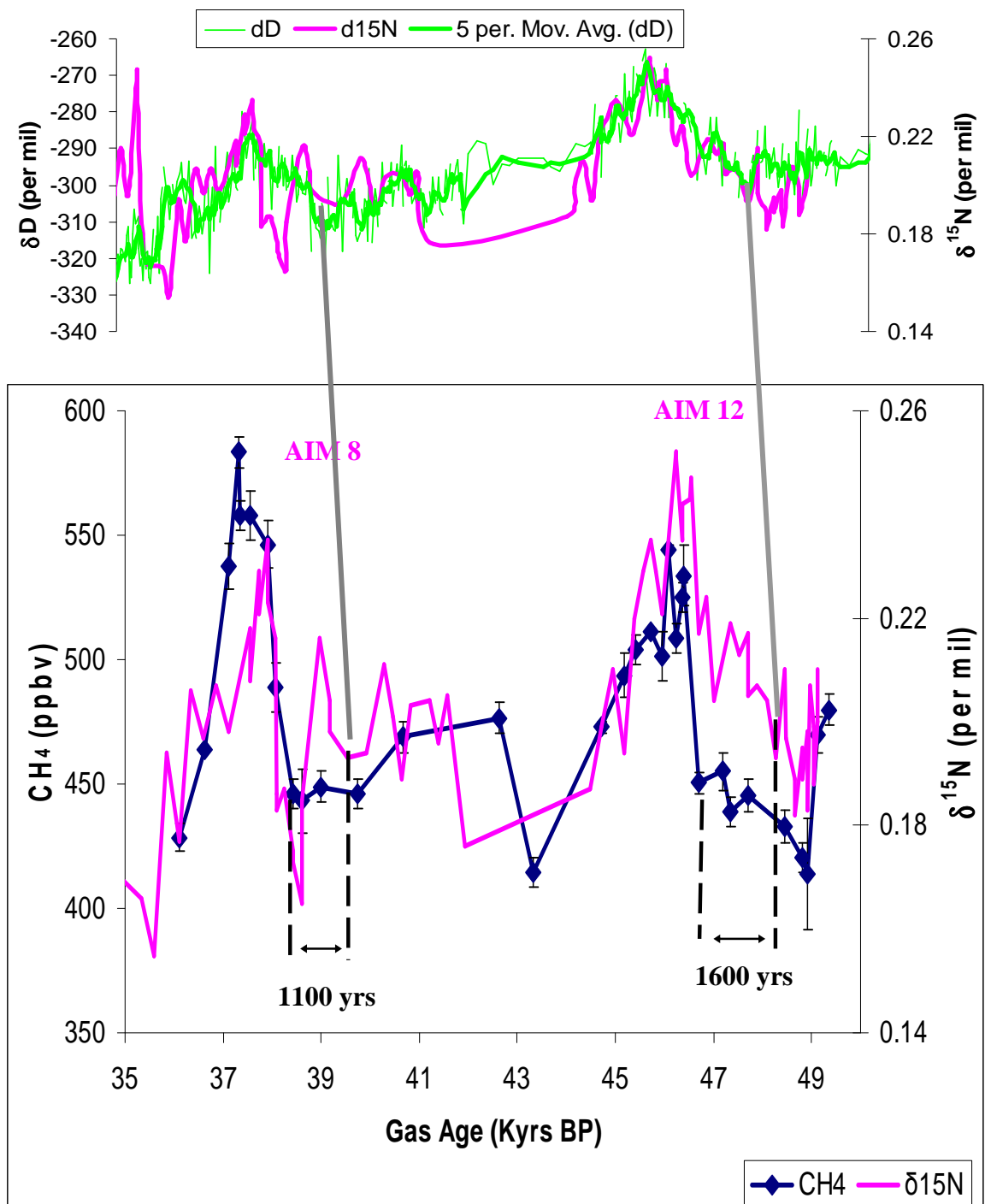
Figure 4.3.1: Top panel shows the δD and $\delta^{15}N$ plotted on the same depth scale. The δD data were corrected for Δdepth. The correlation between δD and $\delta^{15}N$ was used to decipher the starting point of the warming event in the $\delta^{15}N$ profile (grey line). Methane and $\delta^{15}N$ data for the AIM 8 and AIM 12 events plotted on the Berkner gas age scale to estimate the time lag for the onset of climate change between the Northern Hemisphere and Southern Hemisphere.

signal. Similar findings by Bender *et al.* (1999) led them to conclude that rapid climate change in both hemispheres was synchronous. Although the observation of Bender *et al.* (1999) is correct, i.e. that the maxima coincide, it is however misleading to suggest that the onset of that climate change in both hemispheres are in phase as there seems to be a time lag between the onset of warming events in Antarctica and Greenland during the last glacial period.

The data suggest a time lag of 1100 ± 360 yrs between the onset of warming for the AIM 8 and the DO 8 event and a time lag of 1600 ± 350 yrs between the start of warming for AIM 12 and the DO 12 event. The error associated with the time lag estimate was calculated from the midpoint age difference between the bottom and the increasing methane value during the transition of the DO event, which was then added to the age resolution of the $\delta^{15}N$ measurements at the beginning of the $\delta^{15}N$ peak (that is the age resolution per bag of sample at that particular depth, which is in the range of ~ 150 – 200 yrs). The error estimates given here are believed to be the upper limit.

Assuming the global synchronisation of methane, the methane and the $\delta^{15}N$ data obtained in this study demonstrate that warming events in the Antarctic preceded the rapid DO events in Greenland during the MIS 3 period (see Figure 4.3.1). This finding disagrees with the suggestion of synchronous deglacial climate change between coastal Antarctica and Greenland (following from Steig *et al.*, 1998). It contradicts the suggestion that long interstadials start in the north and spread to the south with Greenland temperature variations leading Antarctic temperature variations over the last 50 Kyrs (Bender *et al.*, 1994c).

The time lag estimates of 1100 ± 360 yrs and 1600 ± 350 yrs are in excellent agreement with the findings of Charles *et al.* (1996) who used isotopic signatures of benthic and planktonic foraminifera in a marine core from the Southern Ocean. Charles *et al.* (1996) concluded that Northern Hemisphere climate changes lag Southern Hemisphere climate by ~ 1500 yrs. The time lag estimate between AIM 8 and DO 8 and between AIM 12 and DO 12 obtained in this study are within the range of 1000 – 2500 yrs obtained by Blunier *et al.* (1998). Delmotte *et al.* (2004) calculated that CH_4 lagged temperature (derived from the δD signal) by 1100 ± 200 yrs from the Vostok ice core on timescales

of 50 – 400 kyr, suggesting that the mechanisms for the millennial scale climate variability in the last glacial period were operational beyond the last glacial period. Nevertheless the time lag estimate from Vostok should be considered cautiously as large Δage corrections of the order of 5000 yrs were applied.

Blunier *et al.* (1998) studied the same Antarctic warming events, A1 (AIM 8) and A2 (AIM 12), as we have investigated in our study. Although the time lag estimates from both studies are in agreement, the approach taken to derive these estimates are quite different. Blunier *et al.* (1998) synchronised the isotopic ice core records from both hemispheres by correlating CH_4 records and then calculating Δage values to assign an ice age. Hence, Blunier's time lag estimate of 1000 – 2500 yrs is subject to uncertainties arising from synchronising the ice core records from both hemispheres and as well as uncertainties from the Δage calculations. Even taking into account the synchronisation error of 200 yrs and a Δage of 500 ± 300 yrs during A1 and A2 in the Byrd ice core (Blunier *et al.*, 1998; Blunier and Brook 2001) the isotopic records of Antarctica and Greenland would not be in phase. Blunier *et al.* (1998) therefore concluded that Antarctic climate definitely leads Greenland climate.

In this study $\delta^{15}N$ and CH_4 data were used to assess the phase relationship between the northern and southern hemispheres. Since both are gas signals this overcomes the need for Δage (between ice and air) calculation and its associated uncertainties in estimating the time lags. The only uncertainty in the time lag estimates given here are from the error in the absolute Berkner gas age chronology that results from the initial work on synchronisation of ice core records via gases. The recent high resolution methane measurements could place additional constraints on the gas age chronology for the AIM 8 and AIM 12 events. Fast high resolution CH_4 variations during warming events could improve the synchronisation error to better than 200 years. However, it is very unlikely that the synchronisation error in the current gas age chronology could be as large as 1000 yrs which would be necessary in order to bring the $\delta^{15}N$ and CH_4 variations in phase for the two Antarctic warming events. For future work it is recommended that high resolution methane data should be used to derive a more robust gas age chronology for the AIM 8 and AIM 12 event (work in progress by Jean-Marc Barnola, LGGE, Grenoble).

It would also be beneficial to match CH_4 data with the Greenland methane composite record and to synchronise both records on a common GICC05 timescale. This could potentially verify or even improve the time lag estimates given here. Currently the CH_4 variations using the absolute Berkner gas age chronology during the AIM 8 matches the Greenland methane composite record on the GICC05 age scale but there is a slight discrepancy during the AIM 12 event. According to the GICC05 age scale, CH_4 began to rise at 47 kyr BP, approximately 500 yrs earlier than noted from the Berkner gas age chronology. Due to this slight discrepancy in the gas age chronology, the lower limit of 1600 ± 350 yrs should be considered as the best time lag estimate for the onset of the warming of the DO 12 event.

Precise dating of the ice core is critical when trying to assess the leads and lags of paleoclimatic events in two hemispheres (White and Steig, 1998). Δage is the largest uncertainty in deriving the ice age chronologies as this depends on the palaeo-accumulation rates and the temperature of the site. Blunier *et al.* (1998) and Blunier and Brook (2001) used Δage estimation to study phase relationships and concluded that millennial scale warming in Antartica preceded the onset of Greenland warmings by 1500 to 3000 yrs. White and Steig (1998) questioned whether there is truly a lead or lag of such magnitude, which is about half-cycle or even more of the DO events, which have a periodicity of approximately 3000 yrs. White and Steig (1998) also suggested that it may be neither a lead nor a lag but an inverse relationship in climate change between Greenland and Antarctica on those timescales. However, this study support the findings of Blunier *et al.* 1998 and Blunier and Brook (2001). The data obtained in our study clearly show that there is an average time lag of ~1400 yrs (840 – 1950 yrs) between the onset of warming in the Antarctic ($\delta^{15}N$) and in Greenland (CH_4) and once the Antarctic reaches the maximum temperature then Greenland temperature increases very rapidly and is almost in phase with the Antarctic and then cooling is almost synchronous. Therefore, this study disputes the possibility of an inverse relationship in climate change as proposed by White and Steig, (1998). The model also suggested that initiation of the THC after a shutdown is a very rapid process, which rapidly transports heat from the Southern Ocean to the Northern Hemisphere (Stocker, 2000), and causing the maxima of the temperature signal to be almost in phase in both hemispheres.

The approach taken here to study phase relationships in the same ice core is more direct as it does not involve any Δage estimation or corrections for Δage. This approach was adopted from the study of Caillon *et al.* (2003a) which concluded that Antarctic warming corresponding to the MIS 5d/c transition preceded the Greenland DO 24 event by 2000 yrs. The $\delta^{15}N$ and $\delta^{40}Ar$ data of Caillon *et al.* (2003a) were noisy and the sampling resolution was not of high enough resolution to identify the start of the warming trend. The modelled Δdepth estimate was used to locate the signal of the MIS 5d/c transition in the gas phase (see Figure 4.3.2). Caillon *et al.* (2003a) were also unable to rule out whether cooling in Greenland is in phase or out of phase with Antarctica. This study suggests that cooling in both hemispheres is almost synchronous. Calculation of $\delta^{15}N_{excess}$ calculations may perhaps allow an even more detailed phasing relationship to be derived and would add confidence to the interpretation of the data.
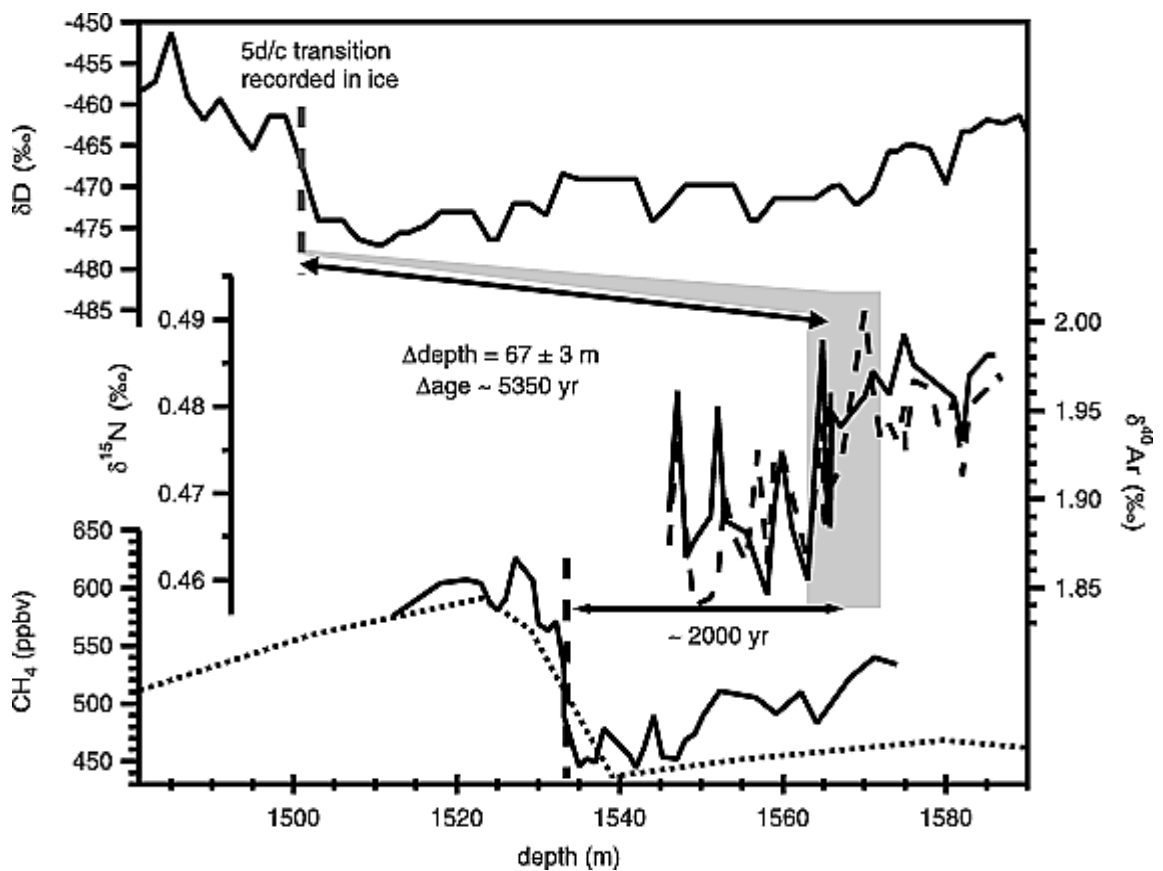
Figure 4.3.2: δD (solid line, Top panel), $\delta^{40}Ar$ (solid line, middle panel), $\delta^{15}N$ (dashed line, middle panel) and CH_4 profile (solid line, bottom panel) for MIS 5d/c transition in Vostok ice core. The modelled Δdepth was used to identify the gas isotope signal with

an uncertainty of 20%. The data showed a time lag of 2000 yrs between the onset of this climate event in Northern and Southern Hemisphere. (Figure adapted from Caillon *et al*., 2003a)

The timing and rate of the cooling phase in both hemispheres seems to be synchronous for AIM 12 whereas for the AIM 8 event cooling in the south appears to be much faster than cooling in the north (refer to Figure 4.3.1). These observations may indicate that millennial scale climate changes during the last glacial period may vary from one event to the other. However there is insufficient evidence here to reach a firm conclusion and that broadly both events studied show a consistent pattern. The GRIP ice core profiles for CH_4 and $\delta^{18}O_{ice}$ show that Greenland was cooling while the methane peak showed the second maxima for the DO 8 event (Chappellaz *et al*., 1993). Hence the Greenland cooling phase for the DO 8 event was not synchronous with the fall in the methane peak and exhibits a similar pattern observed in this study. On this basis it can be concluded that the cooling phase between the two hemispheres for DO 8 is also synchronous. Blunier *et al*. (1998) noted the synchronous nature of temperature decrease in both hemispheres to full glacial levels but also suggested that Antarctica reaches these minimum glacial values earlier than Greenland. However given the data resolution and taking into consideration factors other than temperature affecting the $\delta^{15}N$, it was not possible to verify here whether Antarctic reaches minimum glacial values first. A more precise $\delta^{15}N_{excess}$ may shed a light on this issue.

4.4   Phasing of atmospheric CO_2 and $\delta^{15}N$ for the AIM 12 event.

CO_2 ratios were measured at LGGE by Heinrich Schaffer and discussion on the CO_2 and $\delta^{15}N$ correlation will be further developed in the future by him. This section discusses the timing and variation of the atmospheric CO_2 and Antarctic temperature changes across the AIM 12 warming event during the last glacial period. Understanding the phase relationship is vital in order to understand better how the carbon cycle and climate change are linked. In order to study this phase relationship, a common time scale for the climate proxies and atmospheric CO_2 are required (Stauffer *et al*., 1998). Our study offers the solution for common time scale since both signals ($\delta^{15}N$ as a proxy for temperature and CO_2) are in the gas phase and we can reliably estimate the time lag

between the CO_2 and temperature rise without the need to calculate Δage. This is similar to the approach Caillon *et al.* (2003b) used to estimate the time lag between the timing of changes in atmospheric CO_2 and Antarctic temperature changes across termination III in Vostok ice cores.

Fourteen samples were measured for CO_2 mixing ratios across the AIM 12 event (see Figure 4.4.1). The CO_2 mixing ratio increased by 15.6 ± 2.4 ppmv during the warming event. The magnitude of this increase and the pattern exhibited is similar to CO_2 data for the same event in Byrd and Taylor Dome ice cores (Ahn and Brook, 2007). The onset of the CO_2 rise is about 180 yrs after the initiation of the warming and therefore strongly suggests that CO_2 is not the driver that initiates the abrupt climate changes but that it responds to climatic forcing and being a greenhouse gas amplifies the initial climatic forcing. The phasing between CO_2 and $\delta^{15}N$ reveals that the temperature and CO_2 rise is near synchronous within the limits of sample resolution and error of measurements, an observation that was not very precisely concluded in previous studies (Ahn and Brook, 2007; Ahn and Brook, 2008) due to ice age- gas age complications. Monnin *et al.* (2001) suggested that during the last deglaciation from the Dome C record the onset of the CO_2 increase lagged the start of the δD increase by 800 ± 600 yrs. The large error on this time lag estimate is due to the Δage value of ~550 yrs at Dome C. It is obvious that the phasing technique used in our study provides more precise time lag estimates.

Another interesting finding is that CO_2 apparently peaked after temperature with a time lag of 390 ± 200 yrs (the error arises from the sample resolution) and then decreased much slowly than the Antarctic temperatures. This estimate is based on a single datum and perhaps more measurements should be carried out in future from similar depths to increase the confidence of the time lag between the peaks of CO_2 mixing ratios and temperature. The time lag of ~390 yrs is lower than the previous estimate of 800 ± 200 yrs (Caillon *et al*., 2003b) and 1200 ± 700 yrs (Indermuhle, 2000). However the time lag estimate derived here is within the range of a recent estimate of 720 ± 370 yrs during the millennial scale variation (Ahn and Brook, 2007). A time lag of 300 yrs was also calculated for the last glacial termination (Severinghaus *et al*., 2009). Monnin *et al.* (2001) derived a time lag of 410 yrs for the highest correlation between CO_2 and δD for

the last deglaciation and this difference in timing was considered to be insignificant given the ice age – gas age difference.
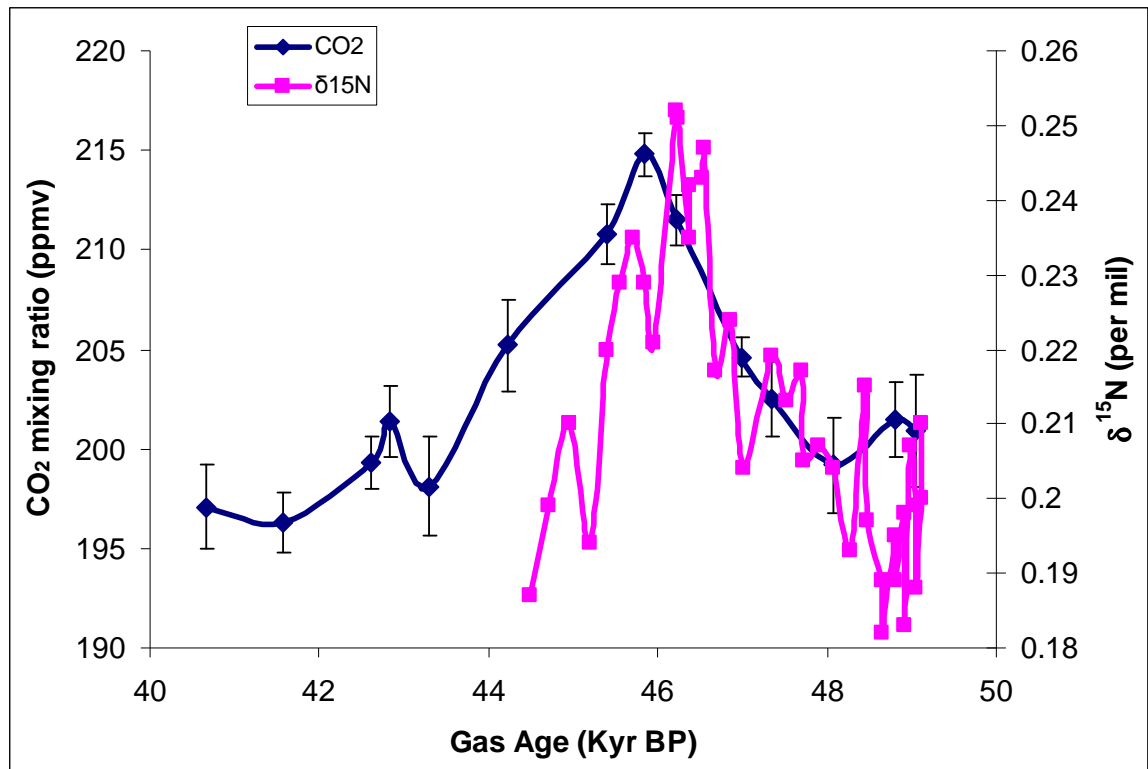
Figure 4.4.1: An illustration of CO_2 and $\delta^{15}N$ measurements in Berkner Island ice core for the AIM 12 event.

A noteworthy feature of Figure 4.4.1 is that CO_2 mixing ratios decrease much slower than the rate of decrease for Antarctic temperatures. The difference between the midpoint of the decreasing slope in CO_2 and $\delta^{15}N$ data is approximately 1000 years. Ahn and Brook (2008) observed that CO_2 levels remained relatively stable for about 1000 – 1500 yrs after reaching maximum levels whilst Antarctic temperatures dropped rapidly. Given the coarse CO_2 data resolution in this study it is impossible to know whether the CO_2 remained relatively stable after reaching the peak but the data certainly suggest that the rate of decrease was slower than the rate of decrease for Antarctic temperatures.

Figure 4.4.2 shows the phase relationship between CO_2 variability for the AIM 12 event and CH_4, a proxy for Greenlandic temperatures across the DO 12 event. It is obvious that CO_2 started increasing when Greenland was still in the cold stadial period or during the Heinrich event. The CH_4 mixing ratios across the DO 12 event might have increased

approximately 1400 yrs after the onset of rapid rise in CO_2. Almost 50% of increase in CO_2 was noted when Greenland was in the stadial period and the remaining 50% was after the onset of the interstadial in Greenland.
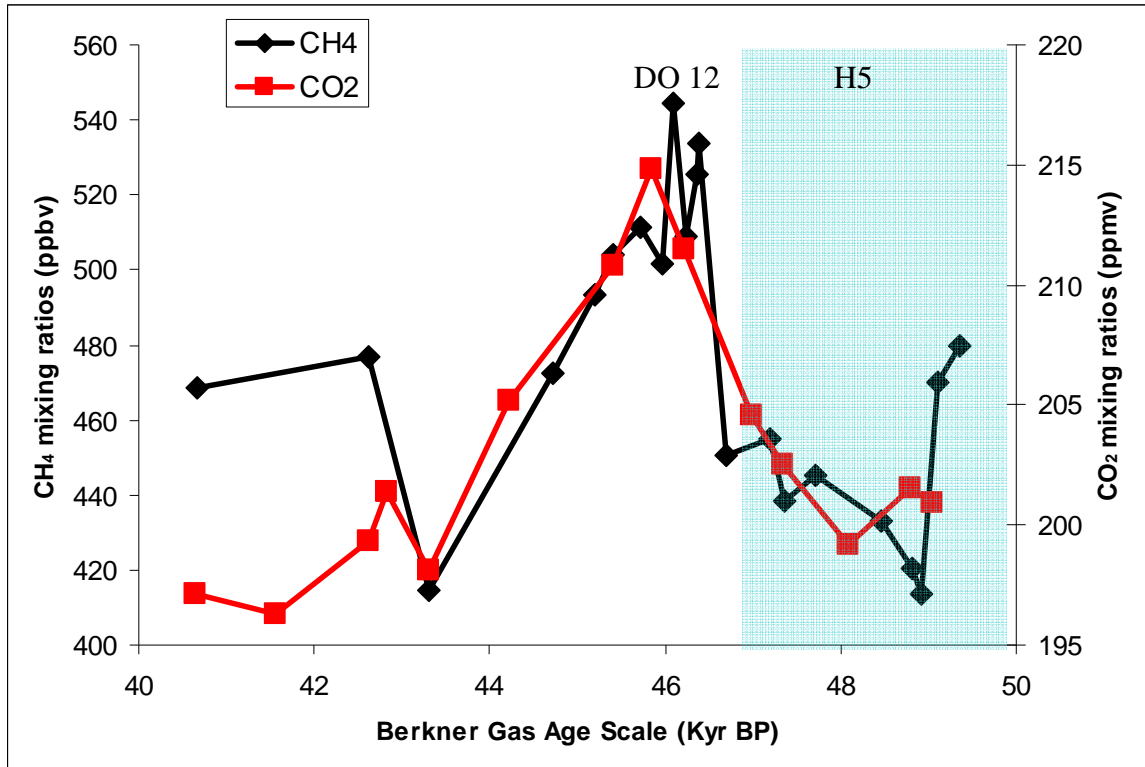
Figure 4.4.2: Timing of CO_2 variability in Antarctica and proxy of Greenlandic temperatures (CH_4). The shaded region shows the timing of the Heinrich Event 5 (H5).

The near synchronous nature of CO_2 rise and Antarctic warming can be explained in terms of Southern Ocean processes. Ahn and Brook (2008) showed that CO_2 concentrations rise most rapidly when the NADW shoaled and stratification in the Southern Ocean was reduced. This oceanic process occurred during stadial periods in the Northern Hemisphere. Other mechanisms proposed to explain the relationship between millennial scale climate variability and CO_2 rise include outgassing from the Southern Oceans due to decreased sea ice extent (Stephens and Keeling, 2000), changes in the position of midlatitude westerlies which affect the overturning of southern deep water (Toggweiler *et al.*, 2006) and changes in the Southern Ocean stratifications (Schmittner and Galbraith, 2008). Model results show that despite significant changes in the land carbon inventory, CO_2 variations are predominantly controlled by oceanic release of biological sequestered carbon in deep ocean, which is enhanced by increase in

Antarctic temperature and Southern Ocean stratification during the shutdown of the AMOC (Schmittner and Galbraith, 2008). However, results obtained in this study suggest that approximately 50% of the increase in CO_2 had occurred when the AMOC resumed and is in contrary to the model results. Such observation raises questions about the impact of higher sea surface temperature in the Northern Hemisphere associated with abrupt warming in Greenland on the global carbon cycle. Monnin *et al.* (2001) also noted simultaneous rapid increases in CO_2 and CH_4 during the Bølling Allerød (BA) warm phase in the North Atlantic region and likewise suggested additional NADW formation related mechanisms in the Northern Hemisphere contributing to the observed CO_2 variations.

4.5   Summary

Methane measurements in ice cores serve an important purpose in dating the ice cores. It is also used as a time marker for climate change in the Northern Hemisphere (since Greenland temperature is virtually synchronous with CH_4). Hence methane measurements in Berkner Island ice cores during the MIS 3 period enabled study of the phase relationship for abrupt climate changes between two hemispheres and could also provide additional constraints for Berkner Island gas age chronology.

In this study, high resolution methane measurements were coupled with $\delta^{15}N$ data to investigate the phase relationship for abrupt climate changes between the two hemispheres. The data indicate that warming in Antarctica leads Greenland warming. The time lag estimate between the onset of AIM 12 and the onset of DO 12 is 1600 ± 350 yrs and between AIM 8 and DO 8 is 1100 ± 360 yrs. The findings support the earlier observations of Blunier *et al.* 1998 and Brook and Blunier (2001). However, the time lag estimates obtained here are more precise because temperature signals from both hemispheres are in the gas phase and therefore overcome the problem of ice age – gas age difference.

A high resolution methane record for MIS 3 was compared to the Greenland methane composite record on the GICC05 age scale. The comparison revealed that the Berkner Island gas age chronology for DO 3, 4, 5 and 6 does not agree with GICC05 age scale

suggesting that this section of Berkner requires more careful dating especially where the strange event occurred. The discrepancy in the Berkner age scale during the timing of the strange event confirms that the water isotope – accumulation relationship failed during this particular time. There is also a slight discrepancy in Berkner Island gas chronology during the onset of the DO 12 event. Work is in progress (by Jean-Marc Barnola of LGGE) to improve the gas age chronology with the new methane data obtained in this study. For future work it is recommended that Berkner Island gas age scale be transferred to GICC05 age scale and therefore the time lag estimates obtained here could be more robust. Methane measurements also indicate that during the occurrence of the anomalous $\delta^{15}N$ signal there is a possibility that the accumulation rate increased by more than a factor of 2. However this needs to be confirmed with some modelling and work is in progress by Jean Marc Barnola.

The $\delta^{15}N$ profile was correlated to CO_2 mixing ratios for the AIM 12 event. The data indicate that the rise in temperature and CO_2 is almost synchronous based on the sample resolution. CO_2 values reach the maximum after the peak in temperature signal. This suggests that the rise of atmospheric CO_2 was in fast response to abrupt climate change but is not the initial driver of climate change. The time difference between the maxima of $\delta^{15}N$ and CO_2 is in the range of 190 – 590 yrs. An interesting outcome from the correlation of CO_2 and CH_4 record for the AIM 12 event show that CO_2 started rising while Greenland was still in the cold stadial period but ~ 50% of the increase occurred when Greenland was warming. This raises the question of the potential role of warming or NADW related mechanism in the Northern hemisphere in the global carbon cycle.

Chapter 5: Oldest Firn Record of Trace Gases (PFCs, HFC-23, SF$_6$ and SF$_5$CF$_3$) from EPICA Dronning Maud Land, Antarctica.

5.1 Introduction

5.2 EDML site description and firn sampling

5.3 Firn air modelling
5.3.1 The firn diffusion model
5.3.2 Iterative dating

5.4 Tetrafluoromethane (CF$_4$)
5.4.1 Results and discussion

5.5 Hexafluoroethane (C$_2$F$_6$)
5.5.1 Results and discussion

5.6 Perfluoropropane (C$_3$F$_8$)
5.6.1 Results and discussion

5.7 Perfluorocyclobutane (c-C$_4$F$_8$)
5.7.1 Results and discussion

5.8 Fluoroform (CHF$_3$)
5.8.1 Results and discussion

5.9 Sulfur hexafluoride (SF$_6$)
5.9.1 Results and discussion

5.10 Trifluoromethylsulfurpentafluoride (SF$_5$CF$_3$)
5.10.1 Results and discussion

5.11 Radiative forcing

5.12 Summary

5.1 Introduction

Firn air is an archive of old air and when extracted and analysed for its gas composition, the firn record could potentially extend the real-time measurements back to early twentieth century. It is particularly useful in reconstructing atmospheric histories and assessing the existence of natural background levels of trace gases. The advantages of reconstructing atmospheric histories from firn air are that large volumes of samples are collected for repetitive measurements and firn air corresponding to different ages can be analysed in a short span of time, therefore overcoming problems of instrumental or reference drift as usually faced in the long term real-time measurements. Nevertheless the atmospheric reconstructions from firn air are subjected to several uncertainties pertaining to the structure of the firn and the physical processes that modifies the trace gas concentrations.

In this study firn air collected from the EPICA Dronning Maud Land (EDML), which is believed to include some of the oldest firn air sampled to date, were measured by GC-MS, and their atmospheric histories were reconstructed with the help of a 1-dimensional firn diffusion model and an iterative dating technique. A range of compounds (PFCs, HFCs, Halons and CFCs) were measured but the discussions are limited to PFCs, HFC-23, SF_6 and SF_5CF_3. All of these fluorinated compounds, except SF_5CF_3, are included in the Kyoto Protocol and therefore there is a need to understand how these gases evolved over time, identifying the natural and anthropogenic contributions to the atmospheric abundance and enforcing mitigation options to reduce its emissions.

The principal objective of this study is to provide the longest reconstructed atmospheric histories of the fluorinated compounds and also to provide updated trends of the PFCs. These reconstructed trends are then compared with previous firn air reconstructions and any ambient atmospheric measurements or measurements from air archives. This study provides insights into the growth rates of these compounds, natural background levels and emissions estimated from the growth rates obtained.

In this chapter a brief description of the site, sample collection technique, the firn diffusion model and the iterative dating technique are given. This chapter mainly consist

of detailed discussion of each individual species (CF_4, C_2F_6, C_3F_8, c-C_4F_8, CHF_3, SF_6 and SF_5CF_3). Each subsection on the individual species has its own literature review, results and discussion on atmospheric history reconstructions from firn data and estimating emissions from the reconstructed trends.

5.2 EDML site description and firn sampling

A more detailed description of the site and the firn air sampling experiment was outlined in Weiler (2008). Firn air samples were collected during the 2005/2006 field season by University of Bern in cooperation with the Alfred Wegner Institute for Polar and Marine Research (AWI).

The EDML firn air samples were collected from the vicinity of the deep ice core drilling site at Kohnen Station in Dronning Maud Land. The EDML site is characterised by an annual accumulation rate of approximately 7 cm yr^{-1} (ice equivalent) and annual mean surface temperature of 228 K. The firn air sampling was carried out 500 m away from the camp, 1 km away from the runaway and in the direction of the wind to avoid any contamination from the camp and vehicles. Three shallow sample holes were drilled namely B35 (75˚ 0.08'S, 0˚ 4.808'E), B36 (75˚ 0.038'S, 0˚ 4.676'E), B37 (75˚ 0.031'S, 0˚ 4.721'E) to a depth of 30 m, 78 m and 124 m, respectively. The temperature logging took place in B35 and the sampling initially started at B36 but was terminated at 78m depth due to technical fault. Finally the sampling was restarted in a new hole, B37, and was completed within 11 days.

Firn air samples were collected with the bladder method as described by Schwander *et al*. (1993). The bladder assembly consists of a rubber bladder approximately 4 m long and 95 mm in diameter mounted on the end cap and containing three 6 mm in diameter DEKABON–1300 tubes for inflating, purging and sampling. The end cap contains the sampling and purging chambers separated by a metal disc (Figure 5.2.1). The borehole was drilled with the Swiss electromechanical shallow drill to a certain depth and the bladder was lowered to the bottom of the hole and was inflated with clean atmospheric air from tube mounted outside in a remote area. The inflation of the bladder makes a

seal between the bladder and the inside of the borehole, preventing any movement of contemporary air into the borehole contaminating the firn air samples. To further prevent sample contamination, air from between the lowermost end cap of the bladder and the uppermost baffle plate was evacuated and vented into the atmosphere via the purge line. As the air was pumped out, CO_2 concentration was monitored continuously on a LI-COR 7000 CO_2/H_2O analyzer and once it had reached a stable value, only then a sample was collected. This critical step in the sampling procedure ensures that only aged air was collected and that there were no contamination issues. Finally the samples were collected through the sampling inlet between the uppermost and lowermost baffle plates (Figure 5.2.1).

Samples were collected in 3L Silcocans (RESTEK) which were pressurised with moist clean nitrogen gas and were evacuated prior to sampling. The canisters were filled three times with the sample to a pressure of 10^5 Pa and then evacuated before a final sample was filled to a pressure of 40 psi. The samples collected for UEA were not dried during the sampling but samples collected for University of Bern were dried using magnesium perchlorate.
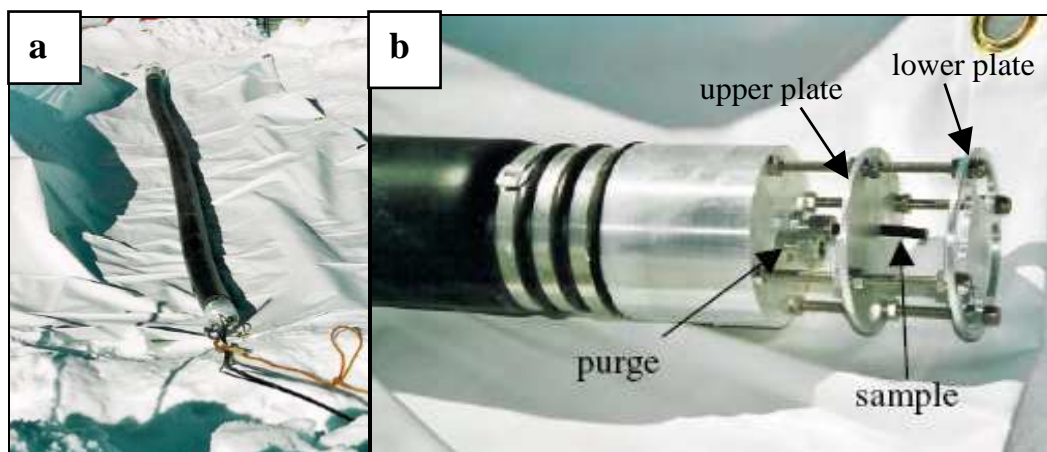
Figure 5.2.1: a) A photography showing 4 m long bladder assembly. b) A photograph showing the details of the bladder plate such as the upper and the lower plates, the purge line and the sample inlet line (Source: Schwander, 2001).

5.3 Firn air modelling

5.3.1 The firn diffusion model

The firn diffusion model is used as a dating tool to interpret the trace gas depth – concentration profiles in terms of their atmospheric trends. The firn diffusion model used was developed by CNRS-LGGE and a detailed description was given by Rommelaere *et al*. (1997). This is a numerical model that simulates the movement of a gas of interest in the firn and incorporates factors that influence transport rate such as mass, molecular diffusivity of the gas and physical processes affected by the firn structure. This model incorporates the same physical processes as in previous models (Schwander *et al*., 1993; Trudinger *et al*., 1997) but in addition it takes into account the effect of trapping on the movement of the air in the firn and as a result it can be used to compute mixing ratios in firn and in bubbly ice simultaneously.

In order to execute the model several site-specific and gas-related parameters (shown in Table 5.3.1), an atmospheric scenario, density and effective diffusivity profile of the site needs to be known. The model was run in the direct mode and it generated concentration depth profile in relation to inputted atmospheric scenario. In the model it was assumed that the snow accumulation rate, temperature and firn structure at a given depth were independent of time. This is justified because the study period is short and climatically stable. The density profile was obtained by measuring the weights and dimensions of ~ 0.55 cm long sections of the firn core. The critical variable in the model is the relationship between the gas molecular diffusivity and the effective diffusivity, which is related to tortuosity and open porosity of the firn. The effective diffusivity profile (see Figure 5.3.1) was obtained through the inverse modelling of CO_2, a gas having a well characterised atmospheric evolution trend and also has a firn depth profile at the EDML site. This was done by Patricia Martinerie at LGGE, Grenoble, France. The effective diffusivity profile was calibrated such that the model result for CO_2 matches the CO_2 measurements in the firn (see Figure 5.3.2). The effective diffusivity is an increasing function of open porosity or rather a decreasing function of depth and therefore does not take into account the effect of refrozen melt layers or other heterogeneities in the firn (Martinerie *et al*., 2008).

Table 5.3.1: Site specific parameters and diffusion coefficients used in the model

Surface accumulation (ice equivalent)	7.2 cm/yr
Annual mean temperature (K)	228 K
Close-off density	0.839
i-windlayer (convective zone)	3

Diffusion coefficients relative to CO_2 :

CF_4	0.7581
C_2F_6	0.5953
C_3F_8	0.5072
$c\text{-}C_4F_8$	0.4938
CHF_3	0.8135
SF_6	0.6045
SF_5CF_3	0.5134
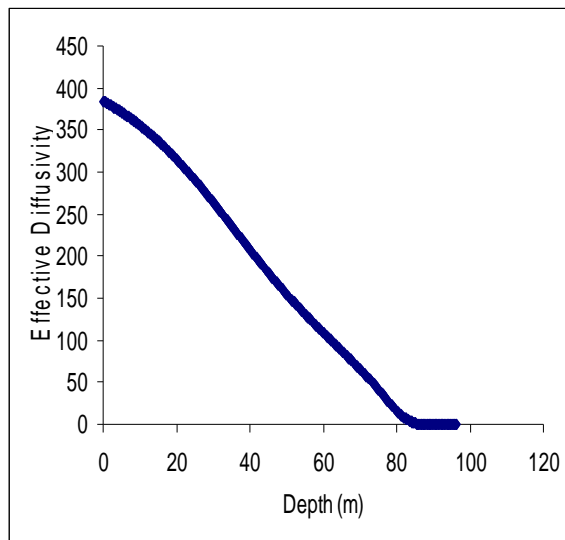
Figure 5.3.1: Effective diffusivity profile for the EDML firn obtained through inverse modelling (Courtesy of University of Bern and LGGE).
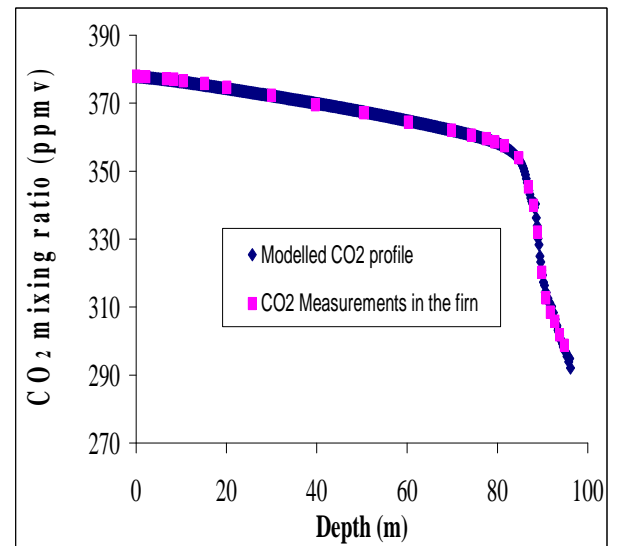
Figure 5.3.2: An illustration of modelled CO_2 firn profile obtained with the effective diffusivity profile matches the observations in the firn.

163

Once the effective diffusivity profile was obtained then the concentration depth profile of any gas can be generated by using diffusion coefficients relative to CO_2. Consequently if there was a bias in the effective diffusivity then this bias is implicated in the data interpretation of all the gases. The diffusion coefficients for trace gases under investigation were estimated from Le Bas molar volumes (Fuller *et al*., 1966) and the values used for the individual gases are given in Table 5.3.1.

The depth of the convective zone is described by the number of windlayers in the model and typically each windlayer is 0.2 m thick. The depth of the convective zone can be interpreted from the stable isotope measurements, such as $\delta^{15}N$, or fast growing species in the atmosphere like HFC 134a. The spatial resolution of samples in the shallow firn was very limited due to technical difficulties in collecting samples from depths shallower than 4 m. On inspection of the preliminary isotope data it was speculated that the convective zone was less than 1 m (Weiler, University of Bern, personal communication). The effective diffusivity profile obtained also showed a convective zone of 0.6 m, which equates to 3 windlayers in the model. The sensitivity of the model to the number of windlayers was investigated. The model was run for C_2F_6 with the same atmospheric scenario but the windlayers were varied. The model output for 3, 10, and 20 windlayers is shown in Figure 5.3.3. The modelled depth concentration profile for the gas was insensitive to the number of windlayers, in particularly for the deeper part of the firn. The modelled concentration depth profile obtained with various windlayers fits the data exceptionally well.
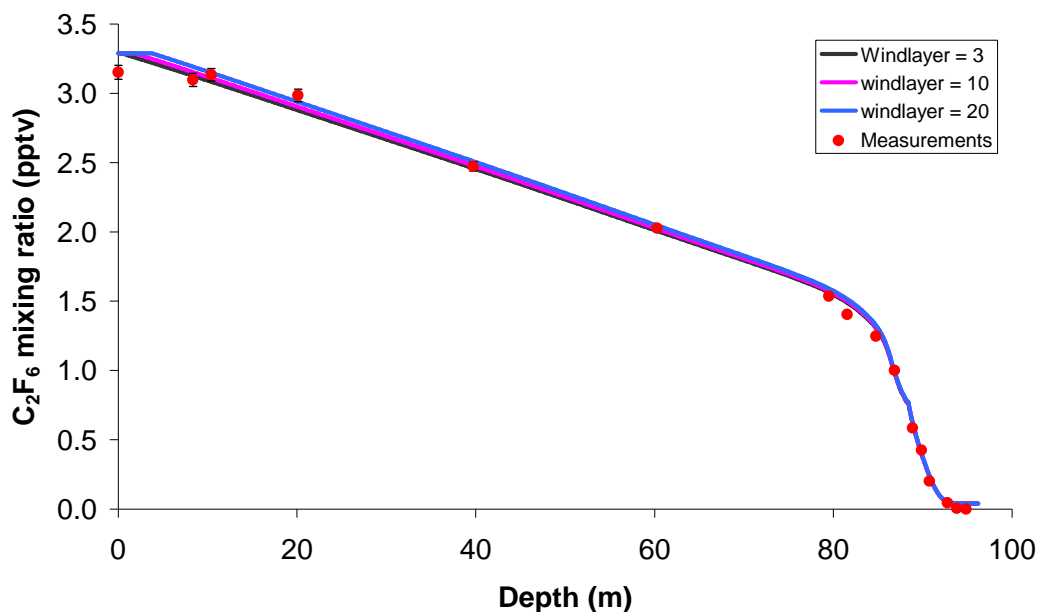
Figure 5.3.3: The model output results for the sensitivity test for different number of windlayers in the model

5.3.2 Iterative dating

To interpret the firn data in terms of atmospheric trends and reconstructing its atmospheric history from old firn air it is a vital requirement to date the firn air samples as accurately as possible. The firn diffusion model can be used to assign effective ages for the firn measurements but it requires an atmospheric input scenario, which is a detailed account of the atmospheric history of the gas. A well-defined atmospheric scenario would result in a better modelled fit to the measured data. However dating would be poorly constrained for species where their atmospheric evolution trend is not known. This obstacle was overcome by an "iterative dating" technique developed by Trudinger *et al.* (2002), which does not require any preconception of a species' atmospheric history. This technique is restricted to species with reasonably simple atmospheric variations that are monotonic in nature and does not show change in the sign of the concentration gradient. This technique has proven to work well in previous studies for several species of anthropogenic origin such as halocarbons, CFC's (Sturrock *et al.*, 2002) and PFCs (Worton *et al.*, 2007).

All of the species under investigation in this study display a monotonic increase in atmospheric burden and therefore satisfy the basic requirement for the application of

this technique. An initial atmospheric scenario was generated through a linear fit to the firn data at the bottom of the firn and at the surface (see black line in Figure 5.3.4), which was used to generate model concentration - depth profile (referred to as run 1 in the illustrations shown in the discussions of the individual species). The output is used as a 'look up table' to assign dates to each sampling depth, based on the modelled concentration at the depth and the corresponding date from the input atmospheric scenario. The concentration – age profile obtained from this run was used to generate another atmospheric scenario through polynomial fitting (blue line and blue equation in Fig. 5.3.4) and this scenario was inputted to generate run 2. This procedure was repeated until the age estimate was refined towards the best fit solution and usually after two runs the atmospheric scenario generated tends to converge towards a similar atmospheric trend.
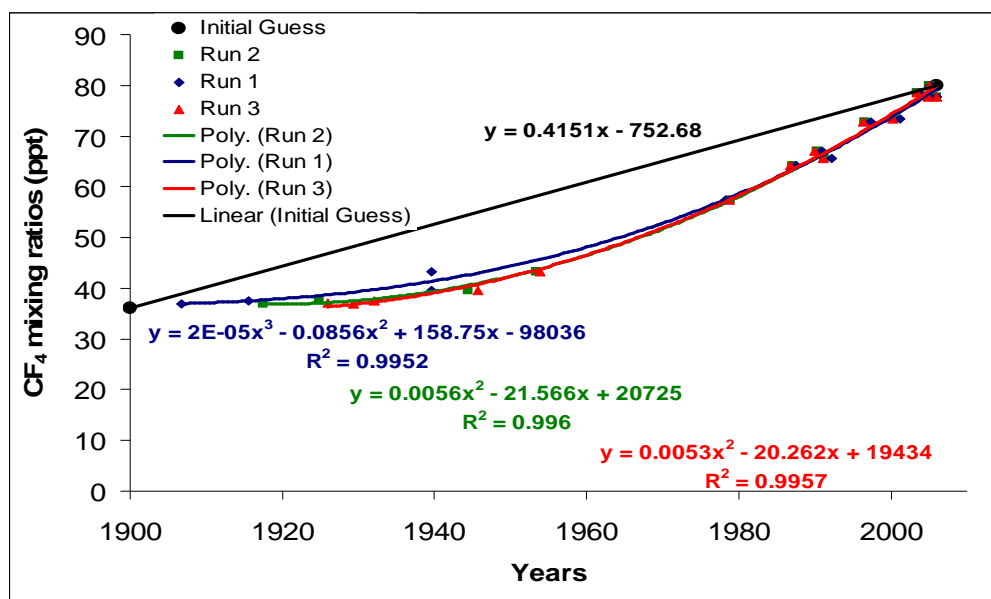
Figure 5.3.4: The generated atmospheric scenarios used in the firn diffusion model to reconstruct the atmospheric history of CF_4. The "initial guess" (solid black line) was used to generate the atmospheric scenario for "Run 1". The polynomial fitting (solid blue line) to the concentration-age profile obtained from Run 1 was used to generate atmospheric scenario for the model Run 2. The polynomial fitting to the model output for Run 2 (Solid green line) was used to generate atmospheric scenario for Run 3. The concentration- age profile for Run 2 and Run 3 (solid red line) converged to similar atmospheric trend so the iterative dating was discontinued.

The iterative dating model was proved to be a success in dating most of the species studied. But it should be noted that the reconstructed histories from firn measurements will be smoothed relative to the original record due to firn processes and mixing. The short scale variations such as inter-annual variations are not recorded and also the medium scale variations are damped. In addition there are further uncertainties associated with the several input parameters for the model. These suggest that if an atmospheric scenario produces an excellent fit to the measured data it does not guarantee the accuracy of that particular atmospheric trend. However the firn diffusion model is probably the best tool at hand currently to infer most likely past atmospheric variations for specific species as opposed to exact reconstruction.

5.4 Tetrafluoromethane

Tetrafluoromethane (CF_4) is one of the longest living trace gases and it contributes to the radiative properties of the atmosphere. Its long atmospheric lifetime, which is currently estimated to be 50,000 years, and strong IR absorption in the "IR Window" region in the terrestrial IR spectrum makes it a potent greenhouse gas (Worton *et al*., 2007). The estimated 100 year GWP for CF_4 is 7600 relative to CO_2 based on the new absorption cross section of $1.90 \times 10^{-16} cm^2 molecule^{-1} cm^{-1}$ (Hurley *et al*., 2005). The radiative forcing of CF_4 is currently at 0.004 Wm^{-2} (Worton *et al*., 2007) and is estimated to increase to 0.033 Wm^{-2} in accordance with 2100 emission scenario (WMO, 2006).

The current atmospheric abundance of CF_4 is approximately 80 ppt (Worton *et al*., 2007; Aoki and Makide, 2000) and has roughly doubled since 1950s. There are several studies documenting atmospheric trends of CF_4: Harnisch *et al.* (1996a) derived tropospheric trends for CF_4 from SF_6 dated stratospheric air that indicated an increase in the growth rate to 1.00 ± 0.05 ppt yr^{-1} for the period 1982 – 1995; Khalil *et al*. (2003) reported data from 1978 – 1997 in Cape Meares, Oregon, air archives and in flasks from Point Barrow, Alaska, and Palmer Station, Antarctica; Infrared high spectral resolution space-based solar occultation measurements of stratospheric CF_4 indicated a slowdown in the rate of accumulation (Rinsland *et al.,* 2003); in-situ measurements of CF_4 at Mace Head, Ireland and Cape Grim as part of the Advanced Global Atmospheric Gases

Experiment (AGAGE) (Greally *et al.*, 2005); atmospheric trends were reconstructed since 1950's from Berkner Island, Antarctica and North Greenland Ice Core Project (NGRIP) firn air (Worton *et al.*, 2007).

The major anthropogenic source of CF_4 is from the production of aluminium. Aluminium is produced by the Heroult-Hall process, which involves the electrolysis of a solution of Alumina (Al_2O_3) in a molten cryolite (Na_3AlF_6) at high temperature. CF_4 and other PFCs are produced when the smelting process is disturbed briefly by a condition known as "anode effects". This condition normally occurs when the concentration of alumina gets very low which results in a sudden increase in voltage causing the cryolite to decompose. The fluorine produced via cryolite decomposition reacts with carbon anode to produce primarily CF_4 and C_2F_6, but also small amounts of C_3F_8 and possibly $CClF_3$ (Harnisch, 2000). The increasing awareness of PFC emissions from the smelting process in recent years led to process optimization to reduce emissions. The semiconductor industry also contributes to the CF_4 atmospheric burden. CF_4 is used as dry etching and in plasma cleaning agents in the semiconductor industry and is released into the atmosphere as a fugitive emission in the absence or failure of any abatement technologies, which are responsible for capturing and destroying CF_4 in the waste stream. The semiconductor industry source is not as significant as compared to the aluminium industry but the Emissions Database for Global Atmospheric Research (EDGAR) shows increasing emissions from the semiconductor industry and therefore emissions from this source needs to be closely monitored and regulated.

In addition to anthropogenic sources there is a natural source of CF_4 which accounts for almost half of the current mixing ratio. Harnisch *et al.* (1996b) analysed two glacial ice samples to highlight a natural or pre-industrial background level of 39 ± 6 ppt and estimated a natural CF_4 flux of < 0.01Gg yr^{-1}. The natural flux is of geochemical origin, mainly from weathering of certain rocks and minerals. More recently, Deeds *et al.* (2008) showed evidence of crustal degassing of CF_4 by measuring groundwater samples in Mojave Desert, California. This study also concluded that the crustal flux was enhanced during tectonically driven fracturing of the continental crust.

The atmospheric destruction of CF_4 is mediated by a photolysis reaction with O^+ ions in the mesosphere, which could result in atmospheric lifetime of 330 kyr (Morris *et al.*,

1995) to 1 million years (Ravishankara *et al.*, 1993). However the atmospheric destruction process seems to be less important than the thermal destruction in high temperature combustion zones of power plants, incinerators and automobiles at ground level, and consequently decreasing the atmospheric lifetime to about few ten thousands of years.

5.4.1 Results and discussion

The concentration - depth profile of CF_4 measured in samples from EDML firn air is shown in Figure 5.4.1. The graph shows that the concentration has risen from ~ 37 ppt in the bottom-most samples to ~ 80 ppt in contemporary air. The most intriguing results are the observed mixing ratios at the bottom of the firn, which are not only the lowest observed to date in any firn air record, but moreover they stabilize and do not continue to decrease with increasing depth. This particular feature confirms that the EDML firn air could probably be the oldest record providing better insights into atmospheric trends by extending the existing firn air records to pre-industrial period. The average concentration observed in the three deepest samples (92.75m, 93.80m, and 94.80m) is 37.1 ± 0.3 ppt as compared to Worton *et al.* (2007) study, which observed lowest values of 47.0 ppt at Berkner Island and 40.6 ppt at NGRIP site. The mixing ratios at the bottom of the firn were not decreasing any further with depth and therefore it can be taken as a representative of the pre-industrial air or the natural background levels. In order to constrain the atmospheric trends it was vital to assign the age scale to the observations. The iterative dating technique was used and as shown in Figure 5.4.1 the model result from run 3 agrees very well with the measurements. The atmospheric scenario used in this model run was used to reconstruct the atmospheric history of CF_4 from the EDML firn air (Figure 5.4.2).

The reconstructed time series of CF_4 in the EDML firn air extends back to 1925 giving the oldest record of CF_4 from firn air. The CF_4 concentration remained almost constant from 1925 until late 1920's to 1930, giving evidence of natural background levels of CF_4. The average value of 37.1 ± 0.3 ppt is within the error limit of the reported natural
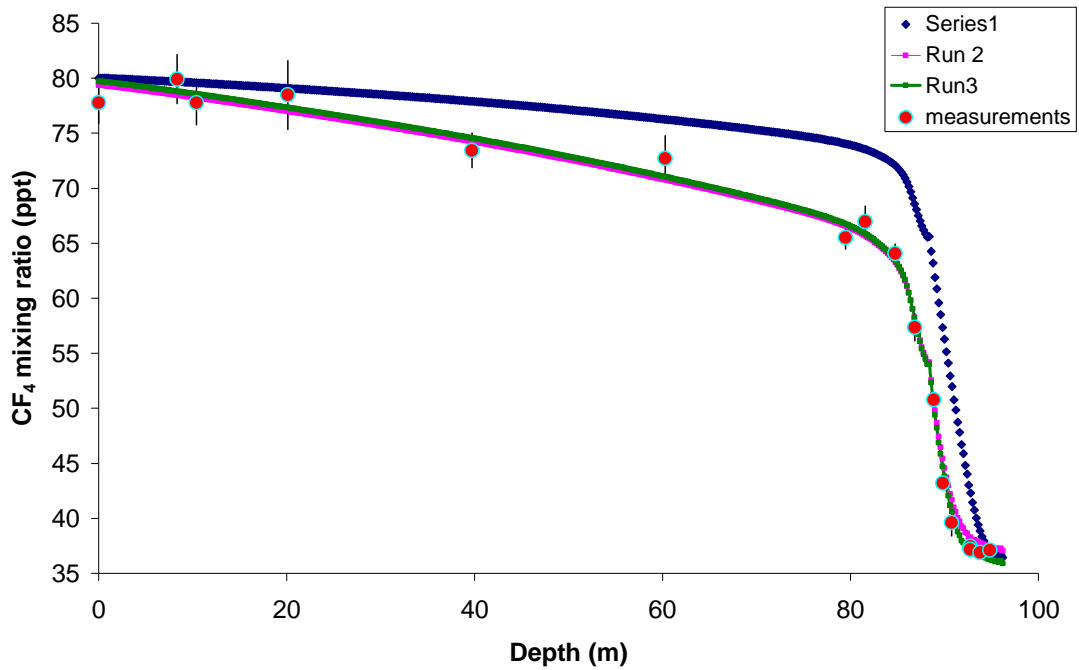
Figure 5.4.1: Depth Profile of CF_4 mixing ratios in EDML firn air. The diffusion model results obtained with different atmospheric scenarios are also shown.
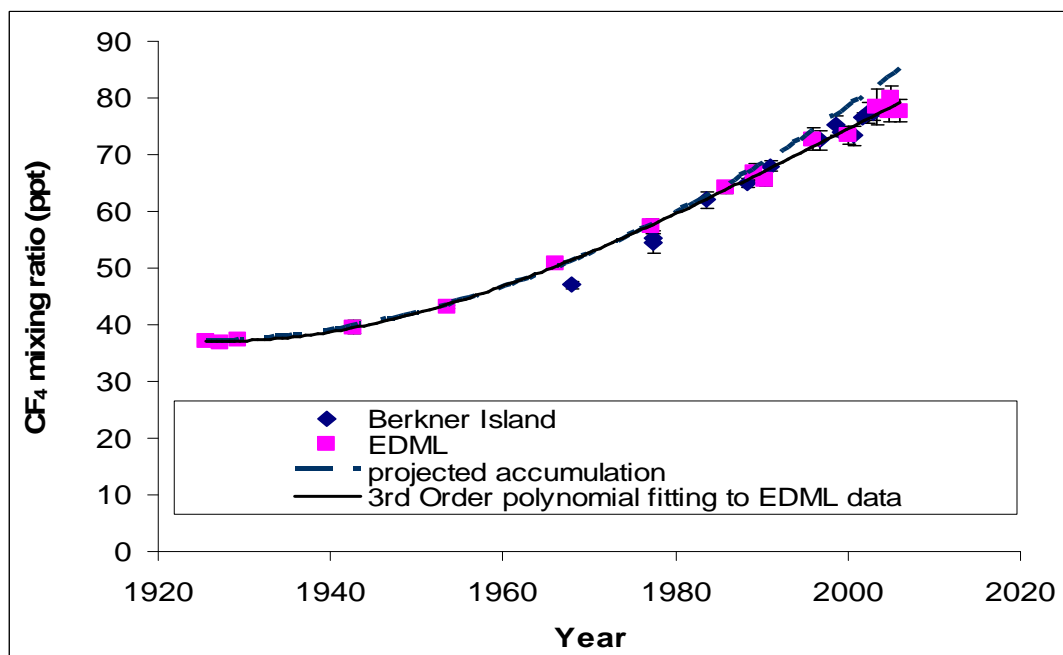
Figure 5.4.2: Atmospheric trend of CF_4 reconstructed from iterative modelling of firn air. The solid line is the 3rd order polynomial fitting to the EDML data. Data from Worton *et al*., (2007) from Berkner Island is also shown. Dashed line (the projected accumulation) is the extrapolation of the modelled mixing ratios from the EDML firn air samples dated before 1980.

background level of 39 ± 6 ppt estimated from glacial ice (Harnisch *et al.*, 1996b). The pre-industrial value obtained in this study is higher than the reported value of 34 ± 1 ppt (Worton *et al.*, 2007) and lower than 44 ppt reported by Khalil *et al.* (2003). These pre-industrial values reported earlier were based on the extrapolation of CF_4:C_2F_6 relationship to zero C_2F_6 concentration. This may not be a very reliable approach to evaluate natural background levels as compared to direct measurement of pre-industrial air because the CF_4:C_2F_6 relationship is variable depending on external factors such as smelter design and its operations.

The mixing ratios of CF_4 increased from a value of 37.3 ± 0.3 ppt in 1930 to 77.8 ± 1.9 ppt in 2006. This increase could be attributed to anthropogenic sources such as the aluminium industry. Although the concentration has increased, the rate of change has decreased in recent years. It increased from 0.1 % yr^{-1} in 1930 to 1.3% yr^{-1} in early 1980s and then decreased to 1% yr^{-1} in 2006. The decreasing trend in accumulation rate also propagated into the stratosphere and it was shown that the rate decreased from 2.77 % yr^{-1} in 1985 to 1.14% yr^{-1} in 2004 (Rinsland *et al.*, 2005). Harnisch *et al.* (1999) reported a tropospheric trend of 0.72 ppt yr^{-1} for the period 1992 – 1998 which is comparable to our estimate of 0.78 ± 0.02 ppt yr^{-1} for the same period. The growth rate observed for 1986 – 1997 was 0.85 ± 0.15 ppt yr^{-1} in Khalil *et al.* (2003), which is in close agreement with the value of 0.79 ± 0.02 ppt yr^{-1} obtained for the similar period in this study. The continuous in-situ measurements of CF_4 at Mace Head suggest an annual growth rate of 0.7% yr^{-1} in 2004 (Greally *et al.*, 2005). The CF_4 measurements in the Cape Grim archive air from 1981 showed a significant decline in the growth rate from the 1980/1990s value of 1.1 ppt yr^{-1} to 0.8 ppt yr^{-1} for 2004 (Greally *et al.*, 2005). The recent growth rate obtained in this study matches with the value obtained in the Greally *et al.* (2005) study for Cape Grim site, however the growth rate (ppt yr^{-1}) from the reconstructed trend did not show any irregularities in the growth rate rather than smooth increase for the same period. The discrepancy could be due to poor temporal resolution of the firn data and the inability of the firn record to capture the inter-annual or short term atmospheric variations and often results in a smoothed record. There are certain levels of disagreement between the absolute values of growth rates reported by different studies due to different approaches taken to estimate the growth rate and differences in the calibration scale.

A polynomial curve was fitted to the data before 1980 when the atmospheric accumulation rate was at the peak and was extrapolated to 2006 (see Figure 5.4.2). Assuming the CF_4 growth was consistent with the rate observed before 1980 then we should expect a current atmospheric value of 85 ppt. The fact that the actual measured value was less than the projected accumulation of CF_4 hints a slowdown in emissions.

The CF_4 emissions could be estimated from the atmospheric measurements or trends because CF_4 has a very long lifetime and without any known natural destruction processes in the lower atmosphere. In this study we used the conversion factor of 1 ppt yr^{-1} = 14.7 Gg yr^{-1} (Khalil et al., 2003) to estimate emission in Gg yr^{-1} from the model-derived atmospheric trend. Figure 5.4.3 shows the emission of CF_4 since late 1920s. During the early years the emission rates were larger than the rate of aluminium production and then increased coherently with the growth of global aluminium production. The reason for the emission rate being higher than the production rate in early years could be due to highly inefficient smelting process. However in the recent years there was a very large offset in the trend of global aluminium production and the emission estimated from the reconstructed history of CF_4 from the firn measurements. This suggests that the emissions from the aluminium industry have decreased significantly as discussed below.
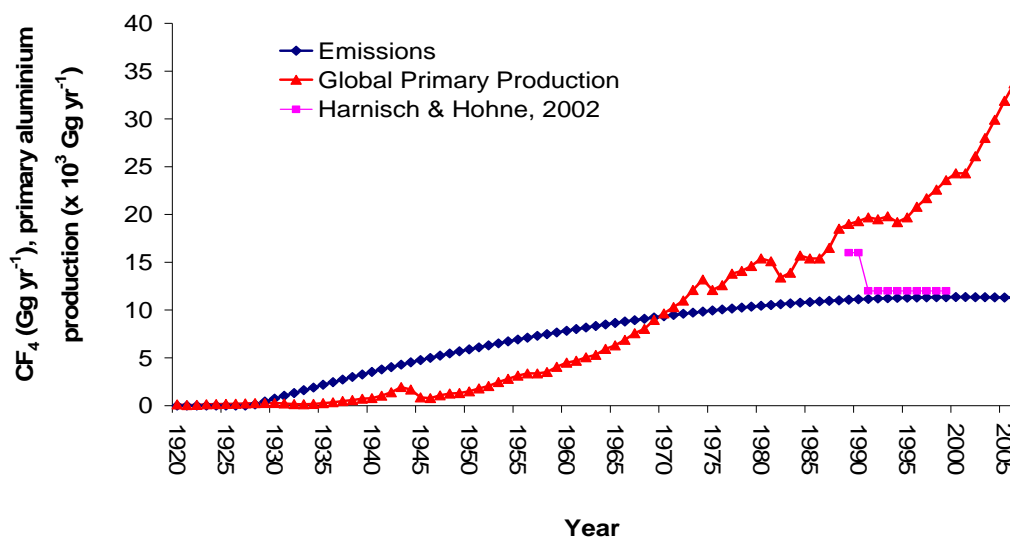
Figure 5.4.3: The emission of CF_4 from 1928 to 2006 based on the model-derived atmospheric trend is compared to global aluminium production. Data from Harnisch and Höhne (2002) are also shown.

To test the validity of the emission pattern derived from the atmospheric trend obtained in this study we compared our values to the updated Emissions Database for Global Atmospheric Research (EDGAR, version 3.3) for the period 1970 – 1998 and 2000 (Olivier *et al*., 2005). The emissions based on the model-derived atmospheric trend are generally in good agreement with EDGAR values except small discrepancies such as a slight underestimation for the period 1970s and a slight overestimation for early 1990s (see Figure 5.4.4). The lack of high resolution firn measurements, smoothing of data due to mixing processes in the firn and the inaccurate input variables in the model could explain the discrepancies between EDGAR estimations and emissions estimated in this study. The differences in emission estimations obtained from direct atmospheric measurements for the period 1989 and 1990 in a study by Harnisch and Höhne (2002) and this study could also be accounted for same reasons stated above. However, for the period 1991 to 1999 the emissions based on atmospheric measurements by Harnisch and Höhne (2002) were in excellent agreement with our estimate (see Figure 5.4.3). Harnisch and Höhne (2002) reported an emission of 16 Gg yr^{-1} for 1989 & 1990 but the Anode Effect Survey (AES) 2008 conducted by International Aluminium Institute (IAI) reported an emission of 13.0 Gg yr^{-1} closer to our estimate of 11.1 Gg yr^{-1}.

It is noteworthy that the EDGAR Database shows negative emission trend from mid 1980s to 1992 and then shows a positive trend (see Figure 5.4.4). This increase in emission after 1992 could be either an increase in emissions from the aluminium industry or some other source, such as the semiconductor industry (Worton *et al*., 2007), or a combination of both. The EDGAR reports an increase in CF_4 from the semiconductor industry from a value of 0.4 Gg yr^{-1} in 1990 to 1.9 Gg yr^{-1} in 2000. Harnisch (2000) reported similar rate of increase in CF_4 emission from the semiconductor industry, that is, from 0.3 Gg yr^{-1} in 1990 to 1.1 Gg yr^{-1} in 1995. Despite the increasing contributions from the semiconductor industry the major emitter is still the aluminium industry. Nevertheless, the emissions from the semiconductor industry needs stringent monitoring to curtail any further increase in emissions.
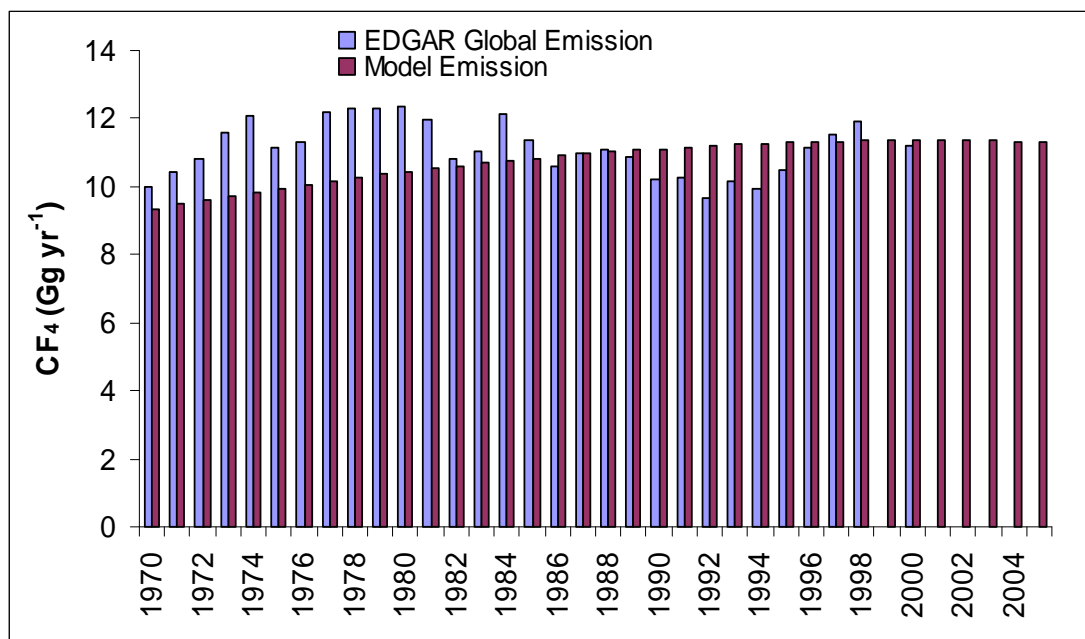
Figure 5.4.4: Comparison of CF_4 emissions obtained in this study with EDGAR Global emissions.

The growing emission rate from the semiconductor industry could to some extent compensate the reduction in emission from the aluminium industry due to concerted effort by aluminium manufacturers to reduce PFC emissions. There are different smelter technologies by which aluminium is extracted from the ore and the emissions vary from one technology to the other. The different technologies are: Horizontal Stud Soderberg (HSS), Vertical Stud Soderberg (VSS), Side Worked Prebake (SWPB) and the newest technology called Point Feed Prebake (PFPB) that was adopted under the PFC emissions reduction program. The PFPB utilizes multiple "point feeders" and other computerized controls for precise aluminium feeding, which minimizes the occurrence of "anode effect". The International Aluminium Institute report on the Aluminium's Global Perfluorocarbon Gas Emissions Reduction Programme described PFPB as the lowest PFC emitting technology that has grown by a factor of three from 1990 to 2006. During this time period the aluminium production increased by 75% and the common smelter design used was the lowest emitting PFPB technology.

The 2006 Anode Effect Survey (AES) calculated emissions from survey participants and estimated emissions from non-participants from 1990 to 2006. The survey concluded that the total emissions of PFCs (i.e. CF_4 and C_2F_6) have been reduced by

75% while global primary aluminium production has increased over the same period by almost 75%. This suggests that CF_4 contribution from this particular industrial activity should plummet causing the atmospheric levels to stabilise. The emissions calculated earlier from the atmospheric trend shown in Fig 5.4.2 indicate emissions stabilising at 11.3 Gg yr^{-1}; however this was much higher than the emissions that were calculated from the Total PFC (only CF_4 and C_2F_6) emissions shown in the 2006 AES report. This could be simply the case of an overestimation due to polynomial fitting to the data.

To investigate if the findings of the AES and this study are consistent we focussed only on the firn data of recent years. The AES reports total PFC emissions in million tonnes of CO_2- equivalent. To convert this value into CF_4 emission only we used the GWP for CF_4 and C_2F_6 used in the AES and also took into account that C_2F_6 constitutes only 10% by mass of CF_4 in the total PFC emissions (EDGAR; Khalil *et al*., 2003). Based on this approach we obtained CF_4 emission values of 7.3 Gg yr^{-1} in 2000, 4.7 Gg yr^{-1} in 2004, 4.1 Gg yr^{-1} in 2005 and 3.2 Gg yr^{-1} in 2006. These AES emission values were back-calculated into rate of change (ppt yr^{-1}) using the conversion factor stated above. The rate of change obtained for the years of survey were then added to the mixing ratios obtained from the atmospheric trend used in this study for the corresponding 1999 and 2003 years. Assuming that the aluminium industry is the major source, and if the emission values quoted in the 2006 AES report are correct, then it should be reflected in the atmospheric measurements. The mixing ratios obtained from the emissions stated in the 2006 AES report were plotted against the observed firn air reconstructed atmospheric measurement for the similar period. Figure 5.4.5 illustrates that the mixing ratios back-calculated from the emission values stated in the 2006 AES are within the error limits of the measurements. Hence the measurements did validate to some extent the findings of the 2006 AES results and showed evidence of stabilizing levels of CF_4 in the atmosphere since 2004 due to highly efficient PFCs reduction protocols adopted by the aluminium industry.
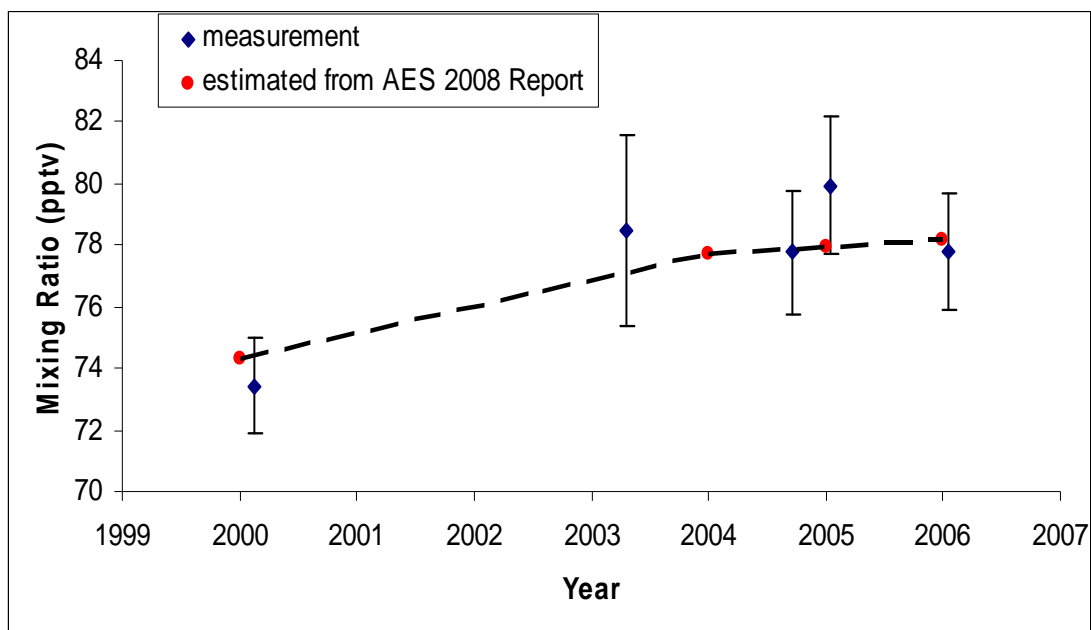
Figure 5.4.5: An illustration of mixing ratios of CF$_4$ reconstructed from the firn air (blue diamonds) from 2000 to 2006 and mixing ratios estimated from the AES 2008 report.

The discrepancies between the mixing ratios back-calculated from the AES and the measurements were very minimal though some variability associated with other sources such as semiconductor industry or electrolytic production of neodymium in Japan or probably some uncharacterised sources were expected. The differences could also be explained by the validity/accuracy of the survey as there were limited participations by Chinese and Russian producers that account for 40% of global primary aluminium production. It should be noted that while comparing the values estimated from the AES report and the firn measurements, the time lag for inter-hemispheric difference was not taken into account. This was not done as it would have very minimal effect in this case and also a small number of participants in the survey were from Southern Hemisphere so therefore it would not be a relatively simple time lag correction.

5.5 Hexafluoroethane

Hexafluoroethane (C_2F_6) was first determined in the atmosphere in 1981. It is also a potent greenhouse gas with an atmospheric lifetime of 10000 years and GWP of 9200. The atmospheric concentration of approximately 3 ppt – 3.5 ppt was observed in recent years (Worton *et al*., 2007, Greally *et al*., 2005). Unlike CF_4 there are no known natural sources of C_2F_6 and it is believed to be entirely man-made. The anthropogenic sources of this gas are from the aluminium industry, semiconductor industry and release from CFC-115 manufacture. The emissions from latter source should have practically dropped to zero due to phasing out of CFC 115 under the Montreal Protocol. The "anode effects" in the aluminium smelting are also responsible for the C_2F_6 emissions. However surveys by International Aluminium Institute showed a reduction in C_2F_6 emission factor from 0.058 to 0.016 kg t^{-1} Al between 1990 and 2004 (IPCC, 2007).

This decrease in emissions from aluminium production in recent years could be compensated by increase in emissions from semiconductor industries that utilizes C_2F_6 to clean chemical vapour deposition chambers (CVDs) and it is also used in silicon etching. Usually C_2F_6 is added to the CVD chambers where it dissociates into highly reactive ionic species such as $C_2F_6^+$ that reacts with contaminants to clean the surface of the chamber. After the cleaning cycle the gas mixtures from the chamber were evacuated, diluted with nitrogen and then passed to a scrubber to remove any remaining reactive species before being vented into the atmosphere. Therefore C_2F_6 is released into the atmosphere as fugitive emissions from inefficient scrubbers.

5.5.1 Results and discussion

The mixing ratios of C_2F_6 measured in EDML firn air increased from below a detection limit of 0.04 ppt in the deepest sample to approximately 3.15 ppt in the ambient air (Figure 5.5.1). It is quite evident that C_2F_6 does not have any natural source and that the emissions were practically zero before anthropogenic influence. Figure 5.5.1 also shows the model results that were obtained with the diffusion model with varying atmospheric scenarios derived from the iterative dating technique. Model run 3 matches closely with the measurements and therefore the atmospheric scenario used in this model execution was used to reconstruct the atmospheric history of C_2F_6. The model fit to measurements

was excellent except a data point was underestimated by the model at 20 m and it also overestimated at ambient levels. Such disagreement could be due to procedural errors or uncertainties in the iterative dating model not being capable of capturing the measurements if the concentrations start to level off, which could most likely be the cause in this case.
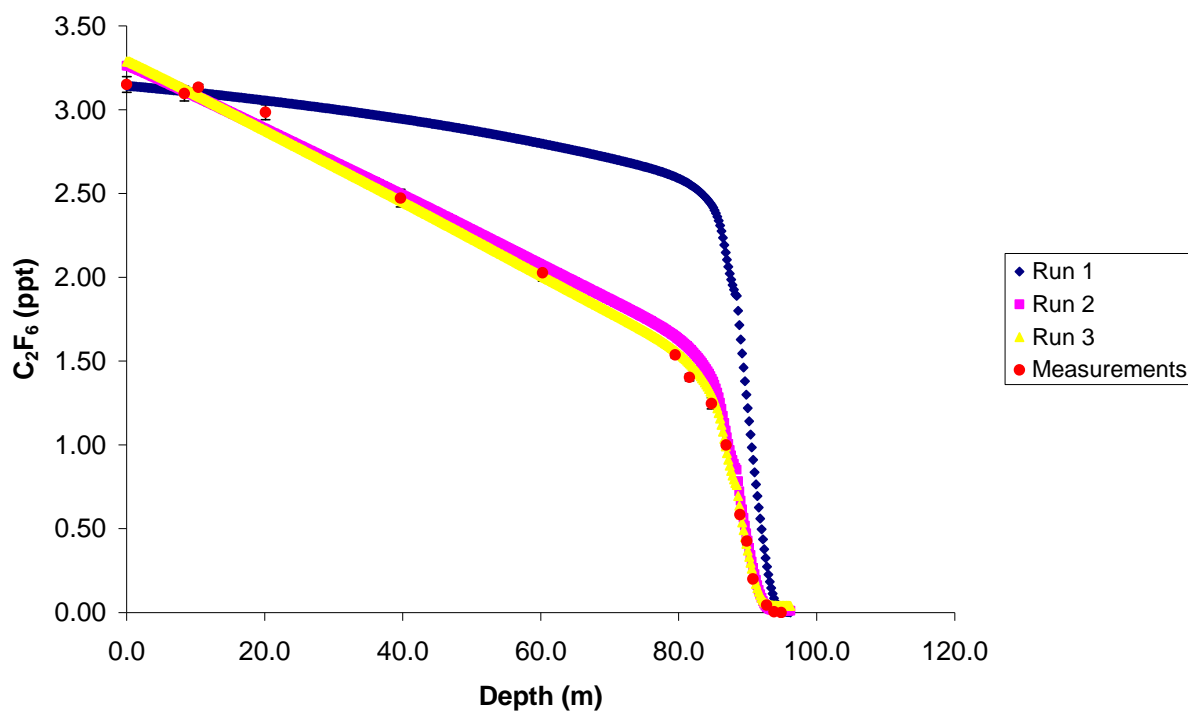
Figure 5.5.1: Depth Profile of C_2F_6 mixing ratios in EDML firn air. The diffusion model results obtained with different atmospheric scenarios are also shown.

The atmospheric burden of C_2F_6 started rising after 1920 at a linear growth rate as shown by the red line in the Figure 5.5.2. From 1920 until late 1980s the growth rate was about 0.02 ppt yr^{-1} but then it increased by almost a factor of five to 0.1 ppt yr^{-1}. The behaviour of the C_2F_6 atmospheric trend is in contrast to that of CF_4, which showed steady growth (in % yr^{-1}) and then decreased after mid 1980s. The change in growth rate reflected a change in source strengths. The data were plotted against CF_4 (Figure 5.5.3) to fully understand the underlying cause for the changing atmospheric growth rate of C_2F_6. The relationship obtained in this study is in agreement with the relationship obtained in Worton *et al*. (2007) and also clearly showed the extension of the steeper gradient obtained in Worton *et al*. (2007). Hence this study supports the findings of Worton *et al*. (2007).
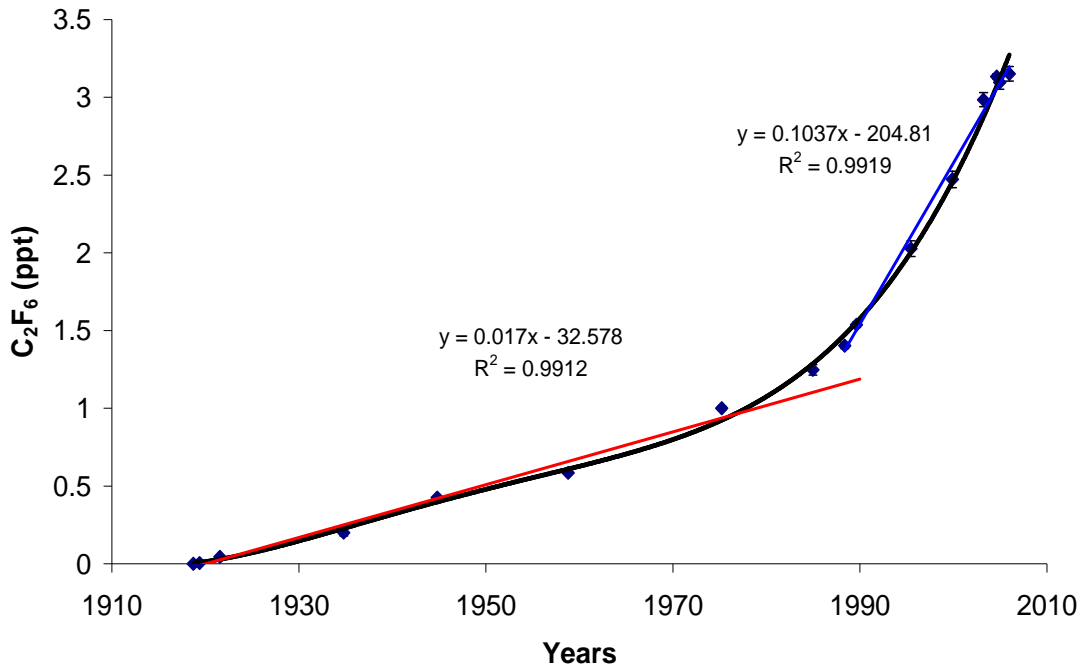
Figure 5.5.2: Atmospheric trends of C_2F_6 reconstructed from iterative modelling of firn air.
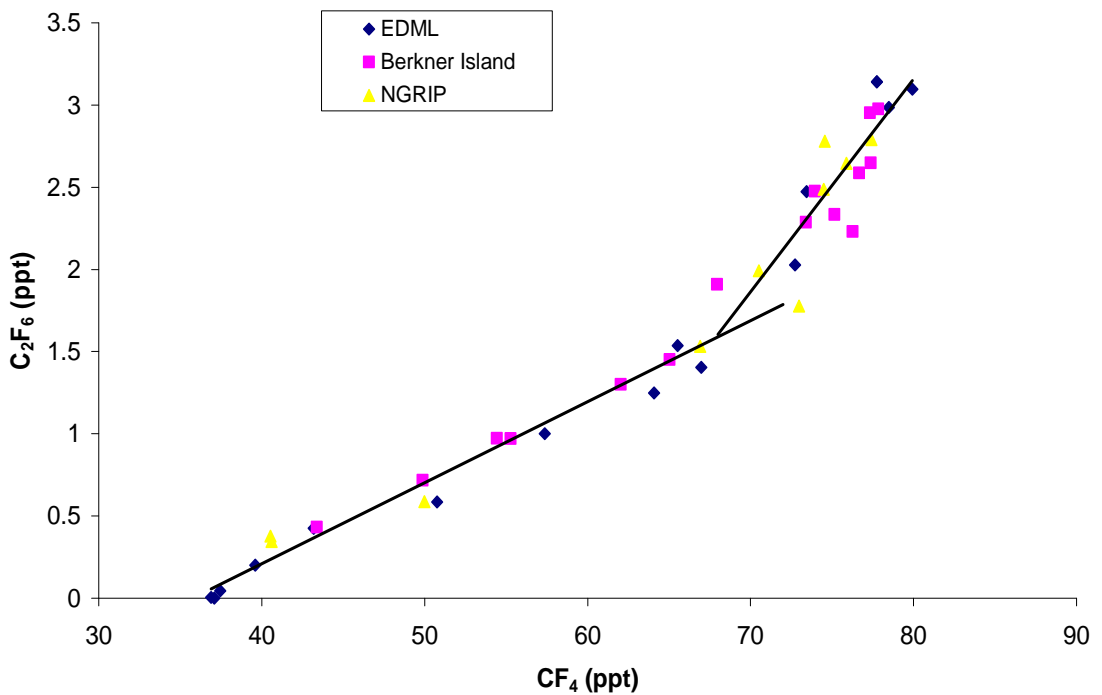
Figure 5.5.3: A plot of C_2F_6 Vs CF_4 illustrates the changing relationship between CF_4 and C_2F_6 from EDML firn air. The figure also shows data from Berkner Island and NGRIP in the Northern Hemisphere (Worton *et al.*, 2007). The solid lines were determined by linear least- squares curve fitting to the two obvious trends.

The growth rate of C_2F_6 increases linearly with respect to the CF_4 growth rate before late 1980s suggesting that the C_2F_6 emissions were primarily from the aluminium industry. Characteristically C_2F_6 emissions were based on CF_4 emissions, equating to approximately 10 - 12% of CF_4 by mass (Khalil *et al*., 2003; Greally *et al*., 2005). However in late 1980s the trend in growth rate of C_2F_6 deviated significantly from the initial trend. The steeper gradient suggests that in the recent years C_2F_6 emissions have increased, with the growth rate larger than the CF_4 growth rate. Since the implementation of PFC emissions reduction program, the C_2F_6 emissions from the aluminium industry have decreased significantly so therefore it can be concluded that increasing emissions from the semiconductor industries caused the increase in the C_2F_6 growth rate. Moreover, the in-situ continuous measurements of C_2F_6 at Mace Head highlighted that above baseline elevations in the mixing ratios of C_2F_6 were not correlated with the CF_4 above baseline events (Greally *et al*., 2005). It was concluded that an additional stronger source for C_2F_6, such as stronger European emission source from semiconductor industries resulted in this non-correlation between CF_4 and C_2F_6.

According to the model-derived atmospheric trend the growth rate increased from 0.04 ppt yr^{-1} in mid 1980s to an average of 0.14 ppt yr^{-1} for the period 2004 to 2006. Khalil *et al*. (2003) and Harnisch *et al*. (1996a) estimated the growth rate to be approximately 0.09 ppt yr^{-1} for the period 1987 – 1997, which is comparable to the value of 0.08 ppt yr^{-1} obtained in this study for the similar period. Greally *et al*. (2005) reported a value of 0.05 ppt yr^{-1} for baseline growth rate which is significantly lower than earlier reported values in other studies and in this study as well.

The conversion factor of 1 ppt yr^{-1} = 23 Gg yr^{-1} (Khalil *et al*., 2003) was used to convert the atmospheric trend derived from the model into emission estimates. Figure 5.5.4 highlighted that the emission estimates from the model-derived atmospheric trend were generally in good agreement with the EDGAR values and the emission estimates from Harnisch and Höhne (2002), which published the total emissions reported by countries under Annex I Parties. However the Russian Federation only reported for the period 1990 – 1994 and for the rest of the years the emissions were interpolated or were assumed constant. The Russian Federation is responsible for 40 – 50% of the global emission and its actual emission not being known could explain the discrepancy

between our data set and those reported by Harnisch and Höhne(2002). There are again slight discrepancies between estimates obtained in this study and the EDGAR values, and these are observed at similar periods in comparison with the CF_4 case. The discrepancies could be the result of the smoothing of data due to lack of direct atmospheric measurements or, quite possibly, in early 1970s the CF_4:C_2F_6 emission ratio may have not been constant (a constant ratio of 10 is used to estimate C_2F_6 emission from CF_4 emissions), and this seems logical because different smelters would have different CF_4:C_2F_6 ratios.
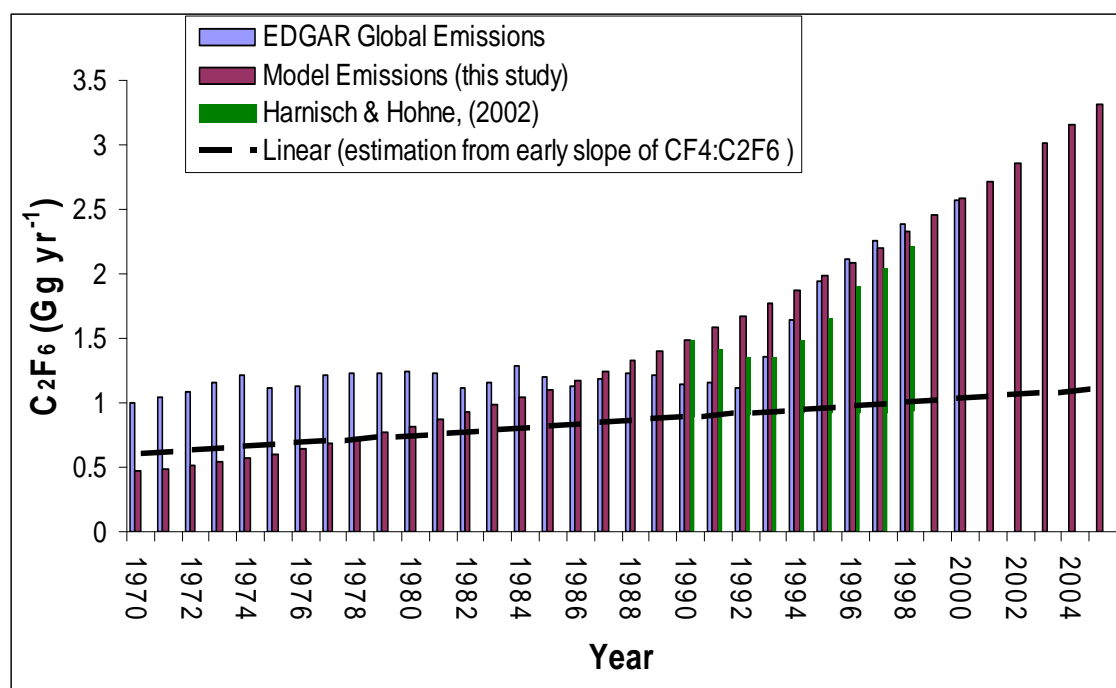
Figure 5.3.4 Comparison of C_2F_6 emissions obtained in this study with EDGAR Global emissions and emissions stated in Harnisch and Hohne (2002), which was the total emission estimates reported by countries under "Annex 1 Parties" to the United Nations Framework Convention on Climate Change.

The emissions reported by EDGAR were in the proximity of 1 Gg yr^{-1} from 1970s to 1990 and then increased by a factor of 3 in recent years. The dashed line in Figure 5.3.4 depicts almost constant values of 0.8 Gg yr^{-1}, which was assumed to be contributed solely by the aluminium industry as estimated from the early slope of correlation between CF_4 and C_2F_6. The 2006 AES documented a decrease in C_2F_6 emissions from the aluminium production from 1.4Gg yr^{-1} in 1990 to 0.4 Gg yr^{-1} in 2006. The emission estimate of 1.5 Gg yr^{-1} in 1990 obtained in this study is in close agreement with the

industrial estimate but the emission for 2006 obtained in this study and by the 2006 AES is in vast disagreement. The differences could be explained by increasing emissions from additional sources such as semiconductor industry. Assuming that the emissions reported by the 2006 AES are valid then it can be approximated that the emissions from the semiconductor industry increased from 0.4 Gg yr^{-1} in mid 1980s to ~1.70 Gg yr^{-1} in 2000. The rate of increase is consistent with the findings of Worton *et al*. (2007), who reported an increase from 0.47 ± 0.21 to 1.8 ± 0.11 Gg yr^{-1} between 1990 and 2001 due to non-aluminium source.

The more recent emission estimates such as 2.96 Gg yr^{-1} in 2006 could not be validated, as the EDGAR (version 3.2) database was only available until 2000. These emission estimates are subject to uncertainties in the atmospheric trend used in this study. The model-derived atmospheric trend tends to overestimate the mixing ratio in the ambient air sample collected at the EDML and underestimated the concentration of a sample dated at 2003 although the polynomial fitting curve for the entire dataset had a value of $r^2 = 0.99$. From the depth profile (see Figure 5.5.1), the C_2F_6 concentration seems to stabilise more recently. The measurements from air samples dated 2000 onwards were plotted and an atmospheric trend was obtained by a polynomial fitting of order 2 that fits all the data (Figure 5.5.5). The emission estimates were revised based on the atmospheric trend for the recent years and it showed that emissions decreased from 4.36 Gg yr^{-1} in 2001 to 0.63 Gg yr^{-1} in 2006.
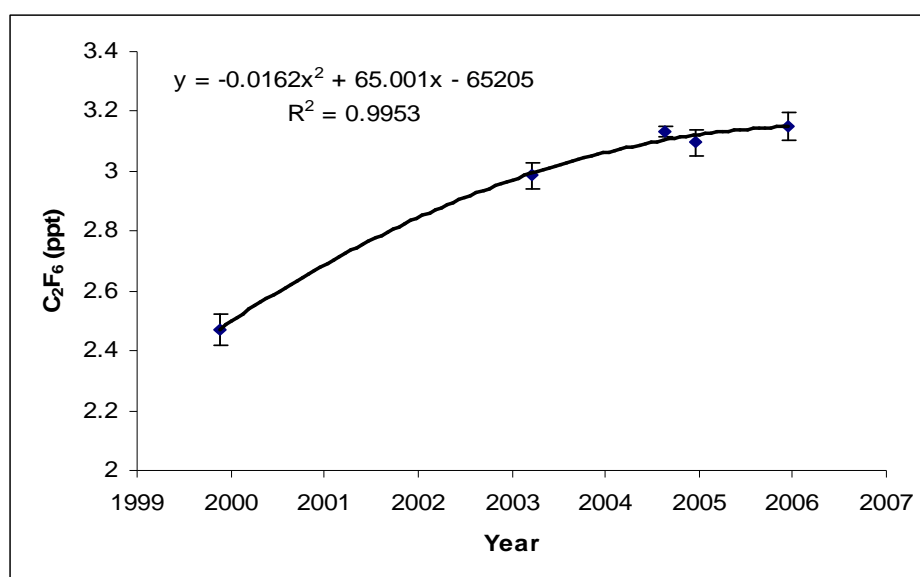
Figure 5.5.5: C_2F_6 atmospheric trend for the period 2000 – 2006.

Figure 5.5.5 clearly demonstrates that the growth rates have decreased significantly from 2003 to 2006. The results obtained here are preliminary evidence of stabilising atmospheric growth of C_2F_6 due to decrease in source emissions. This finding can be confirmed by more high-resolution atmospheric measurements of air archives to current date. The World Semiconductor Council (WSC) is committed to implement emission reduction strategy to reduce global emissions to 10% below the baseline year (1995) by the year 2010. Several industrial practices were adopted to achieve this goal and these include: replacement of perfluorocarbons with NF_3 and other compounds that are degradable in the chamber, high temperature furnace-scrubber to efficiently destroy any PFCs, and development of membrane systems to recover and recycle PFCs (Wijmans *et al*., 2004).

5.6 Perfluoropropane

Perfluoropropane (C_3F_8), or commonly known as PFC 218, has an atmospheric lifetime of about 2600 years with a radiative forcing of 0.26 Wm^{-2} ppb^{-1} and a GWP of 8830 based on a 100 year time horizon (IPCC, 2001). The atmospheric sources are entirely anthropogenic resulting from its application in plasma etching in semiconductor production, primary aluminium production and its use in a blended refrigerant such as R-413a. The atmospheric measurement of C_3F_8 is very scarce and therefore very little is known about its atmospheric history. There is only one published long term trend data (1978 – 1997) for C_3F_8 in Cape Meares, Oregon, air archives and in flask data from Point Barrow, Alaska, and Palmer Station, Antarctica (Khalil *et al*., 2003; Culbertson *et al*., 2004), which showed the rising atmospheric burden from 0.08 ppt in 1978 to 0.22 ppt in 1997. More recently in-situ measurements at Mace Head, Ireland in 2004 observed a mixing ratio of 0.47 ppt (Greally *et al*., 2005).

The atmospheric measurements of C_3F_8 have not been updated since 2004 and therefore this study not only provides insights into the longest atmospheric trend but also the most updated atmospheric record of C_3F_8, and consequently, should confirm the findings of Greally *et al*. (2005), which stated more than doubling of C_3F_8 mixing ratios in the atmosphere since 1997.

5.6.1 Results and discussion

Figure 5.6.1 illustrates the concentration - depth profile of C_3F_8 measurements in the EDML firn air. A value of 0.83 ppt was measured in the ambient air sample (January 2006) in Antarctica. This suggests that the atmospheric concentration has increased by a factor of 4 since 1997. The zero concentration of C_3F_8 in few deepest-most samples of the firn also suggests that this species does not have a long atmospheric history unlike the other major PFCs.
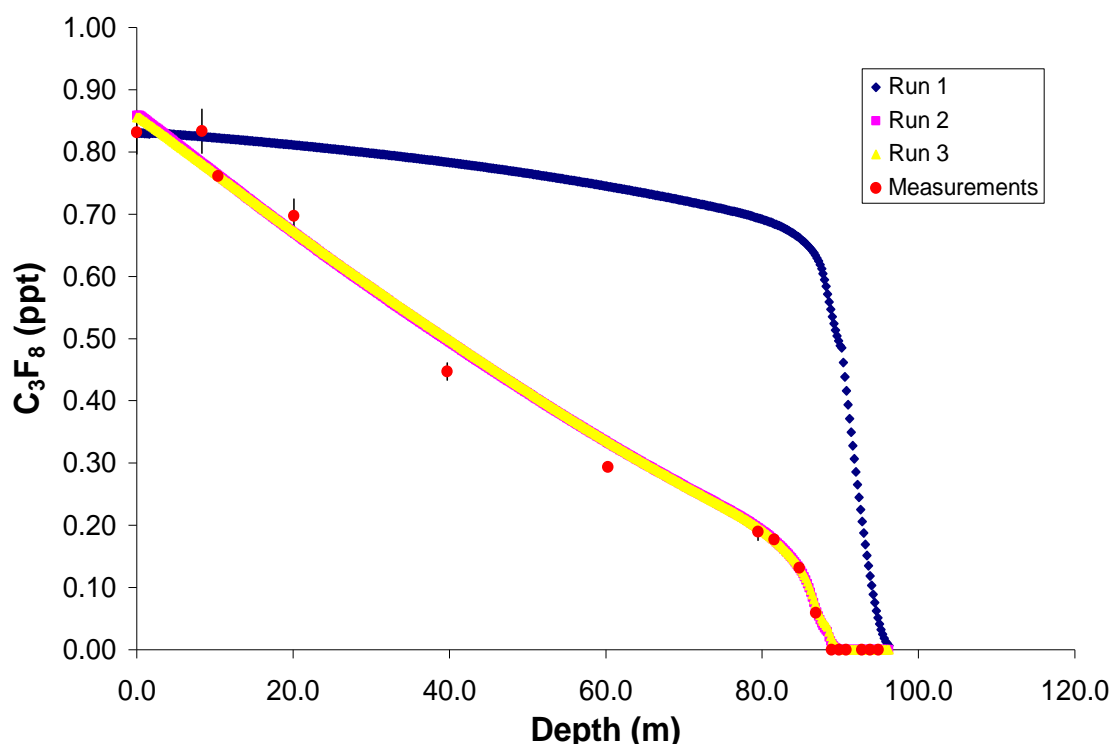
Figure 5.6.1: Depth Profile of C_3F_8 mixing ratios in the EDML firn air. The diffusion model results obtained with different atmospheric scenarios are also shown.

The atmospheric trend derived in this study revealed that the atmospheric C_3F_8 was only evident after early 1960s and grew at a slow but steady rate to early 1970s. It remained almost constant at ~0.1 ppt until mid 1980s and then increased to 0.22 ppt in mid 1990s before escalating to a value of 0.83 ppt in the ambient air samples. The reconstructed atmospheric trend obtained from the EDML firn measurements correlates very well with the UEA Cape Grim data, particularly in the later part of the reconstructed trend. The atmospheric trend shown in Figure 5.6.2 closely resembles the trend observed at Cape Meares, Oregon and Palmer Station, Antarctica for the period 1978 - 1992 by
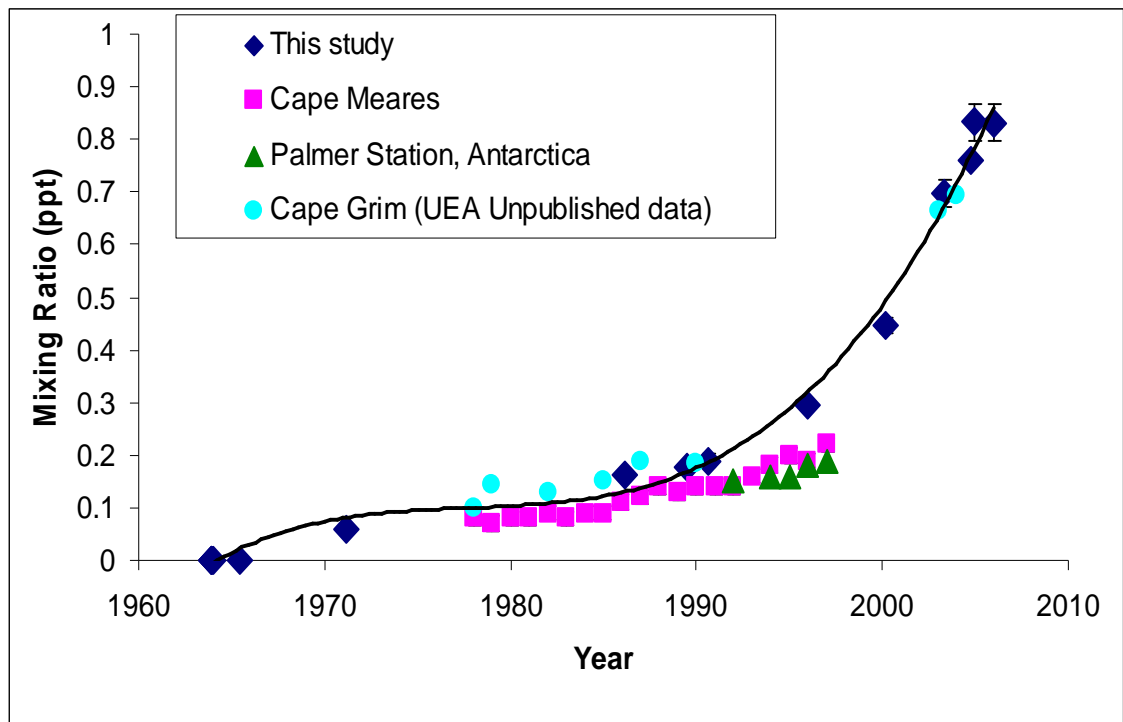
Figure 5.6.2: Model-derived Atmospheric trend for C_3F_8 obtained by iterative dating technique. The atmospheric trend obtained is compared with other published (Culbertson *et al*., 2004) and unpublished data from Cape Grim measured at UEA.

Khalil *et al*. (2003) and Culbertson *et al*. (2004). The measurements in this period are in good agreement and the small disparity in absolute values between the two datasets could have resulted from differences in the calibration scales. The two datasets (UEA and Culbertson *et al*., 2004) are in obvious disagreement in absolute values but not so much in the general trend from mid 1990s until 1997.

The discrepancies between the two datasets (between this study and Culbertson *et al*., 2003) could be an overestimation by the model-derived atmospheric trend due to lack of data points in that particular period, or they simply could be attributed to uncertainties in the assigned age scale. The discrepancies for this particular period could be easily compensated for if the age scale for the atmospheric trend was moved to the right by approximately 4 years. The uncertainty in the age scale would arise from an incorrect atmospheric scenarios input and as a result the model runs overestimated the concentration at 60 m depth which actually corresponds to the disagreement region in

the age scale. Culbertson *et al*. (2004) reported values of 0.16 ppt to 0.23 ppt in 1996 and such scatter in the data could also partially explain the discrepancy between the firn smoothed data and the annual averaged trend from Culbertson *et al*. (2003). However it seems there are some serious calibration issues with C_3F_8. When the absolute values were decreased by 1/3 only then the two datasets were coherent, hence providing a convincing case that the UEA calibration scale for C_3F_8 was 33% higher than the Culbertson's scale.

Despite the apparent discrepancy in absolute values between the datasets the pattern of atmospheric growth is very similar. The average growth rate calculated from the model trend for the period 1986 - 1992 was 10% yr^{-1} and is comparable to the average growth rate of 9.3% yr^{-1} observed in 1986 at Cape Meares (Culbertson *et al*., 2004). Both datasets depict a change in the growth rate at 1993 although the growth rate illustrated by the model trend is more dramatic then that of Culbertson *et al*. (2004). The average growth rate for the years 2000 – 2005 was estimated to be ~0.06 ppt yr^{-1}. Such a large increase in the growth rate means an increase in source emissions.

The pattern of reconstructed atmospheric trend is very similar to the C_2F_6 reconstructed atmospheric trend. Figure 5.6.3 shows the correlation between C_2F_6 and C_3F_8 data with a correlation coefficient of 0.96. This could indicate that the timing of change in growth rate could be similar for both species hence the basis for speculation that the origin of the emissions could also be similar. As highlighted in the above section the increase in C_2F_6 atmospheric burden was due to increase in emissions from the semiconductor industry and therefore the rapid increase in the C_3F_8 growth rate observed since 2000 could also be attributed to the semiconductor industry. In addition, the in-situ continuous measurements at Mace Head revealed a similar sort of pattern for above baseline observations for both gases suggesting that the sources are similar and most likely linked to the semiconductor industries in Europe (Greally *et al*., 2005). However this is not very conclusive for two reasons. Firstly, there are no emission estimates available from semiconductor industries to suggest that the emissions are increasing and secondly it has been reported that there were growing emissions due to its use in refrigerants like R-413a (Harnisch, 2000).

Although it is certain that emissions have increased rapidly in the past decade it was difficult to pinpoint a particular source responsible for the increase at this stage and therefore demands further investigation in this aspect. Given the current growth rate it is vital to identify the sources and implement emission reduction strategies.
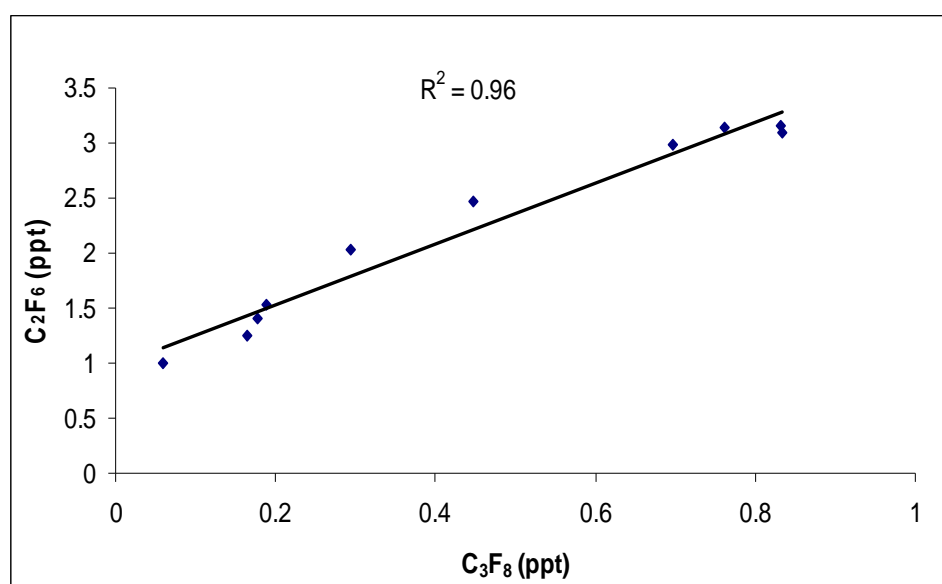
Figure 5.6.3: An illustration of linear correlation between atmospheric trends for C_2F_6 and C_3F_8. Only those samples were correlated where non-zero values of C_3F_8 were observed.

The emissions were calculated based on the growth rate obtained from the reconstructed atmospheric trend and the values from 1970 to 2005 are shown in Figure 5.6.4. It portrays a decrease in emissions from 1970 to 1979 and then a slow increase in 1980 with more rapid growth from the early 1990s. The average emission for 1970 - 1979 was about 0.1 Gg yr^{-1} and is a typical emission value from the aluminium smelting, which are on the order of 0.1 Gg yr^{-1} (Harnisch, 2000). The emission estimates for the second half of 1990s were calculated to be 1.1 Gg yr^{-1} and this strongly supports the tentative emission of 0.70 ± 0.45 Gg yr^{-1} estimated by Harnisch (2000). The average emission for the period 2000 – 2005 obtained in this study was 1.8 Gg yr^{-1}. The emissions obtained in this study for more recent years could not be verified due to the lack of more recent atmospheric measurements, and inaccurate and inconsistent

emission inventories. The EDGAR values available were much less than those values obtained in this study. This clearly reflects some inconsistencies in the reporting procedures, and is an indication that some potential sources were not accounted for.
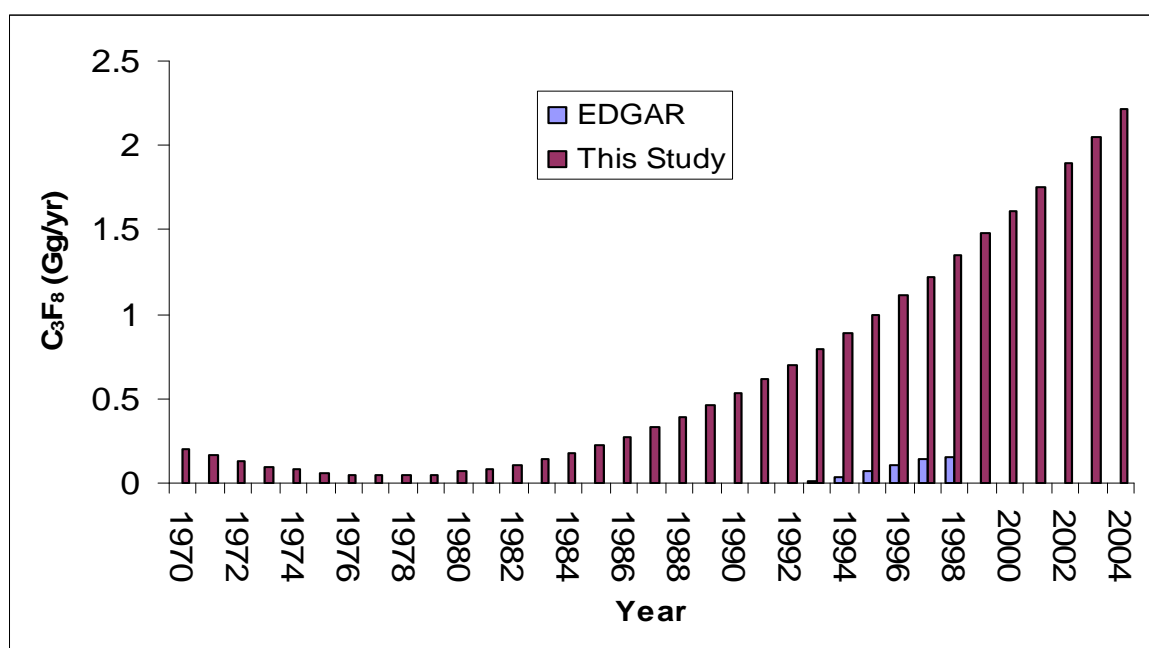
Figure 5.6.4: Emission estimation based on the growth rate obtained from the reconstructed atmospheric trend for the period 1970 – 2005. The emission estimations obtained are compared to the EDGAR values.

5.7 Perfluorocyclobutane

Perfluorocyclobutane (c-C_4F_8) has an atmospheric lifetime of 3200 years, radiative efficiency of 0.32 $Wm^{-2}ppb^{-1}$ and a GWP of 10 090 for a 100-year time horizon (Velders et al., 2005). There is very limited knowledge about its atmospheric abundance and the nature of sources for this particular species remains largely unexplained. It has some economic relevance in plasma etching in semiconductor production. It could be formed through dimerization of tetrafluoroethene or possibly through combustion or thermal decomposition of fluoropolymers (Harnisch, 2000). The possibility of military

applications of c-C_4F_8 in radar systems and as specialised refrigerant in submarines were also mentioned (Harnisch, 2000).

Harnisch (2000) reported an annual mixing ratio of 0.7 ppt in 1997 based on an unpublished study of stratospheric air measurements. This study provides the first and the longest atmospheric trend of c-C_4F_8 derived from the EDML firn air measurements.

5.7.1 Results and discussion

Figure 5.7.1 shows that the mixing ratio increased from below detection limit at the bottom of the firn to 1.17 ppt in January 2006. The atmospheric history was reconstructed using the diffusion model and the iterative dating technique, and the results obtained are shown in Figure 5.7.2. It illustrates that the mixing ratios increased very slowly from 0 ppt in 1940 to ~ 0.1 ppt in early 1960s and then increased at a linear growth rate. In fact, a linear fit to the 1957 – 1997 data ($R^2 = 0.99$) yields a growth rate of 0.03 pptv yr^{-1}. Since 2000 the growth rate decreased drastically stabilizing the atmospheric mixing ratios. The reconstructed trend shows the mixing ratios levelled at 1.15 ± 0.02 pptv for the period 2000 – 2006.
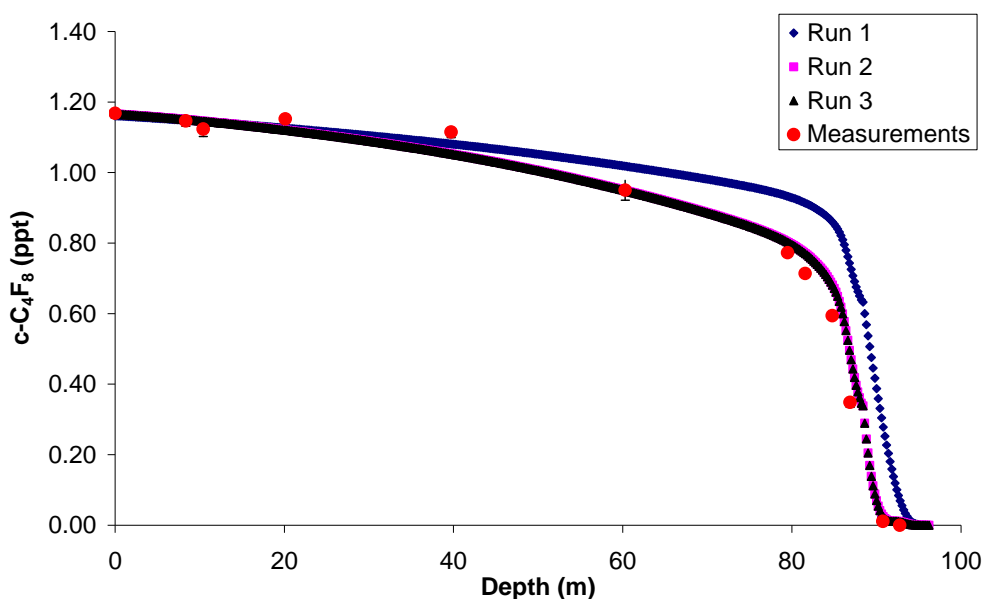
Figure 5.7.1 The depth profile and the diffusion model results for c-C_4F_8 in EDML firn air.

Figure 5.7.2: Model-derived atmospheric trend for c-C_4F_8 obtained by polynomial fitting curve to the data. The trend obtained in this study was compared with measurements from Cape Grim data reported by Oram (1999).

The reconstructed atmospheric trend was compared to atmospheric measurements of archive air samples from Cape Grim from 1978 – 1995 (Oram, 1999) and updated measurements from the same site until 2003. All these measurements were done on the same UEA calibration scale. The general pattern of the reconstructed atmospheric trend is coherent with Oram's (1999) data except a minor disagreement around 1990 – 1995. Oram (1999) noted that the atmospheric values started stabilising around 1990 – 1995 with the growth rate decreasing by nearly 80%. Obviously our reconstructed trend does not show this feature due to lack of temporal resolution of the firn measurements. A linear regression of the 1990 – 1995 Cape Grim data yielded a poor correlation due to scatter in data. The precision of the measurement was better than the degree of the scatter observed in the dataset, suggesting that there was a local influence on this compound (Oram, 1999). However the absolute concentration values from the firn measurements in the same time period as in Oram's study were in excellent agreement with the reconstructed trend and therefore increased the confidence in the validity of the reconstructed trend.

The c-C_4F_8 depth profile was compared with other species such as CF_4 and C_2F_6 whose atmospheric abundance and the fate of its sources were well constrained. Figure 5.7.3 shows remarkable similarities in the growth patterns between CF_4 and c-C_4F_8. Apparently c-C_4F_8 started to increase approximately at the time when CF_4 growth rate increased rapidly due to aluminium smelting. CF_4 and c-C_4F_8 both had their peak growth rates during similar time period and therefore could strongly suggest that the nature of the sources could be same. The growth rates of c-C_4F_8 and C_2F_6 were distinctly different (see Figure 5.7.4), the initial growth rate of c-C_4F_8 was much faster than C_2F_6. The period where the semiconductor industry had a significant impact on the atmospheric C_2F_6 it could also have contributed to the increasing levels of c-C_4F_8 but clearly is not the major source of c-C_4F_8. Due to strong resemblance to CF_4 growth rate patterns it is convincing that aluminium industry was responsible for the increase in c-C_4F_8 but the fact that c-C_4F_8 started to stabilise in the atmosphere before CF_4 is quite perplexing. This could be only possible if the emissions decreased much faster than CF_4 due to improvement in technologies and other mitigation strategies.
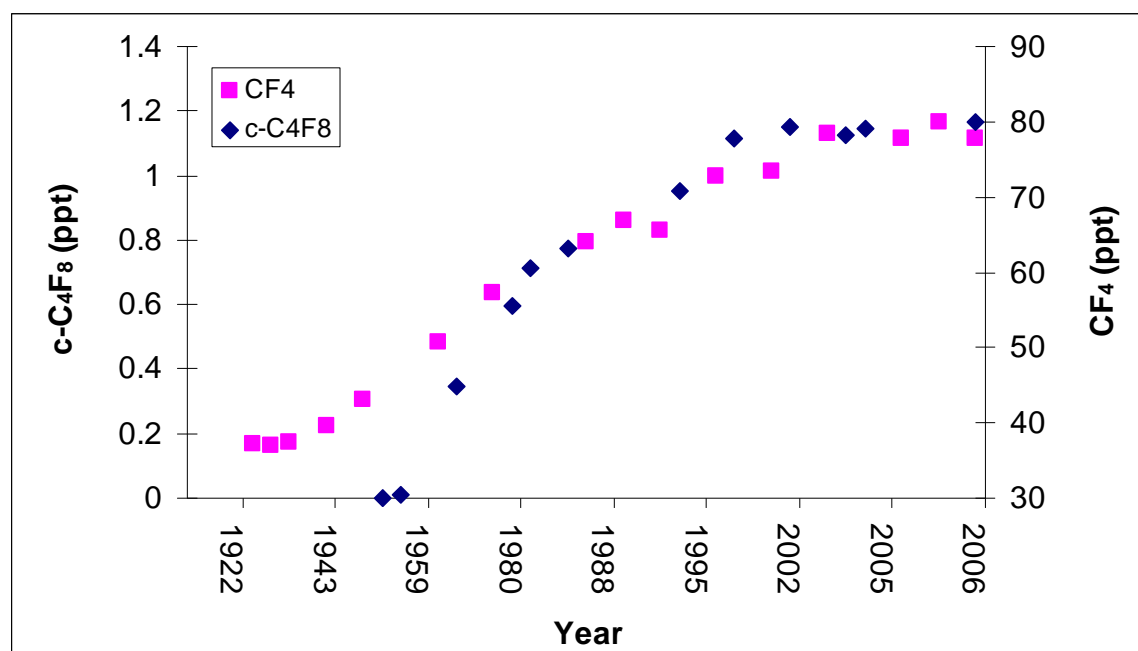
Figure 5.7.3: A scatter plot of CF_4 vs c-C_4F_8
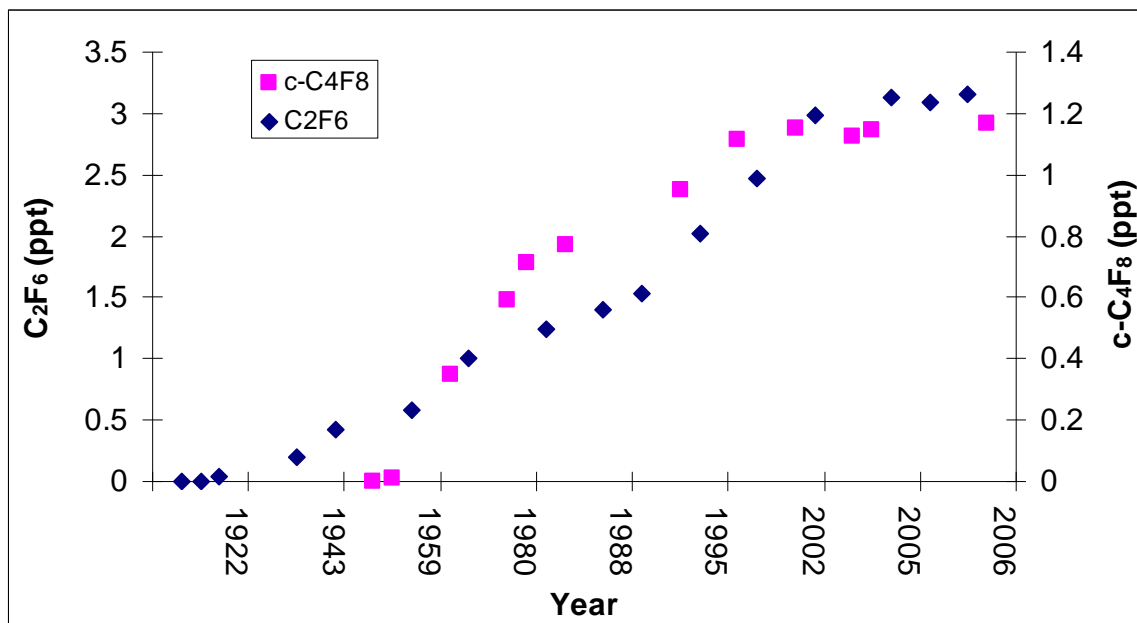
Figure 5.7.4: A scatter plot C_2F_6 vs. $c\text{-}C_4F_8$

Like the other PFCs discussed earlier, emission estimates of $c\text{-}C_4F_8$ were obtained by similar process. The model-derived atmospheric trend was converted into emission estimates using the conversion factor of 1 pptv yr^{-1} = 33.4 Gg yr^{-1}. Figure 5.7.5 shows that the emissions increased from 0.8 Gg yr^{-1} in 1971 to 1.1 Gg yr^{-1} in mid 1980s and then decreased to almost 0 Gg yr^{-1} in recent years. The emissions obtained in this study were compared to Oram (1999) and to the EDGAR values. The emission values reported by EDGAR were underestimated and were almost insignificant in comparison to the values obtained by this study and Oram (1999). There is a good agreement in the emissions for the period 1976 – 1981 between this study and Oram (1999), but for the other periods although the absolute values are in disagreement, the general trend for emission is similar. Oram (1999) highlighted a much faster decrease from 1990 – 1995 but our study showed a steady decrease in emissions. As discussed previously such discrepancies could arise due to the lack of temporal resolution in data from the firn record, due to smoothing effect in the firn and also due to the polynomial fitting to the data used to obtain the atmospheric trend.
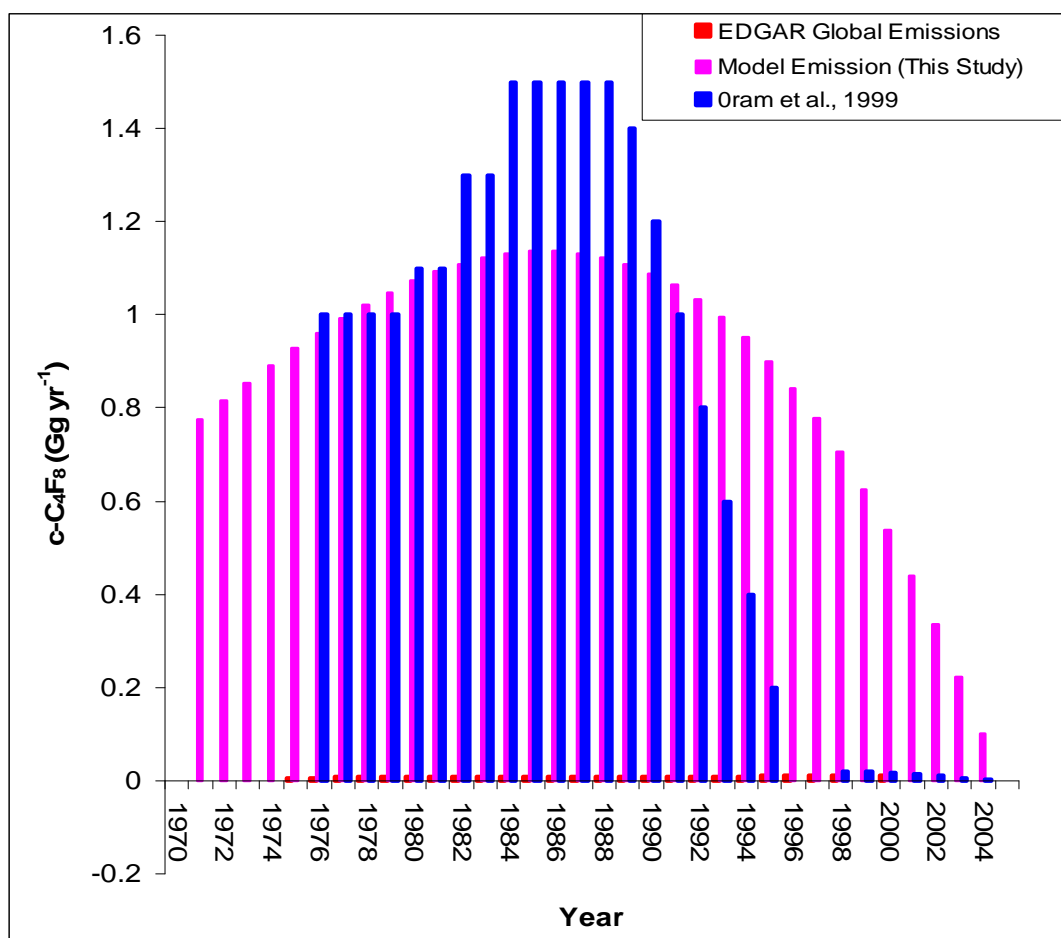
Figure 5.7.5: Emission estimates of c-C_4F_8 based on the reconstructed atmospheric trend from firn measurements. These emission estimates are compared to EDGAR database and Oram (1999) study.

An annual emission of 0.17 Gg yr^{-1} for the year 2003 was noted based on interspecies ratios observed in aircraft profiles near Tokyo, Japan (Yokouchi *et al.*, 2005). This is approximately 77% of the global emission derived from the firn measurement for the year 2003. The emissions decreased from 1.13 Gg yr^{-1} to 0 Gg yr^{-1} for the period 1990 - 2005, implying a decrease by 100% as compared to 75% reduction in total PFCs emissions from the aluminium industry (AES, 2006). To date c-C_4F_8 has not been detected in the anode gas and warrants further investigation to pinpoint the aluminium industry as the major source. The similarity in behaviour between CF_4 and c-C_4F_8 could be coincidental and therefore we may not have achieved much in terms of understanding the sources of this particular greenhouse gas, but we are convinced that this particular greenhouse gas is not increasing in the atmosphere and its emission has almost decreased to 0 Gg yr^{-1}.

5.8 Fluoroform

Fluoroform (CHF_3, HFC-23) is another potent greenhouse gas with a GWP of 11, 700 based on 100-year time horizon (WMO, 2006) and a radiative efficiency of 0.19 Wm^{-2} ppb^{-1}. The atmospheric lifetime is about 270 years owing to its very slow removal process predominantly via reaction with tropospheric OH radicals. HFC-23 is the most abundant and is probably the longest existing HFC in the atmosphere. Initially HFC-23 was used as a raw material in the production of Halon-1301 ($CBrF_3$) but this source would have decreased to zero due to the implementation of the Montreal Protocol, which bans halon manufacture in developed countries. It is currently used as a replacement agent for halons in low temperature refrigerant and fire extinguishing applications. Although it is directly dispersed into the atmosphere, emissions from these sources are trivial as compared to emissions from HCFC-22 production. HFC-23 is formed at the reactor stage of the HCFC-22 manufacturing process due to over-fluorination of HCFC-22 with hydrogen fluoride. The HFC-23 produced is separated from HCFC-22 and is vented into the atmosphere. The amount of HFC-23 produced depends on the occurrence of unfavourable reaction conditions but it is estimated to be between 1% and 4% of the production of HCFC-22 (McCulloch & Lindley, 2007).

There are two published long term trends for HFC-23: one from 1978 - 1995 in air archives from Cape Grim (Oram *et al*., 1998) and the other from Cape Meares, Oregon samples from 1978 to 1997 (Culbertson *et al*., 2004). Both studies revealed that the atmospheric levels are increasing unabatedly.

5.8.1 Results & discussion

The depth profile of CF_3H in the EDML firn air is shown in Figure 5.8.1, along with model runs with different atmospheric scenarios obtained from the iterative dating technique. It was quite challenging to model this particular species because it did not reach zero at the bottom of the firn indicating that there might be a natural background level. However it would be difficult to imagine what this natural source could be, and on the basis of there being no documented evidence of any natural sources of this compound, we assumed that the pre-industrial value was zero. Nevertheless the values observed at the bottom of the firn were close to zero. It was measured to be ~ 0.5 ppt,

which is significantly higher than the detection limit, indicating a natural background level or due to some contamination from the sampling device but it is difficult to make any conclusive remarks at this stage of a possible natural background level. A system blank run was done immediately after measuring the deepest firn samples on the instrument and it showed a zero blank. This indicates that samples were either contaminated with HFC-23 during sample collection or probably there might be a natural source. Hence the dates assigned to the deepest samples need to be treated cautiously as they could be older if there was a natural source. Nevertheless the reconstructed atmospheric trend is in absolute agreement with the atmospheric measurements (Figure 5.8.2).
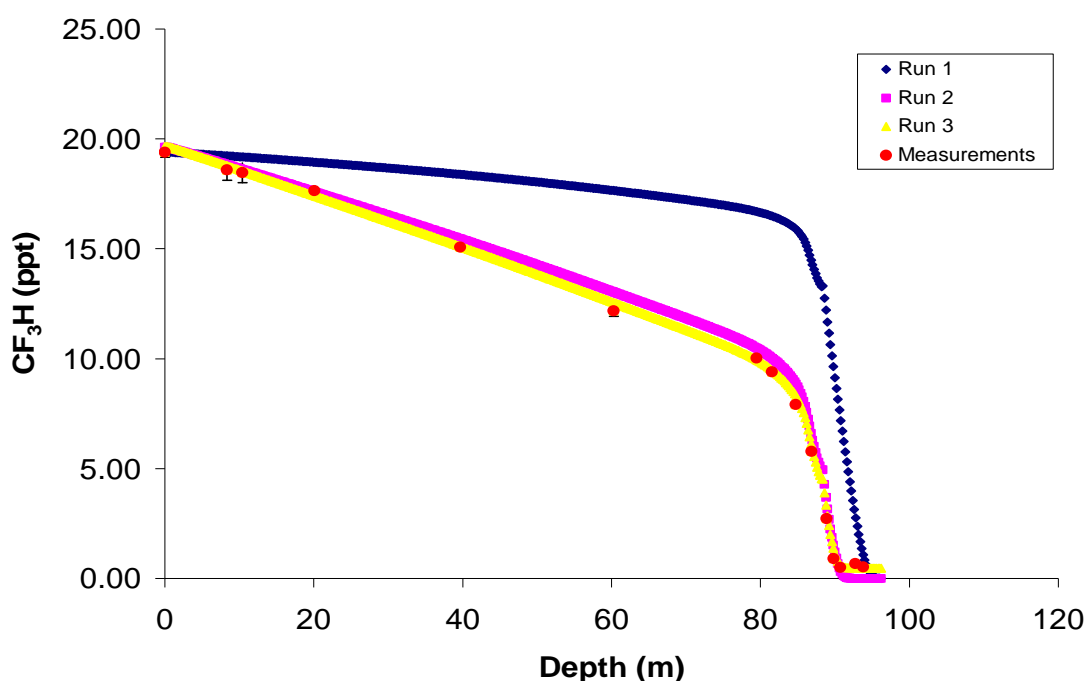
Figure 5.8.1: The concentration-depth profile and the diffusion model results for CHF_3 in the EDML firn air.

The reconstructed atmospheric trend showed that the atmospheric values rose from a value of ~0.5 ppt in 1950 to 19.4 ppt in early 2006. The atmospheric trend derived here is in good agreement especially during the recent part of the derived trend with the trend obtained by Oram *et al.* (1998) and is in agreement with Culbertson *et al.* (2004) for the same period. The reconstructed trend is consistent with the updated trend until 2004 from Cape Grim (WMO, 2006) except minor discrepancies in the earlier part of the
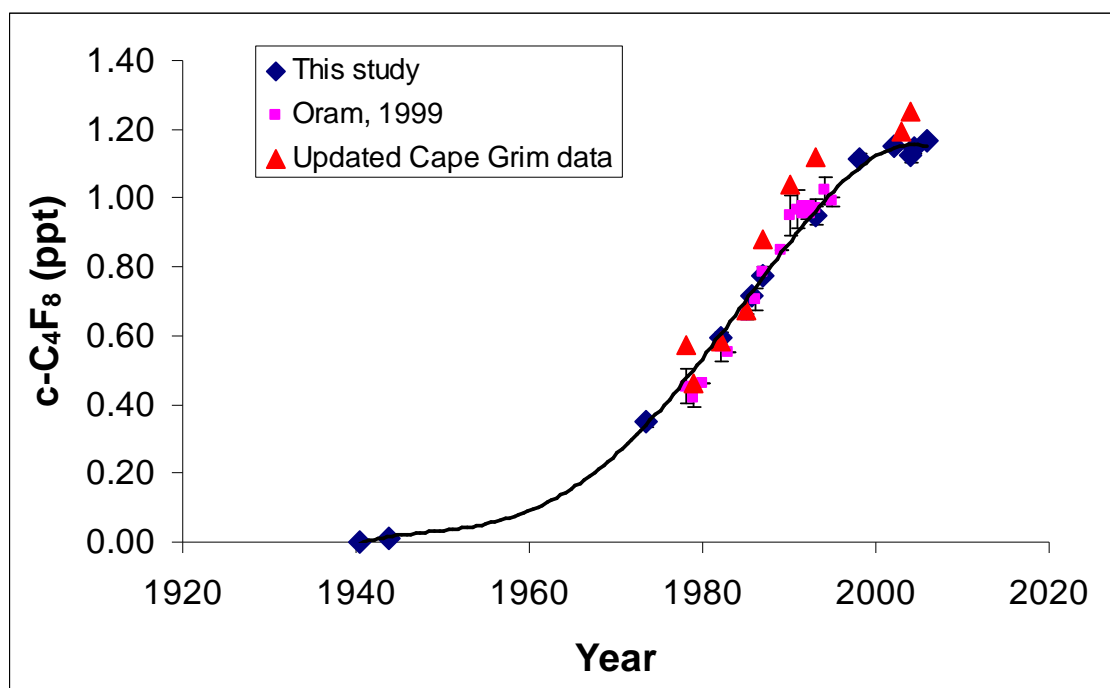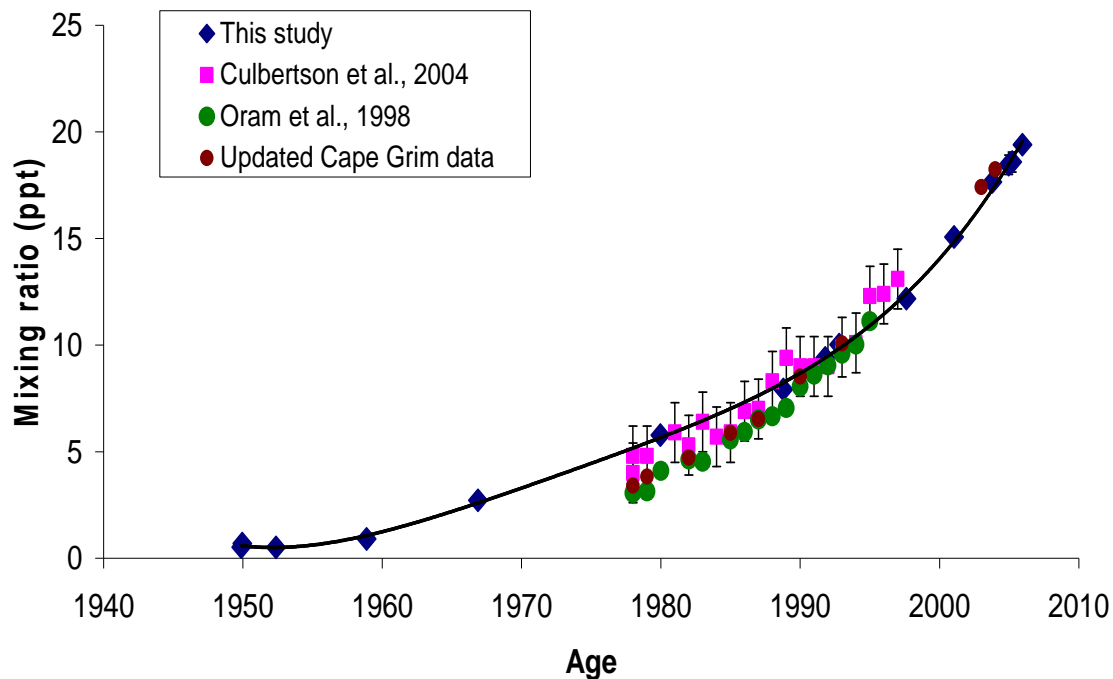
Figure 5.8.2: Model-derived atmospheric trend for CHF_3 obtained by polynomial fitting curve to the data. The trend obtained in this study was compared with measurements from Cape Grim data reported by Oram *et al.* (1998), from Cape Meares by Culbertson *et al.* (2004) and unpublished Cape Grim data.

record. The measurements reported by Culbertson *et al.* (2004) are higher by 1.2 pptv than those reported by Oram *et al.* (1998), reflecting systematic errors in the calibration scale. Since the calibration scale used in this study is essentially the same as Oram *et al.* (1998), the reconstructed trend should be more consistent with the trend obtained in Oram *et al.* (1998) study and the updated trend published in WMO (2006) report. The fact that the model-derived atmospheric trend is consistent with Oram *et al.* (1998) and WMO (2006) report from 1990 onwards eliminates any discrepancies due to dating of the firn air samples. The discrepancy between this study and other trends reported using the same calibration scale is simply because two data points (1978 and 1968) seems to have higher mixing ratios than expected and therefore introduce bias in the derived atmospheric trend. However there are no obvious reasons to justify that these samples were contaminated and should be rejected from data analysis. It was in these samples

that CFCs and H1301 started to deviate accordingly from the natural background levels of 0 ppt, so if there was contamination with the contemporary air then it would be difficult to rule out. Also the in-situ measurements of CO_2 at the site did not record any increase in CO_2 values at these depths. Therefore contamination with modern air can be ruled out but it seems like these two samples were contaminated by sampling device, the fluoro-polymer used in sampling device seems to contaminate samples with CHF_3.

The growth rates were calculated from the equation obtained by fitting fourth order polynomial curve to the entire data ($R^2 = 0.99$). The growth rate escalated from 0.24 ppt yr^{-1} in 1970 - 1980 to 0.87 ppt yr^{-1} in 2000 – 2005. These growth rates are comparable to some of the earlier published growth rates such as 0.7 ppt yr^{-1} in 2001 – 2004 (WMO, 2006). The atmospheric trend obtained in this study shows a steady increase in growth rate. On the contrary, WMO (2006) reported a significantly higher growth rate for the period 1994 – 2001 than 2001 – 2004 based on the high resolution Cape Grim measurements. Due to the lack of temporal resolution of our data it was impossible to suggest that the growth rate could be higher in the past and has slowly declined in the recent years but this could be a possibility. In this study we also obtained a growth rate of 5 ppt yr^{-1} for the period 1995 - 1997, replicating the growth rate observed for the similar period in Oram *et al*. (1998) and Culbertson *et al*. (2004).

The industrial emission estimates are usually based on the annual production of HCFC-22 and an emission function (relationship between HCFC-22 production and HFC-23 emission). Oram *et al*. (1998) obtained an emission function of 2.1% up to 1995 by forcing the predicted concentrations, which was calculated by varying emission functions, to fit the observations at Cape Grim. More recently McCulloch and Lindley (2007) estimated emissions for a "business as usual" scenario in which the emission function of 1.9% was used for developed countries that utilized significant abatement technologies and an emission function of 4% was used for developing countries without any significant abatement technologies.

Figure 5.8.3 compares the emission estimates obtained in this study from the model-derived atmospheric trend with the emission estimates from Oram *et al*. (1998) and McCulloch and Lindley (2007). Generally there is a good agreement between the emission estimates from this study and Oram *et al*. (1998) from mid 1970s to mid

1980s. However the emission estimates of Oram *et al.* (1998) and McCulloch and Lindley (2007) were higher than the emission values obtained in this study, especially from 1990 where values are higher by as much as 24%. Clearly the emission functions used by McCulloch and Lindley (2007) was overestimated and this was hardly surprising because under the business as usual scenario it was assumed that none of the new facilities in developing countries would have basic abatement procedures and that there will be no improvement in abatement technologies to existing facilities in developed countries, resulting in maximum atmospheric concentrations and environmental effects. Despite the discrepancy in the absolute values the trend in emission estimates obtained is consistent with other studies.
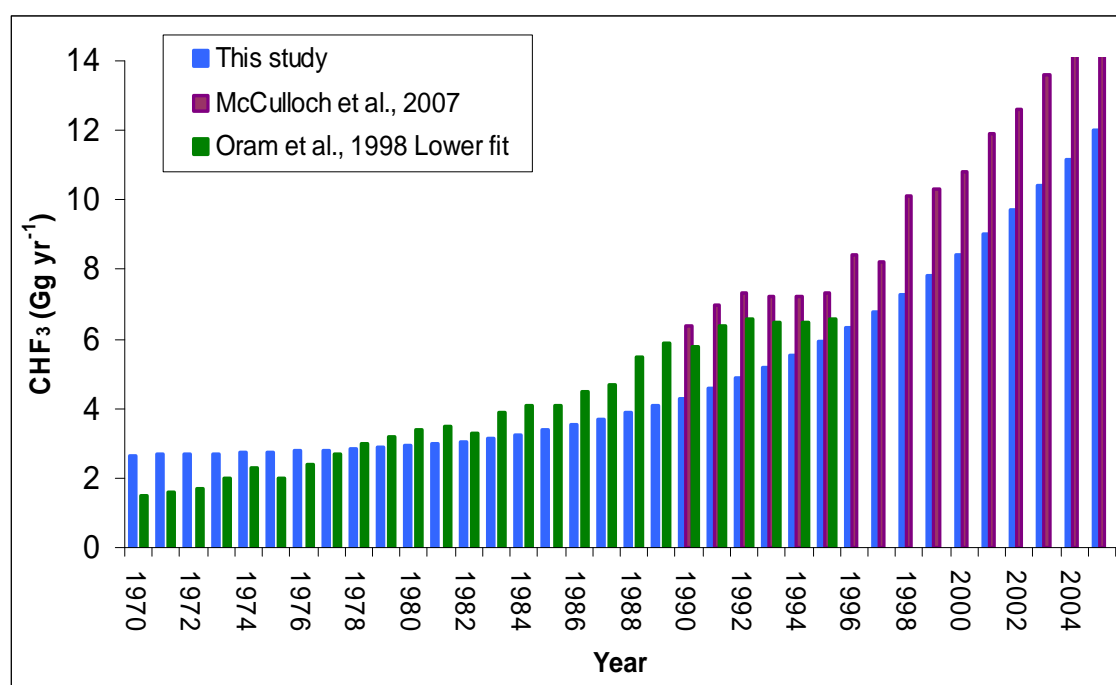
Figure 5.8.3: Emission estimates obtained from the model-derived atmospheric trend were compared to the emission estimates of Oram *et al.* (1998) and McCulloch and Lindley (2007).

The increasing trend in emissions could be reversed if HFC-23 was captured and destroyed. The emissions could be reduced by process optimisation in the reactor and by collecting and treating the vent gases such as the thermal oxidation treatment process. Thermal oxidation is a highly effective treatment option, destroying 99.996% of HFC-23 produced but the system must be designed to cope with halogen acids and the downtime of the destruction facility needs to considered when implementing this

treatment option. McCulloch and Lindley (2007) estimated emissions for the current best practice that would destroy 90% of the total quantity of HFC 23 produced based on the assumption that such destruction facilities be incorporated into all processes over a 10 years period commencing in 2005. By 2015, the predicted emissions for the best practice scenario would be 2.4 Gg yr^{-1}, resulting in an 83% reduction of the 2004 emission value (McCulloch and Lindley, 2007).

5.9 Sulfur hexafluoride

Sulfur hexafluoride (SF_6) is one of the most efficient greenhouse gases with the highest GWP noted to date. It has a GWP of 22 450 based on a 100 year time horizon and an atmospheric lifetime of 3200 years (WMO, 2006). The long atmospheric lifetime is due to its stability in the troposphere and stratosphere, with its only sink being photolysis and high energy electron capture in the mesosphere. Its present atmospheric concentration is about 5.60 ± 0.04 pptv (IPCC, 2007) and therefore contributing only 0.1% of the total man-made global warming effect of CO_2. However due to its long atmospheric lifetimes, increasing atmospheric trends and highest GWP, it was classified as one of the greenhouse gases in the Kyoto protocol that required to reduce its atmospheric burden.

The sources of atmospheric SF_6 are almost entirely anthropogenic but there has been a very small natural source from out gassing of soils containing fluorite minerals (Deeds *et al*., 2008). The natural background level of SF_6 is lower than 0.04 ppt (Maiss and Brenninkmeijer, 1998). The most dominant application of SF_6 is in the insulating fluid in transformers (WMO, 2006). The industrial production began in 1953 with the introduction in the United States market for SF_6 insulated circuit breakers but since 1972 the application of SF_6 insulated switchgear became more widespread (Maiss *et al*., 1998). It is also used as a cover gas in magnesium production to prevent oxidation of molten reactive metal. Some of the minor uses of SF_6 include a cover gas in aluminium smelting, in the electronics industry, filling of tyres, in sound-insulating windows and in sport shoes.

Due to its steady growth rate and well characterised meridional concentration gradients in the atmosphere, SF_6 was measured as a tracer in atmospheric transport and mixing studies. Hence there are numerous studies which have published atmospheric trends for SF_6: long term trend (1972 – 1996) from Cape Grim air archives (Maiss and Brenninkmeijer, 1998), longest high precision record in the NH from Izana (1991-1999) and Spitsbergen (78°N) from 1996 – 1998 (Maiss & Brenninkmeijer, 2000), measurements from high altitude Jungfraujoch Research Station, Switzerland since mid 1980s (Zander *et al.*, 2008), and also, there is an ongoing monitoring at several NOAA sites.

5.9.1 Results and discussion

In this study atmospheric trend was reconstructed from the EDML firn air measurements. Figure 5.9.1 illustrates the depth profile, which clearly points out increasing concentrations from virtually zero levels in the oldest air to 5.5 ppt in January 2006. In order to assign the age scale the standard dating tool, which was used for the earlier species, was also adopted for SF_6. Despite the ability of the model to closely reproduce the firn depth profile, the atmospheric trend (blue line, see Fig 5.9.2) obtained with the iterative dating technique was not coherent with the atmospheric and other firn measurements. The atmospheric trend obtained from iterative dating technique overestimated the mixing ratios from 1970 – early 1980s and underestimated the mixing ratios from early 1990s to late 1990s. Such inconsistencies could arise from the atmospheric scenario that was used in the diffusion model. However there is high-resolution database for SF_6 from late 1970s to present day (from Cape Grim data and NOAA SH data) and from the iterative dating technique it was obvious that the concentration was ~ 0.01 ppt or less before 1940. These information were pieced together to reconstruct an atmospheric scenario for the model by the method of polynomial fitting. The atmospheric scenario was reconstructed from 1900 to January 2006 which was then forced into the model to generate diffusion model result, labelled as run 4 inserted in Figure 5.9.1.
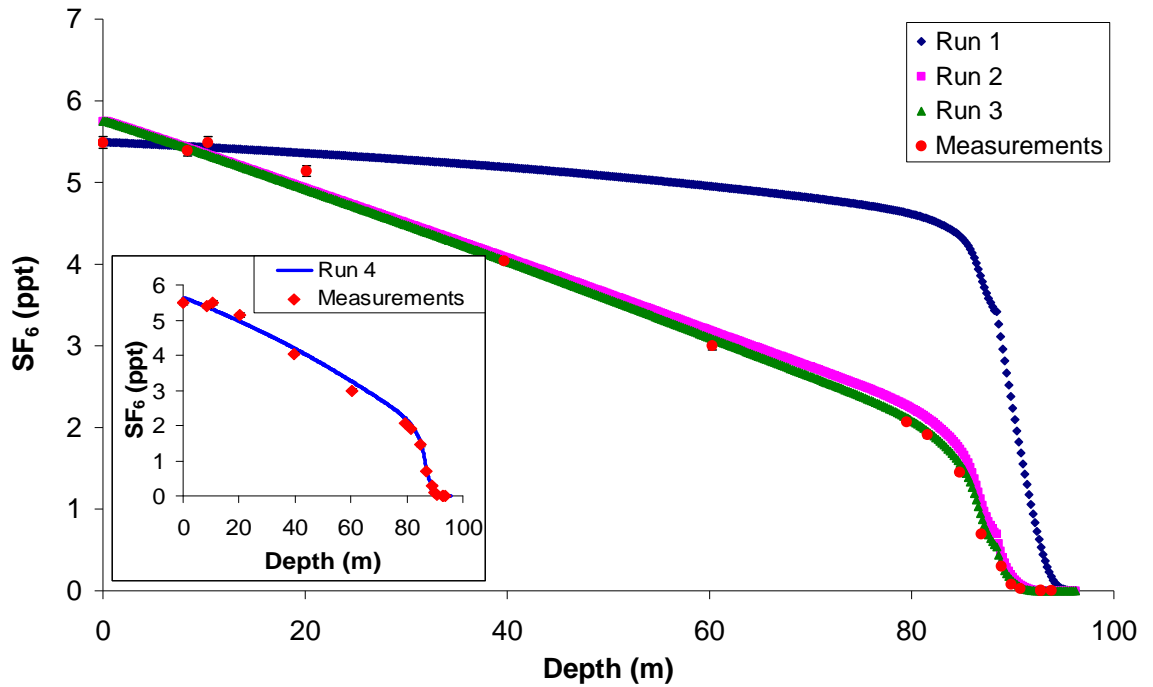
Figure 5.9.1: Depth profile and diffusion model results for SF_6 in the EDML firn air. The atmospheric scenario used in the first three model runs were generated through the iterative dating technique but for the fourth run (inserted in Figure 5.9.1) the atmospheric scenario was a reconstructed trend from atmospheric measurements from Cape Grim archive air and the NOAA/CMDL Southern Hemispheric monthly mean values.

Though the model result from run 4 did not quite match the measurements for the middle depths as it did for deeper and shallower parts of the firn, the atmospheric trend (solid purple line in Figure 5.9.2) obtained from this run is remarkably coherent with other atmospheric and firn measurements. Such an excellent match increases the validity and confidence in the reconstructed atmospheric trend, which was used to evaluate the growth rates and emission rates.
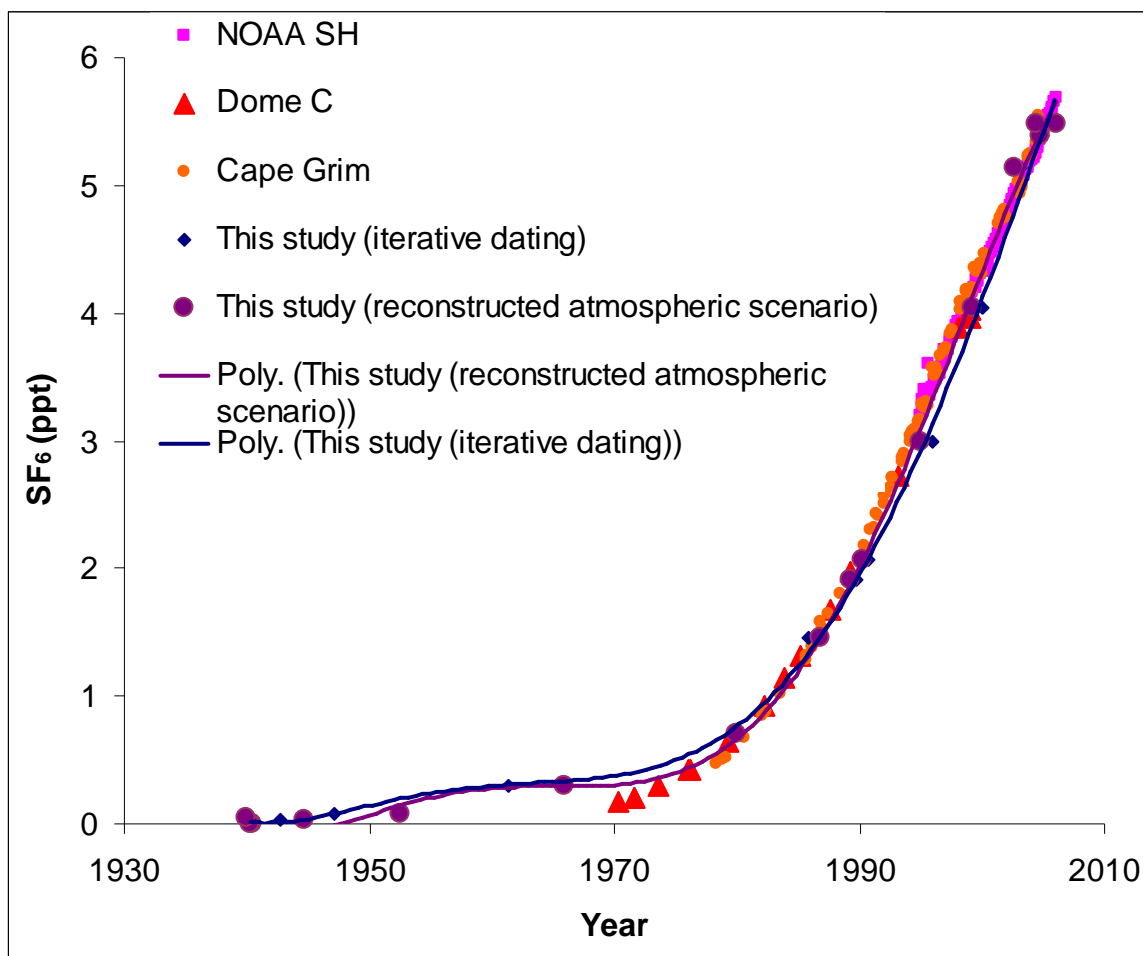
Figure 5.9.2: Model-derived atmospheric trend obtained by curve fitting to the data (purple solid line) was compared to NOAA Southern Hemisphere mean values from 1995 – 2006, Cape Grim (Oram, personal communications), Dome C firn air data (UEA unpublished data).

The reconstruction from firn measurements clearly show that SF_6 had a small background level of 0.04 ± 0.03 ppt before the 1950s, complementing the findings of Maiss & Brenninkmeijmer (1998), who reconstructed the atmospheric history of SF_6 on the basis of SF_6 sales record and suggested a natural background level of approximately 0.04 ppt. The mixing ratios increased to 0.30 ppt in 1960 and such increase could be rivalled by the onset of SF_6 production for use in switch gears in 1950s. However after mid 1960s the atmospheric burden of SF_6 remained constant at 0.30 ppt until 1972 and then started increasing almost unabatedly after 1972 to 5.5 ppt in January 2006. The substantial atmospheric loading of SF_6 commenced when its application in the switch gear became widespread.

Maiss and Brenninkmeijer (1998) reconstructed atmospheric trend from 1953 - 1996 from the sales data. This atmospheric trend was verified with the firn measurements and diffusion model-derived reconstructed history obtained in this study. The reconstructed trend observed in this study agrees well with the reconstruction from sales data and globally observed mixing ratios. The notable feature is the disagreement in both reconstructions from early 1950s to 1965. The reconstruction from the firn measurements shows higher mixing ratios than those reconstructed from sales data. A sudden increase in SF_6 atmospheric loading tends to suggest some point emissions in mid 1950s and then the emission was practically zero until early 1970s. Clearly the firn measurements reveal the atmospheric concentration was higher during the 1950s and early 1960s than those predicted on the basis of the sales data. There was only one firn measurement that resulted in this disagreement and therefore no concrete conclusions could be made at this stage.
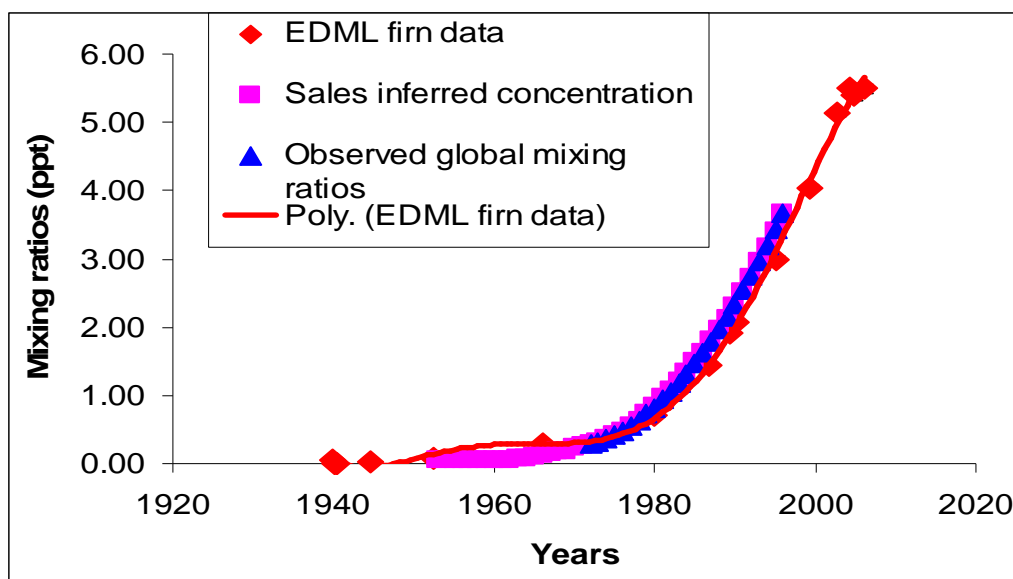
Figure 5.9.3: Reconstructed atmospheric trend from the firn measurements is compared to observed global mixing ratios and the trend reconstructed from the sales inferred concentration (Maiss & Brenninkmeijer, 1998). The EDML firn data were corrected for inter-hemispheric exchange time.

To fully confirm that the atmospheric mixing ratios in the 1950s and early 1960s as inferred from the firn data were higher than the reconstruction based on sales data for the similar period, older air either from firn or ice needs to be analysed. The Dome C

firn air measurements (see Figure 5.9.2), which predates to early 1970s, may imply that the reconstructed atmospheric trend is being overestimated due to this one suspicious datum point.

The growth rate increased steadily from almost 0.006 ppt yr^{-1} in 1972 to 0.25 ppt yr^{-1} in 1998 and then it declined slowly to ~ 0.20 ppt yr^{-1} in 2005. Krieg *et al*. (2005) obtained a trend of 0.24 – 0.31 ± 0.008 ppt yr^{-1} for three sites in the NH from 1993 – 2002, in agreement with the average trend of 0.24 ppt yr^{-1} obtained in this study for the similar period. WMO (2006) noted that the growth rate has remained relatively constant at 0.23 ± 0.02 ppt yr^{-1} since mid 1990s, which is similar to an average trend of 0.24 ± 0.02 ppt yr^{-1} obtained in this study from 1995 – 2005. The growth rate from 2000 – 2005 obtained in this study was in excellent agreement except for the 2005 value. According to NOAA/CMDL data the mean growth rate for the southern hemisphere for 2005 was 0.25 ppt yr^{-1} as compared to 0.20 ppt yr^{-1} obtained in this study. The discrepancy could be due to underestimation of the convective zone layer which would lead to uncertainties in the age assignment of the air from the shallow firn depths or another possibility could be that the mean southern hemispheric values are biased towards higher value due to meridional gradient or variations from one site to the other. Some monitoring sites, particularly those closer to the equator and industrialised countries in the southern hemisphere, would record high mixing ratios. Contrarily, insufficient atmospheric mixing or changes in the atmospheric circulation would mean more polluted air could not be transported to Antarctica. Therefore concentrations observed at Antarctica for any given year could not be taken as a representative for the southern hemisphere. The NOAA/CMDL South Pole (SPO) data showed that the growth rate for 2005 was indeed 0.20 ppt yr^{-1}, supporting the value obtained in this study.

The growth rate calculated from the model-derived atmospheric trend was converted into emissions (Gg yr^{-1}) by multiplying by a factor of 25 (Maiss and Brenninkmeijer, 2000). The emission estimates obtained were compared with emission estimates calculated from direct high-resolution atmospheric observations as given in Maiss & Brenninkmeijer (1998) and Oram (1999). Figure 5.9.4 illustrates that the emission estimates obtained from the firn reconstructed atmospheric trend agrees with the trends of emission with other studies and the absolute values are almost matched from 1986 to 1996, but there are considerable differences in the earlier part of the trend.
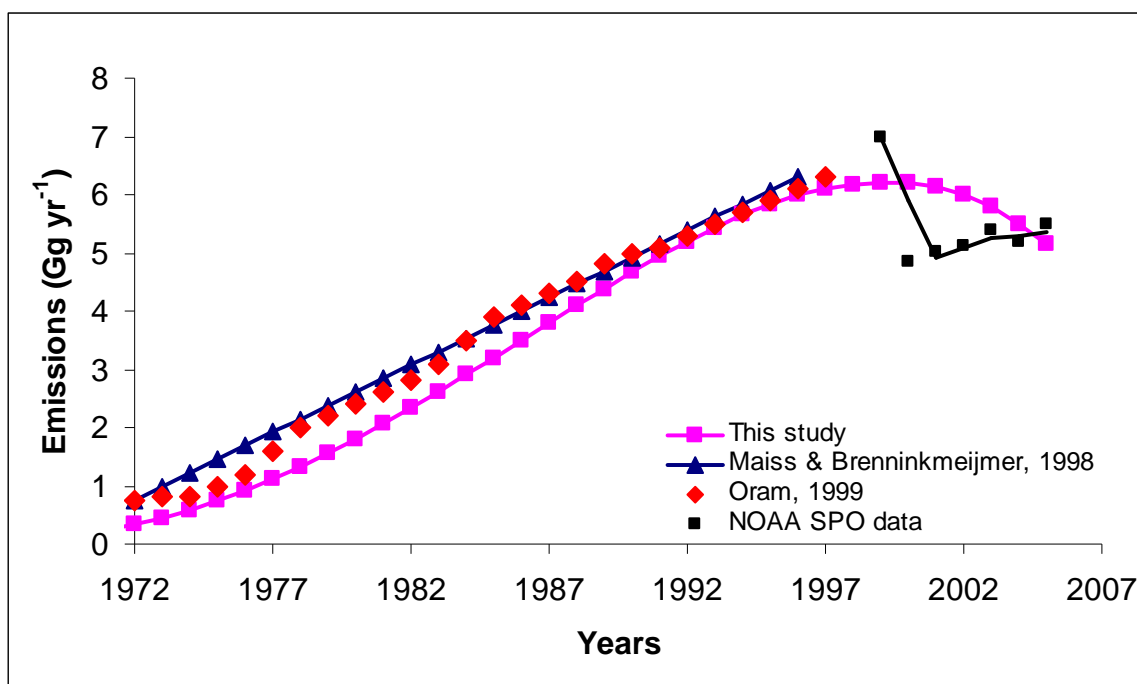
Figure 5.9.4: Emission estimates derived from the reconstructed atmospheric trend. The emission estimates obtained was compared to estimates from Maiss & Brenninkmeijer (1998) and Oram (1999).

The discrepancies could be attributed to the usual reasons of uncertainties associated with the reconstructed trend due to lack of high-resolution data and curve fitting to the data. Maiss and Brenninkmeijer (2000) obtained high-resolution atmospheric measurements from Izana for the period 1991 – 1999 and concluded a 27% reduction in SF_6 emissions after 1996, which was economically driven. Smythe (2004) collected sales data from major companies and showed a decrease of 33% in SF_6 sales in 1996 – 1999, followed by a 27% increase in 1999 – 2003. Certainly the emission estimates obtained in this study does not reflect such variations in emission but rather show a constant emission at 6.3 Gg yr^{-1} until 1999 and then decreased by 24% from 2001 – 2005. The flask data from the NOAA/CMDL SPO showed a decrease of 30% from 1999 – 2000 but then showed an increasing trend since 2000. The emission estimates for EDML and SPO for 2004 and 2005 were similar. However the EDML profile did not record any abrupt decrease from 1999 – 2000 as shown in SPO data because such inter-annual variability would have been lost due to smoothing effect in the firn. The obvious reason for the differences in the interannual variations in emission could be that

the actual emission scenarios were not incorporated into the diffusion model but rather a smoothed trend obtained by polynomial fitting through the Cape Grim and NOAA/CMDL data, resulting in incorrect simulations of the firn data. The reconstructed trend from scant firn air data may not be ideal to assess emissions for species like SF_6, which exhibits inter-annual variations depending on its sales and cost of the product. The reversed trend in emissions observed recently could result from increased environmental awareness about its implication on climate change. Greally *et al*. (2005) observed a decrease in global emissions, with the growth rate of 4.7% observed in 2004 as compared to 6.8 - 7.5 %/yr from 1994 – 1996 (Maiss and Brenninkmeijmer, 1998). The decrease in global emission is consistent with the commitments by industries to decrease emissions by increasing the efficiency of SF_6 trapping in the equipment for the power distribution and semiconductor industries (Graber *et al*., 2008). Also the U.S Environmental Protection Agency (EPA) launched a collaborative initiative called the SF_6 Emission Reduction Partnership for the Magnesium Industry in 1999 to voluntarily eliminate the use of SF_6 by 2010 (Bartos *et al*., 2007).

5.10 Trifluoromethylsulfurpentafluoride

The existence of trifluoromethylsulfurpentafluoride (SF_5CF_3) in the atmosphere was first reported by Sturges *et al*. (2000). This gas has a very large radiative forcing observed to this date, making it a super greenhouse gas (Sturges *et al*., 2000). The initial estimate of the radiative forcing of 0.57 $Wm^{-2}ppb^{-1}$ (Sturges *et al*., 2000) was updated to 0.59 $Wm^{-2}ppb^{-1}$ (Nielson *et al*., 2002) based on the quantification of a new absorption band in a more extensive wavenumber range than previously studied in the pioneer study. The atmospheric lifetime of SF_5CF_3 was not known initially but based on the stratospheric profile it was estimated to be on the order of several hundred years to a few thousand years. The accurate knowledge of atmospheric lifetime is imperative in calculating the GWP; however, based on the assumption that it has the same lifetime as SF_6 the 100-year-mass-normalised GWP was estimated to be in the range of 18,000 – 19,000 (Sturges *et al*., 2000; Nielson *et al*., 2002). This claim was disputed by Xu *et al*. (2004), stating on the basis of theoretical and experimental observations, that the atmospheric lifetime of SF_5CF_3 would be less than the atmospheric lifetime of SF_6 and

therefore its GWP might be overestimated. However, Takashi *et al.* (2002) calculated the atmospheric lifetime of SF_5CF_3 to be in the range of 650 – 950 years depending on solar activity levels, and based on this atmospheric lifetime, the GWP was revised to ~18, 000.

It is a man-made gas and does not have any tropospheric sinks. The atmospheric concentrations grew from 0 ppt in the late 1950s to 0.12 ppt in 1999 (Sturges *et al.*, 2000). An increase in atmospheric abundance indicates an increasing source. A potential source was identified when 3M Environmental Technology and Services admitted the production of SF_5CF_3 as a by-product during the manufacturing of certain fluorochemicals (Santoro, 2000). It is produced most likely via electrochemical fluorination of commonly used intermediates and products such as trifluoromethanesulfonic ("triflic") and fluorosurfactants. The use of such compounds in fluorochemicals production has been standard practice since the late 1950s and was approximately the time when SF_5CF_3 was detected in the atmosphere. Another potential source was recently identified by Huang *et al.* (2005), who concluded that under spark discharge conditions SF_6 reacts with HFC-23 and HFC-32 (CH_2F_2), which may be emitted from the fluoropolymers in high voltage equipment, to produce SF_5CF_3.

SF_5CF_3 has been measured in firn air from Dome C in eastern Antarctica, providing a reconstructed history from 1965 – 1999 (Sturges *et al.*, 2000). It has been also measured in stratospheric balloon flights launched from Kiruna, Sweden (68 °N) in 1997 and Aire sur l'Adour, France in 1999 (Sturges *et al.*, 2000). This study does not only provide the longest atmospheric record but more importantly will update the record of atmospheric SF_5CF_3.

5.10.1 Results and discussion

Figure 5.10.1 shows the concentration-depth profile of SF_5CF_3 from the EDML firn air and it is obvious that it grew from zero concentration in the oldest firn air to 0.16 ppt in 2006. The diffusion model results replicate the firn depth profile reasonably well except at a few depths such as 10.40m, 39.70m and 81.56m, which are within ± 10%. An iterative dating technique was used to date the firn air and the results obtained are plotted in Figure 5.10.2.
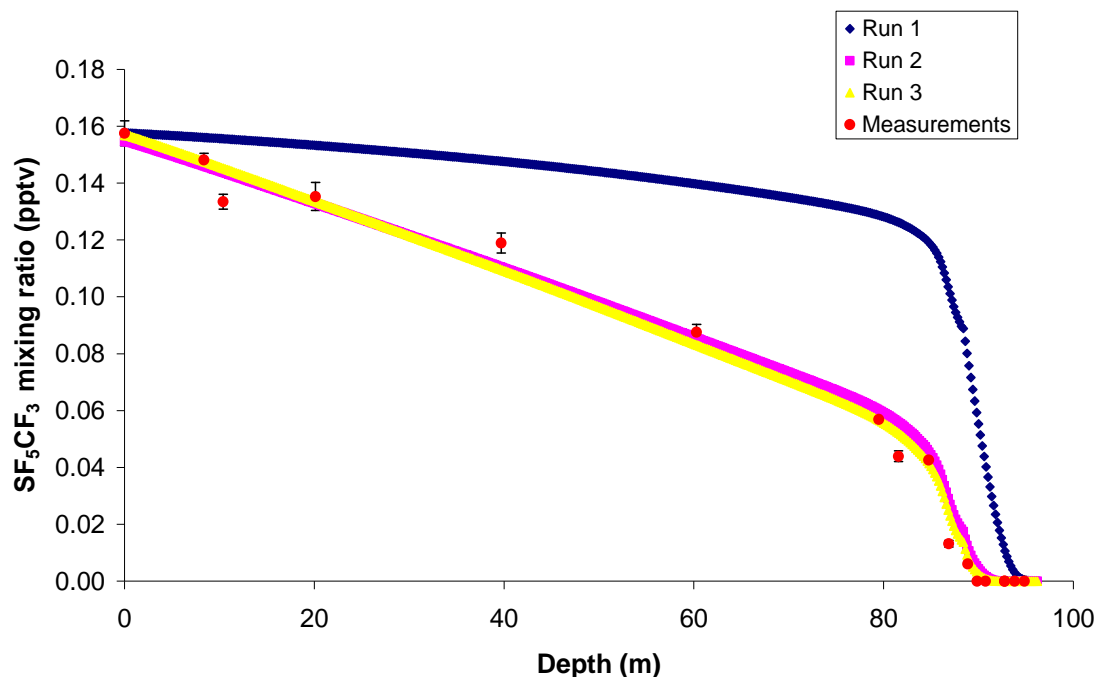
Figure 5.10.1: An illustration of firn air depth profile of SF_5CF_3 fitted with the firn diffusion model results obtained with three different atmospheric scenarios.
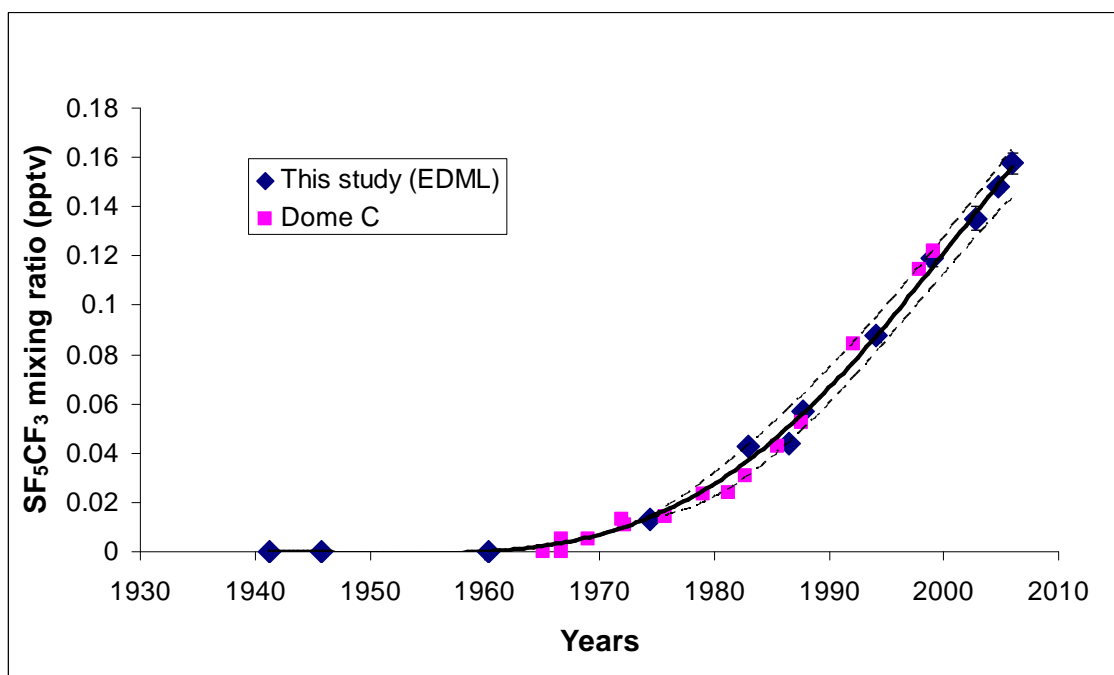
Figure 5.10.2: Model-derived atmospheric trend for SF_5CF_3 obtained by polynomial fitting curve to the data (the solid line). The dotted lines signify $\pm$ 10% of the atmospheric trend. The trend obtained in this study was compared with measurements in the Dome C firn air samples reported by Sturges *et al*. (2000).

The atmospheric trend was derived by fitting a 5th order polynomial through the data after assigning the age scale. The upper and lower error estimates in the reconstructed history (dashed lines) represents ± 10% of the curve fitting and it accommodates any data points that were outside the polynomial curve fitting. The Dome C values fall within this envelope and match favourably with the reconstructed trend from the EDML firn air, making the reconstructed trend more robust. It is noteworthy that Dome C firn air reconstruction was based on an entirely different approach, where atmospheric scenario for SF_5CF_3 was obtained by scaling the SF_6 atmospheric scenario, and consequently could explain very minor discrepancies in both records.

The EDML firn data provides atmospheric history of SF_5CF_3 from 1940s to 2006. The mixing ratios were zero before 1960 and then started increasing slowly until 1980, after which the growth rate accelerated. In fact a linear regression of 1960 – 1981 data (r^2 = 0.98) yielded a gradient of 0.001 pptv yr^{-1} and the linear regression for 1983 – 2006 data (r^2 = 0.98) gave a gradient of 0.005 pptv yr^{-1}, which is comparable to the growth rate of 0.006 pptv yr^{-1} obtained for Dome C for the 1983 – 1999 period (r^2 = 0.99). Currently the growth rate is increasing at 3 – 4% per year. It was clear from both firn records that the growth rate changed by a factor of 5 since early 1980s, which implied a change in source strengths.

The increasing growth rate might not be attributed to the production of fluorochemicals by 3M because the company claimed that it had reduced its emission by more than 40% in 2000 and a further reduction of 50% was to be implemented over next 1 to 5 years (Santoro, 2000). Probably the increasing mixing ratios could be attributed to the other potential source, that is, reaction of SF_6 with HFCs under spark discharge conditions in high voltage equipment or maybe continued fluorosurfactant production elsewhere other than by 3M in USA. Figure 5.10.3 shows a 1:1 correlation between SF_6 and SF_5CF_3 atmospheric trends. The fact that the trends of SF_5CF_3 and SF_6 have tracked each other so remarkably since the last 30 years, suggest the existence of a common source or SF_5CF_3 produced via reaction involving SF_6. It is apparent from the figure that the growth rate increased approximately at the time when SF_6 emissions increased due its application in switchgears in high voltage equipments. Another interesting feature of Figure 5.10.3 is that before 1960 the SF_6 mixing ratios started to increase prior to any detectable increase in SF_5CF_3. The deviation from this 1:1 relationship suggests the

presence of an uncommon source such as SF_6 emissions from magnesium production but is not very conclusive at this stage since this speculation is based on a single measurement and is the same sample that is anomalously high in SF_6.

Emissions of SF_5CF_3 were estimated from the atmospheric trend by using the conversion factor of 1 ppt yr^{-1} = 32.75 Gg yr^{-1}. Figure 5.10.4 shows that the emissions increased from 0.01 Gg yr^{-1} in 1960 to almost 0.18 Gg yr^{-1} in 1999, and remained almost constant until 2002. Since 2003 to 2006 the emissions decreased by 0.01 ppt yr^{-1} and I speculate this could be the result of zero emissions from fluorochemical productions. An increased awareness of detrimental environmental effects of SF_6 and SF_5CF_3 applications resulted in growing research into ways of decomposing these gases such as the photoreduction of SF_6 and SF_5CF_3 in the presence of propene (Huang *et al*., 2008)
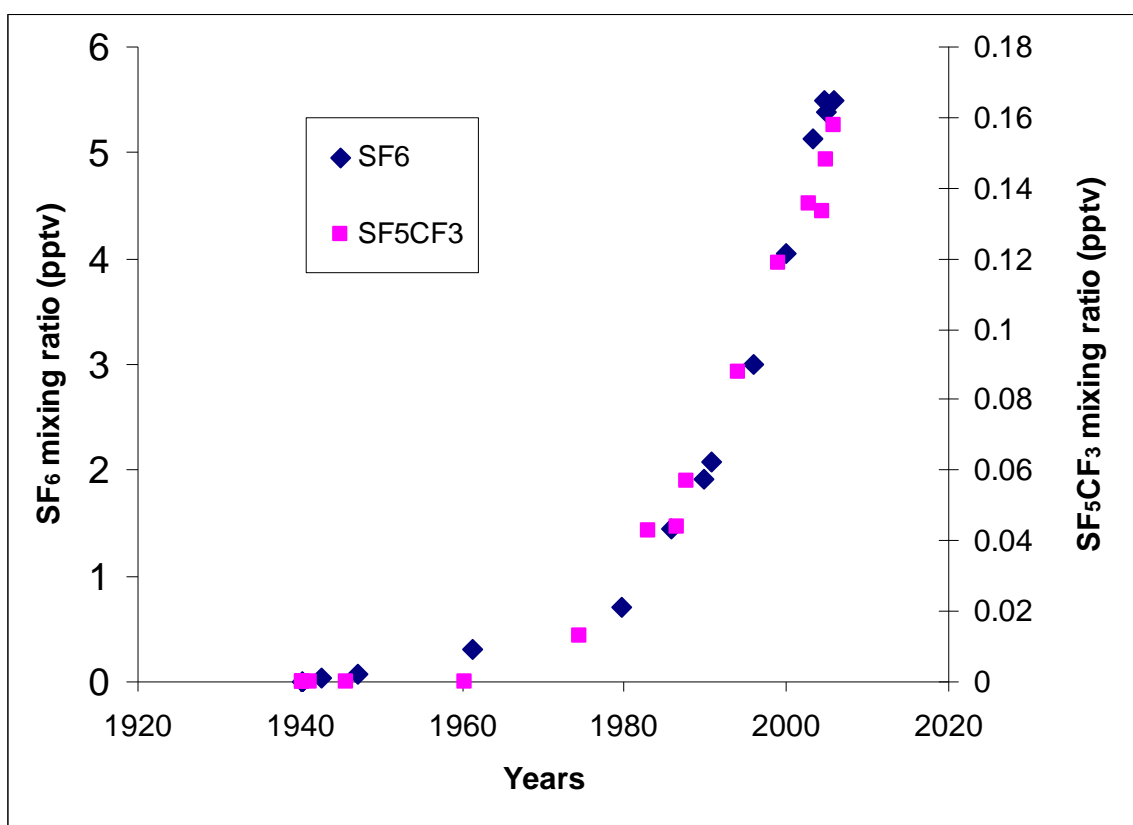
Figure 5.10.3: An illustration of remarkable correlation between SF_5CF_3 and SF_6 in the EDML firn air.
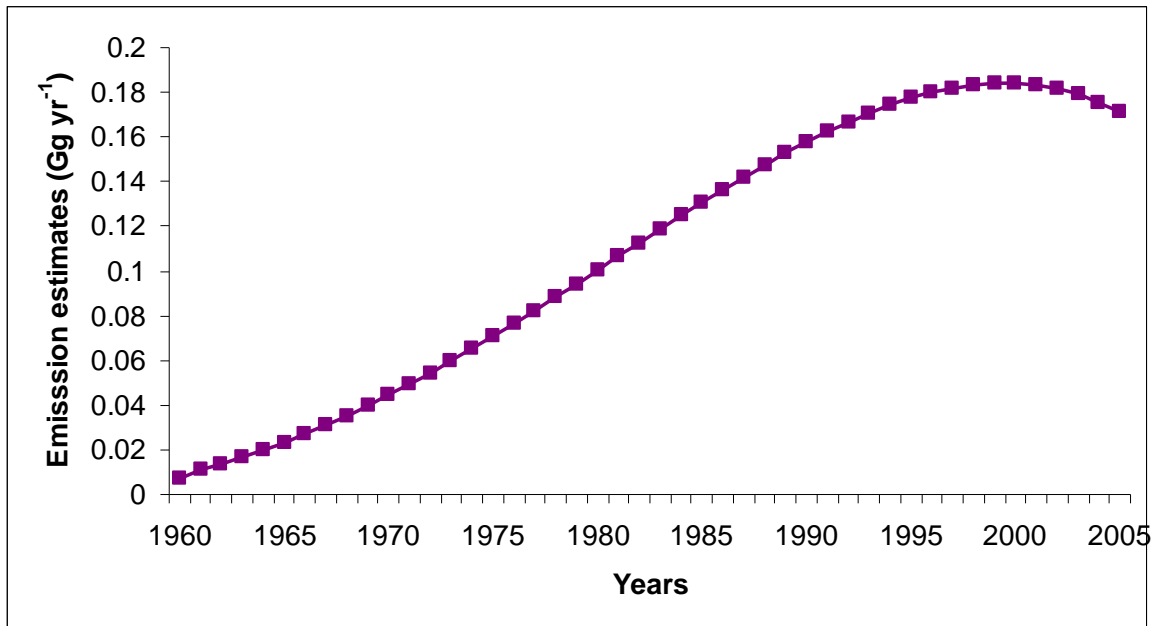
Figure 5.10.4: Emission estimates calculated from the average atmospheric trend obtained in figure 5.10.2.

5.11 Radiative forcings

Radiative forcing (RF) is defined as a concept used for quantitative comparisons of the strengths of different human and natural drivers of climate change (IPCC, 2007). In this study the time history of the RF of individual species was calculated from the concentration change (since preindustrial times, taken as the year 1750, and a given year) which was then multiplied by the radiative efficiency of the individual gases shown in Table 5.11.1. In this approach of estimating RF, the RF varies linearly with the atmospheric concentrations and as a result the time history of the RF of that particular greenhouse gas is similar to the model derived atmospheric concentration trend.

Table 5.11.1: Radiative efficiency used in this study to derive radiative forcing of individual species and also includes the current estimate of radiative forcing given in IPCC, (2007).

Species	Radiative Efficiency $(W\ m^{-2}\ ppbv^{-1})$	Radiative Forcing IPCC 2007 estimate $(W\ m^{-2})^b$
CF_4	0.10^c	0.0034
C_2F_6	0.27	0.0008
C_3F_8	0.26^d	-
$c\text{-}C_4F_8$	0.32	-
HFC-23	0.19	0.0033
SF_6	0.52	0.0029
SF_5CF_3	0.57	-

Figure 5.11.1 shows the RF of the individual gases. The 2005 estimate for the RF of CF_4 is 0.004 W m^{-2} as compared to 0.0008, 0.0002, 0.0004, 0.0035, 0.0028, 0.00008 W m^{-2} for C_2F_6, C_3F_8, $c\text{-}C_4F_8$, HFC-23, SF_6 and SF_5CF_3 respectively. The estimated RF values for CF_4, C_2F_6, SF_6 and HFC-23 agree with the IPCC (2007) estimates except a slight discrepancy in the CF_4 value. The differences could be due to discrepancies in the atmospheric concentrations estimated for 2005 in this study and the IPCC (2007) and also the natural background concentration used here and those used in the calculation in the IPCC report. The discrepancy in the CF_4 RF value could also result from the radiative efficiencies calculated in Worton et al. (2007) and the one quoted by Velders et al. (2005). If a radiative efficiency of 0.08 Wm^{-2} ppbv^{-1} (Velders et al., 2005) was used instead of 0.1 Wm^{-2} ppbv^{-1} then the radiative forcing of 0.0033 W m^{-2} would be obtained that matches with the IPCC estimates.

---

[b] The actual reference for these data is Forster et al., 2007.

[c] The radiative efficiency for CF_4 and C_2F_6 was given in Worton *et al.* (2007).

[d] The radiative efficiency for C_3F_8, $c\text{-}C_4F_8$, HFC-23, SF_6 and SF_5CF_3 was given in Velders *et al.* (2005).
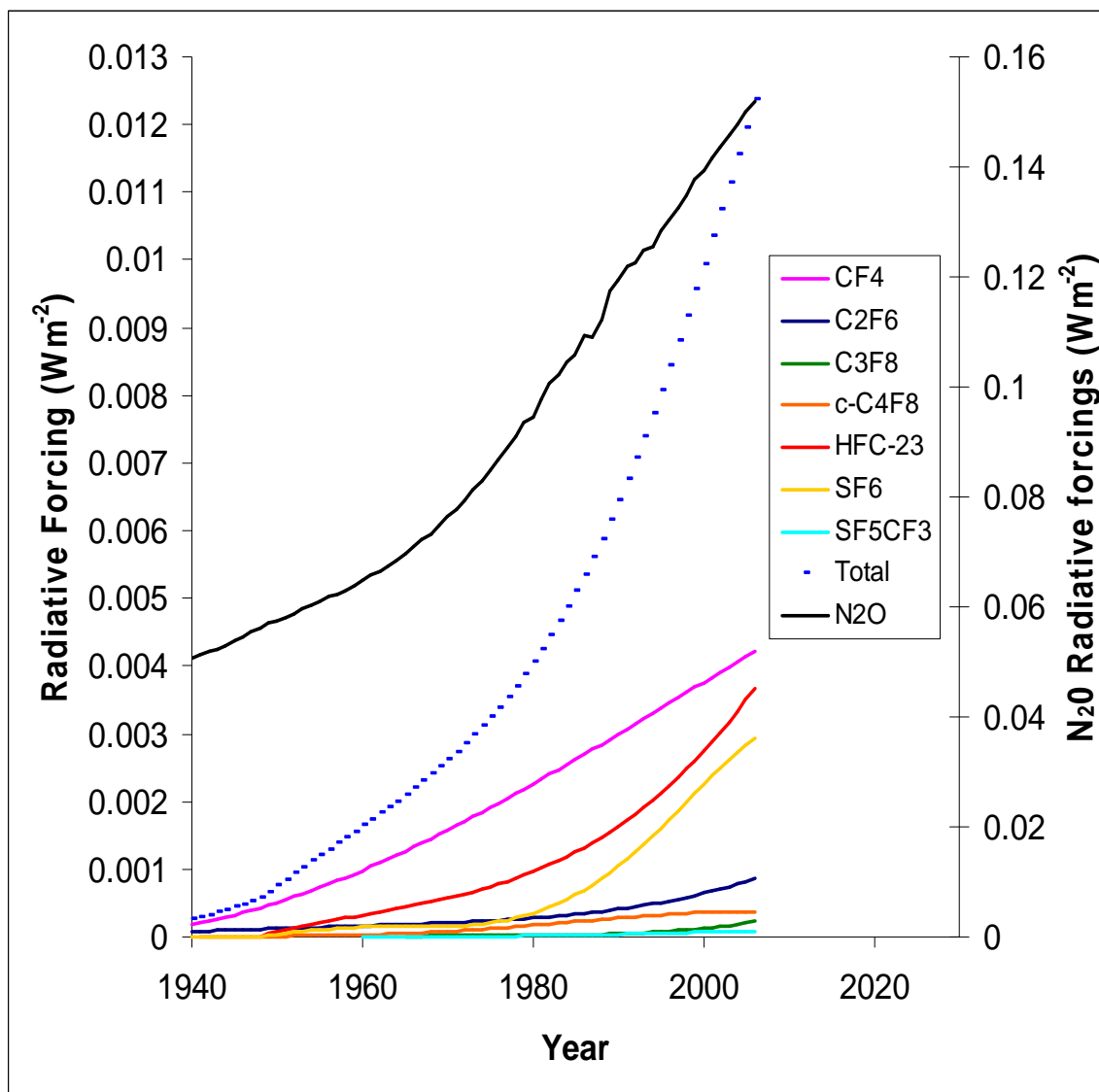
Figure 5.11.1: Time history of the global annual mean radiative forcings for CF_4, C_2F_6, C_3F_8, c-C_4F_8, HFC-23, SF_6, SF_5CF_3, and the sum or total radiative forcings for all gases studied (dashed blue line) relative to that of N_2O (solid black line).

The largest calculated RF is for CF_4, owing to its large concentration change since 1750. The exponential growth rate in the RF for SF_6 and HFC-23 since 1980 is also noteworthy. The CF_4, SF_6 and HFC-23 contribute significantly to the total RF calculated whereas all the other species have RF in the order of < 0.001 W m^{-2}. The sum of the RF obtained for the gases studied here is 0.012 Wm^{-2}. The sum of the RF obtained in this study is comparable to the sum of RF for HFCs, PFCs and SF_6 of 0.017 W m^{-2} (IPCC, 2007). The IPCC estimate is logically higher as it may have considered the full suite of HFCs whereas only HFC-23 was considered in the estimate derived

here. For example, HFC-134a is a fast growing species and it contributes ~0.005 W m^{-2} to the total RF estimate given by IPCC (2007). The total RF obtained for the gases studied is small when compared to major greenhouse gases. The total RF for PFCs, HFC-23, SF_6 and SF_5CF_3 estimated in this study is 0.7, 2.5, and 8% of the RF of CO_2, CH_4 and N_2O respectively. Figure 5.11.1 compares the RF time history for N_2O and the total RF for the gases studied. It clearly illustrates that the rate of change in RF is larger than the rate of change in the RF for N_2O. Since 1995 the total RF for the gases studied changed by +35% whereas the RF for N_2O changed by +15 %. The overall contribution of PFCs, HFCs, SF_6 and SF_5CF_3 to the RF is small but the rate of change is high and therefore the emissions of these gases should be curtailed.

5.12 Summary

Trace gases with very high Global Warming Potentials such as perfluorocarbons (CF_4, C_2F_6, C_3F_8, c-C_4F_8), HFC-23, SF_6 and SF_5CF_3 were measured by high resolution GC-MS in firn air from EPICA Dronning Maud Land (EDML), Antarctic drill site. The EDML firn provides some of the oldest firn air that has been sampled to date hence constraining the historical atmospheric record for these species over the last century. This study not only reveals the updated atmospheric trends for these gases from early 20th century to 2006 but also for the first time highlights the long term atmospheric trend for c-C_4F_8 and C_3F_8 from the firn air reconstructions. Figure 5.12.1 shows the atmospheric trends for all the species studied here. Table 5.12.1 summarises the atmospheric trends, growth rates, emissions and radiative forcings for the individual gases.
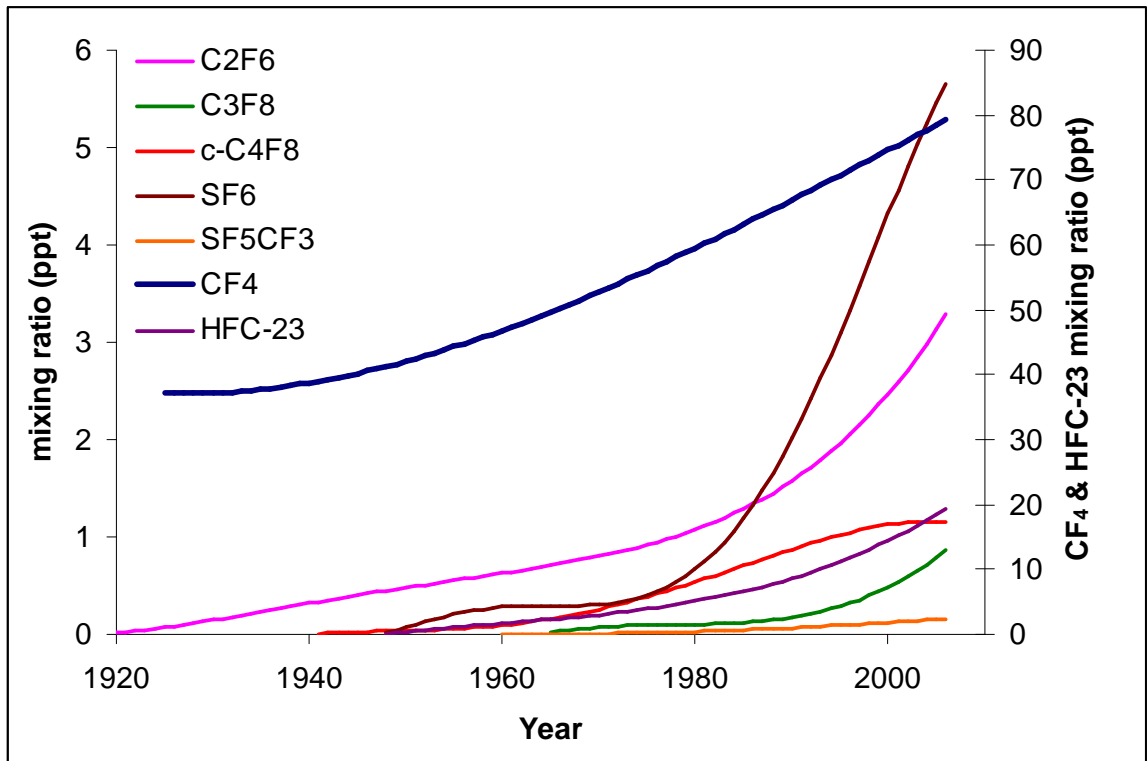
Figure 5.12.1: The best estimate long term atmospheric trend reconstruction from the EDML firn air measurements for CF_4 (blue line), C_2F_6 (Pink line), C_3F_8 (green line), c-C_4F_8 (red line), HFC-23 (purple line), SF_6 (brown line) and SF_5CF_3 (orange line).

Table 5.12.1: Summary of atmospheric trends, growth rates, emissions and radiative forcings for the individual species.

Species	Atmospheric Trend	Growth Rate (ppt yr^{-1})	Emissions (Gg yr^{-1})	2005 Radiative Forcing (W m^{-2})
CF_4	The natural background level of 37 ppt was obtained based on the three oldest firn air samples and in 2006 the mixing ratio was ~80 ppt. The mixing ratio started increasing from early 1930s.	In 1990 the growth rate was 0.79 ppt yr^{-1} and then increased only slightly to 0.82 ppt yr^{-1}. Polynomial fitting to recent dated firn air measurements shows a slow-down in the growth rate and the atmospheric CF_4 mixing ratios stabilizing.	Emission stabilising at 11.3 Gg yr^{-1}. The emission estimates compared well with the EDGAR database. The emission values obtained from the AES report is much lower than the estimate obtained in this study.	0.004
C_2F_6	No natural background level of this compound was observed. The mixing ratios increased from 0 ppt to 3.15 ppt in 2006. The mixing ratio started rising around 1920. There was a linear relationship between CF_4	From 1920 – 1980, the growth rate was linear at 0.02 ppt yr^{-1}. The growth rate increased from 0.06 ppt yr^{-1} in 1990 to 0.14 ppt yr^{-1} in 2005. This	The emission in 1990 was about 1.5 Gg yr^{-1} and in 2005 increased to 3.5 Gg yr^{-1}. The 2006 AES suggest that the emissions from Aluminium production decreased to 0.35 Gg	0.0008

C_3F_8	and C_2F_6 but this relationship changed after 1990 due to uncommon source like the semiconductor industry. The concentration was 0 ppt in1965 and rose to 0.83 ppt in 2006. The concentration was 0.22 ppt in early 1990s but since then increased three fold to its present day concentration. Has a very high correlation with C_2F_6 atmospheric trend. Probably semiconductor industries play a significant role in increasing the atmospheric burden of C_3F_8	increase in growth rate is attributed to the semiconductor industry. Prior to 1992 the growth rate was < 0.02 ppt yr^{-1}. For the period 2000 – 2005 the growth rate was 0.06 ppt yr^{-1}.	yr^{-1}. Increasing emissions suggest that semiconductor industry is contributing significantly. In 1970s the emission was about 0.01 Gg yr^{-1}, which is the typical emission value from aluminium smelting. In 1992 the emission was 0.6 Gg yr^{-1} and the average emission for the period 2000 – 2005 obtained in this study is 1.8 Gg yr^{-1}.	0.0002
c-C_4F_8	Increased from 0 ppt in 1940 to ~ 0.1 ppt in early 1960s. It then increased linearly to 1 ppt before 2000. The atmospheric mixing ratio started to stabilise after 2000. The mixing ratios levelled out at 1.15 ± 0.02 ppt for the period 2000 – 2006.	Linear growth rate of 0.03 ppt yr^{-1} from 1957 – 1997. Since 1998 the growth rate started to decrease to the current value of 0 ppt yr^{-1}.	In mid 1980s the emission increased to 1.13 Gg yr^{-1} and then decreased to present value of 0 Gg yr^{-1}.	0.0004
HFC-23	The atmospheric values increased from 0.5 ppt in 1950 to 19.4 ppt in early 2006. The trend derived is consistent with other published long term records.	The average growth rate for the period 1970 – 1980 was 0.24 ppt yr^{-1}. It increased to 0.87 ppt yr^{-1}	In 1990 the emission was 4 Gg yr^{-1} but increased to 12 Gg yr^{-1} in 2005.	0.0035

		for the period 2000 – 2005.		
SF$_6$	The mixing ratios increased from ~ 0.04 ppt prior to 1950 and rose steadily to 5.5 ppt in early 2006.	The growth increased from 0.01 ppt yr^{-1} in 1972 to 0.25 ppt yr^{-1} in 1999 and then declined to 0.20 ppt yr^{-1} in 2005.	The emission increased from a value of 0.3 Gg yr^{-1} in 1972 to a value of 6.2 Gg yr^{-1} in 1999 and then declined to 5 Gg yr^{-1} in 2005.	0.003
SF$_5$CF$_3$	The mixing ratio started to increase from 0 ppt in 1960s to the current value of 0.16 ppt in 2006. Shows a strong 1:1 relationship between SF$_6$ and SF$_5$CF$_3$, suggesting a common source or it being produced via reaction involving SF$_6$.	The growth rate for 1960 – 1981 was 0.001 ppt yr^{-1} and then increased to 0.005 ppt yr^{-1} for the period 1983 – 2006. Growth rate is increasing at 3 – 4 % per year.	Emissions increased from 0.01 Gg yr^{-1} in 1960 to almost 0.18 Gg yr^{-1} in 1999 and remained constant until 2002 and in 2005 the emission decreased to 0.17 Gg yr^{-1}	0.00008

Chapter 6: CF$_4$ measurements in Berkner Island ice core

6.1 Introduction

6.2 CF$_4$ measurements in Berkner Island ice cores

6.3 Discussion

6.1 Introduction

CF_4 is the most abundant perfluorocarbon (PFC) in the atmosphere and is a potent greenhouse gas with an atmospheric lifetime of at least 50,000 years (IPCC, 2007). Currently the mixing ratio is ~ 80 ppt but almost half of the current atmospheric mixing ratios is contributed from the natural background level. Khalil *et al*. (2003) and Worton *et al*. (2007) predicted background concentration of 40 and 33 ppt respectively, based on the extrapolation of the CF_4 and C_2F_6 relationship obtained from firn air measurements. Whereas the CF_4 measurements in the deepest EDML firn air samples show the atmospheric values were stable at 37 ppt, indicating that the background level was higher than what was suggested by Worton *et al*. (2007). Harnisch *et al*. (1996) is the only study that measured preindustrial air from ice core samples from a glacier at the Swiss/Italian border. A natural background value of 39 ± 6 ppt was reported based on only two ice samples dated to be 1790 ± 30 and 1860 ± 15 (Harnisch *et al*., 1996).

Harnisch *et al*. (1996) melted 1 kg of ice and then extracted the dissolved gases by 'bubbling out' with synthetic air. The extraction method utilized in this method is different. A dry extraction method was used to prevent any dissolving of gases in water, and the sample size of the ice used was also smaller (~ 200 g). Harnisch *et al*. (1996) attributed the natural background level to slow degassing of CF_4 produced by fluoride minerals in the earth's crust. An emission in the range of $0.1 – 10$ Tg yr^{-1} was estimated (Harnisch *et al*., 1996). More recently it was shown that crustal degassing is a potential natural source for CF_4 and the flux is enhanced by tectonic activities (Deeds *et al*., 2008). A total lithospheric CF_4 flux in the range of $0.0009 – 0.005$ Gg yr^{-1} was estimated. Certainly the natural emission rates obtained is negligible compared to the current anthropogenic emission rates. It was assumed that the natural emissions were small and therefore the atmospheric value of CF_4 during pre-industrial times would be almost invariable. Hence this justifies the goal of this study to investigate the natural variability in CF_4 measured from deep ice core samples.

6.2 CF$_4$ measurements in Berkner Island ice cores

In total fifteen samples (~200 g) were measured in the age range of 95 – 2 kyr BP. However, four measurements were rejected due to minor leaks during the extraction procedure. The measurements were rejected on the basis of elevated levels of contaminants such as SF$_6$ and F12. Replicate measurements of samples were not carried out because there was only sufficient volume of sample from 1 extraction for a single run on the instrument. The error bars on the measurements were gauged from the replicate analyses of the standard. There were two samples that have an age difference of 7 years and therefore could be an ideal substitute for duplicate samples because CF$_4$ has a long lifetime. Based on the two samples the reproducibility of the measurements is in the range of ± 0.2 ppt. Three clusters of data are shown for Berkner in Figure 6.2.1. Table 6.1 highlights these three clusters of data and some basic statistics.

Table 6.1: Shows the average CF$_4$ concentration in Berkner Island ice cores for three different time period.

Mean Age (kyr)	Average CF$_4$ mixing ratio (ppt)	Standard deviation (ppt)
2.04 ± 0.02	38.1	0.7
2.95 ± 0.02	39.3	0.2
94 ± 2	39.3	0.1

From Table 6.1 it can be inferred that the CF$_4$ concentration was stable at 39.3 ppt from 94 – 3 kyr BP[5] period and then slowly declined to 38.1 ppt around 2 kyr BP. The scatter on the data around 2 kyr BP is large as compared to the other cluster of data. The large standard deviation is due to two points (39.2 and 37.1 ppt) around 2 kyr BP. These two data could not be eliminated due to leaks during the extractions but it could be attributed to instability of the instrument, particularly the sample containing 37.1 ppt has a large error.

---

[5] Note that BP notation used here refers to number of years before 2006.
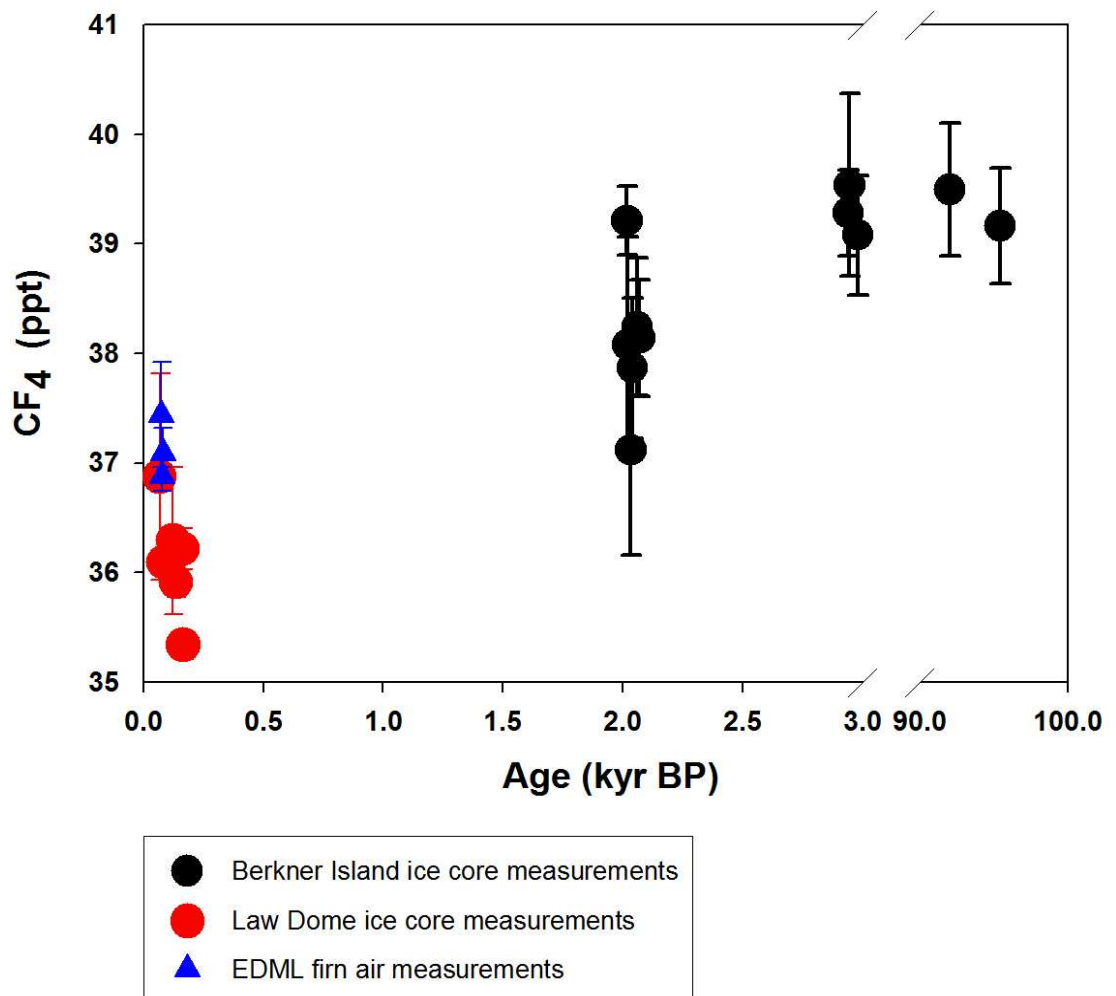
Figure 6.2.1: CF$_4$ mixing ratios measured in ancient air from Berkner island ice cores (black dots), in 19th and early 20th century air extracted from Law Dome ice core (red dot) and bottom-most firn samples from the EDML site (blue triangles).

6.3 Discussion

The CF$_4$ mixing ratios measured in Berkner Island was slightly higher than those observed at the bottom of the firn air which was dated to be 1930 A.D. The mixing ratio was stable at 39 ppt prior to 2.9 kyr BP but then started to decline very slowly to 38 ppt around 2 kyr BP. The values obtained at 2 kyr BP are not significantly different from

those obtained at the bottom of the EDML firn air especially when the lower range of the values measured would be very close to 37.4 ppt. However when the unpublished Law Dome CF_4 data from the 19th century was plotted it makes a very convincing case that indeed the mixing ratios did decline to 36.0 ± 0.5 ppt (see Figure 6.2.1). A value of 35.3 ppt is observed at 1840 AD in the Law Dome ice core. The maximum value of 36.9 ppt in Law Dome ice core air dated to be 1937 is closer to what was measured at the bottom of the EDML firn air. It is obvious that the average background levels observed in 19th century from the Law Dome ice cores is lower than the background levels predicted from the EDML firn air. The mixing ratios observed at the bottom of the EDML firn would be biased towards higher concentrations than those observed in older air extracted from the ice cores due to mixing of gases in the firn.

The age range of Law Dome data is 100 yrs and shows the similiar degree of scatter in CF_4 concentration as observed in the Berkner Island ice core measurements. The extraction method used for the Law Dome ice cores was different to the one developed here at UEA. The Law Dome ice cores were extracted at Commonwealth Scientific and Industrial Research Organisation (CSIRO) trace gas lab in Melbourne, Australia, where the extracted gases were trapped cryogenically using liquid helium. The CF_4 measurements in Berkner Island ice cores are significantly higher than the Law Dome ice cores and this could be due to real variability in natural background levels of CF_4 or could be due to some bias introduced by activated charcoal used for trapping during the extraction. The test extraction runs performed with the EDML firn air does not show bias and agrees with the firn air measurements. However, in future the extractions should be performed with liquid helium cryo-trapping and the data obtained should be compared with activated charcoal extraction method.

The atmospheric CF_4 trend obtained after 3 kyr BP was examined in more detail. It was assumed that there were no emissions after 3 kyr BP and the concentration decreased in accordance with the first order exponential decay (See Figure 6.2.2).
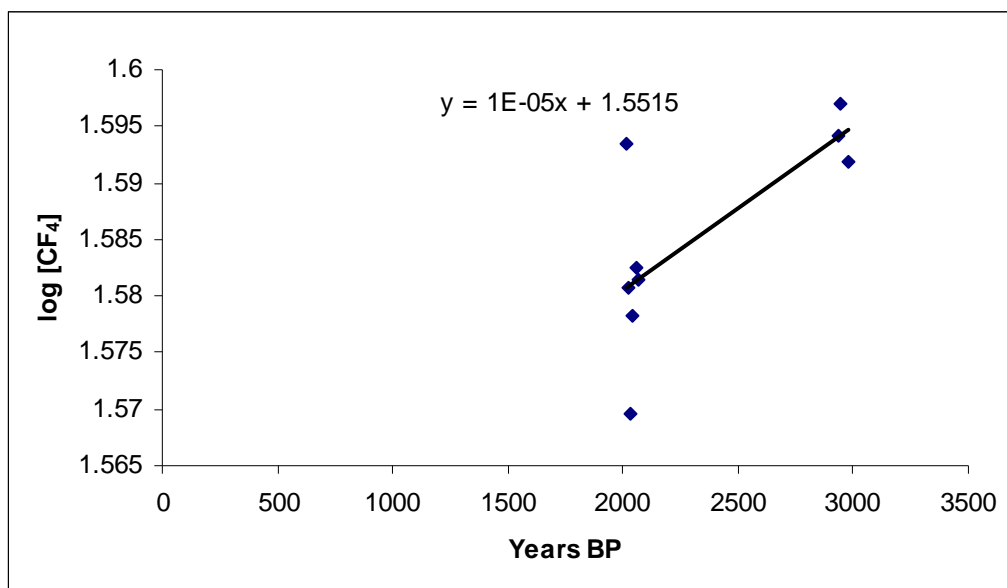
Figure 6.2.2: 1st order exponential decay curve for atmospheric CF_4 after 3 kyr BP.

If the exponential decay curve, $\log[CF_4]_t = -kt + \log[CF_4]$ is linear and takes the form of $y = mx + c$ then it is a first order decay. The k in the above equation is the slope of Figure 6.2.2 and is 1×10^{-5}. The mean atmospheric lifetime would be $1/k = 1/1 \times 10^{-5} =$ 100, 000 yrs. The decay curve could be extrapolated to 1840 AD by substituting $t = 166$ in the equation shown in Figure 6.2.2. This gives an atmospheric mixing ratio of 35. 6 ppt for 1840 AD. The atmospheric lifetime of 100, 000 yrs is higher than the modern day atmospheric life. This is expected due to the absence of thermal destruction of CF_4 in high temperature combustion zones of power plants, incinerators and automobiles at ground level. The pre-industrial atmospheric lifetime obtained here is similar to the value of 110 - 170 kyr obtained based on the atmospheric loss processes (Deeds *et al*., 2008). Deeds *et al*. (2008) estimated an atmospheric lifetime of 100 – 620 kyr on the total lithospheric sources to sustain a steady state atmospheric abundance of 34 ± 1 ppt. The estimation by Deeds *et al*. (2008) has large uncertainties due to limited geographical sampling and assumption regarding the global crustal flux. The mixing ratio of 35.6 ppt, obtained from extrapolating the decay curve to 1840 AD or (166 yr BP), is in good agreement with the Law Dome ice core data of 35.3 ppt. These observations suggest that probably CF_4 concentration did decline after 3 kyr BP.

To summarise, the results indicate that the background level of CF_4 was not stable. It was few ppt higher than what was observed in the Law Dome ice cores and the deepest

samples of the EDML firn air. The mixing ratios started to decline after 3 kyr BP. If the concentration did decline after 3 kyr BP then it raises the question why the mixing ratios were stable between 3 kyr BP and 95 kyr BP. There could have been continuous emissions from the geological sources, which were balanced by the loss rate. On the contrary, there could have been a major geological flux between 3 - 95 kyr BP and then atmospheric burden started to decline. It would be interesting to measure CF_4 trapped in ice cores before and after the Toba volcanic event that occurred about 70 kyr BP. Ideally it would be also interesting to investigate the CF_4 levels in very old ice samples from the EDC ice core. If the concentrations were even higher at 800 kyr BP, it would pose an interesting situation because then million of years back CF_4 could have been a major greenhouse gas as the GWP is much higher than CO_2. Currently the resolution of the ice core measurements is extremely poor and more measurements are needed particularly in the range of 3 – 95 kyr BP and from 2 – 0.1 kyr BP for better understanding of the natural variability in atmospheric CF_4.

Chapter 7: Conclusions and Recommendations

7.1 Method development

7.2 δ^{15}N measurements and data interpretation with the firn densification model

7.3 Methane measurements in Berkner Island ice core

7.4 Trace gas measurements in the EDML firn air

7.5 CF_4 measurements in Berkner Island ice cores

7.1 Method development

A goal of the project was to improve the precision of the measurement of $\delta^{15}N$ in ice core air in order to be able to measure $\delta^{15}N$ in Antarctica ice samples, where typically, the signal amplitude is lower than seen in Greenland. The technique of removing all the interfering species such as O_2, CO_2, H_2O and other trace gases from the sample air and having the reference gas of similar composition as the extracted sample air improved the precision of the measurement. This method had not been applied to ice core $\delta^{15}N$ measurements prior to the analysis of Berkner Island ice core samples presented in this thesis. Later it was discovered that Kobashi *et al.* (2007 & 2008a) referred to this method as a "new copper method" but since I had no prior knowledge of the application of this technique to ice core measurements it seems that there had been a parallel development in both laboratories.

Overall procedural precisions (extraction and analysis) of 0.003 ‰ (n = 7) for replicate ambient air samples, and 0.006 ‰ (n = 9) for ice core samples were obtained. The technique developed does not involve any isobaric interference corrections, and therefore eliminates the need for quantifying the carbon dioxide concentrations in ice cores which has associated analytical uncertainties. The technique developed at UEA does not require any corrections, which is usually about 0.03‰ (~ 40 - 50% of the $\delta^{15}N$ signal observed during the deglaciation). The precision obtained was an order of magnitude lower than the observed $\delta^{15}N$ anomaly during the last deglaciation in Antarctica.

In addition to the method development, the importance of oxygen removal was highlighted and a possible mechanism for the isobaric effects due to the presence of oxygen in samples, more commonly referred to as the 'chemical slope' was investigated. The presence of oxygen in the mass spectrometer produces carbon monoxide (CO), which interferes with mass 29 and 28. This novel finding was confirmed with $^{18}O^{18}O$ enriched samples, which did not show large enrichments in measured $\delta^{15}N$ but in the mass scan showed an amplified peak at m/z = 30 which was due to the production of $^{12}C^{18}O$ in the ion source.

Recommendations:

- The extraction procedure is time consuming and perhaps for future work, the extraction line should be modified to accommodate three – six simultaneous extractions, which will be time and cost effective compared to the single extraction and measurement.

- Despite the fact that CO which has m/z = 28 and 29 could interfere with $\delta^{15}N$ measurements, CO is not commonly removed from the sample because it is considered that the amount of CO in the ancient air from ice core is negligible, and should not cause any significant enrichment in the measured $\delta^{15}N$ value. Any variations in $\delta^{15}N$ due to the presence of minute amounts of CO would be within the error estimate. However in the future, CO should be removed from the samples using I_2O_5 reagent and this could further improve the precision.

7.2 $\delta^{15}N$ measurements and data interpretation with the firn densification model

The goal of the project was to measure $\delta^{15}N$ across two warming events (AIM 8 and AIM 12) in Berkner Island ice core to evaluate the magnitude of the warming and to calibrate the $\delta D – T$ relationship.

The deuterium profile clearly showed the two distinct isotopic anomalies for the two warming events, AIM 8 and AIM 12, during the MIS 3 period. The $\delta^{15}N$ measurements across these two warming events revealed a signal of +0.07 ‰. The signal obtained for the two warming events are larger than the $\delta^{15}N$ signal obtained for the last deglaciation period in the EDML ice core and this could be attributed to the newly developed high precision $\delta^{15}N$ method. The rate of change in $\delta^{15}N$ signal for the AIM 12 event was +0.07‰ in 2400 yrs, although 50% of the change occurred in 800 yrs. The rate of change observed for the AIM 12 event is six times slower than the observed rate of change for the Greenland DO 12 event. The behaviour of $\delta^{15}N$ signal for the AIM 8 event is not straightforward. It shows an increase and then a rapid decrease and then a rapid increase in $\delta^{15}N$ data. When the $\delta^{15}N$ data was combined with the Δdepth corrected δD data, it became clear that the onset of the warming for the AIM 8 in $\delta^{15}N$

signal coincides with the start of the warming in the δD profile. This suggested that a rapid increase in temperature could cause rapid firn densification and as result the firn became thinner decreasing the gravitational fractionation component of the measured $\delta^{15}N$ signal. There was a good correlation ($r^2 = 0.78$) between the Δdepth corrected δD and $\delta^{15}N$ signal for the AIM 12 event.

A strange behaviour was observed in $\delta^{15}N$ data after the AIM 8 event, an apparent enrichment of 0.2 ‰ in $\delta^{15}N$ was obtained. This signal did not correspond to any peaks in the depth corrected δD profile and therefore it was ruled out to be any warming event. This event was labelled as the "Strange Event" because the mechanism for such large fractionation for this event is yet to be discovered. There was a strong correlation between the timings of "strange event" and large altitudinal increase of Berkner Island ice sheet. An increase of 39 m in the diffusive column height would explain the enrichment of 0.2 ‰. Increase in diffusive column height or close-off depth are linked to colder temperatures and higher accumulation at the site. However the accumulation rates estimated from the water isotopes did not show any apparent increase and therefore suggest that at this particular time the accumulation – water isotopes empirical relationship failed. This is not unusual especially for the coastal sites and has been proven by several studies that accumulations derived from water isotopes are often underestimated.

Another important outcome of the $\delta^{15}N$ measurements across the two warming events is that it provides validation for the model Δage calculations, which is used to derive the ice age chronology. The Δdepth or Δage calculated from the difference in warming maxima in ice (δD) and gas phase ($\delta^{15}N$) agrees with the modelled Δage or Δdepth. The agreement between the calculated and modelled Δage not only verifies the ice chronology across the two warming events but leads to three main suggestions:

- That the assumptions used in the model such as the 6.04 ‰ / °C coefficient for isotope – temperature relationship which is valid at EDC may be also valid at Berkner Island.
- This may provide further evidence that the present day δD – T relationship could be used as a surrogate in the glacial period for temperature reconstructions.

- That the warming during the two events was not significantly different from the continental Antarctica

To develop these suggestions into conclusive evidence, it is vital to use a firn densification model to simulate the measured $\delta^{15}N_{excess}$, by varying the $\delta D - T$ coefficient. The $\delta^{40}Ar$ measurements were carried out to calculate $\delta^{15}N_{excess}$ but the data were very noisy and not reliable for interpretations. Although the $\delta^{40}Ar$ were noisy in general, most of the measurements ($\delta^{40}Ar/4$) during the AIM 12 events matched $\delta^{15}N$ data, signifying that most of the observed signal for the AIM 12 is due to gravitational fractionation. This could be attributed to the slow change in temperature and as a result the thermal fractionation is not as large as those observed during the DO events in Greenland. This may prove a point again that the rate of change for the millennial scale climate variability during the last glacial at Berkner Island is typical of any other sites in central Antarctica. The agreement between $\delta^{40}Ar/4$ and $\delta^{15}N$ for the AIM 12 event also increases the confidence in the newly developed $\delta^{15}N$ method. The $\delta^{40}Ar/4$ data for the AIM 8 event matches the $\delta^{15}N$ data at the beginning of the transition and then decreases further than the $\delta^{15}N$ data. This offset could result from the presence of a thermal gradient but due to the apparent scatter in the data the existence of a large temperature gradient could not be ruled out. However the decrease in $\delta^{40}Ar/4$ during the AIM 8 event suggests thinning of the firn column.

Since the attempts to reconstruct the $\delta^{15}N_{excess}$ profile failed it was decided to use the firn densification model to correct for the gravitational fractionation. This procedure has been used in numerous studies where only $\delta^{15}N$ data are used to reconstruct the temperature changes. The firn densification model is unable to simulate the magnitude of the observed $\delta^{15}N$ signals at Berkner Island and as a result it is ineffective to interpret the $\delta^{15}N$ signal in terms of gravitational and thermal components. The two accumulation scenarios (accumulation derived from the water isotopes and from gas synchronisation) used in the model lead to the conclusion that palaeo-accumulation rate estimation in the model is highly uncertain and that the evolution of $\delta^{15}N$ from the model is sensitive to rapid changes in accumulation rate. The model is able to simulate the $\delta^{15}N$ values observed for the Holocene and the disagreement between the data and model during the glacial period is not as large when compared to the results of Landais *et al*. (2006a). However, if it can be proven that Berkner Island experienced large variations in

accumulation rates during the warming events then there is hope that the firn densification model could work for this site.

An important outcome of the firn densification modelling work was phasing the firn temperature gradient with the obtained $\delta^{15}N$ signal. The firn temperature gradients during the two warming events, obtained from the model, using the accumulation rate derived from the deuterium isotopes, are in phase with the $\delta^{15}N$ signal. An excellent correlation between the firn temperature gradient and the $\delta^{15}N$ signal confirms that the signal is definitely a climate signal. The absolute values of the firn temperature gradient are very small and suggest that the change in temperature was slow and gradual. The rate of climate change at Berkner Island during MIS 3 was more in accordance with the rate and magnitude of climate change observed at other sites in Antarctica, that is, no abrupt rapid climate change was observed during the MIS 3 period at Berkner Island.

The thermal fractionation could not be isolated from the total $\delta^{15}N$ signal due to limitations such as noisy $\delta^{40}Ar$ and the ineffectiveness of the firn densification model. However, indirectly the $\delta^{15}N$ signal obtained is likely to be a complex proxy for climate change at Berkner Island responding to both temperature and accumulation. The high correlation between $\delta^{15}N$ and depth corrected δD and between $\delta^{15}N$ and the firn temperature gradient reinforces that $\delta^{15}N$ signals obtained can be reliably considered as a proxy for climate.

Recommendations

The agreement between the model derived Δage and experimental Δage indicates that the modern day relationship between δD – T relationship of 6.04 ‰ / °C may be valid at Berkner during the glacial period. However this could be further confirmed with $\delta^{15}N_{excess}$ calculations or improving the parameters in the firn densification model so that it fits the data. To this end the recommendations for future work are:

- Obtaining high precision $\delta^{40}Ar$ and preferably some samples measured in duplicates.

- At present the model is prescribed with two unknowns, the temperature and accumulation history both derived from water isotopes. It seems that the

accumulation is the obvious reason for the model-data mismatch and in future high resolution chemistry measurements such as Na^+ ions should be carried out for assessing the past accumulation rates. The accumulation rates derived independently from water isotopes should be inputted into the model and then other parameters such as convective zones and the sensitivity coefficient of δD – T relationship should be varied to fit the observed $\delta^{15}N$ signal. This could actually validate the isotope-temperature relationship and also quantify the magnitude of warming during the AIM 8 and AIM 12 events.

• To explain the "strange event" in terms of increasing DCH due to increased accumulation rates requires high resolution chemistry measurements to assess the accumulations rates and changes in the atmospheric circulation processes. The high precision $\delta^{40}Ar$ measurements in future should also indicate if this strange signal is due to gravitational mechanism and whether it could provide a means for reconstructing past DCH.

7.3 Methane measurements in Berkner Island ice core

The goal of the project is to study the phase relationship of the two warming events between Greenland and Antarctica.

The high resolution methane measurements were obtained for Berkner Island in the depth range of 680 – 760 m, encompassing the MIS 3 period. Methane is used as a time marker for climate change in the northern hemisphere since Greenland temperature during the DO events is virtually synchronous with CH_4. Hence the methane data (signal for climate change in northern hemisphere in gas phase) were coupled with $\delta^{15}N$ signal (climatic signal in gas phase from Berkner Island in southern hemisphere) to investigate the phase relationship for abrupt climate changes between the two hemispheres without the need to calculate Δage.

The data here indicate that the southern hemisphere leads the global warming signal. The time lag estimate measured in this study between the onset of AIM 12 and the onset

of DO 12 is 1600 ± 350 yrs and between AIM 8 and DO 8 is 1100 ± 360 yrs. The findings support the "See-Saw" hypothesis. The time lags estimated here are more precise than previous studies since the climatic signals from both hemispheres are in the gas phase and therefore overcome the problem of taking into account the highly uncertain Δage calculations.

The high resolution methane data could be used in dating the ice core. The Berkner methane record for MIS 3 was compared to Greenland methane composite record on GICC05 age scale. The comparison shows some discrepancies in the Berkner age scale especially during the timing of the "strange event" and suggest tentatively that the accumulation rate increased by more than a factor of two during this time period if the thinning rate was assumed to be constant.

Recommendations

- The Berkner age scales should be synchronised to GICC05 age scale. This would make the time lag estimates calculated in this study more robust. It will also allow comparison with the climate record from the northern hemisphere and confirm that Antarctica was warming when the northern hemisphere was in the cold stadial period.

- The number of annual layers are known between the DO 5 and DO 6 and between DO 6 and DO 7. If the thinning rate can be obtained in the future by the ice flow model during this period then the palaeo-accumulation rates can be calculated from this during the occurrence of strange of the strange event.

7.4 Trace gas measurements in the EDML firn air

The goal of the project was to measure and derive the longest atmospheric histories of PFCs, HFC-23, SF_6 and SF_5CF_3 from the EDML firn air samples. The atmospheric histories of these species were reconstructed using the firn diffusion model and the iterative dating technique. The reconstructed atmospheric trend is probably the longest atmospheric record derived from firn air. Table 7.1 shows the summary of the findings.

Table 7.1: Summary of mixing ratios, growth rates and radiative forcings of individual gases estimated from the atmospheric trend reconstructed from the EDML firn air.

Chemical Species	Mixing ratios (ppt)			Growth (ppt yr^{-1})		Radiative forcings 2006 (mW m^{-2})
	1960	1990	2006	1990	2006	
CF_4	45.9	66.3	77.8	0.8	0.8	4
C_2F_6	0.63	1.6	3.2	0.06	0.15	0.8
C_3F_8	0	0.18	0.8	0.02	0.08	0.2
$c\text{-}C_4F_8$	0.09	0.87	1.2	0.03	0	0.4
HFC-23	1.24	4.3	19.4	0.4	1.0	3.5
SF_6	0.28	2.0	5.5	0.2	0.2	3
SF_5CF_3	0	0.06	0.16	0.005	0.005	0.08

The CF_4 concentration in bottom most firn air samples levelled at ~37 ppt. This is the first evidence from the firn record indicating the pre-industrial value of CF_4 and also proving that the EDML firn air provided the longest record of reconstructed atmospheric PFCs trends. The CF_4 mixing ratio seems to have stabilised in recent years. Initially the C_2F_6 emissions were based on the linear relationship between CF_4 and C_2F_6, assuming that both species have the same source (aluminium smelting). However, the firn air data shows that in early 1990s this relationship changed due to additional atmospheric loading of C_2F_6 from the semiconductor industry.

The most interesting result is that of C_3F_8 which shows that the atmospheric abundance has multiplied four times since early 1990s. There is a high correlation between C_2F_6 and C_3F_8 ($r^2 = 0.96$) which suggests that their atmospheric trends could be attributed to same sources. Probably the semiconductor industry is also contributing to the atmospheric budget of C_3F_8 significantly. Currently the $c\text{-}C_4F_8$ atmospheric concentration is not increasing in the atmosphere. There is no published literature on

atmospheric histories of c-C_4F_8 and this study has contributed significantly to understanding the history of this species in the atmosphere. Although the sources of this particular gas are unknown, it displays a great resemblance to the CF_4 atmospheric trend.

The HFC-23 emission estimated from the reconstructed trend shows that the recent industrial emission estimate (based on HCFC-22 production) is overestimated by 24%. There is a 1: 1 relationship between SF_6 and SF_5CF_3, which suggests a common source or SF_5CF_3 is produced via a reaction involving SF_6. Table 7.1 shows the radiative forcing for individual gases. The combined radiative forcing for all the species studied is 0.012, which is 8% of the radiative forcing of N_2O. The overall contribution of PFCs, HFCs, SF_6 and SF_5CF_3 to the radiative forcings is small but the rate of change is high. The total radiative forcings for the gases studied changed by +35% since 1995 whereas the radiative forcings for N_2O changed by +15 % for the similar time period.

Recommendations

- The calibration scale for C_3F_8 is on UEA "preliminary scale" and needs to be verified in future with rigorous calibration techniques. There is some constant offset between the atmospheric measurements and reconstructed trend from the EDML firn air, which is probably due to calibration issues.

- Future monitoring is very important for all the species studied here. These species are potent greenhouse gases and the total contribution to the radiative forcings is increasing at an alarming rate. Consequently it will be very important to monitor the changing atmospheric levels of these species to support mitigation options should these be needed to curtail industrial emissions. There is evidence that the atmospheric levels of certain species such as CF_4, C_2F_6 and c-C_4F_8 have stabilised or the growth rate is declining and this needs monitoring to confirm this finding. According to industry, they are committed to reduce the emissions of PFCs and this should be reflected in the future atmospheric growth rate.

7.5 CF$_4$ measurements in Berkner Island ice cores

The goal of this pilot study was to investigate the variability in natural background levels of CF$_4$ during the last glacial period and late Holocene.

In very ancient air the background levels of CF$_4$ was higher than the Pre-Industrial period. The CF$_4$ had an average mixing value of 39.5 ppt during the glacial period and was very much constant until 3000 yrs BP. Since then the CF$_4$ concentration decreased at a linear rate to 36.5 ppt, comparable to the pre-industrial values that were observed at the bottom of the firn. The atmospheric lifetime obtained with the first order exponential decay curve was 100 000 yrs, which agrees with the published literature that suggests that the lifetime would be longer in the absence of destruction of CF$_4$ high combustion furnace. The trend obtained suggests that there may have been an emission between 95 – 3 kyr BP or a continuous slow geological emissions. Since 3 kyr BP there were no emissions and the CF$_4$ decreased at a linear rate.

Recommendations

- Although the extraction method is verified using static standard transfers and oxygen free nitrogen it is still recommended that the trapping of sample should be done using a cryogen such as liquid helium. This will eliminate the use of activated charcoal and will also confirm that the variability observed is not due to some artefacts in the trapping procedure.

- The data resolution is very poor and some more samples should be measured in between 95 – 3 kyr BP periods and from late Holocene to early pre-industrial period. More measurements between 95 – 3 kyr BP period would enable us to determine if geological activity increased the CF$_4$ concentration in the atmosphere, or if it was a continuous slow geological emission. It would be interesting to measure samples before and after major volcanic events during the last glacial period. This would certainly show if past major volcanic events contributed to the natural abundance of CF$_4$. Equally it would be interesting to measure CF$_4$ in very old ice samples such as EDC ice core to see if CF$_4$ was even higher than in the last glacial period. If so then this would present a strong

case that CF_4 may have been one of the major greenhouse gas compared to CO_2 million of years ago because of its high GWP.

References

Ahn, J., and Brook, E. J.: Atmospheric CO_2 and climate from 65 to 30 ka B.P, Geophysical Research Letters, 34, 2007.

Ahn, J., and Brook, E. J.: Atmospheric CO_2 and climate on millennial time scales during the last glacial period, Science, 322, 83-85, 2008.

Alley, R. B., Mayewski, P. A., Sowers, T., Stuiver, M., Taylor, K. C., and Clark, P. U.: Holocene climatic instability: A prominent, widespread event 8200 yr ago, Geology, 25, 483-486, 1997.

Aoki, N., and Makide, Y.: Precise determination of the atmospheric CF_4 concentration by using natural Kr in the atmosphere as an internal reference in the preconcentration-GC-MS analysis, Chemistry Letters, 33, 1634-1635, 2004.

Arnaud, L., Barnola, J.-Mand Duval, P.: Physical modelling of the densification of snow/firn and ice in the upper part of polar ice sheets. In: Hondoh, T. (ed.), Physics of Ice Core Records. Sapporo, pp. 285 – 305.

Barbante, C., Fischer H., Masson-Delmotte, V., Waelbroeck, C. and Wolff, E.W.: Climate of the last million years: new insights from EPICA and other records, Quaternary Science Reviews, 29, 1-7, 2010.

Barnes, P.R.F., Wolff, E.W., and Mulvaney, R.: A 44 kyr paleoroughness record of the Antarctic, Journal of Geophysical Research, 111, D03102, doi: 03110.012029/02005JD006349, 2006.

Barnola, J. M., Pimienta, P., Raynaud, D., and Korotkevich, Y. S.: CO_2 climate relationship as deduced from the Vostok ice core: A re- examination based on new measurements and on a re-evaluation of the air dating, Tellus, Series B, 43 B, 83-90, 1991.

Bartos, S., Laush, C., Scharfenberg, J., and Kantamaneni, R.: Reducing greenhouse gas emissions from magnesium die casting, Journal of Cleaner Production, 15, 979-987, 2007.

Bender, M. L., Sowers, T., Barnola, J. M., and Chappellaz, J.: Changes in the O_2/N_2 ratio of the atmosphere during recent decades reflected in the composition of air in the firn at Vostok station, Antarctica, Geophysical Research Letters, 21, 189-192, 1994a

Bender, M.L., Tans, P.P., Ellis, J.T., Orchardo, J. and Habfast, K.: A high precision isotope ratio mass spectrometry method for measuring the O_2/N_2 ratio of air, Geochimica et Cosmochimica Acta, 58(21), 4751-4758, 1994b.

Bender, M., Sowers, T., Dickson, M. L., Orchardo, J., Grootes, P., Mayewski, P. A., and Meese, D. A.: Climate correlations between greenland and antarctica during the past 100,000 years, Nature, 372, 663-666, 1994c.

Bender, M., Sowers, T., and Lipenkov, V.: On the concentrations of o2, n2, and ar in trapped gases from ice cores, Journal of Geophysical Research, 100, 18,651-618,660, 1995.

Bender, M.L., Malaize, B., Orchado, J., Sowers, T., Jouzel, J.: High precision correlations of Greenland and Antarctic ice core records over the last 100 ky. In Mechanisms of Global Climate Change at Millennial Time Scales, pp. 149-164,1999.

Bender, M. L.: Orbital tuning chronology for the vostok climate record supported by trapped gas composition, Earth and Planetary Science Letters, 204, 275-289, 2002

Blunier, T., Schwander, J., Stauffer, B., Stocker, T., Dällenbach, A., Indermühle, A., Tschumi, J., Chappellaz, J., Raynaud, D., and Barnola, J. M.: Timing of the Antarctic cold reversal and the atmospheric CO_2 increase with respect to the younger dryas event, Geophysical Research Letters, 24, 2683-2686, 1997.

Blunier, T., Chappellaz, J., Schwander, J., Dällenbach, A., Stauffer, B., Stocker, T. F., Raynaudt, D., Jouzel, J., Clausen, H. B., Hammer, C. U., and Johnsen, S. J.:

Asynchrony of antarctic and greenland climate change during the last glacial period, Nature, 394, 739-743, 1998.

Blunier, T., and Brook, E. J.: Timing of millennial-scale climate change in Antarctica and Greenland during the last glacial period, Science, 291, 109-112, 2001.

Blunier, T., Schwander, J., Chappellaz, J., Parrenin, F., and Barnola, J. M.: What was the surface temperature in central Antarctica during the last glacial maximum?, Earth and Planetary Science Letters, 218, 379-388, 2004.

Blunier, T., Spahni, R., Barnola, J. M., Chappellaz, J., Loulergue, L., and Schwander, J.: Synchronization of ice core records via atmospheric gases, Climate of the Past, 3, 325-330, 2007.

Boyle, E. A.: Cool tropical temperatures shift the global $\delta^{18}O$-T relationship: An explanation for the ice core $\delta^{18}O$ - borehole thermometry conflict?, Geophysical Research Letters, 24, 273-276, 1997.

Brion, C.E. and Stewart, W.B.: Mass Spectrometric Analysis of Oxygen, Nature, 217, 946, 1968.

Broecker, W. S., Andree, M., Wolfli, W., Oeschger, H., Bonani, G., Kennett, J., and Peteet, D.: The chronology of the last deglaciation: Implications to the cause of the younger dryas event, Paleoceanography, 3, 1-19, 1988.

Brook, E. J., White, J. W. C., Schilla, A. S. M., Bender, M. L., Barnett, B., Severinghaus, J. P., Taylor, K. C., Alley, R. B., and Steig, E. J.: Timing of millennial-scale climate change at Siple dome, West Antarctica, during the last glacial period, Quaternary Science Reviews, 24, 1333-1343, 2005.

Burgess, A. B., Grainger, R. G., Dudhia, A., Payne, V. H., and Jay, V. L.: Mipas measurement of sulphur hexafluoride (SF_6), Geophysical Research Letters, 31, 2004.

Butler, J. H., Battle, M., Bender, M. L., Montzka, S. A., Clarke, A. D., Saltzman, E. S., Sucher, C. M., Severinghaus, J. P., and Elkins, J. W.: A record of atmospheric halocarbons during the twentieth century from polar firn air, Nature, 399, 749-755, 1999.

Caillon, N., Severinghaus, J. P., Barnola, J. M., Chappellaz, J., Jouzel, J., and Parrenin, F.: Estimation of temperature change and of gas age - ice age difference, 108 kyr b.P., at Vostok, Antarctica, Journal of Geophysical Research D: Atmospheres, 106, 31893-31901, 2001.

Caillon, N., Jouzel, J., Severinghaus, J. P., Chappellaz, J., and Blunier, T.: A novel method to study the phase relationship between Antarctic and Greenland climate, Geophysical Research Letters, 30, 2003a.

Caillon, N., Severinghaus, J. P., Jouzel, J., Barnola, J. M., Kang, J., and Lipenkov, V. Y.: Timing of atmospheric CO_2 and Antarctic temperature changes across termination III, Science, 299, 1728-1731, 2003b.

Chappellaz, J., Barnola, J. M., Raynaud, D., Korotkevich, Y. S., and Lorius, C.: Ice-core record of atmospheric methane over the past 160,000 years, Nature, 345, 127-131, 1990.

Chappellaz, J., Blunier, T., Raynaud, D., Barnola, J. M., Schwander, J., and Stauffer, B.: Synchronous changes in atmospheric CH_4 and greenland climate between 40 and 8 kyr bp, Nature, 366, 443-445, 1993.

Chappellaz, J., Blunier, T., Kints, S., Dällenbach, A., Barnola, J. M., Schwander, J., Raynaud, D., and Stauffer, B.: Changes in the atmospheric CH_4 gradient between Greenland and Antarctica during the Holocene, Journal of Geophysical Research D: Atmospheres, 102, 15987-15997, 1997.

Charles, C. D., Lynch-Stieglitz, J., Ninnemann, U. S., and Fairbanks, R. G.: Climate connections between the hemisphere revealed by deep sea sediment core/ice core correlations, Earth and Planetary Science Letters, 142, 19-27, 1996.

Colbeck, S. C.: Air movement in snow due to windpumping, Journal of Glaciology, 35, 209-213, 1989.

Craig, H.: Standard for reporting concentrations of deuterium and oxygen-18 in natural waters, Science, 133, 1833-1834, 1961.

Craig, H., Horibe, Y., and Sowers, T.: Gravitational separation of gases and isotopes in polar ice caps, Science, 242, 1675-1678, 1988.

Cuffey, K. M., Alley, R. B., Grootes, P. M., and Anandakrishnan, S.: Toward using borehole temperatures to calibrate an isotopic paleothermometer in central greenland, Palaeogeography, Palaeoclimatology, Palaeoecology, 98, 265-268, 1992.

Cuffey, K. M., Clow, G. D., Alley, R. B., Stuiver, M., Waddington, E. D., and Saltus, R. W.: Large arctic temperature change at the Wisconsin-Holocene glacial transition, Science, 270, 455-458, 1995.

Cuffey, K. M., and Vimeux, F.: Covariation of carbon dioxide and temperature from the vostok ice core after deuterium-excess correction, Nature, 412, 523-527, 2001.

Culbertson, J. A., Prins, J. M., Grimsrud, E. P., Rasmussen, R. A., Khalil, M. A. K., and Shearer, M. J.: Observed trends for CF_3-containing compounds in background air at Cape Meares, Oregon, Point Barrow, Alaska, and Palmer Station, Antarctica, Chemosphere, 55, 1109-1119, 2004.

Dällenbach, A., Blunier, T., Flückiger, J., Stauffer, B., Chappellaz, J., and Raynaud, D.: Changes in the atmospheric CH_4 gradient between Greenland and Antarctica during the last glacial and the transition to the Holocene, Geophysical Research Letters, 27, 1005-1008, 2000.

Dahl-Jensen, D., Mosegaard, K., Gundestrup, N., Clow, G. D., Johnsen, S. J., Hansen, A. W., and Balling, N.: Past temperatures directly from the Greenland ice sheet, Science, 282, 268-271, 1998.

Dansgaard, W.: Stable isotopes in precipitation, Tellus, 16, 436-467, 1964.

Dansgaard, W., White, J. W. C., and Johnsen, S. J.: The abrupt termination of the Younger Dryas climate event, Nature, 339, 532-534, 1989.

Dansgaard, W., Johnsen, S. J., Clausen, H. B., Dahl-Jensen, D., Gundestrup, N. S., Hammer, C. U., Hvidberg, C. S., Steffensen, J. P., Sveinbjärnsdottir, A. E., Jouzel, J., and Bond, G.: Evidence for general instability of past climate from a 250-kyr ice-core record, Nature, 364, 218-220, 1993.

Deeds, D. A., Vollmer, M. K., Kulongoski, J. T., Miller, B. R., Mühle, J., Harth, C. M., Izbicki, J. A., Hilton, D. R., and Weiss, R. F.: Evidence for crustal degassing of CF_4 and SF_6 in mojave desert groundwaters, Geochimica et Cosmochimica Acta, 72, 999-1013, 2008.

Delmotte, M., Chappellaz, J., Brook, E., Yiou, P., Barnola, J. M., Goujon, C., Raynaud, D., and Lipenkov, V. I.: Atmospheric methane during the last four glacial-interglacial cycles: Rapid changes and their link with Antarctic temperature, Journal of Geophysical Research D: Atmospheres, 109, 2004.

Dreyfus, G. B., Parrenin, F., Lemieux-Dudon, B., Durand, G., Masson-Delmotte, V., Jouzel, J., Barnola, J. M., Panno, L., Spahni, R., Tisserand, A., Siegenthaler, U., and Leuenberger, M.: Anomalous flow below 2700 m in the epica dome c ice core detected using $\delta^{18}O_{atm}$ of atmospheric oxygen measurements, Climate of the Past, 3, 341-353, 2007.

Dreyfus, G. B., Jouzel, J., Bender, M. L., Landais, A., Masson-Delmotte, V., and Leuenberger, M.: Firn processes and $\delta^{15}N$: Potential for a gas-phase climate proxy, Quaternary Science Reviews, 29, 28-42, 2010.

EDGAR: (The EDGAR V3.2 FT2000 database, . Accessed 27 January 2008, 2008.

EPICA Community Members: Eight glacial cycles from an Antarctic ice core, Nature, 429, 623-628, 2004.

EPICA Community Members: One-to-one coupling of glacial climate variability in Greenland and Antarctica, Nature, 444, 195-198, 2006.

Etheridge, D. M., Steele, L. P., Langenfelds, R. L., Francey, R. J., Barnola, J. M., and Morgan, V. I.: Natural and anthropogenic changes in atmospheric CO_2 over the last 1000 years from air in Antarctic ice and firn, Journal of Geophysical Research D: Atmospheres, 101, 4115-4128, 1996.

Etheridge, D. M., Steele, L. P., Francey, R. J., and Langenfelds, R. L.: Atmospheric methane between 1000 a.D. And present: Evidence of anthropogenic emissions and climatic variability, Journal of Geophysical Research D: Atmospheres, 103, 15979-15993, 1998.

Ferretti, D. F., Miller, J. B., White, J. W. C., Etheridge, D. M., Lassey, K. R., Lowe, D. C., MacFarling Meure, C. M., Dreier, M. F., Trudinger, C. M., Van Ommen, T. D., and Langenfelds, R. L.: Atmospheric science: Unexpected changes to the global methane budget over the past 2000 years, Science, 309, 1714-1717, 2005.

Fischer, H., Wahlen, M., Smith, J., Mastroianni, D., and Deck, B.: Ice core records of atmospheric CO_2 around the last three glacial terminations, Science, 283, 1712-1714, 1999.

Flückiger, J., Blunier, T., Stauffer, B., Chappellaz, J., Spahni, R., Kawamura, K., Schwander, J., Stocker, T. F., and Dahl-Jensen, D.: N_2O and CH_4 variations during the last glacial path epoch: Insight into global processes, Global Biogeochemical Cycles, 18, 2004.

Forster, P., Ramaswamy, V., Artaxo, P., Berntsen, T., Betts, R., Fahey, D.W., Haywood, J., Lean, J., Lowe, D.C., Myhre, G., Nganga, P., Prinn, R., Raga, G., Schulz, M., and Van Dorland, R.: Changes in Atmospheric Constituents and in Radiative Forcing. In: Climate Change 2007: The Physical Science Basis. Contribution of Working Group I to the Fourth Assessment Report of the Intergovernmental Panel on Climate Change [Solomon, S., D. Qin, M. Manning, Z. Chen, M. Marquis, K.B. Averyt, M.Tignor and H.L. Miller (eds.)]. Cambridge University Press, Cambridge, United Kingdom and New York, NY, USA, 2007.

Goujon, C., Barnola, J. M., and Ritz, C.: Modelling the densification of polar firn including heat diffusion: Application to close-off characteristics and gas isotopic fractionation for Antarctica and Greenland sites, Journal of Geophysical Research D: Atmospheres, 108, 2003.

Graber, L., Bonfigli, G., and Müller, S.: Improving SF_6 leakage detection in switchgear by reducing the influence of solar radiation on density measurement, Conference Record of IEEE International Symposium on Electrical Insulation, 2008, 441-444,

Grachev, A. M., and Severinghaus, J. P.: Laboratory determination of thermal diffusion constants for $^{29}N_2/^{28}N_2$ air at temperatures from -60 to 0 °C for reconstruction of magnitudes of abrupt climate changes using the ice core fossil-air plaeothermometer, Geochimica et Cosmochimica Acta, 67, 345-360, 2003a.

Grachev, A. M., and Severinghaus, J. P.: Determining the thermal diffusion factor for $^{40}Ar/^{36}Ar$ in air to aid paleoreconstruction of abrupt climate change, Journal of Physical Chemistry A, 107, 4636-4642, 2003b.

Grachev, A. M., and Severinghaus, J. P.: A revised + 10 ± 4 °C magnitude of the abrupt change in Greenland temperature at the younger dryas termination using published gisp2 gas isotope data and air thermal diffusion constants, Quaternary Science Reviews, 24, 513-519, 2005.

Greally, B. R., Simmonds, P. G., O'Doherty, S., McCulloch, A., Miller, B. R., Salameh, P. K., Mühle, J., Tanhua, T., Harth, C., Weiss, R. F., Fraser, P. J., Krummel, P. B., Dunse, B. L., Porter, L. W., and Prinn, R. G.: Improved continuous in-situ measurements of $C_1 - C_3$ pfcs, hfcs, hcfcs, cfcs and SF_6 in europe and australia, Environmental Sciences, 2, 253 - 261, 2005.

Gross, J.H.: Mass Spectrometry: A textbook, Springer, berlin, Heidelberg, New York, ISBN: 3-54040739-1, 2005.

Harnisch, J., Borchers, R., Fabian, P., Gaggeler, H. W., and Schotterer, U.: Effect of natural tetrafluoromethane [2], Nature, 384, 32, 1996a.

Harnisch, J., Borchers, R., Fabian, P., and Maiss, M.: Tropospheric trends for CF_4 and C_2F_6 since 1982 derived from SF_6 dated stratospheric air, Geophysical Research Letters, 23, 1099-1102, 1996b.

Harnisch, J., Borchers, R., Fabian, P., and Maiss, M.: CF_4 and the age of mesospheric and polar vortex air, Geophysical Research Letters, 26, 295-298, 1999.

Harnisch, J.: Atmospheric Perfluorocarbons: Sources and Concentrations. in: Non CO_2 greenhouse gases: scientific understanding, control and implementation , Proceedings of the second international symposium, edited by Ham, J.V., Baede, A.P.M., Meyer, L.A., and Ybema, R., pp 199 – 204, Kluwer Academic Publishers, Dordrecht, Noordwijkerhout, The Netherlands, 2000.

Harnisch, J., and Höhne, N.: Comparison of emissions estimates derived from atmospheric measurements with national estimates of HFCs, PFCs and SF_6, Environmental Science and Pollution Research, 9, 315-320, 2002.

Headly, M. A., and Severinghaus, J. P.: A method to measure Kr/N_2 ratios in air bubbles trapped in ice cores and its application in reconstructing past mean ocean temperature, Journal of Geophysical Research D: Atmospheres, 112, 2007.

Heard, D.E.: Analytical Techniques for Atmospheric Measurements, Blackwell, Oxford, UK, ISBN: 1495123575, 2006.

Herron, M. M., and Langway Jr, C. C.: Firn densification: An empirical model, Journal of Glaciology, 25, 373-385, 1980.

Huang, L., Zhu, L., Pan, X., Zhang, J., Ouyang, B., and Hou, H.: One potential source of the potent greenhouse gas SF_5CF_3: The reaction of SF_6 with fluorocarbon under discharge, Atmospheric Environment, 39, 1641-1653, 2005.

Huang, L., Shen, Y., Dong, W., Zhang, R., Zhang, J., and Hou, H.: A novel method to decompose two potent greenhouse gases: Photoreduction of SF_6 and SF_5CF_3 in the presence of propene, Journal of Hazardous Materials, 151, 323-330, 2008.

Huber, C., Beyerle, U., Leuenberger, M., Schwander, J., Kipfer, R., Spahni, R., Severinghaus, J. P., and Weiler, K.: Evidence for molecular size dependent gas fractionation in firn air derived from noble gases, oxygen, and nitrogen measurements, Earth and Planetary Science Letters, 243, 61-73, 2006a.

Huber, C., Leuenberger, M., Spahni, R., Flückiger, J., Schwander, J., Stocker, T. F., Johnsen, S., Landais, A., and Jouzel, J.: Isotope calibrated greenland temperature record over marine isotope stage 3 and its relation to CH_4, Earth and Planetary Science Letters, 243, 504-519, 2006b.

Hurley, M. D., Wallington, T. J., Buchanan, G. A., Gohar, L. K., Marston, G., and Shine, K. P.: IR spectrum and radiative forcing of CF_4 revisited, Journal of Geophysical Research D: Atmospheres, 110, 1-8, 2005.

Huybrechts, P.: Sea-level changes at the LGM from ice-dynamic reconstructions of the Greenland and Antarctic ice sheets during the glacial cycles, Quaternary Science Reviews, 21, 203-231, 2002.

Indermuhle, A., Monnin, E., Stauffer, B., Stocker, T. F., and Wahlen, M.: Atmospheric CO concentration from 60 to 20 kyr BP from the Taylor Dome ice core, Antarctica, Geophysical Research Letters, 27, 735-738, 2000.

IAI: The International Aluminium Institute report on The Aluminium Industry's Global Perfluorocarbon Gas Emissions Reduction Programme. Results of the 2006 Anode Effect Survey, 2008.

Ikeda-Fukazawa, T., Fukumizu, K., Kawamura, K., Aoki, S., Nakazawa, T., and Hondoh, T.: Effects of molecular diffusion on trapped gas composition in polar ice cores, Earth and Planetary Science Letters, 229, 183-192, 2005.

Jouzel, J., Alley, R. B., Cuffey, K. M., Dansgaard, W., Grootes, P., Hoffmann, G., Johnsen, S. J., Koster, R. D., Peel, D., Shuman, C. A., Stievenard, M., Stuiver, M., and White, J.: Validity of the temperature reconstruction from water isotopes in ice cores, Journal of Geophysical Research, 102, 26471-26487, 1997.

Jouzel, J., Vimeux, F., Caillon, N., Delaygue, G., Hoffmann, G., Masson-Delmotte, V., and Parrenin, F.: Magnitude of isotope/temperature scaling for interpretation of central Antarctic ice cores, Journal of Geophysical Research D: Atmospheres, 108, 2003.

Jouzel, J., Masson-Delmotte, V., Cattani, O., Dreyfus, G., Falourd, S., Hoffmann, G., Minster, B., Nouet, J., Barnola, J. M., Chappellaz, J., Fischer, H., Gallet, J. C., Johnsen, S., Leuenberger, M., Loulergue, L., Luethi, D., Oerter, H., Parrenin, F., Raisbeck, G., Raynaud, D., Schilt, A., Schwander, J., Selmo, E., Souchez, R., Spahni, R., Stauffer, B., Steffensen, J. P., Stehni, B., Stocker, T. F., Tison, J. L., Werner, M., and Wolff, E. W.: Orbital and millennial Antarctic climate variability over the past 800,000 years, Science, 317, 793-796, 2007a.

Jouzel, J., Stiävenard, M., Johnsen, S. J., Landais, A., Masson-Delmotte, V., Sveinbjornsdottir, A., Vimeux, F., von Grafenstein, U., and White, J. W. C.: The grip deuterium-excess record, Quaternary Science Reviews, 26, 1-17, 2007b.

Kaspers, K. A., van de Wal, R. S. W., de Gouw, J. A., Hofstede, C. M., van den Broeke, M. R., van der Veen, C., Neubert, R. E. M., Meijer, H. A. J., Brenninkmeijer, C. A. M., Karläf, L., and Winther, J. G.: Analyses of firn gas samples from Dronning Maud Land, Antarctica: Study of nonmethane hydrocarbons and methyl chloride, Journal of Geophysical Research D: Atmospheres, 109, 2004.

Kaspers, K. A., van de Wal, R. S. W., van den Broeke, M. R., Schwander, J., vanLipzig, N.P.M., and Brenninkmeijer, C. A. M.:Model calculations of the age of firn air across the Antarctic continent, Atmopsheric Chemistry and Physics., 4, 1-15, 2004.

Kaspers, K.A.: Chemical and physical analyses of firn and firn air from Dronning Maud Land, Antarctica. PhD thesis, University of Utrecht, Netherlands, 2005.

Kawamura, K., Severinghaus, J. P., Ishidoya, S., Sugawara, S., Hashida, G., Motoyama, H., Fujii, Y., Aoki, S., and Nakazawa, T.: Convective mixing of air in firn at four polar sites, Earth and Planetary Science Letters, 244, 672-682, 2006.

Kawamura, K., Parrenin, F., Lisiecki, L., Uemura, R., Vimeux, F., Severinghaus, J. P., Hutterli, M. A., Nakazawa, T., Aoki, S., Jouzel, J., Raymo, M. E., Matsumoto, K., Nakata, H., Motoyama, H., Fujita, S., Goto-Azuma, K., Fujii, Y., and Watanabe, O.: Northern hemisphere forcing of climatic cycles in Antarctica over the past 360,000 years, Nature, 448, 912-916, 2007.

Khalil, M. A. K., Rasmussen, R. A., Culbertson, J. A., Prins, J. M., Grimsrud, E. P., and Shearer, M. J.: Atmospheric Perfluorocarbons, Environmental Science and Technology, 37, 4358-4361, 2003.

Kobashi, T., Severinghaus, J. P., Brook, E. J., Barnola, J. M., and Grachev, A. M.: Precise timing and characterization of abrupt climate change 8200 years ago from air trapped in polar ice, Quaternary Science Reviews, 26, 1212-1222, 2007.

Kobashi, T., Severinghaus, J. P., and Barnola, J. M.: 4 ± 1.5 ℃ abrupt warming 11,270 yr ago identified from trapped air in Greenland ice, Earth and Planetary Science Letters, 268, 397-407, 2008a.

Kobashi, T., Severinghaus, J. P., and Kawamura, K.: Argon and nitrogen isotopes of trapped air in the GISP2 ice core during the Holocene epoch (0-11,500 b.P.): Methodology and

implications for gas loss processes, Geochimica et Cosmochimica Acta, 72, 4675-4686, 2008b.

Krieg, J., Nothholt, J., Mahieu, E., Rinsland, C. P., and Zander, R.: Sulphur hexafluoride (SF_6): Comparison of FTIR-measurements at three sites and determination of its trend in the northern hemisphere, Journal of Quantitative Spectroscopy and Radiative Transfer, 92, 383-392, 2005.

Lüthi, D., Le Floch, M., Bereiter, B., Blunier, T., Barnola, J. M., Siegenthaler, U., Raynaud, D., Jouzel, J., Fischer, H., Kawamura, K., and Stocker, T. F.: High-resolution carbon dioxide concentration record 650,000-800,000 years before present, Nature, 453, 379-382, 2008.

Landais, A., Barnola, J. M., Masson-Delmotte, V., Jouzel, J., Chappellaz, J., Caillon, N., Huber, C., Leuenberger, M., and Johnsen, S. J.: A continuous record of temperature evolution over a sequence of Dansgaard-Oeschger events during marine isotopic stage 4 (76 to 62 kyr bp), Geophysical Research Letters, 31, 1-4, 2004a.

Landais, A., Caillon, N., Goujon, C., Grachev, A. M., Barnola, J. M., Chappellaz, J., Jouzel, J., Masson-Delmotte, V., and Leuenberger, M.: Quantification of rapid temperature change during do event 12 and phasing with methane inferred from air isotopic measurements, Earth and Planetary Science Letters, 225, 221-232, 2004b.

Landais, A., Caillon, N., Severinghaus, J., Barnola, J. M., Goujon, C., Jouzel, J., and Masson-Delmotte, V.: Isotopic measurements of air trapped in ice to quantify temperature changes, Analyse isotopique de l'air piégé dans la glace pour quantifier les variations de tempÃ©rature, 336, 963-970, 2004c.

Landais, A., Jouzel, J., Masson-Delmotte, V., and Caillon, N.: Large temperature variations over rapid climatic events in greenland: A method based on air isotopic measurements, Larges variations de tempÃ©rature au Groenland pendant les Ã©vÃ©nements climatiques rapides: Une mÃ©thode basÃ©e sur la mesure des isotopes de l'air piÃ©gÃ© dans la glace, 337, 947-956, 2005.

Landais, A., Barnola, J. M., Kawamura, K., Caillon, N., Delmotte, M., Van Ommen, T., Dreyfus, G., Jouzel, J., Masson-Delmotte, V., Minster, B., Freitag, J., Leuenberger, M., Schwander, J., Huber, C., Etheridge, D., and Morgan, V.: Firn-air in modern polar sites and glacial-interglacial ice: A model-data mismatch during glacial periods in Antarctica?, Quaternary Science Reviews, 25, 49-62, 2006a.

Landais, A., Masson-Delmotte, V., Jouzel, J., Raynaud, D., Johnsen, S., Huber, C., Leuenberger, M., Schwander, J., and Minster, B.: The glacial inception as recorded in the northgrip greenland ice core: Timing, structure and associated abrupt temperature changes, Climate Dynamics, 26, 273-284, 2006b.

Lang, C., Leuenberger, M., Schwander, J., and Johnsen, S.: 16 °C rapid temperature variation in central greenland 70,000 years ago, Science, 286, 934-937, 1999.

Lee, J.: determination of stratospheric lifetimes of HCFCs and other halogenated hydrocarbons from ballon-bourne profile measurements. Ph.D. Thesis, University of East Anglia, Norwich, UK., 1994.

Leuenberger, M. C., Lang, C., and Schwander, J.: $\delta^{15}N$ measurements as a calibration tool for the paleothermometer and gas-ice age differences: A case study for the 8200 B.P. Event on grip ice, Journal of Geophysical Research D: Atmospheres, 104, 22163-22170, 1999.

MacFarling Meure, C., Etheridge, D., Trudinger, C., Steele, P., Langenfelds, R., Van Ommen, T., Smith, A., and Elkins, J.: Law dome CO_2, CH_4 and N_2O ice core records extended to 2000 years BP, Geophysical Research Letters, 33, 2006.

Maiss, M., Steele, L. P., Francey, R. J., Fraser, P. J., Langenfelds, R. L., Trivett, N. B. A., and Levin, I.: Sulfur hexafluoride - a powerful new atmospheric tracer, Atmospheric Environment, 30, 1621-1629, 1996.

Maiss, M., and Brenninkmeijer, C. A. M.: Atmospheric SF$_6$: Trends, sources, and prospects, Environmental Science and Technology, 32, 3077-3086, 1998.

Maiss, M., and Brenninkmeijer, C. A. M.:A reversed trend in emissions of SF$_6$ into the atmosphere?, in: Non CO$_2$ greenhouse gases: scientific understanding, control and implementation , Proceedings of the second international symposium, edited by Ham, J.V., Baede, A.P.M., Meyer, L.A., and Ybema, R., pp 199 – 204, Kluwer Academic Publishers, Dordrecht, Noordwijkerhout, The Netherlands, 2000.

Mariotti, A.: Atmospheric nitrogen is a reliable standard for natural abundance measurements, Nature, 303, 685-687, 1983.

Martinerie, P., Nourtier-Mazauric, E., Barnola, J.-M., Sturges, W.T., Atlas, E., Gohar, L.K., Shine, K.P., and Brasseur, G.P.:Long-lived halocarbon trends and budgets from atmospheric chemistry modelling constrained with measurements in polar firn, Atmospheric Chemistry and Physics

Masson-Delmotte, V., Delmotte, M., Morgan, V., Etheridge, D., van Ommen, T., Tartarin, S., and Hoffmann, G.: Recent southern Indian ocean climate variability inferred from a law dome ice core: New insights for the interpretation of coastal antarctic isotopic records, Climate Dynamics, 21, 153-166, 2003.

Masson-Delmotte, V., Jouzel, J., Landais, A., Stievenard, M., Johnsen, S. J., White, J. W. C., Werner, M., Sveinbjornsdottir, A., and Fuhrer, K.: Atmospheric science: Grip deuterium excess reveals rapid and orbital-scale changes in Greenland moisture origin, Science, 309, 118-121, 2005.

Masson-Delmotte, V., Dreyfus, G., Braconnot, P., Johnsen, S., Jouzel, J., Kageyama, M., Landais, A., Loutre, M. F., Nouet, J., Parrenin, F., Raynaud, D., Stenni, B., and Tuenter, E.: Past temperature reconstructions from deep ice cores: Relevance for future climate change, Climate of the Past, 2, 145-165, 2006.

Masson, V., Vimeux, F., Jouzel, J., Morgan, V., Delmotte, M., Ciais, P., Hammer, C., Johnsen, S., Lipenkov, V. Y., Mosley-Thompson, E., Petit, J. R., Steig, E. J., Stievenard, M., and Vaikmae, R.: Holocene climate variability in Antarctica based on 11 ice-core isotopic records, Quaternary Research, 54, 348-358, 2000.

Mayewski, P. A., Meeker, L. D., Twickler, M. S., Whitlow, S., Qinzhao, Y., Berry Lyons, W., and Prentice, M.: Major features and forcing of high-latitude northern hemisphere atmospheric circulation using a 110 000-year-long glaciochemical series, Journal of Geophysical Research, 102, 26345-26366, 1997.

McCulloch, A., and Lindley, A. A.: Global emissions of hfc-23 estimated to year 2015, Atmospheric Environment, 41, 1560-1566, 2007.

Monnin, E., Indermühle, A., Dällenbach, A., Flückiger, J., Stauffer, B., Stocker, T. F., Raynaud, D., and Barnola, J. M.: Atmospheric CO$_2$ concentrations over the last glacial termination, Science, 291, 112-114, 2001.

Monnin, E., Steig, E. J., Siegenthaler, U., Kawamura, K., Schwander, J., Stauffer, B., Stocker, T. F., Morse, D. L., Barnola, J. M., Bellier, B., Raynaud, D., and Fischer, H.: Evidence for substantial accumulation rate variability in Antarctica during the Holocene, through synchronization of CO$_2$ in the Taylor dome, Dome C and DML ice cores, Earth and Planetary Science Letters, 224, 45-54, 2004.

Morris, R. A., Miller, T. M., Viggiano, A. A., Paulson, J. F., Solomon, S., and Reid, G.: Effects of electron and ion reactions on atmospheric lifetimes of fully fluorinated compounds, Journal of Geophysical Research, 100, 1287-1294, 1995.

Mulvaney, R., Röthlisberger, R., Wolff, E. W., Sommer, S., Schwander, J., Hutterli, M. A., and Jouzel, J.: The transition from the last glacial period in inland and near-coastal antarctica, Geophysical Research Letters, 27, 2673-2676, 2000.

Mulvaney, R., Alemany, O., and Possenti, P.: The Berkner Island (Antarctica) ice-core drilling project, Annals of Glaciology, 47, 115-124, 2007.

NGRIP members: High-resolution record of northern hemisphere climate extending into the last interglacial period, Nature, 431, 147-151, 2004b.

Nielsen, O. J., Nicolaisen, F. M., Bacher, C., Hurley, M. D., Wallington, T. J., and Shine, K. P.: Infrared spectrum and global warming potential of SF_5CF_3, Atmospheric Environment, 36, 1237-1240, 2002.

Olivier, J.G.J., Van Aardenne, J.A., Dentener, F., Ganzeveld, L. and Peters, J.A.W.H.: Recent trends in global greenhouse emissions: regional trends and spatial distribution of key sources. In: "Non-CO_2 Greenhouse Gases (NCGG-4)", A. van Amstel (coord.), page 325-330. Millpress, Rotterdam, ISBN 90 5966 043 9, 2005.

Oram, D. E., Sturges, W. T., Penkett, S. A., McCulloch, A., and Fraser, P. J.: Growth of fluoroform (CHF_3) in the background atmosphere, Geophysical Research Letters, 25, 35-38, 1998.

Oram, D.E., Trends of long lived anthropogenic halocarbons in the Southern Hemisphere and model calculations of global emissions, Ph.D. Thesis, University of East Anglia, Norwich, 1999.

Parrenin, F., Rémy, F., Ritz, C., Siegert, M. J., and Jouzel, J.: New modeling of the vostok ice flow line and implication for the glaciological chronology of the Vostok ice core, Journal of Geophysical Research D: Atmospheres, 109, 2004.

Parrenin, F., Barnola, J. M., Beer, J., Blunier, T., Castellano, E., Chappellaz, J., Dreyfus, G., Fischer, H., Fujita, S., Jouzel, J., Kawamura, K., Lemieux-Dudon, B., Loulergue, L., Masson-Delmotte, V., Narcisi, B., Petit, J. R., Raisbeck, G., Raynaud, D., Ruth, U., Schwander, J., Severi, M., Spahni, R., Steffensen, J. P., Svensson, A., Udisti, R., Waelbroeck, C., and Wolff, E.: The EDC3 chronology for the EPICA Dome C ice core, Climate of the Past, 3, 485-497, 2007.

Petit, J. R., Jouzel, J., Raynaud, D., Barkov, N. I., Barnola, J. M., Basile, I., Bender, M., Chappellaz, J., Davis, M., Delaygue, G., Delmotte, M., Kotiyakov, V. M., Legrand, M., Lipenkov, V. Y., Lorius, C., PÃ©pin, L., Ritz, C., Saltzman, E., and Stievenard, M.: Climate and atmospheric history of the past 420,000 years from the Vostok ice core, Antarctica, Nature, 399, 429-436, 1999.

Petrenko, V.V., Severinghaus, J.P., Brook, E.J., Reeh, N. and Schaefer, H.: Gas records from the West Greenland ice margin covering the Last Glacial Termination: a horizontal ice core, Quat. Sci. Rev., 25, 865-875, 2006.

Ravishankara, A. R., Solomon, S., Turnipseed, A. A., and Warren, R. F.: Atmospheric lifetimes of long-lived halogenated species, Science, 259, 194-199, 1993.

Raynaud, D., Chappellaz, J., Barnola, J. M., Korotkevich, Y. S., and Lorius, C.: Climatic and ch4 cycle implications of glacial-interglacial CH_4 change in the Vostok ice core, Nature, 333, 655-657, 1988.

Raynaud, D., Lipenkov, V., Lemieux-Dudon, B., Duval, P., Loutre, M. F., and Lhomme, N.: The local insolation signature of air content in Antarctic ice. A new step toward an absolute dating of ice records, Earth and Planetary Science Letters, 261, 337-349, 2007.

Rinsland, C. P., Mahieu, E., Zander, R., Nassar, R., Bernath, P., Boone, C., and Chiou, L. S.: Long-term stratospheric carbon tetrafluoride (CF_4) increase inferred from 1985-2004 infrared space-based solar occultation measurements, Geophysical Research Letters, 33, 2006

Rommelaere, V., Arnaud, L., and Barnola, J. M.: Reconstructing recent atmospheric trace gas concentrations from polar firn and bubbly ice data by inverse methods, Journal of Geophysical Research D: Atmospheres, 102, 30069-30083, 1997.

Salamatin, A. N., Lipenkov, V. Y., Barkov, N. I., Jouzel, J., Petit, J. R., and Raynaud, D.: Ice core age dating and paleothermometer calibration based on isotope and temperature profiles from deep boreholes at Vostok station (east Antarctica), Journal of Geophysical Research D: Atmospheres, 103, 8963-8977, 1998.

Santoro, M. A.: Clarifying the SF_5CF_3 record [4] (multiple letters), Science, 290, 935-936, 2000.

Schmittner, A., and Galbraith, E. D.: Glacial greenhouse-gas fluctuations controlled by ocean circulation changes, Nature, 456, 373-376, 2008.

Schwander, J.,Stauffer, B. and Sigg, A.: Air mixing in firn and the age of the air at pore close-off, Annals of Glaciology, 10, 141-145, 1989.

Schwander, J.: The age of the air in the firn and the ice at summit, greenland, Journal of Geophysical Research, 98, 2831-2838, 1993.

Schwander, J., Sowers, T., Barnola, J. M., Blunier, T., Fuchs, A., and MalaizÃ©, B.: Age scale of the air in the summit ice: Implication for glacial-interglacial temperature change, Journal of Geophysical Research D: Atmospheres, 102, 19483-19493, 1997.

Severi, M., Becagli, S., Castellano, E., Morganti, A., Traversi, R., Udisti, R., Ruth, U., Fischer, H., Huybrechts, P., Wolff, E., Parrenin, F., Kaufmann, P., Lambert, F., and Steffensen, J. P.: Synchronisation of the EDML and EDC ice cores for the last 52 kyr by volcanic signature matching, Climate of the Past, 3, 367-374, 2007.

Severinghaus, J. P., Bender, M. L., Keeling, R. F., and Broecker, W. S.: Fractionation of soil gases by diffusion of water vapor, gravitational settling, and thermal diffusion, Geochimica et Cosmochimica Acta, 60, 1005-1018, 1996.

Severinghaus, J. P., Sowers, T., Brook, E. J., Alley, R. B., and Bender, M. L.: Timing of abrupt climate change at the end of the Younger Dryas interval from thermally fractionated gases in polar ice, Nature, 391, 141-146, 1998.

Severinghaus, J. P., and Brook, E. J.: Abrupt climate change at the end of the last glacial period inferred from trapped air in polar ice, Science, 286, 930-934, 1999.

Severinghaus, J. P., Grachev, A., and battle, M.: Thermal fractionation of air in polar firn by seasonal temperature gradients, Geochemistry Geophysics Geosystems, Vol 2, paper number 2000GC000146, 2001.

Severinghaus, J. P., Grachev, A., Luz, B., and Caillon, N.: A method for precise measurement of argon 40/36 and krypton/argon ratios in trapped air in polar ice with applications to past firn thickness and abrupt climate change in Greenland and at Siple Dome, Antarctica, Geochimica et Cosmochimica Acta, 67, 325-343, 2003.

Severinghaus, J. P., and Battle, M. O.: Fractionation of gases in polar ice during bubble close-off: New constraints from firn air Ne, Kr and Xe observations, Earth and Planetary Science Letters, 244, 474-500, 2006.

Severinghaus, J. P.: Climate change: Southern see-saw seen, Nature, 457, 1093-1094, 2009.

Severinghaus, J.P., Albert, M.R., Courville, Z.R., Fahnestock, M.A., Kawamura, K., Montzka, S.A., Mühle, J., Scambos, T.A., Shields, E., Shuman, C.A., Suwa, M., Tans, P., and Weiss, R.F.: Deep air convection in the firn at zero-accumulation site, central Antarctica, Earth and Planetary Science Letters, 293, 359-367, 2010.

Siegenthaler, U., Stocker, T. F., Monnin, E., Lüthi, D., Schwander, J., Stauffer, B., Raynaud, D., Barnola, J. M., Fischer, H., Masson-Delmotte, V., and Jouzel, J.: Atmospheric science: Stable carbon cycle-climate relationship during the late pleistocene, Science, 310, 1313-1317, 2005.

Sime, L. C., Wolff, E. W., Oliver, K. I. C., and Tindall, J. C.: Evidence for warmer interglacials in east Antarctic ice cores, Nature, 462, 342-345, 2009.

Singleton, J.H.: Interaction of oxygen with hot tungsten, J. Chem. Phys., 45, 2819 – 2826, 1966.

Skoog, D.A., West, D.M., Holler, F.J.: Fundamentals of Analytical Chemistry, Saunders College Publishing, 1996.

Sowers, T., Bender, M., and Raynaud, D.: Elemental and isotopic composition of occluded O_2 and N_2 in polar ice, Journal of Geophysical Research, 94, 5137-5150, 1989.

Sowers, T., Bender, M., Raynaud, D., and Korotkevich, Y. S.: $\delta^{15}N$ of N_2 in air trapped in polar ice: A tracer of gas transport in the firn and a possible constraint on ice age-gas age differences, Journal of Geophysical Research, 97, 1992.

Sowers, T., and Bender, M.: Climate records covering the last deglaciation, Science, 269, 210-214, 1995.

Spahni, R., Chappellaz, J., Stocker, T. F., Loulergue, L., Hausammann, G., Kawamura, K., Flückiger, J., Schwander, J., Raynaud, D., Masson-Delmotte, V., and Jouzel, J.: Atmospheric science: Atmospheric methane and nitrous oxide of the late pleistocene from Antarctic ice cores, Science, 310, 1317-1321, 2005.

Steig, E. J., Brook, E. J., White, J. W. C., Sucher, C. M., Bender, M. L., Lehman, S. J., Morse, D. L., Waddington, E. D., and Clow, G. D.: Synchronous climate changes in Antarctica and the North Atlantic, Science, 282, 92-95, 1998.

Steig, E. J.: Climate change: The south-north connection, Nature, 444, 152-153, 2006.

Stenni, B., Jouzel, J., Masson-Delmotte, V., Röthlisberger, R., Castellano, E., Cattani, O., Falourd, S., Johnsen, S. J., Longinelli, A., Sachs, J. P., Selmo, E., Souchez, R., Steffensen, J. P., and Udisti, R.: A late-glacial high-resolution site and source temperature record derived from the EPICA Dome C isotope records (East Antarctica), Earth and Planetary Science Letters, 217, 183-195, 2004.

Stenni, B., Masson-Delmotte, V., Selmo, E., Oerter, H., Meyer, H., Röthlisberger, R., Jouzel, J., Cattani, O., Falourd, S., Fischer, H., Hoffmann, G., Iacumin, P., Johnsen, S. J., Minster, B., and Udisti, R.: The deuterium excess records of EPICA Dome C and Dronning Maud Land ice cores (East Antarctica), Quaternary Science Reviews, 29, 146-159, 2010.

Stephens, B. B., and Keeling, R. F.: The influence of Antarctic sea ice on glacial-interglacial CO_2 variations, Nature, 404, 171-174, 2000.

Stocker, T. F.: The seesaw effect, Science, 282, 61-62, 1998.

Stocker, T. F.: Past and future reorganizations in the climate system, Quaternary Science Reviews, 19, 301-319, 2000.

Stuiver, M., Grootes, P. M., and Braziunas, T. F.: The GISP2 $\delta^{18}O$ climate record of the past 16,500 years and the role of the sun, ocean, and volcanoes, Quaternary Research, 44, 341-354, 1995.

Sturges, W. T., Wallington, T. J., Hurley, M. D., Shine, K. P., Sihra, K., Engel, A., Oram, D. E., Penkett, S. A., Mulvaney, R., and Brenninkmeijer, C. A. M.: A potent greenhouse gas identified in the atmosphere: SF_5CF_3, Science, 289, 611-613, 2000.

Sturges, W. T., McIntyre, H. P., Penkett, S. A., Chappellaz, J., Barnola, J. M., Mulvaney, R., Atlas, E., and Stroud, V.: Methyl bromide, other brominated methanes, and methyl iodide in polar firn air, Journal of Geophysical Research D: Atmospheres, 106, 1595-1606, 2001.

Sturrock, G. A., Etheridge, D. M., Trudinger, C. M., Fraser, P. J., and Smith, A. M.: Atmospheric histories of halocarbons from analysis of Antarctic firn air: Major Montreal protocol species, Journal of Geophysical Research D: Atmospheres, 107, 2002.

Takahashi, K., Nakayama, T., Matsumi, Y., Solomon, S., Gejo, T., Shigemasa, E., and Wallington, T. J.: Atmospheric lifetime of sf5cf3, Geophysical Research Letters, 29, 7-1, 2002.

Taylor, K. C., Mayewski, P. A., Alley, R. B., Brook, E. J., Gow, A. J., Grootes, P. M., Meese, D. A., Saltzman, E. S., Severinghaus, J. P., Twickler, M. S., White, J. W. C., Whitlow, S., and Zielinski, G. A.: The Holocene-younger dryas transition recorded at summit, Greenland, Science, 278, 825-827, 1997.

Taylor, K. C., White, J. W. C., Severinghaus, J. P., Brook, E. J., Mayewski, P. A., Alley, R. B., Steig, E. J., Spencer, M. K., Meyerson, E., Meese, D. A., Lamorey, G. W., Grachev, A., Gow, A. J., and Barnett, B. A.: Abrupt climate change around 22 ka on the Siple Coast of Antarctica, Quaternary Science Reviews, 23, 7-15, 2004.

Thomas, E. R., Wolff, E. W., Mulvaney, R., Steffensen, J. P., Johnsen, S. J., Arrowsmith, C., White, J. W. C., Vaughn, B., and Popp, T.: The 8.2 ka event from Greenland ice cores, Quaternary Science Reviews, 26, 70-81, 2007.

Thomas, E. R., Wolff, E. W., Mulvaney, R., Johnsen, S. J., Steffensen, J. P., and Arrowsmith, C.: Anatomy of a Dansgaard-Oeschger warming transition: High-resolution analysis of the North Greenland ice core project ice core, Journal of Geophysical Research D: Atmospheres, 114, 2009.

Toggweiler, J. R.: Origin of the 100,000-year timescale in Antarctic temperatures and atmospheric CO_2, Paleoceanography, 23, 2008.

Trudinger, C. M., Enting, I. G., Etheridge, D. M., Francey, R. J., Levchenko, V. A., Steele, L. P., Raynaud, D., and Arnaud, L.: Modeling air movement and bubble trapping in firn, Journal of Geophysical Research D: Atmospheres, 102, 6747-6763, 1997.

Trudinger, C. M., Etheridge, D. M., Rayner, P. J., Enting, I. G., Sturrock, G. A., and Langenfelds, R. L.: Reconstructing atmospheric histories from measurements of air composition in firn, Journal of Geophysical Research D: Atmospheres, 107, 2002.

Trudinger, C. M., Etheridge, D. M., Sturrock, G. A., Fraser, P. J., Krummel, P. B., and McCulloch, A.: Atmospheric histories of halocarbons from analysis of Antarctic firn air: Methyl bromide, methyl chloride, chloroform, and dichloromethane, Journal of Geophysical Research D: Atmospheres, 109, 1-15, 2004.

Udisti, R., Becagli, S., Castellano, E., Delmonte, B., Jouzel, J., Petit, J. R., Schwander, J., Stenni, B., and Wolff, E. W.: Stratigraphic correlations between the European Project for Ice Coring in Antarctica (EPICA) Dome C and Vostok ice cores showing the relative variations of snow accumulation over the past 45 kyr, Journal of Geophysical Research D: Atmospheres, 109, 2004.

Uemura, R., Yoshida, N., Kurita, N., Nakawo, M., and Watanabe, O.: An observation-based method for reconstructing ocean surface changes using a 340,000-year deuterium excess from the Dome Fuji ice core, Antarctica, Geophysical Research Letters, 31, 2004.

Van Ommen, T. D., Morgan, V., and Curran, M. A. J.: Deglacial and Holocene changes in accumulation at law dome, east Antarctica, Annals of Glaciology, 39, 359-365, 2005.

Velders, G.J.M., and Madronich, S., Clerbaux, C., Derwent, R.G., Grutter, M., Hauglustaine, D.A., Incecik, S., Ko, M.K.W., Libre, J.-M., Nielsen, O.J., Stordal, F., and Zhu, T.: Chemical and radiative effects of halocarbons and their replacement compounds, Chapter 2 in: IPCC/TEAP Special Report on Safeguarding the Ozone Layer and the Global Climate System edited by Metz, B., L.Kuijpers, S. Solomons, S.O. Andersen, O. Davidson, J. Pons, D. de Jager, T. Kestin, M. Manning, and L.A. Meyer, 478 pp., Cambridge University Press, Cambridge, U.K., 2005.

Vimeux, F., Masson, V., Delaygue, G., Jouzel, J., Petit, J. R., and Stievenard, M.: A 420,000 year deuterium excess record from east Antarctica: Information on past changes in the origin of precipitation at Vostok, Journal of Geophysical Research D: Atmospheres, 106, 31863-31873, 2001.

Watanabe, O., Jouzel, J., Johnsen, S., Parrenin, F., Shoji, H., and Yoshida, N.: Homogeneous climate variability across east Antarctica over the past three glacial cycles, Nature, 422, 509-512, 2003.

Weiler, K.: On the composition of Firn air and its Dependence on Seasonally Varying Atmospheric Boundary Conditions and the Firn Structure, PhD thesis, University of Bern, Bern, Switzerland, 2008.

White, J. W. C., and Steig, E. J.: Timing is everything in a game of two hemispheres, Nature, 394, 717-718, 1998.

Wijmans, J. G., He, Z., Su, T. T., Baker, R. W., and Pinnau, I.: Recovery of perfluoroethane from chemical vapor deposition operations in the semiconductor industry, Separation and Purification Technology, 35, 203-213, 2004

WMO: Scientific Assessment of Ozone Depletion: 2006, Global Ozone Research and Monitoring Project, Report 50, World Meteorological Organization, Geneva, 2006. .

Wolff, E. W.: Understanding the past - climate history from Antarctica, Antarctic Science, 17, 487-495, 2005.

Wolff, E. W., Fischer, H., and Röthlisberger, R.: Glacial terminations as southern warmings without northern control, Nature Geoscience, 2, 206-209, 2009.

Worton, D.R.: Alkyl nitrates (C_1-C_5), trihalomethanes and related compounds in contemporary air and air preserved in polar firn and ice., Ph.D. Thesis, University of East Anglia, Norwich, 2005.

Worton, D. R., Sturges, W. T., Gohar, L. K., Shine, K. P., Martinerie, P., Oram, D. E., Humphrey, S. P., Begley, P., Gunn, L., Barnola, J. M., Schwander, J., and Mulvaney, R.: Atmospheric trends and radiative forcings of CF_4 and C_2F_6 inferred from firn air, Environmental Science and Technology, 41, 2184-2189, 2007.

Xu, W., Xiao, C., Li, Q., Xie, Y., and Schaefer Iii, H. F.: Structures, thermochemistry, vibrational frequencies and integrated infrared intensities of SF_5CF3, with implications for global temperature patterns, Molecular Physics, 102, 1415-1439, 2004.

Yokouchi, Y., Inagaki, T., Yazawa, K., Tamaru, T., Enomoto, T., and Izumi, K.: Estimates of ratios of anthropogenic halocarbon emissions from Japan based on aircraft monitoring over Sagami Bay, Japan, Journal of Geophysical Research D: Atmospheres, 110, 1-7, 2005.

Zander, R., Mahieu, E., Demoulin, P., Duchatelet, P., Roland, G., Servais, C., MaziÃ¨re, M. D., Reimann, S., and Rinsland, C. P.: Our changing atmosphere: Evidence based on long-term infrared solar observations at the Jungfraujoch since 1950, Science of the Total Environment, 391, 184-195, 2008.